PB82-231713

EPA Complex Terrain Model Development
First Milestone Report, 1981

Environmental Research and Technology, Inc.
Concord, MA

Prepared for

Environmental Sciences Research Lab.
Research Triangle Park, NC

Apr 82

U.S. Department of Commerce
National Technical Information Service
NTIS

PB82-231713

United States
Environmental Protection
Agency

Environmental Sciences Research
Laboratory
Research Triangle Park NC 27711

EPA-600/3-82-036
April 1982

Research and Development

ŞEPA

EPA Complex Terrain Model Development

First Milestone Report - 1981

RESEARCH REPORTING SERIES

Research reports of the Office of Research and Development, U.S. Environmental Protection Agency, have been grouped into nine series. These nine broad categories were established to facilitate further development and application of environmental technology. Elimination of traditional grouping was consciously planned to foster technology transfer and a maximum interface in related fields. The nine series are:

1. Environmental Health Effects Research
2. Environmental Protection Technology
3. Ecological Research
4. Environmental Monitoring
5. Socioeconomic Environmental Studies
6. Scientific and Technical Assessment Reports (STAR)
7. Interagency Energy-Environment Research and Development
8. "Special" Reports
9. Miscellaneous Reports

This report has been assigned to the ECOLOGICAL RESEARCH series. This series describes research on the effects of pollution on humans, plant and animal species, and materials. Problems are assessed for their long- and short-term influences. Investigations include formation, transport, and pathway studies to determine the fate of pollutants and their effects. This work provides the technical basis for setting standards to minimize undesirable changes in living organisms in the aquatic, terrestrial, and atmospheric environments.

This document is available to the public through the National Technical Information Service, Springfield, Virginia 22161.

TECHNICAL REPORT DATA
(Please read Instructions on the reverse before completing)

1. REPORT NO. EPA-600/3-82-036	2.	3. RECIPIENT'S ACCESSION NO. PB82-231713
4. TITLE AND SUBTITLE EPA COMPLEX TERRAIN MODEL DEVELOPMENT First Milestone Report - 1981		5. REPORT DATE April 1982
		6. PERFORMING ORGANIZATION CODE
7. AUTHOR(S) T. F. Lavery, A. Bass, D. G. Strimaitis, A. Venkatram, B. R. Greene, P. J. Drivas, and B. A. Egan		8. PERFORMING ORGANIZATION REPORT NO.
9. PERFORMING ORGANIZATION NAME AND ADDRESS Environmental Research & Technology, Inc. 696 Virginia Road Concord, Massachusetts 01742		10. PROGRAM ELEMENT NO. CABN1D/01-0566 (FY-82)
		11. CONTRACT/GRANT NO. 68-02-3421
12. SPONSORING AGENCY NAME AND ADDRESS Environmental Sciences Research Laboratory - RTP, NC Office of Research and Development U.S. Environmental Protection Agency Research Triangle Park, North Carolina 27711		13. TYPE OF REPORT AND PERIOD COVERED Interim 6/80-12/81
		14. SPONSORING AGENCY CODE EPA/600/09

15. SUPPLEMENTARY NOTES

16. ABSTRACT

The U.S. Environmental Protection Agency is sponsoring the Complex Terrain Model Development program, a multi-year integrated program to develop and validate practical plume dispersion models of known reliability and accuracy for simulating one-hour average ground-level concentrations downwind of elevated sources during stable atmospheric conditions in complex terrain. The first major component of the Complex Terrain Model Development program was a field study conducted during the fall of 1980 at Cinder Cone Butte, a roughly axisymmetric, isolated 100-meter-tall hill located in the broad Snake River Basin near Boise, Idaho. The field program consisted of ten flow visualization experiments and eighteen multi-hour tracer gas experiments conducted during stable flow conditions.

This report presents an overview of the Cinder Cone Butte field program and the results of the modeling analyses completed through June 1, 1981. The objectives of this phase of the modeling program were to begin the development of new dispersion models using the Cinder Cone Butte data base and to compare their performance with existing complex terrain dispersion models.

17. KEY WORDS AND DOCUMENT ANALYSIS

a. DESCRIPTORS	b. IDENTIFIERS/OPEN ENDED TERMS	c. COSATI Field/Group

Dis.

18. DISTRIBUTION STATEMENT RELEASE TO PUBLIC	19. SECURITY CLASS *(This Report)* UNCLASSIFIED	21. NO. OF PAGES 331
	20. SECURITY CLASS *(This page)* UNCLASSIFIED	22. PRICE

EPA Form 2220-1 (9-73)

ATTENTION

PORTIONS OF THIS REPORT ARE NOT LEGIBLE.
HOWEVER, IT IS THE BEST REPRODUCTION
AVAILABLE FROM THE COPY SENT TO NTIS.

TA,

EPA-600/3-82-036
April 1982

EPA Complex Terrain Model Development

First Milestone Report - 1981

by

T.F. Lavery, A.Bass, D.G. Strimaitis, Venkatram,
B.R. Green, P.J. Drivas,
and
B.A. Egan

Environmental Research & Technology, Inc.
696 Virginia Road
Concord, Massachusetts 01742

Contract No. 68-02-3421

Project Officer

Francis A. Schiermeier
Meterology and Assessment Division
Environmental Sciences Research Laboratory
Research Triangle Park, North Carolina 27711

ENVIRONMENTAL SCIENCES RESEARCH LABORATORY
OFFICE OF RESEARCH AND DEVELOPMENT
U.S. ENVIRONMENTAL PROTECTION AGENCY
RESEARCH TRIANGLE PARK, NORTH CAROLINA 27711

April 1982

DISCLAIMER

This report has been reviewed by the Environmental Sciences Research Laboratory, U.S. Environmental Protection Agency, and approved for publication. Approval does not signify that the contents necessarily reflect the views and policies of the U.S. Environmental Protection Agency, nor does mention of trade names or commercial products constitute endorsement or recommendation for use.

FOREWORD

The Environmental Sciences Research Laboratory (ESRL) conducts an intramural and extramural research program in the physical sciences to detect, define, and quantify air pollution and its effects on urban, regional, and global atmospheres and the subsequent impact on water quality and land use. The Laboratory is responsible for planning, implementing, and managing research and development programs designed to quantitate the relationships between emissions of pollutants from all types of sources and air quality and atmospheric effects and to uncover and characterize hitherto unidentified air pollution problems. Information from ESRL programs and from the programs of other Government agencies, private industry, and the academic community are integrated by the Laboratory to develop the technical basis for air pollution control strategies for various pollutants.

The Complex Terrain Model Development project is designed to develop reliable atmospheric dispersion models that are applicable to large pollutant sources located in complex terrain. The first major field study of this five-year program was conducted during 1980 at Cinder Cone Butte near Boise, Idaho. Data from this field study along with measurements of scaled physical simulations performed in the EPA Fluid Modeling Facility are being used to quantify the effects of terrain obstacles on stable plume dispersion. This interim report presents the performance evaluations of four existing complex terrain models and describes the initial developmental stages of two proposed new models.

A. H. Ellison
Acting Director
Environmental Sciences Research Laboratory

ABSTRACT

The U.S. Environmental Protection Agency (EPA) is sponsoring the Complex Terrain Model Development (CTMD), a multi-year integrated program to develop and validate practical plume models of known reliability and accuracy for simulating 1-hour average ground-level concentrations downwind of elevated sources during stable atmospheric conditions in complex terrain. The first major component of the CTMP was a field program conducted during the fall of 1980 at Cinder Cone Butte (CCB), a roughly axisymmetric, isolated 100-meter hill located in the broad Snake River Basin near Boise, Idaho. The field program consisted of ten flow visualization experiments and 18 multi-hour tracer gas experiments conducted during stable flow conditions.

The data base compiled at CCB includes the following components:

- Source information: emission rates, locations, and heights of SF_6, CF_3Br, and oil-fog releases.
- Meteorological information: descriptions of the undisturbed mesoscale valley flow in the vicinity of CCB as well as information on flow and dispersion on and over CCB itself.
- Hill surface tracer gas concentrations: data from more than 14,000 individual bag samples collected over the 18 days of experiments from as many as 80 sampler locations in a given experiment.
- Lidar data: characterizing the plume trajectory and plume spread upwind and over CCB.
- Photographic data: still photographs taken from fixed locations on and around CCB, aerial photographs taken from an aircraft flying overhead, and 16 mm movies and videotapes.

This report presents an overview of the CCB experiment and the results of the modeling analyses completed through June 1, 1981. The objectives of the model analyses are to develop and evaluate new models using the CCB data base and to compare their performance to the following current complex terrain dispersion models:

- the EPA Valley model worst-case screening algorithm, widely used in regulatory practice to screen elevated sources in complex terrain;
- COMPLEX I and COMPLEX II, two new proposed complex terrain screening models issued by EPA for public testing and evaluation; and
- PFM, a potential flow model for turbulent dispersion of plumes in the presence of simple terrain features.

For these comparisons, 45 case study hours were selected from the 18 field experiment days. (The PFM model comparisons were made with about half of these case study hours.)

Two new modeling approaches suggested by the experimental evidence have been formulated and tested. One new model (called the Impingement model) is used to simulate ground-level concentrations in strongly stable flows in which plumes go horizontally around the side of CCB; another new model (called the Neutral model) simulates slightly stable or neutral flows in which plumes rise over CCB. It must be emphasized, though, that these new models--which thus far represent only a modest level of effort--are tentative first steps toward the goal of practical, reliable complex terrain models. They are not the desired end results and are in no way identified for routine application at this time.

All models were evaluated by comparing 1-hour average observed concentrations with 1-hour average calculated concentrations. The results are encouraging: the two preliminary models appear to simulate maximum concentrations and spatial concentration patterns more realistically than the current models.

This report was submitted in partial fulfillment of Contract 68-02-3421 by Environmental Research & Technology, Inc. under the sponsorship of the U.S. Environmental Protection Agency. This report covers the period June 26, 1980 to June 1, 1981, and work was completed as of June 1, 1981.

CONTENTS

Page

Foreword iii

Abstract iv

Figures ix

Tables xv

Symbols and Abbreviations xviii

Acknowledgements xxi

1. Introduction 1
   - 1.1 Overview of Complex Terrain Model Development . . . 1
   - 1.2 Basic Concepts of Plume Dispersion in Stable Flows . 6
2. Overview of Complex Terrain Field Study 10
   - 2.1 Geographic and Meteorological Setting 10
   - 2.2 Fluid Modeling of Expected Flow Regimes. 17
   - 2.3 Experimental Design of Field Study 23
   - 2.4 Field Study Results 45
3. Quality Assurance Program 70
   - 3.1 Meteorological Data 71
   - 3.2 Tracer Data 95
4. Air Quality Models Evaluated 103
   - 4.1 Introduction 103
   - 4.2 Valley Model 104
   - 4.3 COMPLEX I and COMPLEX II Models 106
   - 4.4 Potential Flow Model 109
   - 4.5 New Experimental Models 114
5. Model Performance Using Cindor Cone Butte Field Data . . 128
   - 5.1 Case Hours Selected for Model Evaluations 128
   - 5.2 Data Preparation 129

CONTENTS (Continued)

Page

5.3 Model Evaluation Methods 132
5.4 Sample Case Study Results - Case 205, Hour 5 145
5.5 Summary of Model Performance 184
6. Conclusions and Recommendations for Further Analysis and Development 221
6.1 Accomplishments in Overview 221
6.2 Comparative Model Performance Evaluations 224
6.3 Recommendations for Further Research 227
References 236

Appendices

A. Summary of Tracer Data Analyzed for Tests 201-218 . 239
B. Laboratory Simulation of Stable Plume Dispersion Cinder Cone Butte 249
C. Use of Model Performance Statistics 302

FIGURES

Number		Page
1	Schematic of flow around a three-dimensional obstacle at very low Froude number	9
2	Topographic map of Cinder Cone Butte region.	11
3	Topography of Cinder Cone Butte.	12
4	Side views of Cinder Cone Butte.	13
5	Aerial view of Cinder Cone Butte from south.	14
6	Aerial view of Cinder Cone Butte from southeast.	15
7	Distribution of wind speed and direction for September 1965-1969 derived from weather observations at Mountain Home AFB.	16
8	Composite estimates of plume paths based on towing tank simulations: wind direction 110°, Fr = 0.4.	21
9	Composite estimates of plume paths based on towing tank simulations: wind direction 300°, Fr = 0.4.	22
10	Field experiment layout.	25
11	Preselected camera locations	28
12	Tracer gas sampler locations	32
13	Reflection mast design	34
14	Tracer gas chromatogram.	36
15	Bag sampling and analysis procedures	37

FIGURES

Number		Page
16	Procedures to obtain tracer gas concentrations	38
17	SF_6 calibration curves	40
18	Illustration of lidar-sampled plumes	42
19	Data collection system configuration	44
20	Number of samples analyzed for each field experiment	49
21	Observed SF_6 concentrations (ppt) for Case 206, 0500-0600.	52
22	Five-minute exposure; camera location 0-15 (Case 206, 0500 MST).	54
23	One-minute exposure looking from northeast (Case 206, 0508 MST).	55
24	Five-minute exposure; camera location 0-15 (Case 206, 0530 MST).	56
25	One-minute exposure looking from North Peak (Case 206, 0540 MST).	57
26	Five-minute exposure; camera location 0-11 (Case 206, 0546 MST).	58
27	Observed SF_6 concentrations (ppt) for Case 211, 0400-0500.	60
28	Observed CF_3Br concentrations (ppt) for Case 211, 0400-0500.	61
29	One-minute exposure from southwest (Case 211, 0414 MST). . .	62
30	One-minute exposure from lee side of Cinder Cone Butte (Case 211, 0435 MST)	63
31	Observed CF_3Br concentrations (ppt) for Case 210 0200-0300.	65
32	Observed SF_6 concentrations (ppt) for Case 210, 0200-0300.	66
33	One-minute exposure looking from South Peak (Case 210, 0209 MST).	67
34	One-minute exposure looking from southwest (Case 210, 0535 MST).	68

FIGURES

Number Page

35 Observed SF_6 concentrations (ppt) for Case 205, 0400-0500 69

36 Example of a data file. 92

37 Example of an edited data file. 93

38a PFM geometry for Cinder Cone Butte calculations 112

38b Illustration of the relationship between the tracer release height and important reference surfaces at CCB. 113

39 Geometry used in formulating Impingement model for low Froude number flows 117

40 Geometry used in formulating Neutral model for high Froude number flows. 120

41 Dependence of lidar-derived σ_z on downwind distance for 15 case hours 126

42 Relationship between model inputs, single concentration observations, and the set of possible concentrations described by model inputs 138

43 Relationship between an observed concentration and estimates of this concentration from models A and B when these models accurately simulate the ensemble mean concentration 139

44 Relative performance of different models. 144

45 Observed SF_6 concentrations for Case 205, 0400-0500 . . . 146

46 COMPLEX I: calculated SF_6 concentrations for Case 205, Hour 5, Stability Class D 148

47 COMPLEX I: calculated SF_6 concentrations for Case 205, Hour 5, Stability Class E 149

48 COMPLEX I: calculated SF_6 concentrations for Case 205, Hour 5, Stability Class F 150

49 COMPLEX II: calculated SF_6 concentrations for Case 205, Hour 5, Stability Class D 151

50 COMPLEX II: calculated SF_6 concentrations for Case 205, Hour 5, Stability Class E 152

FIGURES

Number		Page
51	COMPLEX II: calculated SF_6 concentrations for Case 205, Hour 5, Stability Class F	153
52	COMPLEX I and II: calculated SF_6 concentrations versus observed SF_6 concentrations for Case 205, Hour 5, Stability Class D	155
53	COMPLEX I and II: calculated SF_6 concentrations versus observed SF_6 concentrations for Case 205, Hour 5, Stability Class E	156
54	COMPLEX I and II: calculated SF_6 concentrations versus observed SF_6 concentrations for Case 205, Hour 5, Stability Class F	157
55	PFM: calculated SF_6 concentrations for Case 205, Hour 5, Stability Class D	169
56	PFM: calculated SF_6 concentrations for Case 205, Hour 5, Stability Class E	170
57	PFM: calculated SF_6 concentrations versus observed SF_6 concentrations for Case 205, Hour 5, Stability Class D. .	172
58	PFM: calculated SF_6 concentrations versus observed SF_6 concentrations for Case 205, Hour 5, Stability Class E. .	173
59	Neutral model: calculated SF_6 concentrations for Case 205, Hour 5	179
60	Neutral model: calculated SF_6 concentrations versus observed SF_6 concentrations for Case 205, Hour 5. . . .	180
61	Variation of modeled-to-observed ratios of maximum hourly SF_6 concentrations with modeled concentrations calculated by Valley	187
62	Variation of modeled-to-observed ratios of maximum hourly SF_6 concentrations with modeled concentrations calculated by Valley (centerline)	188
63	Variation of modeled-to-observed ratios of maximum hourly SF_6 concentrations with modeled concentrations calculated by COMPLEX I (Stability Class D)	192
64	Variation of modeled-to-observed ratios of maximum hourly SF_6 concentrations with modeled concentrations calculated by COMPLEX I (Stability Class E)	193

FIGURES

Number | Page

65 Variation of modeled-to-observed ratios of maximum hourly SF_6 concentrations with modeled concentrations calculated by COMPLEX I (Stability Class F) 194

66 Variation of modeled-to-observed ratios of maximum hourly SF_6 concentrations with modeled concentrations calculated by COMPLEX I (Appropriate Stability Class - Turner Scheme) 195

67 Variation of modeled-to-observed ratios of maximum hourly SF_6 concentrations with modeled concentrations calculated by COMPLEX II (Stability Class D) 196

68 Variation of modeled-to-observed ratios of maximum hourly SF_6 concentrations with modeled concentrations calculated by COMPLEX II (Stability Class E) 197

69 Variation of modeled-to-observed ratios of maximum hourly SF_6 concentrations with modeled concentrations calculated by COMPLEX II (Stability Class F) 198

70 Variation of modeled-to-observed ratios of maximum hourly SF_6 concentrations with modeled concentrations calculated by COMPLEX II (appropriate stability class - Turner Scheme) 199

71 Variation of modeled-to-observed ratios of maximum hourly SF_6 concentrations with modeled concentrations calculated by PFM (Stability Class D). 202

72 Variation of modeled-to-observed ratios of maximum hourly SF_6 concentrations with modeled concentrations calculated by PFM (Stability Class E). 203

73 Variation of modeled-to-observed ratios of maximum hourly SF_6 concentrations with modeled concentrations calculated by the Impingement model. 206

74 Variation of modeled-to-observed ratios of maximum hourly SF_6 concentrations with modeled concentrations calculated by the Neutral model. 208

75 Relative performance of models tested with 45 case hours of data from CCB with model performance based on ratios of maximum calculated and observed hourly SF_6 concentrations 212

76 Relative performance of models tested with 45 case hours of data from CCB with model performance based on residuals of maximum calculated and observed concentrations. 213

FIGURES

Number Page

77 Relative performance of models tested with 45 case hours of data from CCB with model performance based on residuals of calculated and observed hourly SF_6 concentration at all samplers. 214

78 Relative performance of models tested with 23 case hours (release height > H_{crit}) of data at CCB with model performance based on ratios of maximum calculated and observed SF_6 concentrations. 217

79 Relative performance of models tested with 23 case hours (release height > H_{crit}) of data at CCB with model performance based on residuals of maximum calculated and observed SF_6 concentrations. 218

80 Relative performance of models tested with 23 case hours (release height > H_{crit}) of data at CCB with model performance based on residuals of calculated and observed SF_6 concentrations at all samplers. 219

TABLES

Number		Page
1	Prevailing Wind Direction and Frequency at Mountain Home AFB (October 1964-1970)	18
2	Tower Instrumentation and Measures	26
3	SF_6 and CF_3Br Release Rates.	31
4	Sample Analysis Programs Available Onsite.	46
5	Summary of Tracer Data Analyzed.	47
6	Audit Results: Climatronics Temperature System.	74
7	Audit Results: Climatronics Delta Temperature System. . . .	75
8	Audit Results: Climatronics UVW Wind Systems.	76
9	Audit Results: F460 Wind Speed System	78
10	Audit Results: Climatronics F460 Wind Direction Alignment to Landmark Test	79
11	Audit Results: Climatronics F460 Wind Direction Linearity Test	80
12	Audit Results: Orientation of V Propellor Crossarm.	81
13	Audit Results: F460 Wind Direction Systems Errors	82
14	Audit Results: Landmark and North Stake Orientation Errors	83

TABLES

Number | | Page

15 Classification Criteria and Data Quality Flags for Hour-Averages Produced from 5-Minute Data 94

16 Recount Statistics. 97

17 Co-Located Sampler Statistics 97

18 Sample Degradation Test 99

19 TRC Audit Results 100

20 Comparison of σ_z Derived from Lidar Observations with Predicted σ_z. 125

21 Data Estimated at Source Height for Case Hours Selected for Model Comparisons 133

22 Descriptive Statistics and Associated Analyses. 136

23 Frequency Distributions of SF_6 Concentrations for COMPLEX I and II Models (Case 205, Hour 5, Stability Class D). 158

24 Frequency Distributions of SF_6 Concentrations for COMPLEX I and II Models (Case 205, Hour 5, Stability Class E). 159

25 Frequency Distributions of SF_6 Concentrations for COMPLEX I and II Models (Case 205, Hour 5, Stability Class F). 160

26 Observed Versus COMPLEX I Paired Concentrations (Case 205, Hour 5, Stability Class D) 161

27 Observed Versus COMPLEX I Paired Concentrations (Case 205, Hour 5, Stability Class E) 162

28 Observed Versus COMPLEX I Paired Concentrations (Case 205, Hour 5, Stability Class F) 163

29 Observed Versus COMPLEX II Paired Concentrations (Case 205, Hour 5, Stability Class D) 164

30 Observed Versus COMPLEX II Paired Concentrations (Case 205, Hour 5, Stability Class E) 165

31 Observed Versus COMPLEX II Paired Concentrations (Case 205, Hour 5, Stability Class F) 166

TABLES

Number Page

32 Summary Statistics for COMPLEX I and II (Case 205, Hour 5) 168

33 Frequency Distributions of SF_6 Concentrations for PFM (Case 205, Hour 5, Stability Class D) 174

34 Frequency Distributions of SF_6 Concentrations for PFM (Case 205, Hour 5, Stability Class E) 175

35 Observed Versus PFM Paired Concentrations (Case 205, Hour 5, Stability Class D). 176

36 Observed Versus PFM Paired Concentrations (Case 205, Hour 5, Stability Class E). 177

37 Summary Statistics for PFM (Case 205, Hour 5) 178

38 Frequency Distributions of SF_6 Concentrations for Neutral Model (Case 205, Hour 5). 181

39 Observed Versus Neutral Paired Concentrations (Case 205, Hour 5) 182

40 Summary Statistics for Neutral Flow Model (Case 205, Hour 5) 183

41 Summary C/Q Statistics for Valley and Centerline Valley Calculations. 185

42 Summary C/Q Statistics for COMPLEX I Calculations 189

43 Summary C/Q Statistics for COMPLEX II Calculations. 190

44 Summary C/Q Statistics for PFM Calculations 201

45 Summary C/Q Statistics for Impingement Model Calculations . 204

46 Summary C/Q Statistics for Neutral Model Calculations . . . 207

47 Summary of Analysis of C/Q Residuals - All Case Hours . . . 210

48 Summary of Analysis of C/Q Residuals for Hours in which $H > H_{crit} + 5$ m 216

LIST OF SYMBOLS AND ABBREVIATIONS

SYMBOL	
β	Horizontal distortion factor
b_{scat}	Scattering coefficient
C	Concentration
C_i	Instantaneous concentration
C_{max}	Maximum hourly averaged concentration
C_o	Observed concentration
C_p	Modeled concentration
d	Distance of source to receptor
$\partial\Theta/\partial z$	Vertical potential temperature gradient
$\partial\rho/\partial z$	Vertical density gradient
D_y, D_z	Ratio of plume spread in complex terrain to plume spread over flat terrain
ϵ	Error or residual
ζ	Ratio of streamline spacing at the source to that at a given downwind distance
f_h	Hill factor
Fr	Froude number
g	Acceleration caused by gravity
h	Hill height
H	Height of the plume centerline above the ground over flat terrain
H_{crit}	Critical dividing streamline height
IX, IY, IZ	Turbulence intensities alongwind, crosswind, and vertical
ℓ_w	Vertical length scale of turbulence
m_g	Geometric mean

N	Brunt-Vaisala frequency
n_o	Height of plume centerline over a terrain feature
η	Fractional height of plume centerline over a terrain feature
θ_d	Angle between stagnation streamline and U
θ_s	Instantaneous angular plume spread
Q	Tracer emission rate
Q_o	Surface heat flux
r, θ, z	CCB polar coordinate system coordinates
s_g	Geometric standard deviation
σ_ϵ	Standard deviation of distribution of model errors or residuals
σ_θ	Standard deviation of horizontal wind direction
σ_w	Standard deviation of vertical velocity fluctuations
σ_y	Standard deviation of crosswind tracer distribution
σ_{yf}, σ_{zf}	Crosswind and vertical standard deviations of tracer concentrations in flat terrain setting
σ_z	Standard deviation of vertical tracer distribution
σ_{ze}	Effective total hourly standard deviation of vertical tracer distribution derived from lidar sections
t_ℓ	Integral time scale
T_o	Average temperature
u_s	Wind speed at source
U, u	Uniform wind speed of flow approaching hill
ψ	Stream function
x	Distance downwind from source
x_1	Set of known model input variables
x_2	Set of unknown variables affecting plume dispersion
z_i	Mixed layer height
z_r	Plume release height

ABBREVIATIONS

CCB	Cinder Cone Butte
DBMS	Data Base Management System

EPA	U.S. Environmental Protection Agency
ERT	Environmental Research & Technology
FMF	Fluid Modeling Facility
GC	Gas chromatograph
MRI	Meteorology Research, Inc.
MST	Mountain Standard Time
NAWC	North American Weather Consultants
NOAA	National Oceanographic and Atmospheric Administration
NRTS	National Reactor Testing Station
ppb	Parts per billion by volume
ppt	Parts per trillion by volume
PG	Pasquill-Gifford
PFM	Potential Flow Model
RTD	Resistance Thermometric Device
TRC	TRC Environmental Consultants, Inc.
WPL	Wave Propagation Laboratory

ACKNOWLEDGMENTS

Many people--far too many, in fact, to acknowledge here individually--contributed their talents and energies to making a success of the Cinder Cone Butte (CCB) experiment. We wish to emphasize the extraordinary efforts of colleagues without whom the experiment would never have flown. First, our colleagues at ERT and WSSI: Mike Onorato and Bob Ledwith, who both worked many long days and nights to configure, program, install, and check out the data base management system; Jim Wallace, who did much of the scientific software development; Jim Wagner, Robert Lehmann, Paul Shultz, and Tom Swafford, who labored literally around the clock to install and check out the tower instrumentation and data communication links; Dan Godden, who captained the computer command center through many long experiments; Bob Hatcher, who devoted many weeks to designing, planning, and supervising the field execution of the CCB experiment; and especially Norm Ricks, whose mechanical wizardry, resourcefulness, and sheer persistence in conquering a myriad of mechanical problems was an inspiration to us all. We also want to thank Tony Curreri and Jack Beebe, who assembled the modeling system so quickly; and especially Don DiCristofaro, Jonathan Pleim, and Bill Adamski, who worked long days and nights to do all the model runs and analyses, accurately and completely, in truly record time.

Next, we can thank but a few of many other colleagues who struggled with us to carry this off:

- Tim Spangler and George Taylor of NAWC, our field general and deputy field general at CCB, who superbly directed the complicated logistics of the field operations. Their fortitude, energy, and unfailing patience throughout many difficulties were crucial to the harmonious operation of the field program.

- Bill Snyder of the EPA Fluid Modeling Facility, the godfather of the "small hill" experiment, whose many helpful suggestions in calling the shots during both phases of the field program were invaluable and whose pyrotechnic and photographic triumphs at CCB are truly memorable!
- Wynn Eberhard and colleagues from the NOAA Wave Propagation Laboratory, who labored with us during Phase II to generate the lidar data base.
- Julian Hunt, for his many useful suggestions for modeling the flow regimes at CCB.

And finally, our special thanks to Frank Schiermeier and George Holzworth, whose unflagging enthusiasm, support, and warm encouragement truly made the difference.

TA,

SECTION 1
INTRODUCTION

1.1 Overview of Complex Terrain Model Development

At a time of growing national pressure to expedite decisions on the regulatory acceptability of new energy-development facilities and other major air pollution sources, it is imperative to improve the air quality models that play critical roles in decision-making--especially when models in wide regulatory use are regarded as insufficient by many of the modelers who use them. In particular, problems of plume transport and dispersion in complex terrain urgently require more reliable models.

The Valley model (Burt 1977), widely used for such problems, is recommended for preliminary screening analyses only. The U.S. Environmental Protection Agency (EPA) does not recognize any current model as generally reliable for refined source analyses in complex terrain.

Recognizing its special responsibility to encourage the development of more reliable complex terrain models for regulatory decision making, EPA's Environmental Sciences Research Laboratory convened an expert technical workshop in July 1979 to address outstanding problems of dispersion model development for sources in complex terrain (Hovind et al. 1979). The workshop's specific objective was to make recommendations to EPA for the design of an extensive research program to support the development of more credible models for regulatory applications.

The general consensus of the workshop supported EPA's suggested focus on stable plume impaction and its multiphased approach to progressive model refinement:

> The Workshop participants agreed in principle that EPA should adopt a two-phased field program approach, starting with a controlled experiment on a small, isolated hill of simple geometric setting, and

then proceeding with a large scale program of increased complexity. It was also recommended that the model development program follow multiple phases. The initial effort should be oriented towards improvements in Gaussian-based models, while the final effort should be aimed towards new model development incorporating complex flow fields in rough terrain with either Gaussian-based or "K theory" based models. Physical modeling programs should be an integral part of the above efforts (Hovind et al. 1979).

Proceeding with the workshop recommendations, EPA undertook the preliminary conceptual design of such a multi-year integrated program in which paramount emphasis was placed upon the "production of a useful model (or models) with demonstrated reliability and prescribed applicability" (Holzworth 1980). During the field measurements and laboratory experiments throughout the program, the observational needs of the modelers were to be foremost in importance. The program was perceived as "an integrated and highly coordinated effort that involves:

(1) model evaluation/improvement/development,
(2) scaled physical modeling in a fluid modeling laboratory,
(3) field measurements/experiments centered on an isolated, simple hill, and
(4) field measurements/experiments centered on a full-scale plant....in terrain with opportunities for plume impaction and other types of plume-terrain interactions" (Holzworth 1980).

In June 1980 a contract was awarded for this program, called the EPA Complex Terrain Model Development.* The stated goal of this study is to develop and validate practical plume models of known reliability and accuracy in order to simulate 1-hour average* ground-level concentrations during stable atmospheric conditions in complex terrain downwind of elevated sources. The models must be reasonably economical and easy to use, and--most importantly--their accuracies, limitations, and restrictions must be well understood.

---

*The prime contractor for the study is Environmental Research and Technology, Inc. (ERT). Its principal subcontractors are Western Scientific Services, Inc. (WSSI), responsible for fixed meteorological data (towers, instrumentation and data communication), and North American Weather Consultants (NAWC), responsible for the experimental field program (tracer and smoke releases, tracer data collection, photography, mobile meteorology, and field logistics). In allied activities, the EPA Fluid Modeling Facility (FMF) has provided laboratory fluid modeling support; the NOAA Wave Propagation Laboratory has supported the field program with a manned lidar system; and TRC, Inc. has provided independent data audits.

In accordance with EPA's preliminary planning to meet this goal, this study comprises field observations and measurements, laboratory fluid modeling, data archiving and analysis, and model development and evaluation. The primary field measurement data gathered by the contractor are supplemented by experiments at the EPA Fluid Modeling Facility (FMF), and the model development and evaluation tasks are guided by complementary work at the EPA Meteorology and Assessment Division.

The first major field program was conducted during the fall of 1980 at Cinder Cone Butte (CCB), a roughly axisymmetric, isolated 100-meter hill located in the broad Snake River Basin near Boise, Idaho. The field program consisted of a preliminary, learning phase followed by a second, intensive measurement phase.

The first phase (September 16-27, 1980) comprised 10 experiments (performed mostly at night) to check out and refine the field program and to gain operational and logistical experience. The objectives of this phase were: (1) to practice techniques for generating and photographing oil-fog plumes and (2) to practice procedures for choosing plume release locations, release heights, and sampler locations on CCB in order to "capture" different flow regimes or different aspects of plume-hill behavior.

---

*Short-term ambient air quality standards and increments for SO_2 and particulates are expressed as maximum 3-hour or 24-hour averages, but the ability to estimate 1-hour averages successfully is a necessary first step toward models for the longer averaging times.

The second phase (October 16-November 12, 1980) comprised 18 multihour experiments conducted in the late evening, night, or early morning hours during primarily stable flow conditions. The experimental program concentrated on measurements of ground-level tracer gas (SF_6 and CF_3Br) concentrations on the butte as well as lidar sections through the plume and an intensive set of fixed and mobile meteorological measurements and photographic documentation. Most experiments lasted eight hours with tracer gas releases during at least five or six hours.

When the project was begun in June 1980, the experimental approach and methods for such a small hill study appeared promising but were untested. Looking back, we may conclude that the CCB experiment was largely successful and fulfilled its basic goal: creating an extensive, well-documented archive of reliable meteorological, plume trajectory, and tracer concentration data to illuminate the physics of plume transport and diffusion in the presence of such a hill under stable nocturnal flow conditions. This unique data archive will provide--more effectively than any previous data base--an empirical foundation for developing models of stable plume impingement on three-dimensional, nearly axisymmetric hills.

The data base compiled at CCB includes the following important components:

- Source information: emission rates, locations, and heights of SF_6, CF_3Br, and oil-fog releases.
- Meteorological information: descriptions of the undisturbed mesoscale valley flow in the vicinity of CCB as well as information on flow and dispersion on and over CCB itself.
- Hill surface tracer gas concentrations: data from more than 14,000 individual bag samples collected over the 18 days of experiments from as many as 80 sampler locations in a given experiment.
- Lidar data: sections across the plume characterizing the plume trajectory and plume spread upwind of CCB.
- Photographic data: still photographs taken from fixed locations on and around CCB, aerial photographs taken from an aircraft flying overhead, and (occasional) 16 mm movies and videotapes.

The problems that developed during the field program were caused mainly by insufficient lead time to procure and successfully install all needed equipment, data communication outages or instrument failures in the real-time monitoring network, and failures in gas sampler collection or processing. Immediately after the field program ended, a substantial effort was undertaken to edit, validate, and assess the reliability of all meteorological and tracer gas data. Although more remains to be done, the result to date is an excellent data base for model development.

The major objectives of the model analyses are to develop and evaluate the performance of new models against the observational data at CCB and to compare their performance to the following current complex terrain dispersion models:

- the EPA Valley model worst-case screening algorithm, widely used in regulatory practice to screen elevated sources in complex terrain;
- COMPLEX I and COMPLEX II, two new proposed complex terrain screening models issued by EPA for public testing and evaluation; and
- PFM, a potential flow model for turbulent dispersion of plumes in the presence of simple terrain features.

For these comparisons, 45 case study hours were selected from the 18 field experiment days. (The PFM model comparisons were made with about half of these case study hours.)

We have begun to formulate and test new modeling approaches suggested by the experimental evidence studied to date. One new model (called the Impingement model) is used to simulate ground-level concentrations in strongly stable flows in which plumes go horizontally around the side of CCB; another new model (called the Neutral model) simulates slightly stable or neutral flows in which plumes rise over CCB. It must be emphasized, though, that these new models--which thus far represent only a modest level of effort--are tentative first steps toward the goal of practical, reliable complex terrain models. They are not the desired end results and are in no way identified for routine application at this time.

All models were evaluated by comparing 1-hour average observed concentrations with 1-hour average predicted concentrations. The descriptive statistical measures used were chosen according to the recommendations of a recent American Meteorological Society workshop (Fox 1981). These were supplemented with special statistical measures to describe the mean and peak concentration ratios that were quite useful for summarizing comparative model performance.

The early results are encouraging: the two provisional models appear to simulate maximum concentrations and spatial concentration patterns more realistically than the screening models. Much of the data base remains to be analyzed, however. In the future, better model results may be achieved--when, for example, all of the lidar data collected at CCB have been analyzed, or the existing photographic and meteorological data archives have been more fully used, in conjunction with fluid modeling experiments, to extend the data base for developing and validating complex terrain plume models.

1.2 Basic Concepts of Plume Dispersion in Stable Flows

Throughout this report, two basic concepts are used to characterize the flow around a hill--the Froude number and the dividing streamline height. Important dynamic features of flow around an isolated hill are characterized by the hill Froude number (Fr), defined by

$$Fr = U/Nh \tag{1}$$

where U is the uniform wind speed of the flow approaching the hill, N is the Brunt-Vaisala frequency, and h is the height of the hill. The stability of the flow is described in terms of the Brunt-Vaisala frequency, N, which can be written as

$$N = \left[\frac{g}{T_o} \frac{\partial \theta}{\partial z} \right]^{1/2} \tag{2}$$

where $\partial \theta / \partial z$ is the stable potential temperature gradient (assumed to be uniform over the height of the hill), g is the acceleration caused by gravity, and T_o is the average temperature.

In physical terms, the hill Froude number is the ratio of the inertia of the flow to the buoyancy force that suppresses motion in the vertical. Another physical interpretation of Fr can be obtained by recasting Equation 1 in terms of the density gradient and squaring both sides:

$$Fr^2 = \frac{\rho U^2}{gh^2(-\partial \rho / \partial z)} \tag{3}$$

Here, Fr^2 is the ratio of the kinetic energy of the fluid to the potential energy gained by the fluid as it rises through the stable density gradient to the top of the hill.

A hill Froude number less than unity implies that a fluid parcel at the bottom of the hill will not have sufficient kinetic energy to rise to the top of the hill and thus will be forced to go around it. A hill Froude number of unity or greater implies that the fluid parcel can rise to the top. These concepts can be refined by introducing the dividing streamline height, H_{crit}, defined by the following integral formula (Snyder 1980a):

$$\frac{1}{2} \rho U^2 = g \int_{H_{crit}}^{h} (h-z) \left(\frac{-\partial \rho}{\partial z} \right) dz \tag{4}$$

where U is evaluated at $z = H_{crit}$ and $(\partial \rho / \partial z)$ is the local density gradient. The left-hand side of Equation 4 is the kinetic energy of a fluid parcel at this critical height, and the right-hand side is the potential energy gained by the fluid parcel rising through the height $h-H_{crit}$. The equality in Equation 4 implies that H_{crit}

is the height at which the fluid has just enough kinetic energy to ascend the hill. If the wind speed increases with height, fluid parcels originating below H_{crit} are forced to either stagnate on the hill or flow horizontally around it.

For a constant wind and density gradient, Equation 4 reduces to

$$H_{crit} = h(1-Fr) \tag{5}$$

Note that H_{crit} embodies the physics of the hill Froude number, but in a more flexible manner: it also accounts for nonuniform temperature and velocity profiles. For $Fr \rightarrow 0$, $H_{crit} \rightarrow h$, suggesting that most of the flow goes around the hill. When $Fr \rightarrow 1$, $H_{crit} \rightarrow 0$, implying that most of the fluid goes over the hill. Under these conditions, the flow pattern away from the surface on the windward side of the hill can be modeled to a first approximation as inviscid potential flow (Hunt et al. 1979).

When Fr is close to zero, the flow around a three-dimensional obstacle such as CCB is essentially horizontal (Drazin 1961). Plumes embedded in such a flow field will not be significantly displaced upward as they disperse around the hill. Hunt et al. (1979) show that, given certain limiting assumptions, this problem of plume impingement can be reduced to that of two-dimensional diffusion of a line source around a cylinder. The axis of the cylinder is parallel to the z-axis, and the cylinder has the same cross section as the hill at the height of release z_r. Figure 1 shows plume behavior under such conditions. When the hill Froude number is greater than unity, the flow (and hence a plume embedded in the flow) will go over the top of the hill.

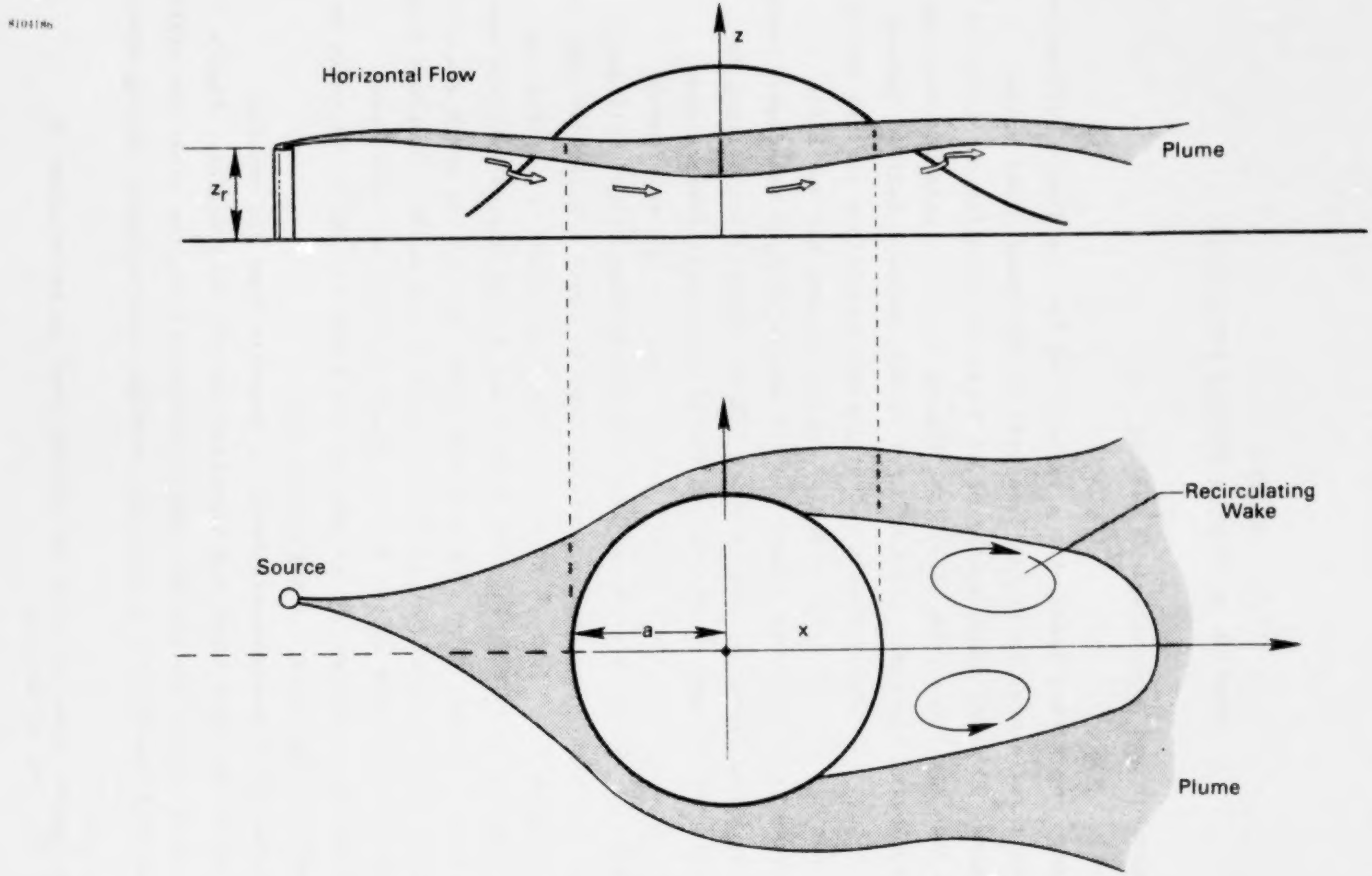
8104186
z
Horizontal Flow
z_r
Plume
Source
a
x
Recirculating Wake
Plume

Figure 1. Schematic of flow around a three-dimensional obstacle at very low Froude number. Adapted from Hunt et al. (1979)

Note: The problem of dispersion is equivalent to dispersion from a line source around the cylinder at the height of release Z_r.

SECTION 2

OVERVIEW OF COMPLEX TERRAIN FIELD STUDY

2.1 Geographic and Meteorological Setting

Cinder Cone Butte, Idaho, the site selected for the flow visualization and tracer experiments, is an isolated hill in the Snake River Basin, located about 30 miles south-southeast of Boise and 15 miles northwest of Mountain Home Air Force Base (AFB) (see Figure 2). This site was selected for the following reasons: (1) the butte is the dominant terrain feature for many miles; (2) fairly simple meteorological conditions prevail during the fall months; (3) the area is easily accessible and has available electric power and telephone lines; (4) the Bureau of Land Management (which manages the Bruno Resource Area in which CCB is located) was willing to grant permission for use of the butte; and (5) the local farmers were willing to lend or rent their facilities and land for the experiments.

Cinder Cone Butte is a two-peaked, roughly axisymmetrical hill about 100 meters (m) high. Its nearly circular base is about 1 kilometer (km) in diameter (Figure 3). Figure 4 presents side views of the butte from the north, northeast, and east; Figures 5 and 6 are aerial views* from the south and southeast. Typical side slopes of the upper part of the butte are about 25°. A road paved with cinder provides access to the peaks. Numerous roads around the hill provided access for the sampling crews and equipment; several roads were constructed as part of the project. The butte could be easily reached from Boise via Interstate 80.

Meteorological measurements taken at Mountain Home AFB provide information on the wind speed and direction for the fall months. Figure 7 shows two wind roses--one for all stability conditions, the other for stable conditions only--derived from September weather observations. During stable

---

*The two figures show elevated and ground-level smoke released on October 24, 1980 at sunrise.

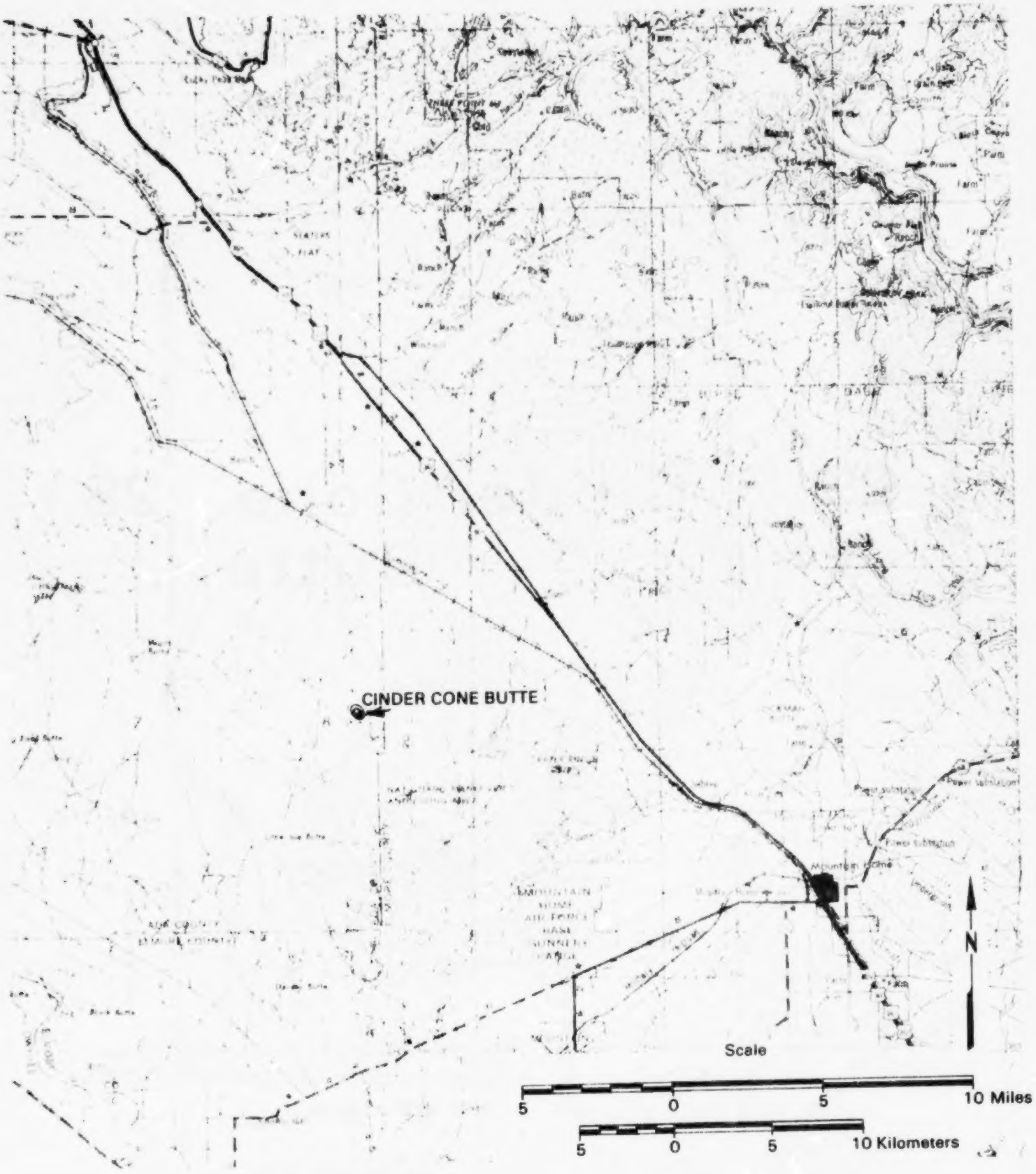
CINDER CONE BUTTE
Mountain Home
MOUNTAIN HOME AIR FORCE BASE GUNNERY RANGE
N
Scale
5
0
5
10 Miles
5
0
5
10 Kilometers

Reproduced from best available copy.

Figure 2. Topographic map of Cinder Cone Butte region.

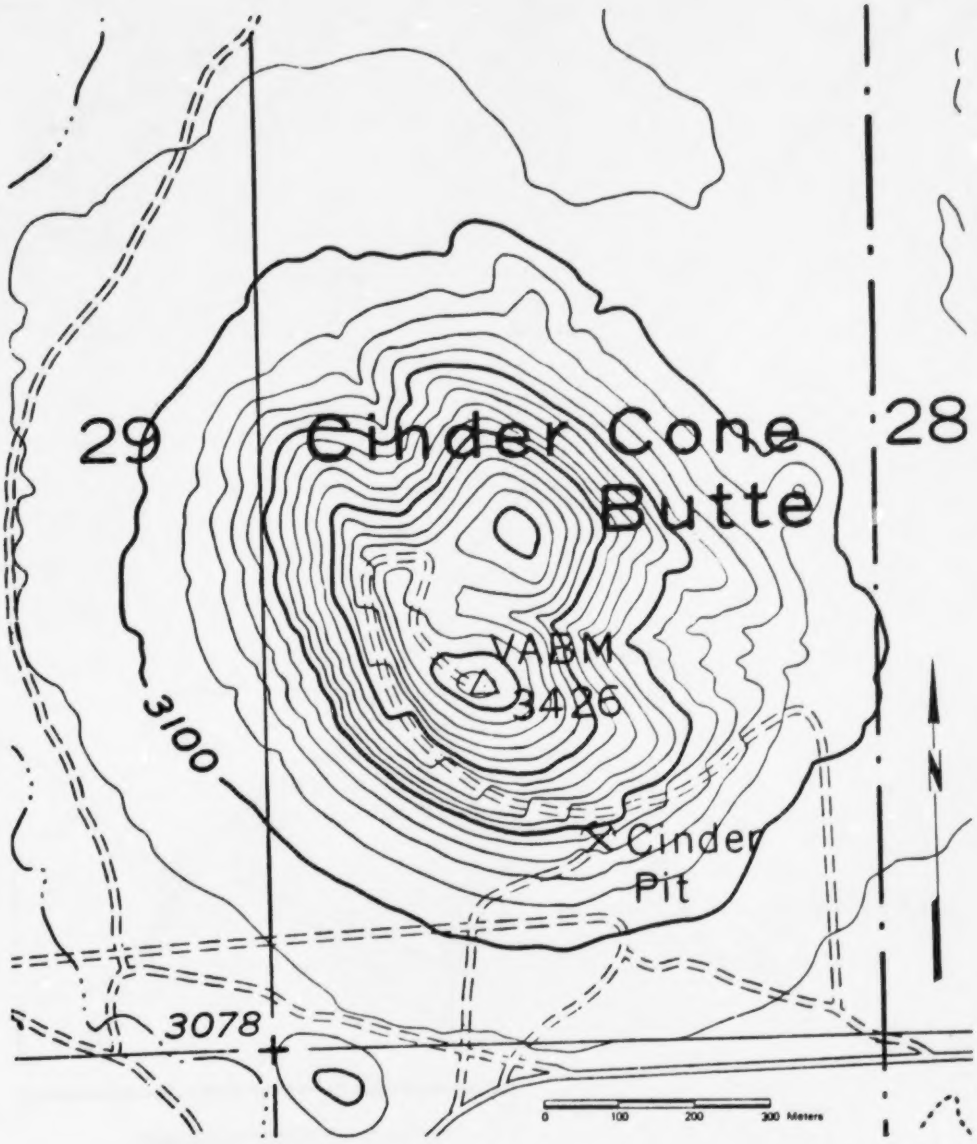
29
Cinder Cone Butte
28
VABM 3426
3100
Cinder Pit
N
3078
0 100 200 300 Meters

Elevation in feet above MSL.
Contour intervals are 20 feet.

Figure 3. Topography of Cinder Cone Butte.

Cinder Cone Butte looking south

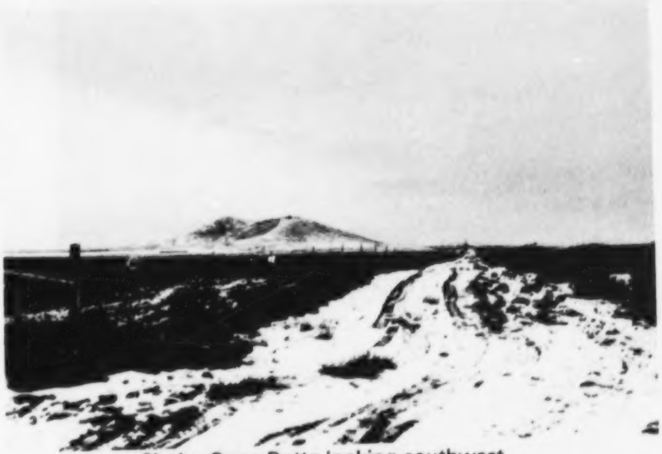

Cinder Cone Butte looking southwest

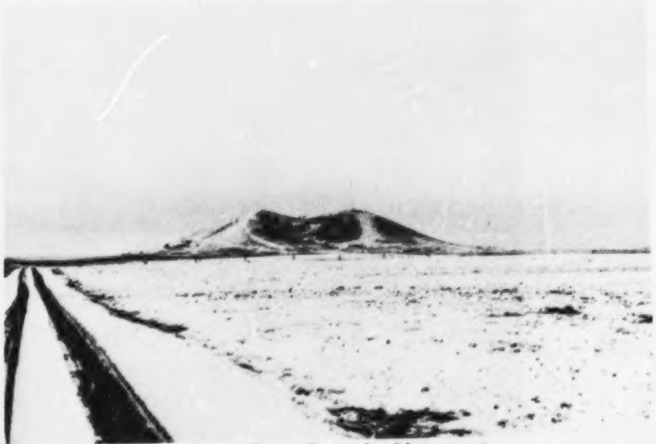

Cinder Cone Butte looking west

Figure 4. Side views of Cinder Cone Butte.

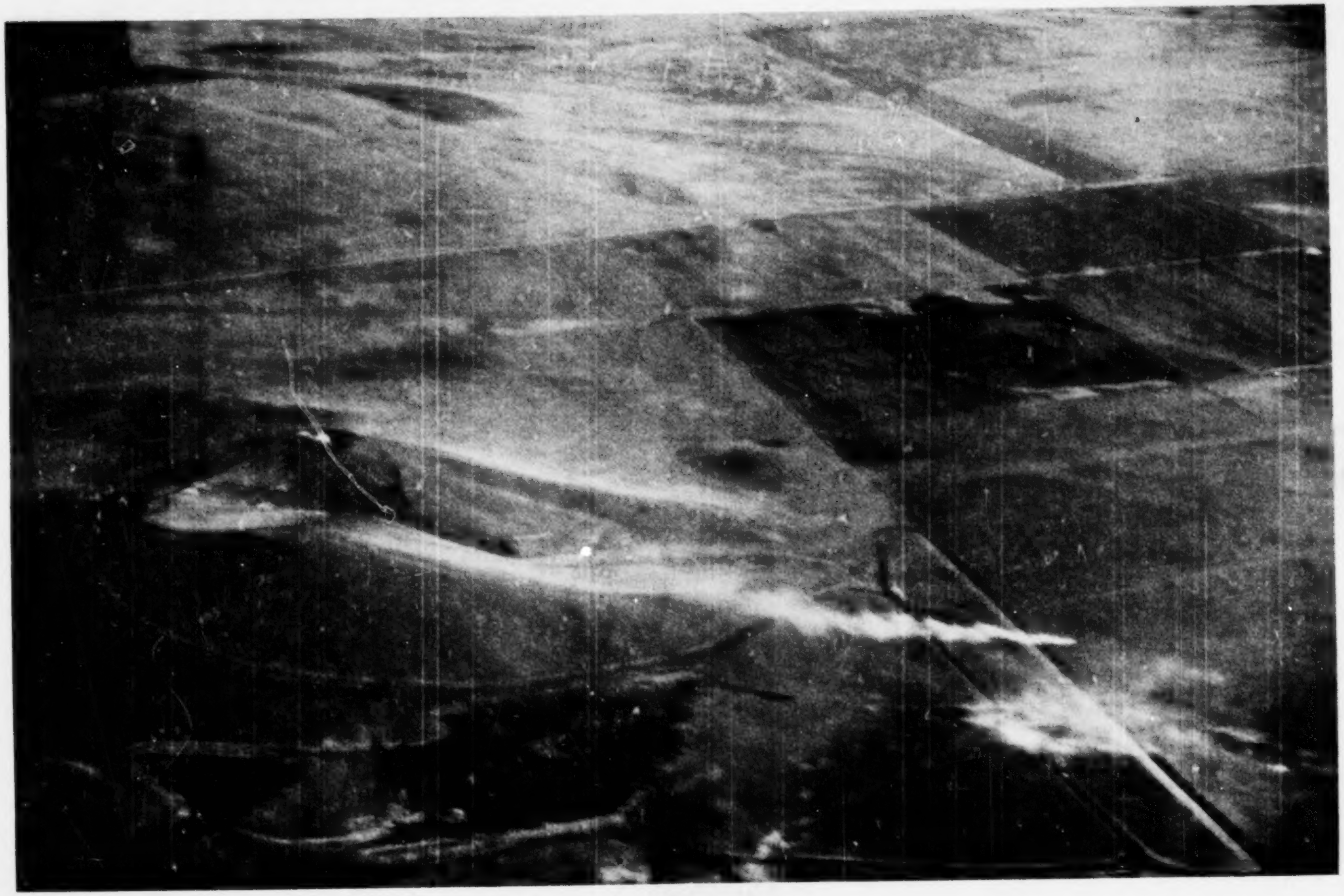

Figure 5. Aerial view of Cinder Cone Butte from south.

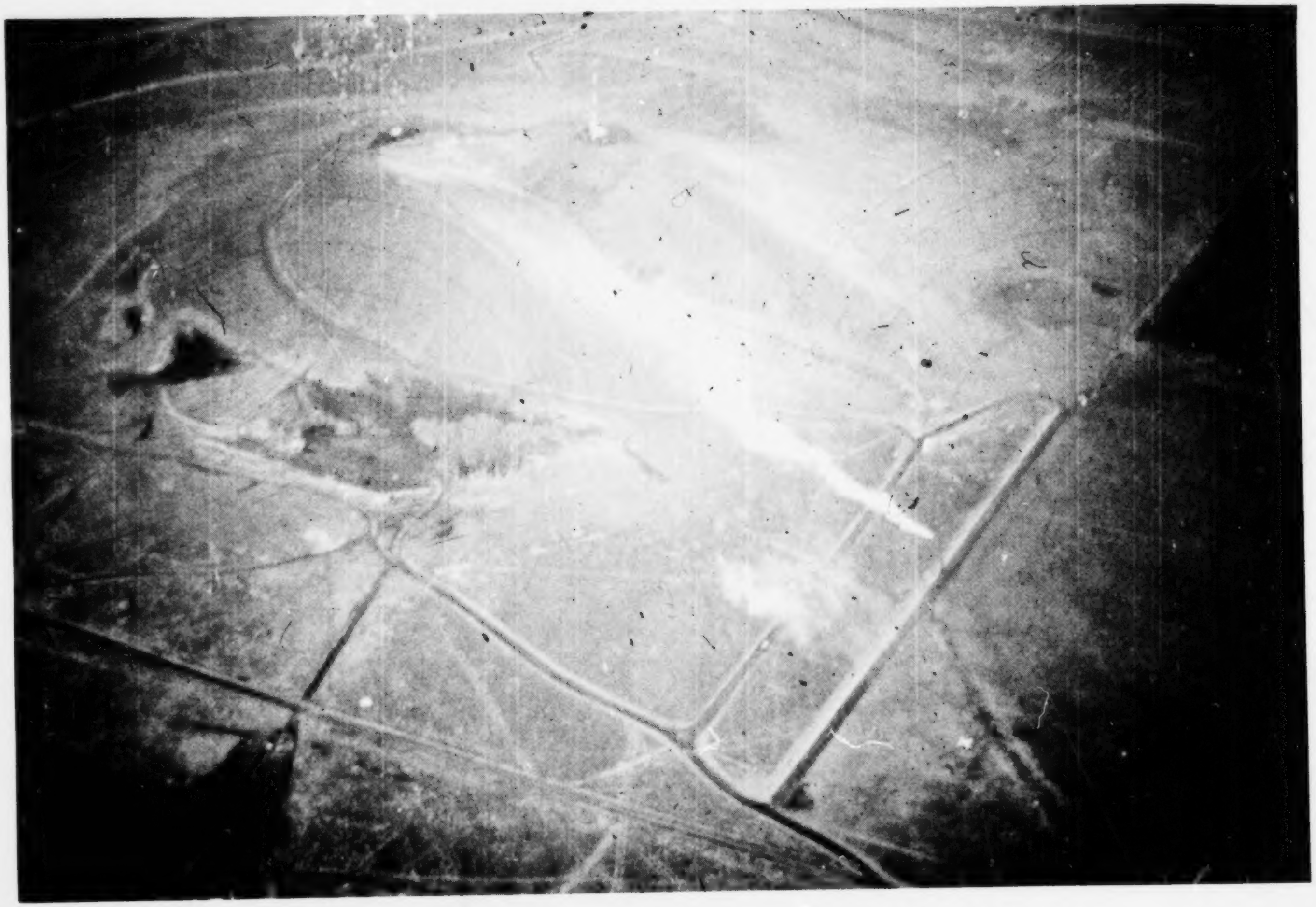

Figure 6. Aerial view of Cinder Cone Butte from southeast.

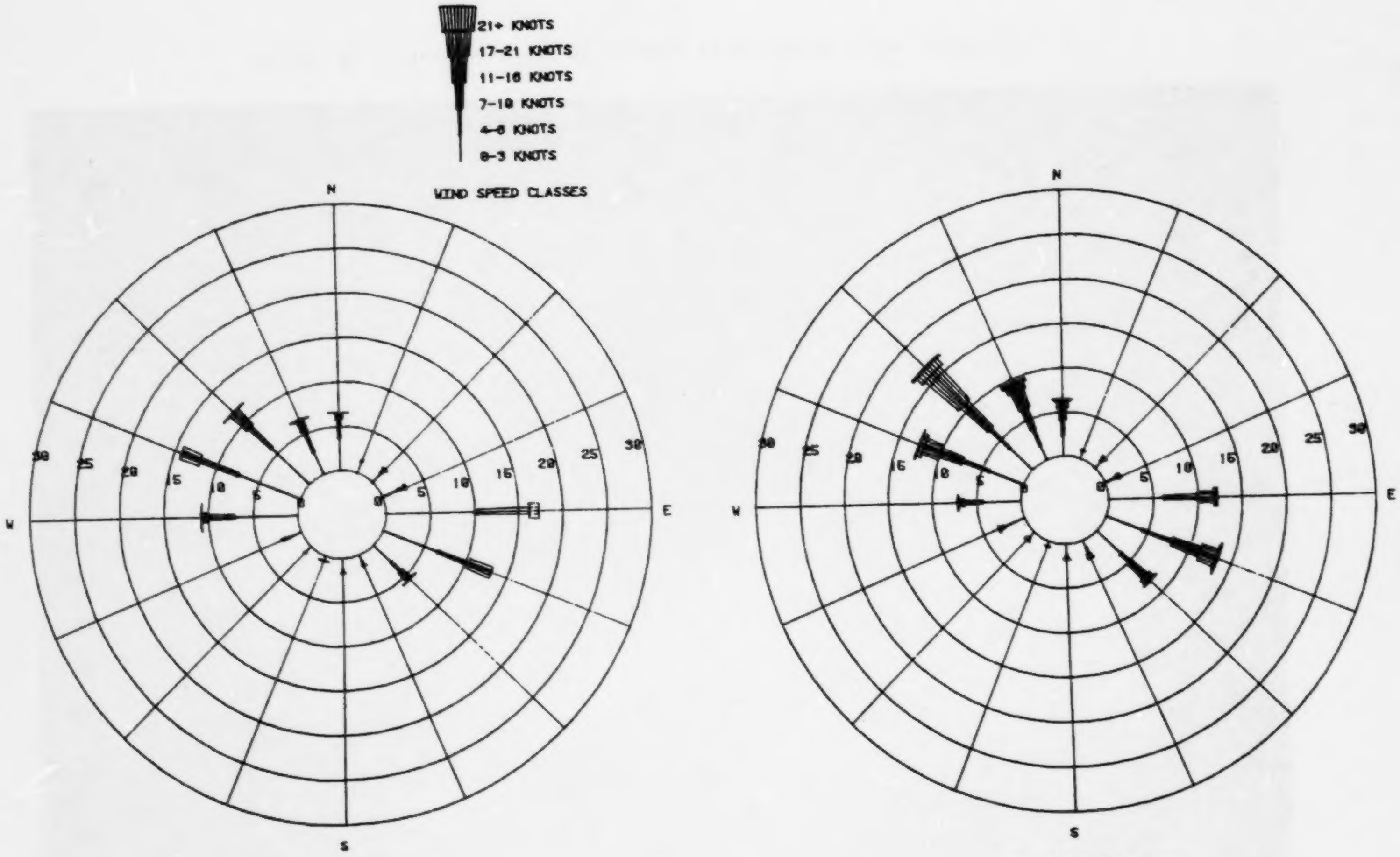

Stable Conditions

All Stabilities

Figure 7. Distribution of wind speed and direction for September 1965-1969 derived from weather observations at Mountain Home AFB.

conditions, which generally occur at night, the most frequent wind directions are east, east-southeast, and west-northwest. Table 1 lists the prevailing wind direction and frequency for every odd hour of the day as derived from Mountain Home AFB data for October. The data illustrate the prevailing up-valley flow (approximately 300°) during the day and down-valley flow (approximately 110°) after midnight. Although the basin circulation appears to occur regularly, it is quite variable about the most frequent wind directions, as may be noted from the wind rose. Evidently, the up-valley flow, most frequently from the west-northwest, can also come from the northwest or west (even occasionally from the north). The down-valley flow can come east-southeast and southeast as well as the most frequent easterly direction shown in the wind rose for stable conditions.

Additional climatological data are available from the National Reactor Testing Station (NRTS) at Idaho Falls, located about 300 km away in the Snake River Basin (Yanskey et al. 1966). This information was assumed to be generally representative of CCB as both sites are in the basin, although the valley axis is northeast-southwest at NRTS and northwest-southeast at CCB. The wind and temperature profiles were also assumed to be similar enough for use in designing the experiments. Vertical temperature profile data suggest the occurrence of inversion conditions more than half the time during the fall, and strong inversions (>3.7°C/100 m) occur approximately 20% of the time (Yanskey et al. 1966). Typical positive temperature gradients and light wind speeds suggest that Froude numbers are frequently less than 1.0 and occasionally as low as 0.2. For example, wind speeds at 75 m are less than 2 meters per second (m/sec) about 20% of the time (Yanskey et al. 1966). If light winds are well correlated with inversion conditions, $Fr < 0.5$ should occur about 20% of the time.

2.2 Fluid Modeling of Expected Flow Regimes

During the summer of 1980, three series of towing tank experiments at the EPA Fluid Modeling Facility (FMF) were conducted by William Snyder to provide input to the design of the CCB field experiment. The first series of experiments was made to assess the perturbations to the mesoscale basin circulation caused by the presence of CCB. The question specifically

TABLE 1. PREVAILING WIND DIRECTION AND FREQUENCY AT MOUNTAIN HOME AFB (OCTOBER 1964-1970)

Hour (MST)	Wind Direction (degrees)	Average Speed (knots)	Frequency (%)
0100	110	5.4	6.5
0300	100	4.0	10.6
0500	100	4.9	14.3
0700	120	7.9	12.0
0900	110	7.8	16.6
1100	120	10.7	13.4
1300	140	7.5	11.1
1500	320	12.1	10.6
1700	310	10.2	14.7
1900	300	4.8	10.6
2100	290, 310, 320	6.0	6.0
2300	300	6.8	6.0

Note: Direction and frequency determined from all weather conditions.

addressed was where to site a 150 m tower relative to CCB so that, given the range of prevailing southeasterly or northwesterly wind directions expected during strongly stable stratification, the flow fields at the proposed tower site would not be appreciably perturbed by the hill.

For this series of tows in the FMF stratified towing tank, a model of CCB was constructed at a scale of 1:1536 (with contours derived from enlargements of USGS maps) and mounted so as to be easily rotated to change the wind direction (Snyder 1980b). Twenty-six tows were made for varied Froude numbers and wind directions. Rakes of tubes emitted a dyed solution for flow visualization. Vertical rakes were used to obtain centerplane streamline patterns and semiquantitative information on vertical velocity profiles (with pulsed releases). Horizontal rakes were used to obtain horizontal streamline patterns at different elevations and information on the horizontal velocity profiles (again, with pulsed releases). From the limited number of wind directions (110°, 120°, 300°) and Froude numbers investigated (Fr = 0.2, 0.4, 0.6) it was estimated that at the proposed 150 m tower site (2 km, 357° relative to hill center), the perturbations in the flow field were negligible and that the streamline patterns appeared independent of wind direction except quite close to the hill surface.

A second series of eleven tow tank experiments was made in the FMF stratified towing tank to (1) guide the design of the smoke and tracer experiments for the CCB field program, (2) preselect possible tracer gas sampler and camera locations, and (3) choose different sampling strategies to account for the variation in wind flows (Bass 1980). The experiments were run using a second model of CCB constructed to a scale of 1:640 and contoured at 20-foot (3/8-inch) intervals. As before, rakes of tubes emitted a dyed solution for flow visualization.

Each tow was filmed from the side with the camera moving with the tow carriage, and from directly below the tow path with the camera held fixed at two or three stationary points pointed upward at the (inverted) model hill. The movie films were viewed with an analyst projector, and the plume patterns were sketched independently by two analysts who used a plan map of CCB identical to the model. The two sketches were then reconciled and smoothed to define the (apparent) envelope of each plume path.

Figures 8 and 9 illustrate the composite estimates of the plume paths and dispersion for two of the towing tank simulations. Figure 8 illustrates the simulation for a wind direction of 110°, Fr = 0.4, and releases equal to 0.25, 0.5, 0.75, and 1.25 of the hill height. Similarly, Figure 9 illustrates flows from 300°, Fr = 0.4, and releases equal to 0.125, 0.25, 0.375, 0.5, 0.75, and 1.25 of the hill height. The results corroborate the suggestions of Hunt and Snyder (1980) that air parcels below H_{crit}, the dividing streamline height, tend to impinge upon and pass around the sides of the hill and that air parcels above the dividing streamline height tend to go over the hill. Note in Figure 8 the uphill-downhill extent of the lowest plume as it impinges in the east "draw" and is swept around the side of CCB; note also that the plumes emitted at one-half and three-quarters hill height ($h > H_{crit}$) are carried over the hill crest with negligible spread before growing on the lee side of the hill.

The qualitative results of the second series of towing tank experiments are summarized as follows:

- Locally, CCB perturbs the general mesoscale wind flow in the Snake River Basin.
- A parcel of air below the dividing streamline height may impinge on the upwind side of the butte if directed along a stagnation streamline and may tend to flow around the butte.
- A plume released just above H_{crit} may produce a maximum ground-level concentration on the upwind side as it passes over the top.
- A plume released substantially above H_{crit} may occasionally produce a maximum ground-level concentration on the lee side of the hill.
- A parcel of air traveling in a direction off the stagnation streamline will tend to pass around CCB without significant impact.

The final series of tow tank experiments conducted to guide the field program design was undertaken to establish more adequately the validity of the general integral expression for the height of the dividing streamline in stably stratified flow (see Section 1.2). Twelve tows of the 1:640 scale

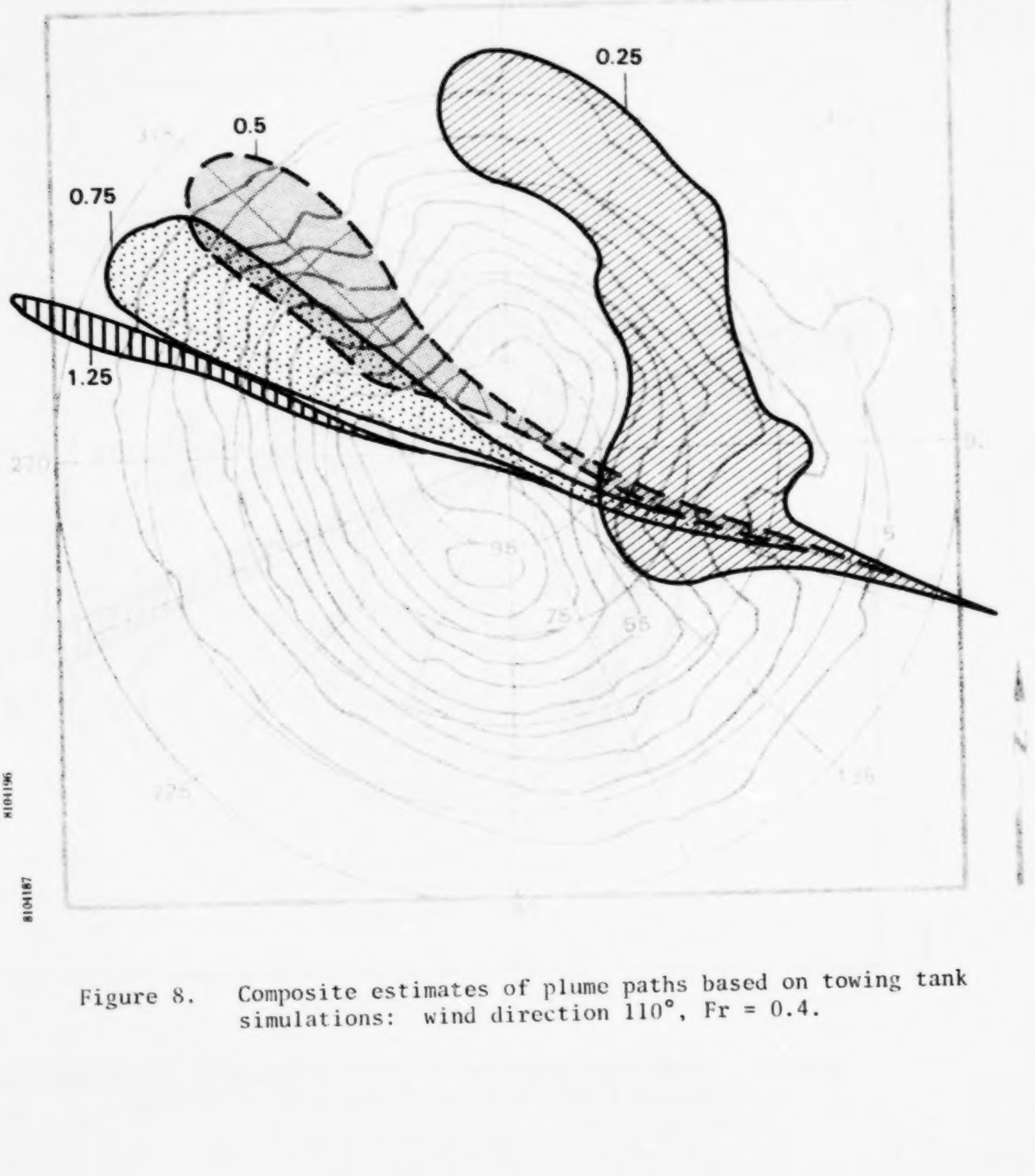
0.25
0.5
0.75
1.25
315
270
95
75
55
5
225
135
N
8104196
8104187

Figure 8. Composite estimates of plume paths based on towing tank simulations: wind direction 110°, Fr = 0.4.

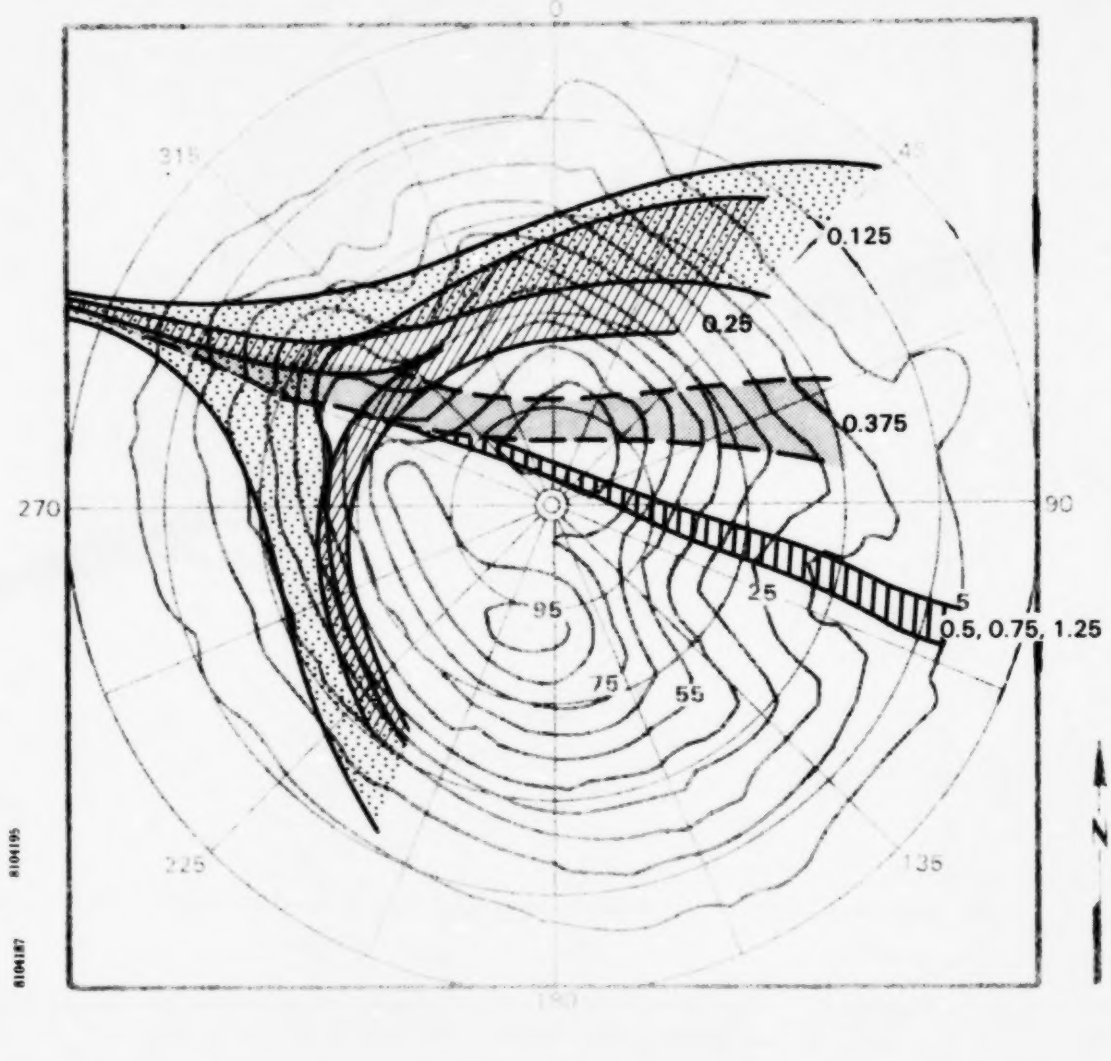
0
315
45
0.125
0.25
0.375
270
90
95
25
5
0.5, 0.75, 1.25
75
55
225
135
180
N
8104195
8104187

Figure 9. Composite estimates of plume paths based on towing tank simulations: wind direction 300°, Fr = 0.4.

model were made under different combinations of density profiles, towing speeds, and source heights (Snyder 1980a), with effective Brunt-Vaisala frequencies (0.86, 0.089 rad sec^{-1}) very close to those expected at CCB under stable nighttime conditions. A vertical rake of three tubes emitted neutrally buoyant colored dyes. For each set of three source heights, the general formula (see Equation 4) was integrated numerically using the measured density profile and towing speed, and the resulting plume path predictions were compared to the observed plume trajectories.

Overall, the agreement was excellent. The validity of the general integral formula (Equation 4) for predicting the height of the dividing streamline as a function of wind speed was demonstrated for a wide range of stable density profiles. It was therefore recommended that the integral formula be used as an operational, real-time decision-making tool during the field study.

2.3 Experimental Design of Field Study

The basic program goal required the measurement of data that, together with information obtained from fluid modeling experiments and recent theoretical work, will be used to develop improved mathematical simulations of plume dispersion and impingement from elevated sources in complex terrain. The basic experimental design involved: (1) meteorological measurements, (2) the emission of tracer gases and a visible plume, (3) quantitative measurements of tracer gas concentrations, and (4) photographic documentation of plume behavior. The variability of the wind flow about the most frequent directions of both up-valley and down-valley flows required that smoke and tracer sources be highly mobile. The regularity of the basin circulation required sampler placement to capture the prevailing west-northwest and east-southeast winds.

The expected perturbations of the air flow by the hill implied the following requirements:

- deployment of samplers to capture plume impacts near the stagnation streamline, as plumes go around the side or up and over CCB;

- the need for real-time meteorological measurements and feedback in order to locate the source azimuth and choose a source height (e.g., release above or below H_{crit});
- meteorological measurements of the unperturbed flow as well as measurements to characterize dispersion on the hill;
- visible elevated and ground-level plumes to capture qualitatively the different classes of plume-terrain interaction; and
- sufficient vertical resolution of meteorological measurements to calculate H_{crit} and Fr.

All of these features were included in the experimental design.

The first field study of the EPA program was conducted at CCB from September through November 1980. The field study encompassed two distinct phases. Phase I ran from September 16 to September 27, 1980 and included a total of 10 experiments. The purpose of this preliminary phase was to gain experience working at the CCB site and photograph various smoke releases for flow visualization. Phase II, the major experimental phase, ran from October 16 to November 12, 1980. Eighteen experiments were run with SF_6 as a tracer, in addition to the smoke plume releases. In nine of these experiments, CF_3Br was simultaneously used as a tracer gas.

2.3.1 Fixed Meteorological Network

ERT assembled at CCB a meteorological monitoring network to characterize the unobstructed approach flow and to analyze the wind field as it encountered the hill. A series of meteorological towers (a 150 m tower located approximately 2 km north of CCB, and a 30 m tower and four 10 m towers located on the hill) documented the local meteorology. The locations of the towers (A, B, C, D, E, and F)* are shown in Figure 10, and the direct measurements and derived parameters at each tower level are given in Table 2.

---

*One other F460 cup-and-vane wind set was on a 10 m mast adjacent to the office trailers at Simco Road (ERT Command Post), but its output was recorded only on strip charts (see Figure 10).

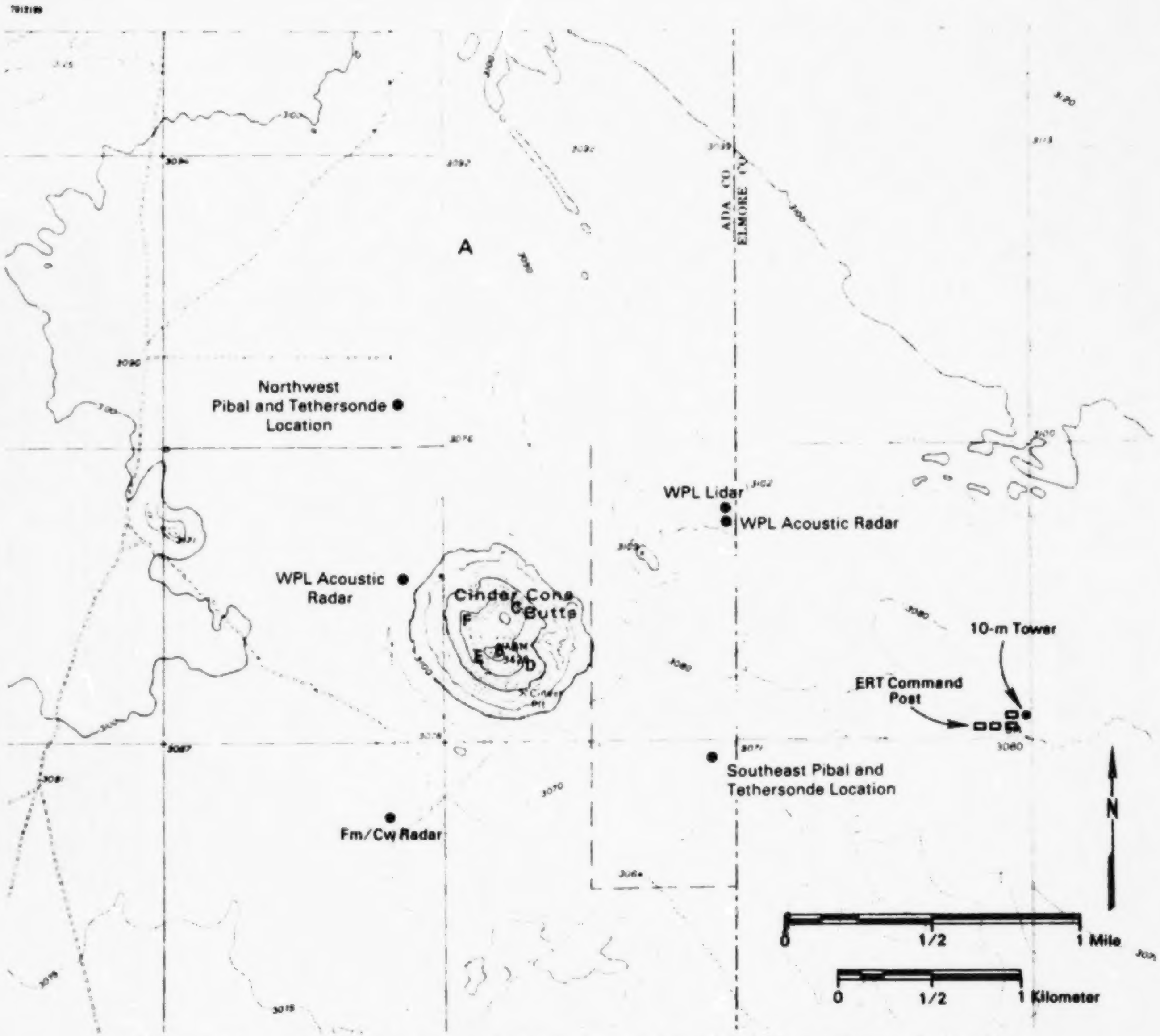
A
ADA CO
ELMORE CO
Northwest Pibal and Tethersonde Location
WPL Lidar
WPL Acoustic Radar
WPL Acoustic Radar
Cinder Cone Butte
B
C
D
E
F
10-m Tower
ERT Command Post
Southeast Pibal and Tethersonde Location
Fm/Cw Radar
N
0
1/2
1 Mile
0
1/2
1 Kilometer

Figure 10. Field experiment layout. A is the 150 m tower; B is the 30 m tower; C, D, E, and F are 10 m towers.

TABLE 2. TOWER INSTRUMENTATION AND MEASURES

Site	Instruments*	Direct Measures**	Derived Measures⁺
Tower A			
Level 0 (1 m)	Pyranometer	Insolation	
	Net radiometer	Net radiation	
Level 1 (2 m)	Triaxial props	U, V, W, IX, IY, IZ	WS, WD
	Cup & vane	UX, VX	SP, DR
	RTD	T	
Level 2 (10 m)	Triaxial props	U, V, W, IX, IY, IZ	WS, WD
	Cup & vane	UX, VX, U, σ_θ,	SP, DR
	RTD	ΔT	T
	Fast bead thermistor	T, σ_T	
Level 3 (20 m)	RTD	T	
Level 4 (40 m)	Triaxial props	U, V, W, IX, IY, IZ	WS, WD
	RTD	ΔT	T
Level 5 (60 m)	RTD	T	
Level 6 (80 m)	Triaxial props	U, V, W, IX, IY, IZ	WS, WD
	RTD	ΔT	T
Level 7 (100 m)	RTD	T	
Level 8 (120 m)	Triaxial props	U, V, W, IX, IY, IZ	WS, WD
	Cup & vane	UX, VX	SP, DR
	RTD	ΔT	T
	Fast bead thermistor	T, σ_T	
Tower B			
2 m	Triaxial props	U, V, W, IX, IY, IZ	WS, WD
	RTD	T	
10 m	Triaxial props	U, V, W, IX, IY, IZ	WS, WD
	Cup & vane	UX, VX	SP, DR
	RTD	ΔT	T
30 m	Triaxial props	U, V, W, IX, IY, IZ	WS, WD
	Cup & vane	UX, VX	SP, DR
	RTD	ΔT	T
Towers C, D, E, F			
2 m	Triaxial props	U, V, W, IX, IY, IZ	WS, WD
	RTD	T	
10 m	Triaxial props	U, V, W, IX, IY, IZ	WS, WD
	Cup & vane	UX, VX	SP, DR
	RTD	ΔT	T

Reproduced from
best available copy.

---

*All temperature sensors were mounted in aspirated radiation shields; an RTD is a Resistance Thermometric Device.

**"Direct" measures are those calculated by the data station microprocessors from the outputs of the instrument translators. The turbulence data (IX, IY, IZ, σ_θ, σ_T) were calculated for both 5-min and 1-hr data periods. All direct measures were updated once per minute by the data stations. UX and VX are the westerly and southerly components of the wind calculated from the cup and vane outputs at the 4 Hz sampling frequency.

⁺"Derived" measures are those calculated by the data collector computer from the 5-min averages provided by the data stations. These derived measures comprise 5-min average values of the measures indicated as well as 1-hr averages of all direct and derived measures except the turbulence data, 1-hr averages of which were calculated by the data stations.

The 150 m tower was instrumented at eight levels to characterize the approach flow for the experiments. This tower had an unobstructed view of the wind for almost all wind directions. The 30 m tower, mounted on the southern peak of CCB, was instrumented at 2, 10, and 30 m. The four 10 m towers were located in the northeast, southeast, southwest, and northwest quadrants of the hill, each tower at a height approximately 65 m above the plain.

2.3.2 Photography Program

A primary objective of the CCB experiment was to document photographically the behavior of the plume as it encountered the hill. This objective was achieved only in part, because most of the experiments were conducted during hours of darkness, and lighting of the smoke plume was a problem. During both Phase I and Phase II, several photographic media were used, including black-and-white as well as color still photographs (35 mm), motion-picture film (16 mm), and videotape.

Five 35 mm cameras were operated simultaneously during the field experiments. Locations were chosen on the basis of the climatological data, the towing tank results, and previous experience with the aid of a professional photographer. Cameras were operated manually at the desired exposure. Exposure times at night were generally 3-5 minutes. Each camera operator was in continuous contact with the lead photographer to synchronize shots. Figure 11 shows the preselected camera locations.

When lighting allowed, a 16 mm motion picture camera was used in a time-lapse mode. This camera, operated by a professional photographer, was generally located at the top of CCB looking toward the plume. The videotape camera was a valuable management tool, especially during debriefing and planning sessions, for near-real-time review of visual experimental evidence.

Lighting of the plume proved to be extremely difficult. Under clear conditions and a full moon, no lighting was required. For other conditions, a carbon arc lamp was invaluable. The arc lamp was generally placed approximately 2 miles away so that the light beam and the plume were nearly perpendicular. The lamp was put in an automatic sweep mode that passed along the plume at 30-second intervals.

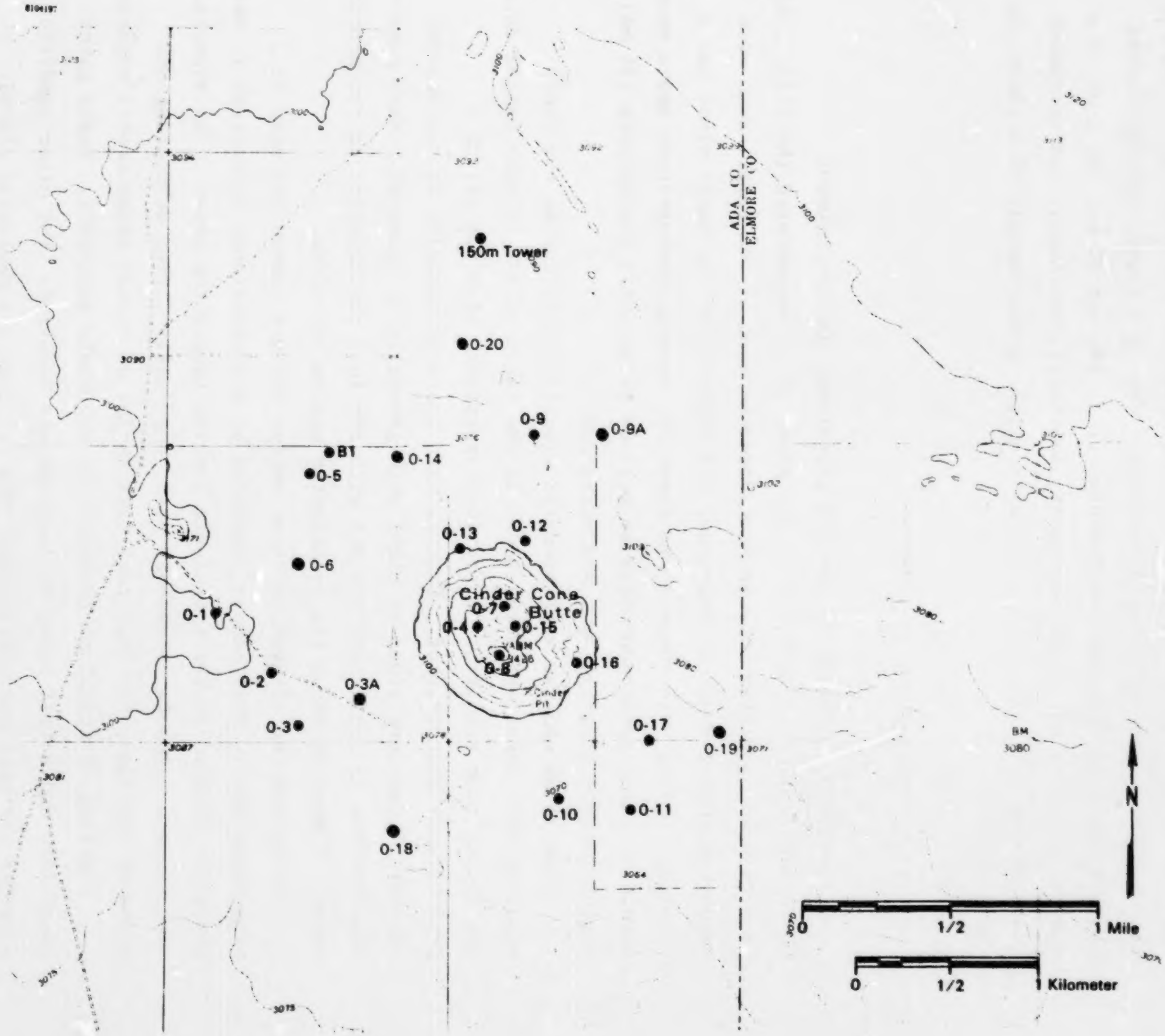
150m Tower
0-20
0-9
0-9A
B1
0-14
0-5
0-13
0-12
0-6
Cinder Cone Butte
0-7
0-4
0-15
0-8
0-16
Cinder Pit
0-1
0-2
0-3A
0-3
0-17
0-19
0-10
0-11
0-18
ADA CO
ELMORE CO
BM 3080
N
0
1/2
1 Mile
0
1/2
1 Kilometer

Figure 11. Preselected camera locations.

Aerial photographs were taken with a still 35 mm camera from a single-engine airplane flying as slowly as safety allowed. ASA 400 black-and-white film was normally used at night, and ASA 64 color film was used when sufficient sunlight was available. The plane flew at a range of heights between 250 and 1,500 feet above the local basin level. Light-gathering power at night was increased by a "Starscope" borrowed from the Army, but the images obtained were not very satisfactory. In the later experiments, aerial photographs were attempted only when there was sufficient natural light.

2.3.3 Tracer Release, Sampling, and Analysis

Tracer Release System

Two tracer gases, SF_6 and CF_3Br, were released at different heights from the boom of a mobile crane. The mobility of the release system resulted in a high number of successful hours per test (normally six or seven hours out of eight) in which significant tracer concentrations were recorded on the hill. In only one experiment (Test 212) were the wind patterns so variable that it was not possible to align the release system upwind of the hill.

The SF_6 and CF_3Br tracer gases were stored in individual compressed gas cylinders kept at ground level; flexible Tygon tubing, approximately 100 m long, led from the gas cylinders to different release heights on the crane boom. For the first nine experiments (Cases 201-209), the tracer release tube was attached to the smoke generator platform at the smoke release height but from 0.5 m to 1 m away, horizontally. For the last nine experiments (Cases 210-218), the tracer release tube was on a separate pulley system independent of the smoke generator platform and about 1 m away, horizontally, from the smoke release. The gas flow was monitored by separate rotameters on the SF_6 and CF_3Br cylinders, and the weight loss of each cylinder was monitored by a separate electronic digital scale.

Because of the difficulty in calibrating rotameters with 100 m of tubing attached, the rotameters were used simply to monitor a constant flow rate of tracer; the weight loss of the cylinders (as recorded by the digital scales) was used to determine the emission rate of each tracer. The scales could be read accurately only to the nearest 0.05 lb, however, and because the SF_6 flow rate was initially as low as 0.06 g/sec (0.5 lb/hr), the possible uncertainty in the hourly emission rate determination could be up to 10%. This problem was alleviated in the later experiments by increasing the SF_6 flow rate to about 0.18 g/sec (1.5 lb/hr), thus reducing the emission rate uncertainty to about 3%. Table 3 presents the average tracer release rates in each experiment; release rates ranged from 0.06 g/sec to 0.20 g/sec for SF_6 and from 0.86 g/sec to 0.98 g/sec for CF_3Br.*

Tracer Sampling System

Tracer sampling was accomplished by means of approximately 90 individual battery-operated samplers capable of either 10-minute or 1-hour sequential operation. Each sampler contained 12 individual pumps, each of which intermittently** filled a Tedlar bag over the time period of interest. Thus, each sampler could take sequential 1-hour samples over a 12-hour period or sequential 10-minute samples over a 2-hour period. Normally, 1-liter bags were used for both hourly and 10-minute samples. Except for samples taken from reflection masts (described below), all samples were taken at 1 m above ground level.

Figure 12 shows the locations of the 70 fixed samplers and also the 10 movable samplers that were placed on either the northwest or southeast side of the hill, depending on the prevailing wind direction. Of these 80 samplers, typically 60 were used for 1-hour average samples and 20 were used for 10-minute average samples. Another 10 samplers were used for reflection masts, for background ambient air samples, and for co-located samplers.

---

*In analysis by electron-capture gas chromatography, CF_3Br is about 20 times less sensitive than SF_6.

**For a 1-hour average sample, a pump sampled intermittently for about 1 second every 15 seconds.

TABLE 3. SF_6 AND CF_3Br RELEASE RATES (g/sec)

Case	SF_6 Average Release Rate	CF_3Br Average Release Rate
201	0.09	-
202	0.08	-
203	0.08	-
204	0.09	-
205	0.09	-
206	0.06	-
207	0.16	-
208	0.19	0.97
209	0.16	-
210	0.17	0.97
211	0.17	0.97
212	0.16	-
213	0.20	0.96
214	0.17	0.94
215	0.20	0.96
216	0.18	0.96
217	0.16	0.98
218	0.15	0.86

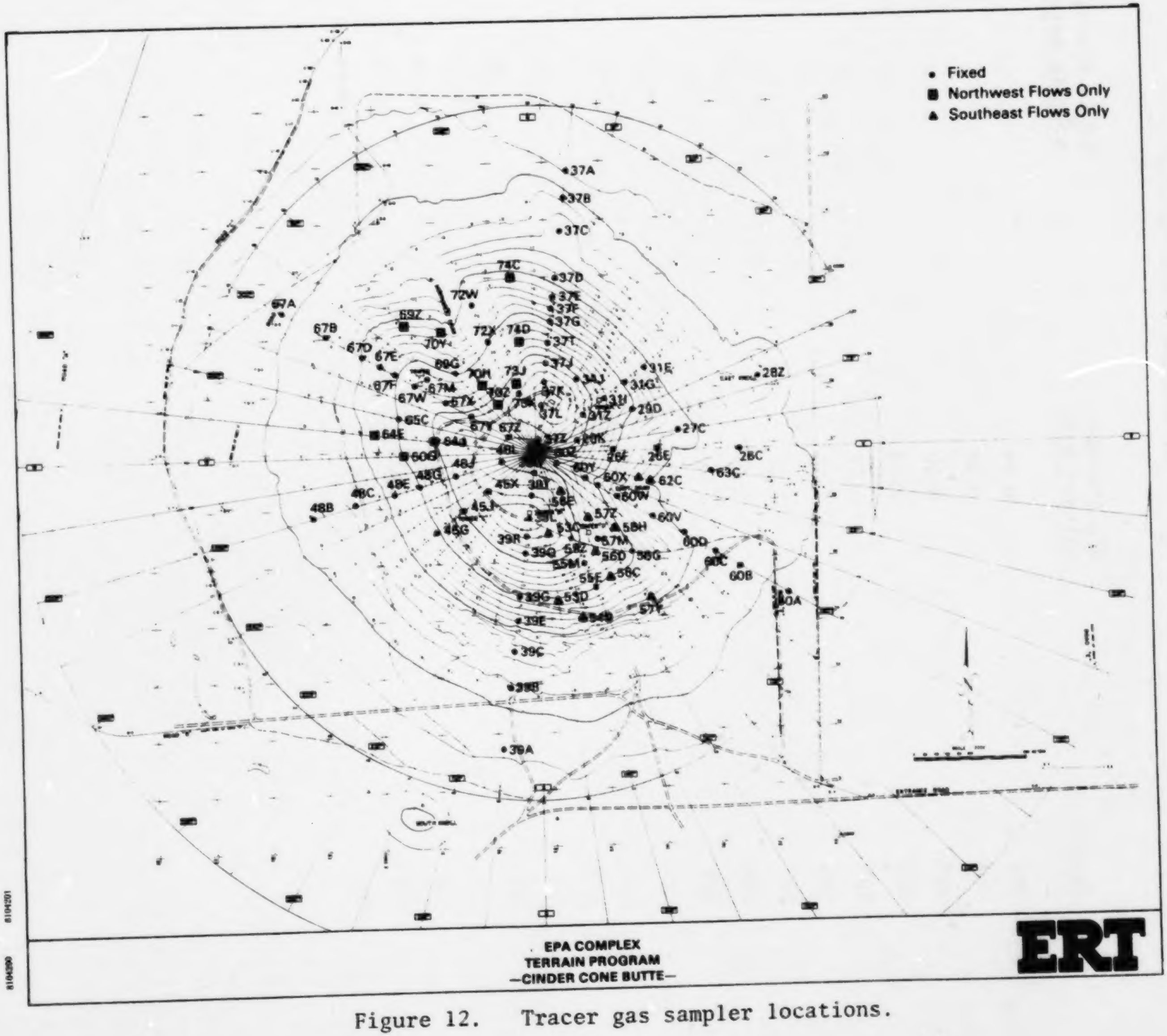
• Fixed
■ Northwest Flows Only
▲ Southeast Flows Only
37A
37B
37C
37D
37E
37F
37G
37T
37J
34J
31E
31G
31H
31Z
28Z
28D
27C
28C
63C
26E
26F
62C
60X
60W
60V
60Y
60D
60C
60B
60A
57Z
58H
57M
56D
58G
58C
55E
55M
57F
53D
54B
39G
39E
39C
39B
39A
39Q
39R
45X
45J
46G
48G
48E
48C
48B
48J
48L
60G
64J
64E
65C
67W
67M
67F
67E
67D
67B
67A
69Z
69G
70Y
70H
72W
72X
73J
74D
74C
67Y
67Z
37Z
37K
37L
EPA COMPLEX
TERRAIN PROGRAM
—CINDER CONE BUTTE—
ERT

Figure 12. Tracer gas sampler locations.

The design of a reflection mast is shown in Figure 13. Air samples were drawn in from 3 m and 6 m (in addition to the normal 1 m height) and also at an uphill site equal in elevation to the 6 m height. The purpose of this sampling strategy was to determine if tracer concentrations would "reflect" off the surface as predicted by some dispersion models. Four of these reflection masts were used during Cases 203-218. Normally, the 3 m height was sampled on only one of the reflection masts; the other masts were sampled at 6 m and 1 m, in addition to the uphill site.

Background air was sampled during each experiment by at least one sampler upwind of the tracer release point. At two locations during each test, an extra sampler was placed next to the normal sampler and set to sample at the same time. These co-located samplers were used to assess the variability in the sampling technique; the results from the co-located samplers are discussed in Section 3.2.

The mechanical reliability of the samplers was relatively poor, with a typical pump breakdown rate of about 20% during each test. During the earlier experiments, the mechanical breakdown problems, when combined with sampler crew mistakes in setting the sampler times, resulted in fairly low data capture for some of the experiments. However, as the sampler crew gained experience, the data capture during the later experiments was limited mainly by mechanical problems.

The design of the sampling system proved to be a good compromise between total flexibility of the system and personnel endurance. For example, it was not possible to operate many more 10-minute samplers because bags had to be manually changed by the sampler crew every two hours for each 10-minute sampler. The utility of the reflection mast system cannot be properly assessed at present because a more detailed study of the results is necessary.

Tracer Analysis System

The analysis of the bag samples by electron-capture gas chromatography was accomplished in the NAWC laboratory in Boise. Six gas chromatographs were used to analyze for the SF_6 tracer; however, because of problems in obtaining adequate column packing material, only one of the chromatographs

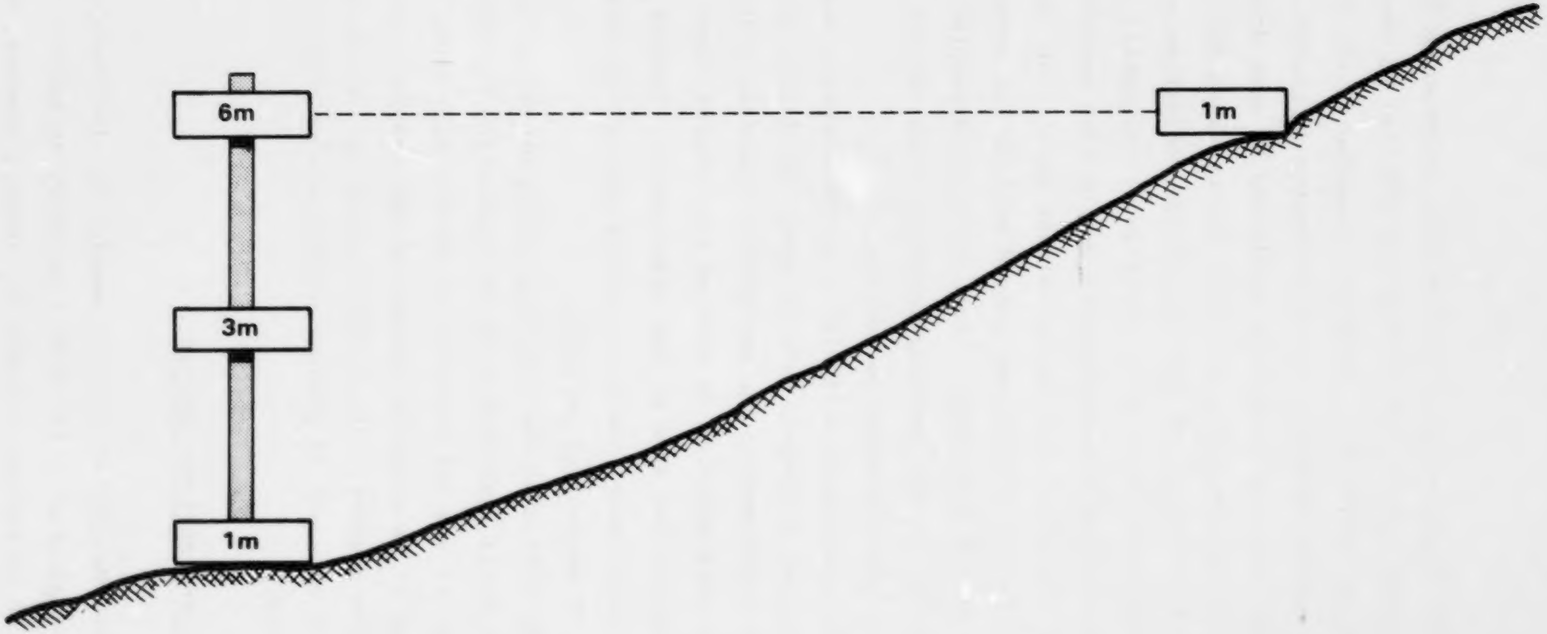
8104172
6m
3m
1m
1m

Figure 13. Reflection mast design.

could analyze for the CF_3Br tracer as well as SF_6. The detection limit of the chromatographs was about 5 parts per trillon (ppt) for SF_6 and about 100 ppt for CF_3Br.

A chromatogram showing a good separation of the tracer gases using a 5A molecular sieve column is illustrated in Figure 14. The SF_6 and CF_3Br* elute before the large oxygen peak, with a total analysis time of about 4 minutes per sample. The SF_6 areas were calculated by an electronic digital integrator (the area under the peaks is directly proportional to concentration). With six chromatographs and an average of 4 minutes per sample, a total of 90 samples per hour could be analyzed.

For quality assurance, about 5% of the samples were analyzed twice on different gas chromatographs. The results of these recounts are discussed in Section 3.2. Most analyzed bags were then flushed two times with nitrogen and returned to the field. The exceptions were bags that contained high tracer concentrations (>1 part per billion (ppb) SF_6; >10 ppb CF Br). These bags were discarded to prevent any possible contamination caused by tracer desorption from the bag walls. Figure 15 illustrates the flow of procedures followed in bag sampling and analysis.

Calibrations were performed on each gas chromatograph at the start and finish of each analysis day. Nine calibration gases, ranging from about 10 ppt to 40 ppb SF_6 and from about 200 ppt to 800 ppb CF_3Br, were used to calibrate each chromatograph in the early experiments. The calibration points were reduced to seven (10 ppt to 10 ppb SF_6) in later experiments because no SF_6 tracer concentration greater than 10 ppb was ever detected in the field studies. A check with one calibration gas (usually 100 ppt SF_6) was performed every four hours on every chromatograph; if this span check showed a greater than 5% difference from the last calibration, that chromatograph was completely recalibrated with all of the calibration gases.

Figure 16 presents the procedures followed to obtain tracer gas concentrations as a function of time and location. The data sheets from each field sampler location that contained times and bag numbers were transferred to the laboratory in Boise along with the bags, and the analysis

---

*On the remaining five columns, the CF_3Br peak could not be separated from the oxygen peak.

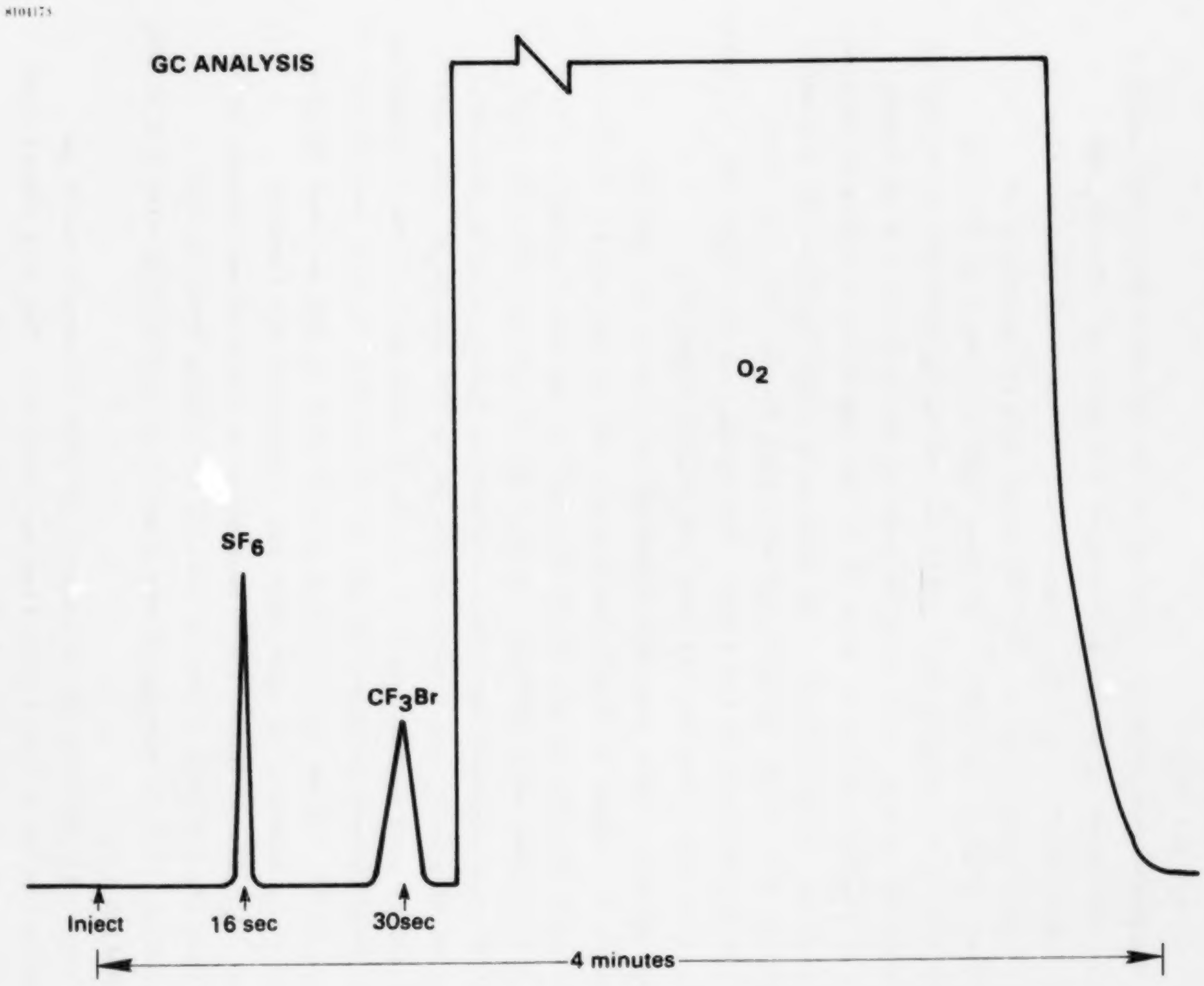

Figure 14. Tracer gas chromatogram.

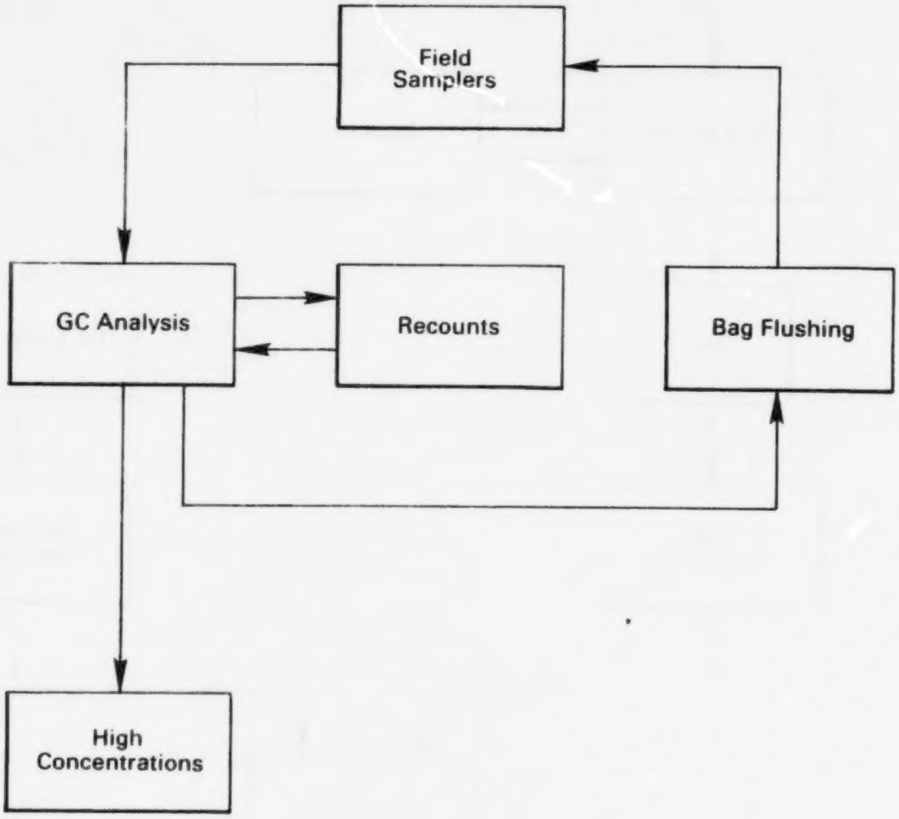
Field Samplers
GC Analysis
Recounts
Bag Flushing
High Concentrations

Figure 15. Bag sampling and analysis procedures.

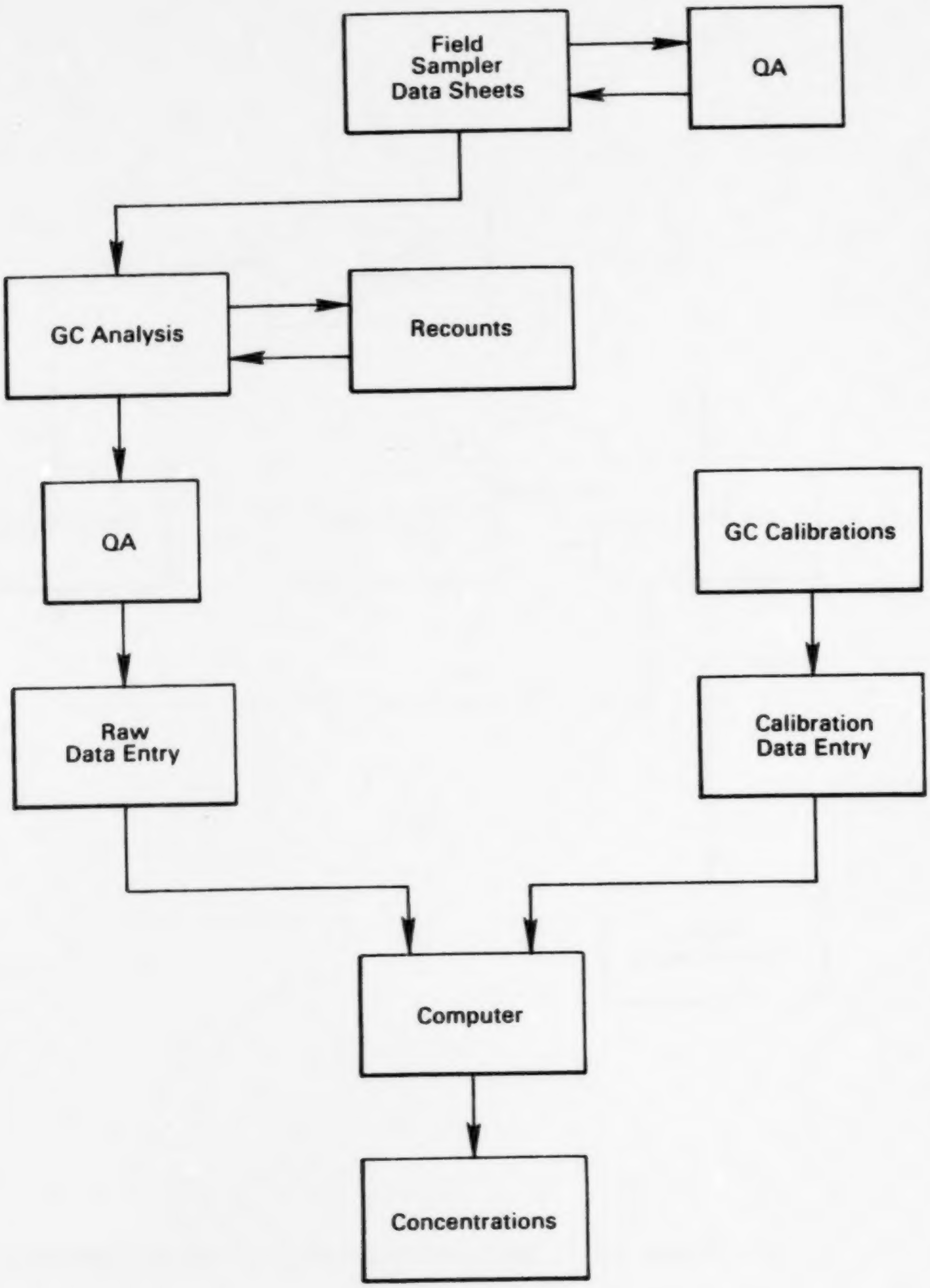
Field Sampler Data Sheets
QA
GC Analysis
Recounts
QA
GC Calibrations
Raw Data Entry
Calibration Data Entry
Computer
Concentrations

8104170

Figure 16. Procedures to obtain tracer gas concentrations.

information (date, time, and integrator area) was then written on the same data sheet. These data were then entered into the ERT data base during the field study from a console at the Boise laboratory.

Calibration data for each chromatograph were also entered separately into the ERT data base. At first, a cubic spline interpolation was used to fit a continuous curve to the calibration points. However, this cubic spline technique resulted in too many degrees of freedom for some calibration curves and produced inaccurate results for high concentrations, as shown in Figure 17. Another function was selected to provide a better fit to the calibration data:

$$y = ax\,(1 - e^{-b/x}), \tag{6}$$

where y is the area or peak height and x is the concentration. This function is based on the response of the electron-capture detector at low and high concentrations (Maggs et al. 1971) and fits the calibration data quite well, as shown in Figure 17. Tracer concentrations of SF_6 and CF_3Br were then calculated by computer from a linear interpolation in time between the two closest calibrations before and after the analysis time of each sample.

In view of the huge number of tracer samples and the operation of the gas chromatographs for 16 hours per day, the tracer analysis system worked quite well. All samples were analyzed within 48 hours of sample collection. The main deficiency was that only one chromatograph could analyze both SF_6 and CF_3Br. The only major instrument problem occurred during the early experiments when it was difficult to obtain reproducible results from three of the chromatographs. These chromatographs were subsequently replaced, and the analysis proceeded quite smoothly thereafter. The preliminary recount statistics, as discussed in Section 3.2, showed good reproducibility of the tracer analysis system.

2.3.4 Lidar Measurements

Under funding through an EPA/NOAA Interagency Agreement, the NOAA Wave Propagation Laboratory (WPL) operated a lidar to measure the back scattering

8104171

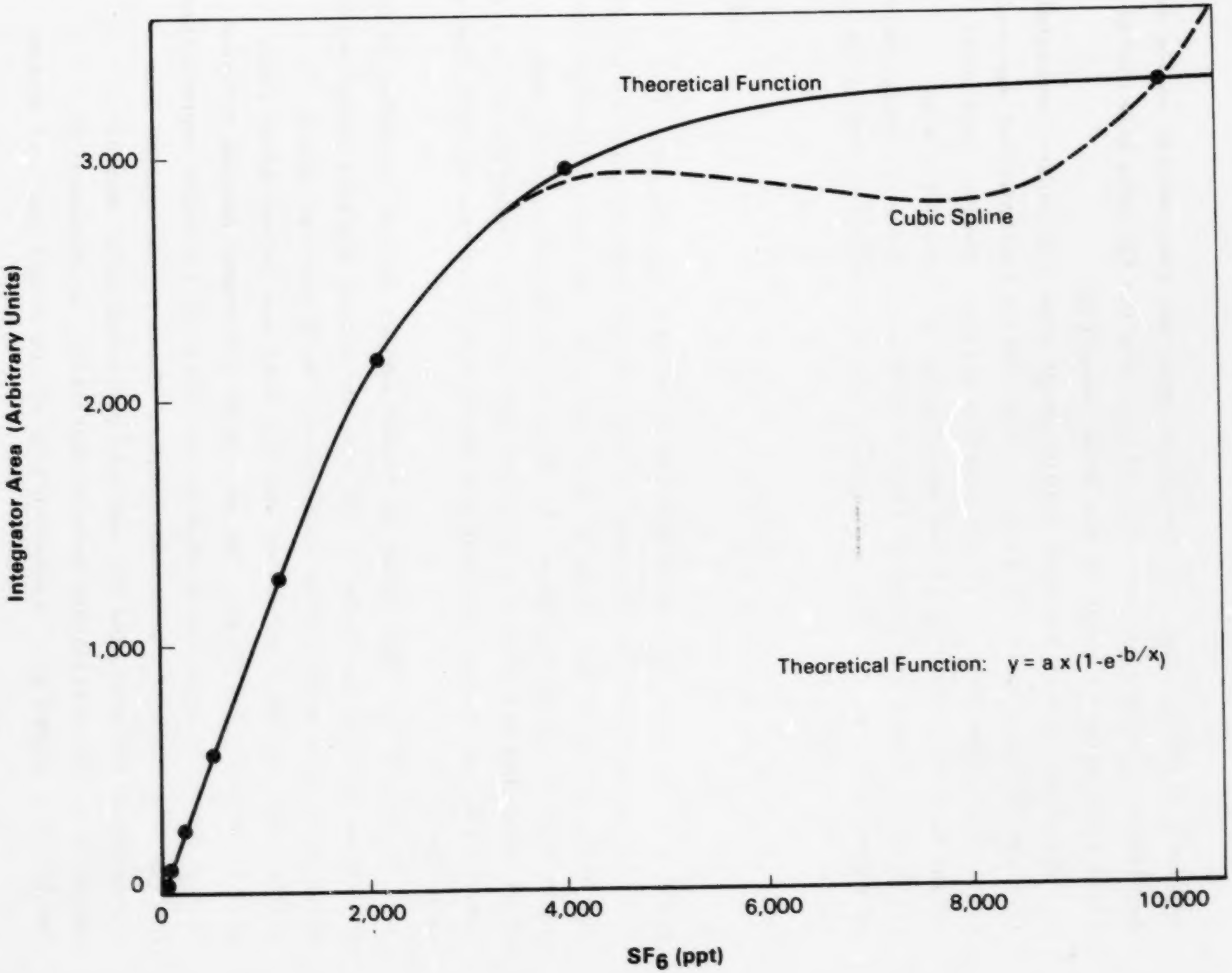

Figure 17. SF_6 calibration curves.

of the oil-fog plume. The basic purpose of the lidar measurements was to determine plume dimensions and to locate the plume centerline before it reached the hill. A sampling protocol was developed so that WPL took regularly scheduled measurements at three locations upwind of CCB. The lidar proved to be also useful for operations management. The WPL crew frequently provided sketches of the plume (see Figure 18), providing nearly real-time feedback of plume location.

2.3.5 Other Measurements

To obtain katabatic wind information, cup-and-vane wind sensors and temperature sensors were arranged at about 1 m above the axis of the east draw at five locations separated by about 50 m. Three hot-wire anemometers were located in a vertical array in the draw near the base of the butte. These instruments were set out to quantify the flow character as a function of height on the hill and longitudinal position down the east draw. A field of orange and white fluorescent streamers was constructed and located across the bottom of both the east and northwest draws to qualitatively assess the depth and extent of downhill flows. The cup-and-vane sets and temperature sensors were connected to a tape recorder and the hot-wire anemometers to a chart recorder.

To define the plume before it interacted with the hill, nephelometer measurements of b_{scat} were taken by instruments suspended from a crane that was driven across the plume path. A 10 m tower with three nephelometers was located near the top of the east draw on CCB. Also, one nephelometer was located at the top of each peak of the butte and one at Tower D.

Supplementing the measurements from the six main meteorological towers were various sounding devices operated by NAWC and WPL (see Figure 10). NAWC operated a tethersonde from the more upwind of two locations about 1.3 km from the center of the butte. These sites were therefore usually within 700 m of the primary release point. An ascent-descent sequence yielding profiles of temperature, pressure, and wind speed and direction was normally performed once an hour (or more frequently) to heights at least 200 m above the local terrain.

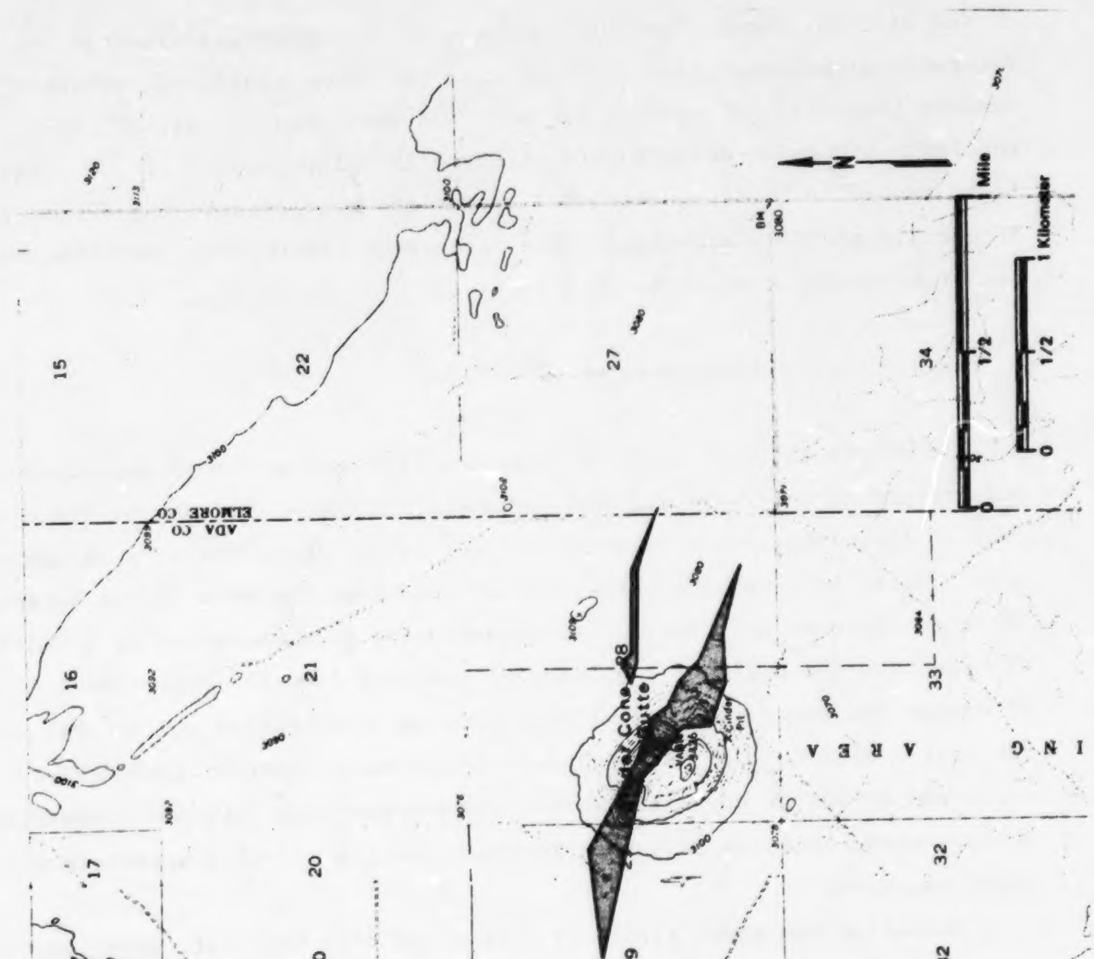
ADA CO
ELMORE CO
Cinder Cone Butte
Cinder Pit
A R E A
I N G
15
16
17
20
21
22
27
28
29
32
33
34
N
Mile
1 Kilometer
0
1/2

Figure 18. Illustration of lidar-sampled plumes.

When this tethered balloon system was not available because wind speeds were too high to allow tethersonde operation, the supplementary profiles were obtained from minisonde flights. (The minisonde profiles were less frequent than the tethersonde profiles.) Wind profiles were also derived from pilot balloons (pibals) released approximately once an hour. The pilot balloon flights were tracked by two theodolites for 10 minutes, if possible, and the balloons rose at approximately 200 m/min; thus, many of the pibal profiles extended as high as 2,000 m above the surface. (The azimuth and elevation angles taken during the balloon flights have not as yet been transformed by NAWC into heights and wind speed and direction profiles.)

WPL operated its frequency-modulated, continuous-wave (FM/CW) radar from a point south of the butte as well as two monostatic acoustic radars, one to the east and one to the west of the butte, to provide information on the atmospheric boundary layer in the vicinity of the butte. Information from these instruments has not yet been received by ERT.

2.3.6 Data Base Management

To house the enormous amount of data that was collected, ERT utilized a Data Base Management System (DBMS) that was designed for efficient handling of data at all levels of input, validation, reduction, processing, and archiving. A Data General Nova minicomputer was located on-site to serve as the prime data collector. This minicomputer provided maintenance information, automatic calibration support, automatic screening of status and value, hourly system summary reports, and data communications in addition to data collection. An on-site hardcopy output printer and three CRT terminals gave scientists direct access to the meteorological data in real time. Data were permanently archived as both 5-minute and 1-hour averages.

Figure 19 illustrates the configuration of the data collector system and the ERT central data processing system. Measurements taken at the 150 m tower were initially processed and averaged at a transponding data station, telemetered to a shelter at the top of CCB, and transmitted to the data collector. Similarly, meteorological data collected from instruments located on the butte were first processed at the data stations there and

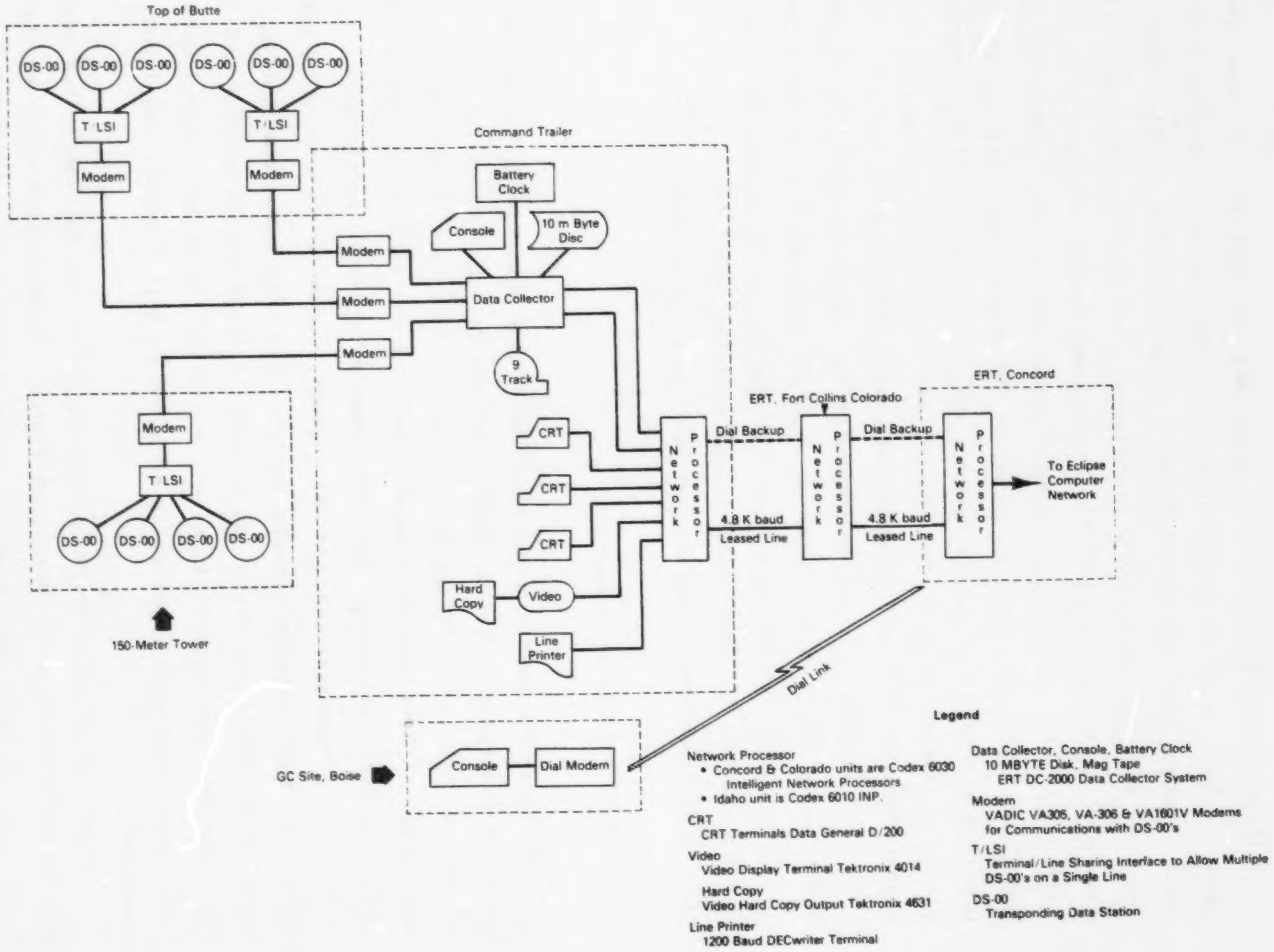
Top of Butte
DS-00
DS-00
DS-00
DS-00
DS-00
DS-00
T/LSI
T/LSI
Modem
Modem
Command Trailer
Battery Clock
Console
10 m Byte Disc
Modem
Modem
Modem
Data Collector
9 Track
Modem
T/LSI
DS-00
DS-00
DS-00
DS-00
150-Meter Tower
CRT
CRT
CRT
Hard Copy
Video
Line Printer
Network Processor
ERT, Fort Collins Colorado
Dial Backup
4.8 K baud
Leased Line
Network Processor
Dial Backup
4.8 K baud
Leased Line
ERT, Concord
Network Processor
To Eclipse Computer Network
Dial Link
GC Site, Boise
Console
Dial Modem

Legend

Network Processor
- Concord & Colorado units are Codex 6030 Intelligent Network Processors
- Idaho unit is Codex 6010 INP.

CRT
CRT Terminals Data General D/200

Video
Video Display Terminal Tektronix 4014

Hard Copy
Video Hard Copy Output Tektronix 4631

Line Printer
1200 Baud DECwriter Terminal

Data Collector, Console, Battery Clock
10 MBYTE Disk, Mag Tape
ERT DC-2000 Data Collector System

Modem
VADIC VA305, VA-306 & VA1601V Modems for Communications with DS-00's

T/LSI
Terminal/Line Sharing Interface to Allow Multiple DS-00's on a Single Line

DS-00
Transponding Data Station

Figure 19. Data collection system configuration.

then transmitted to the data collector located at the field headquarters. Data were displayed in real time at the data collector for analysis and operations management purposes. Data were transmitted to the ERT office in Fort Collins, Colorado, and sent to the ERT central computer in Concord, Massachusetts, via a dedicated telephone line. A computer terminal was available at the NAWC Boise laboratory to allow entry of the SF_6 and CF_3Br data into the data base. In addition to data analysis efforts at CCB, meteorological data were analyzed at the ERT central data processing facilities, and selected analysis results were sent back to the field headquarters for use during the experiment. Table 4 lists examples of the analysis programs used during the experiment.

2.4 Field Study Results

2.4.1 Summary of Field Data

When the project began in June 1980, the experimental methods to be used in the small hill study were untested and unproven. We can now conclude that the CCB dispersion experiment was successful. Extensive data sets of meteorological conditions and ground-level tracer gas concentrations have been assembled which will permit the development of models of plume interaction with three-dimensional, approximately axisymmetric hills in stable flows. Problems in the field occurred primarily because of insufficient lead time, communications failure in the real-time meteorological monitoring system, and tracer gas sampler failure. However, the end result is an excellent data base for model development purposes.

A summary of the total number of tracer data samples analyzed for each case (both 1-hour and 10-minute samples) is presented in Table 5. More detailed data summaries presenting hour-by-hour data capture for each case are tabulated in Appendix A. Table 5 shows a total of over 14,000 data points for the 18 cases, or roughly 800 tracer samples analyzed per case. Overall, 33% of the samples were 1-hour averages and 67% were 10-minute averages. Two tracers (SF_6 and CF_3Br) were released at different heights in nine of the experiments (Cases 208, 210-211, and 213-218). The

TABLE 4. SAMPLE ANALYSIS PROGRAMS AVAILABLE ONSITE

GRAD

Tabulates local temperature, potential temperature gradient, gradient Richardson number, Froude number, and square of Brunt-Vaisala frequency as a function of height for a specified tower and time.

TOWR

Tabulates U, V wind components, mean wind, and wind shear profiles as a function of height for a specified tower and time.

FDIF

Computes the gradient Richardson number, square of Brunt-Vaisala frequency, potential temperature gradient, and Froude number in finite difference form as a function of selected heights for Z_1 and Z_2 for a specified tower and time.

SURF

Computes the Bulk Richardson number, Monin-Obuhkov length, surface friction velocity, surface heat flux, and surface temperature scale as a function of roughness height (Z_0), Z_1 and Z_2 for a specified tower and time.

ZO

Computes the roughness height from data from the 150 m tower for a specified time. Heights used are 40, 10, and 2 m.

HCRIT

Calculates the dividing streamline height using data collected at all eight levels of Tower A or from data collected at the other five (B-F) towers.

TABLE 5. SUMMARY OF TRACER DATA ANALYZED

Case	Number of 1-hr Average Samples		Number of 10-min Average Samples		Total
	SF_6	CF_3Br	SF_6	CF_3Br	
201	73	-	292	-	365
202	169	-	404	-	573
203	79	-	440	-	519
204	222	-	507	-	729
205	225	-	422	-	647
206	228	-	446	-	619
207	150	-	469	-	841
208	173	64	461	-	608
209	240	-	368	-	608
210	251	109	471	89	920
211	291	149	596	81	1,117
212	86	-	202	-	288
213	216	62	352	93	723
214	233	61	478	194	966
215	278	64	567	341	1,250
216	368	98	693	167	1,326
217	339	95	664	88	1,186
218	382	74	713	169	1,338
TOTAL	4,003	776	8,545	1,365	14,689

CF_3Br data account for only 15% of the total because only one of the six chromatographs could analyze for CF_3Br.

It should be noted that Table 5 presents only the number of samples that were analyzed. In most experiments, a number of presumably valid samples were never analyzed because of assumed zero tracer concentrations (e.g., the plume missed the hill for one or two hours). Figure 20 shows the total number of samples analyzed for each case. The severe drop in number for Case 212 was not caused by system failures but rather by a decision to analyze only a few samples; the variable wind patterns during this experiment made it impossible to align the release system upwind of the hill.

These are some of the specific achievements of the CCB experiment:

- Demonstration that the small-hill design concepts successfully generated new knowledge of stable plume dispersion around an isolated, three-dimensional, roughly axisymmetric hill.
- Assembly of a meteorological data base that adequately characterizes the wind and temperature fields around CCB.
- Assembly of a SF_6 and CF_3Br tracer concentration data base that will assist in the development of sound models of stable plume impact on elevated terrain.
- Design, implementation, and operation of a data base management system that generated useful real-time feedback for field operations management and that subsequently will allow users to combine the source, meteorological, and tracer concentration data in a variety of useful formats to aid in developing models.
- Demonstration of the utility of a photographic record of plume behavior in understanding the physics of flows.
- Corroboration of the utility of fluid modeling experiments in understanding flows and dispersion in complex terrain and in designing the CCB experiment.
- Demonstration of the utility of the lidar measurements--both in managing operations and in providing information on plume behavior upwind of CCB.

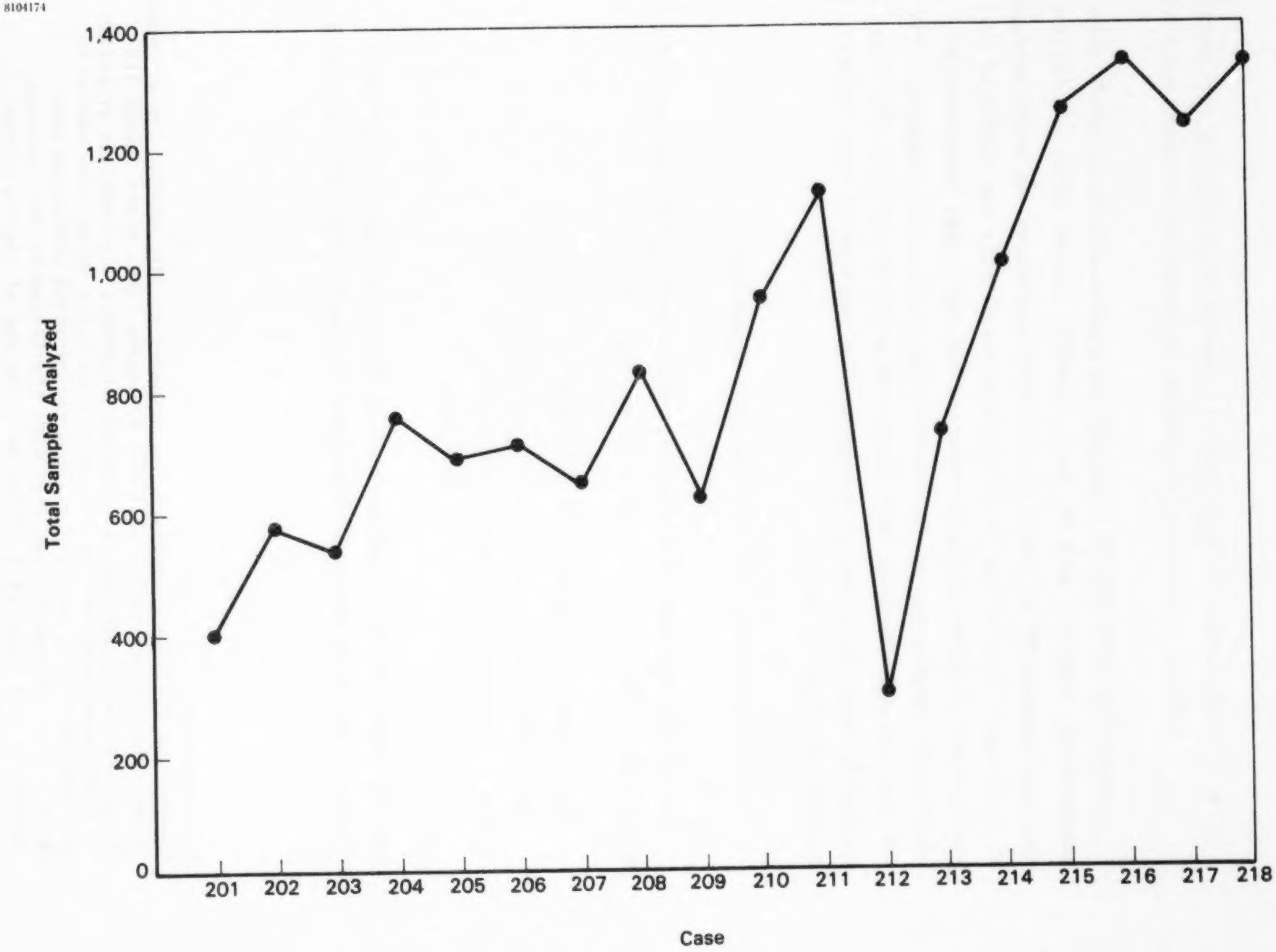

Figure 20. Number of samples analyzed for each field experiment.

- Confirmation in part that the concept of a dividing streamline usefully describes flows around isolated, three-dimensional hills.*

Because we have not yet examined the nephelometer data, FM/CW radar measurements, sampling mast SF_6 data, acoustic sounder data, and katabatic wind measurements,** we cannot assess their usefulness for model development at this time. Most of the 35 mm pictures (especially the nighttime aerial photographs) provided little information and the formal fixed-location photography program was too inflexible from a scientific viewpoint. Many of the most valuable pictures were taken from arbitrary vantage points by interested scientists free to change viewing position in order to best capture the plume dynamics.

2.4.2 Example Results from Specific Experiments

To illustrate some of the experimental results, the remainder of this section will describe four case study hours:

- Case 206 (10/24/80) - 0500-0600+
- Case 211 (10/31/80) - 0400-0500
- Case 210 (10/30/80) - 0200-0300
- Case 205 (10/23/80) - 0400-0500

Case 206 represents a situation in which the plume remained basically horizontal but quite unsteady throughout the hour. Case 211 illustrates an experiment with the emission of both SF_6 and CF_3Br. The smoke and CF_3Br were released at an elevation above the dividing streamline height; SF_6 was emitted below it. Case 210 is an example of a situation in which the higher concentrations occurred on the lee side of CCB. Case 205 is the hour used to illustrate the model evaluations described in the next two sections.

---

*During the field experiments H_{crit} appeared to distinguish instantaneous plume behavior reasonably well for averaging times short enough that H_{crit} remained approximately constant; however, fluctuations primarily in wind speed rendered the 1-hour average H_{crit} value less useful in determining hourly-averaged maximum ground-level concentrations.

**Much of the information was lost when the katabatic wind sensors, recorders, and tapes were stolen near the end of the experiment.

+All times are in Mountain Standard Time (MST).

Case 206 (0500-0600)

The morning of October 24, 1980 exemplifies a situation with light east-southeasterly (126°) drainage winds down the Snake River Basin. The source crane was located about 595 m from the hill center at an orientation of 123.5°. The hourly average wind direction and speed (estimated for the source height) were 126° and 2.0 m/sec, respectively. The SF_6 was released 35 m above the local ground elevation. H_{crit} was estimated as 40 m. On the average, therefore, the SF_6 was emitted at a level slightly below the dividing streamline height, suggesting flow around and toward the north side of CCB during most of the hour (the average wind direction being more southerly than the source orientation).

Figure 21 shows the observed SF_6 concentrations for the hour 0500 - 0600. All concentration labels are placed so that the lower left-hand corner of the right-most digit lies at the sample location. Height contours are presented at 10 m intervals, beginning with the 5 m height contour. The zero height coincides with 945 m (3,100 ft) above sea level. The grid marks radial distance increments of 100 m and angular increments of 22.5°. (The numbers in parentheses represent averages of 10-minute average concentrations; the number of 10-minute averages used to construct the value is the subscript listed at the right. All other values in the figure are hourly average concentrations.*)

H_{crit} values calculated from the archived 5-minute meteorological data range from 29 m to 45 m. Local Fr (calculated at 35 m) ranged from 0.3 to 0.8, and the wind direction varied from 81° to 157°. Most of the plume

---

*Subscripts greater than 6 indicate sampling mast results, which are averaged over all heights sampled (1, 3, and 6 m). A subscript of 2 can also indicate two co-located, hourly averaged samples.

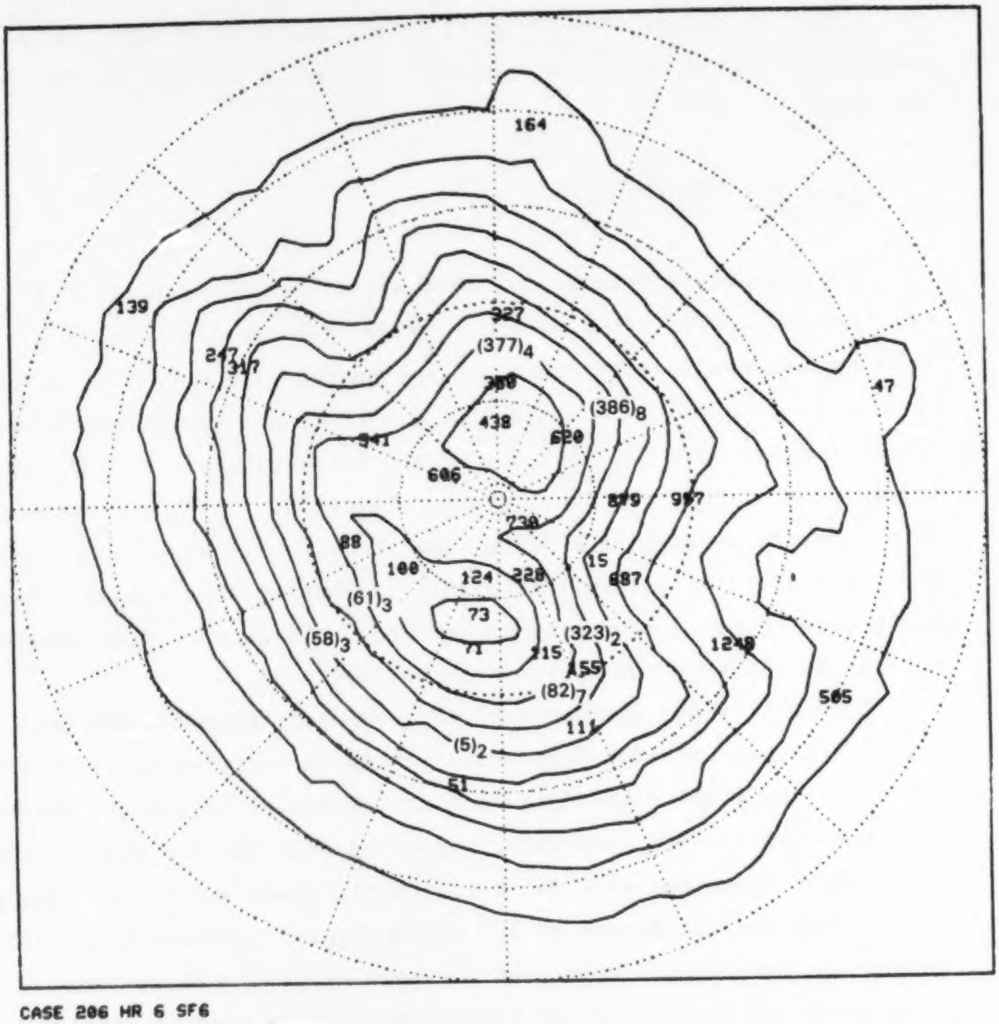

Figure 21. Observed SF_6 concentrations (ppt) for Case 206, 0500-0600. Source: r = 595 m, θ = 123.5°, relative height = 29.5 m, Q = 0.06 g/sec.

material could be expected to be transported toward or along the north side of the butte, at elevations close to the release height. With the changing H_{crit} and wind direction, some SF_6 could be transported through the draw and up the north peak. The hill concentration pattern confirms the transport pattern suggested by the meteorological observations. The higher concentrations (879, 957, and 687 ppt) were measured north of the mean incident wind trajectory at contour heights of between 30 m and 45 m. (Note that a contour height of zero lies approximately 5 m above the local terrain at the release location.) High concentrations were also measured further up in the draw (730 ppt) and on the north peak (606 and 438 ppt), and also towards the base of the draw (1,248 ppt).

Figure 22 is a photograph (5-minute exposure) of the plume taken from the north peak (camera location 0-15) at 0505. The photograph shows the plume bending toward the north and staying at an elevation below the top of the butte. Figure 23, a photograph (1-minute exposure) of the experimental setting taken from the northeast three minutes later (0508), shows a continuous plume going up the north peak and some plume material going around the north side (indicative of the observed concentration pattern). Two photographs, Figures 24 and 25, taken near the middle of the hour--at 0530 and 0540--from the north peak, show the initial plume trajectory toward the butte with subsequent deflection toward the north side. These two photographs suggest substantial crosswind plume diffusion and indicate that the plume path stayed below the top of CCB. Figure 26, shot from the southeast (camera location 0-11) at 0546, shows plume material moving up the draw toward the north peak (but below its top) and around to the north.

Case 206 is a good example of plume transport and diffusion when the release height is near or below the dividing streamline height during most of the hour. Most plume material went toward and around the north side of the butte, although the plume path varied with changes in meteorological conditions.

Case 211 (0400-0500)

Halloween morning 1980 also experienced an east-southeasterly (119°) drainage flow. During the experiment the source crane was located about 1,156 m from the hill center at an orientation of 120.5°. SF_6 was

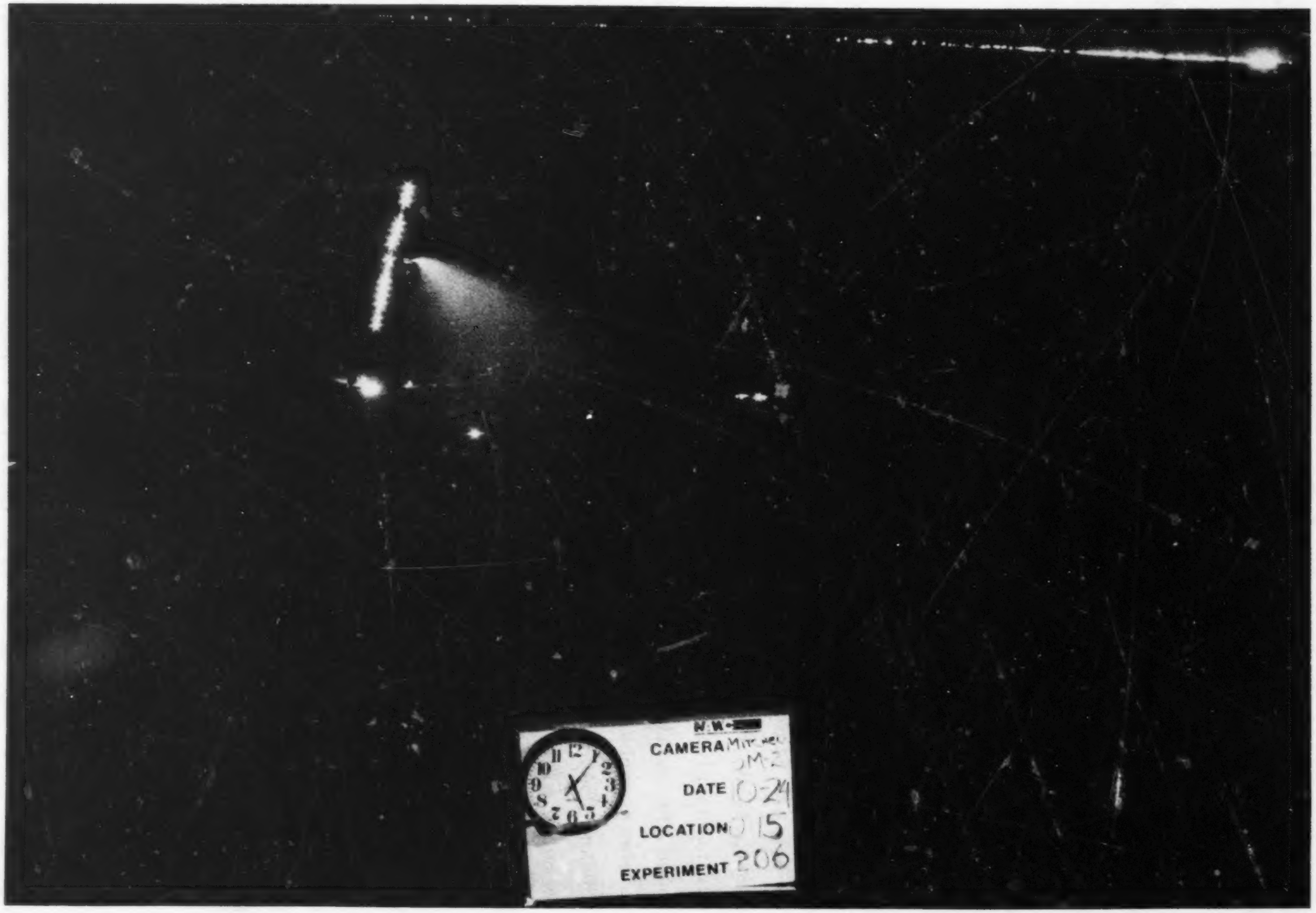
N.W.-[redacted]
CAMERA Mitchell
JM-2
DATE 10-24
LOCATION 015
EXPERIMENT 206

Figure 22. Five-minute exposure; camera location O-15 (Case 206, 0505 MST).

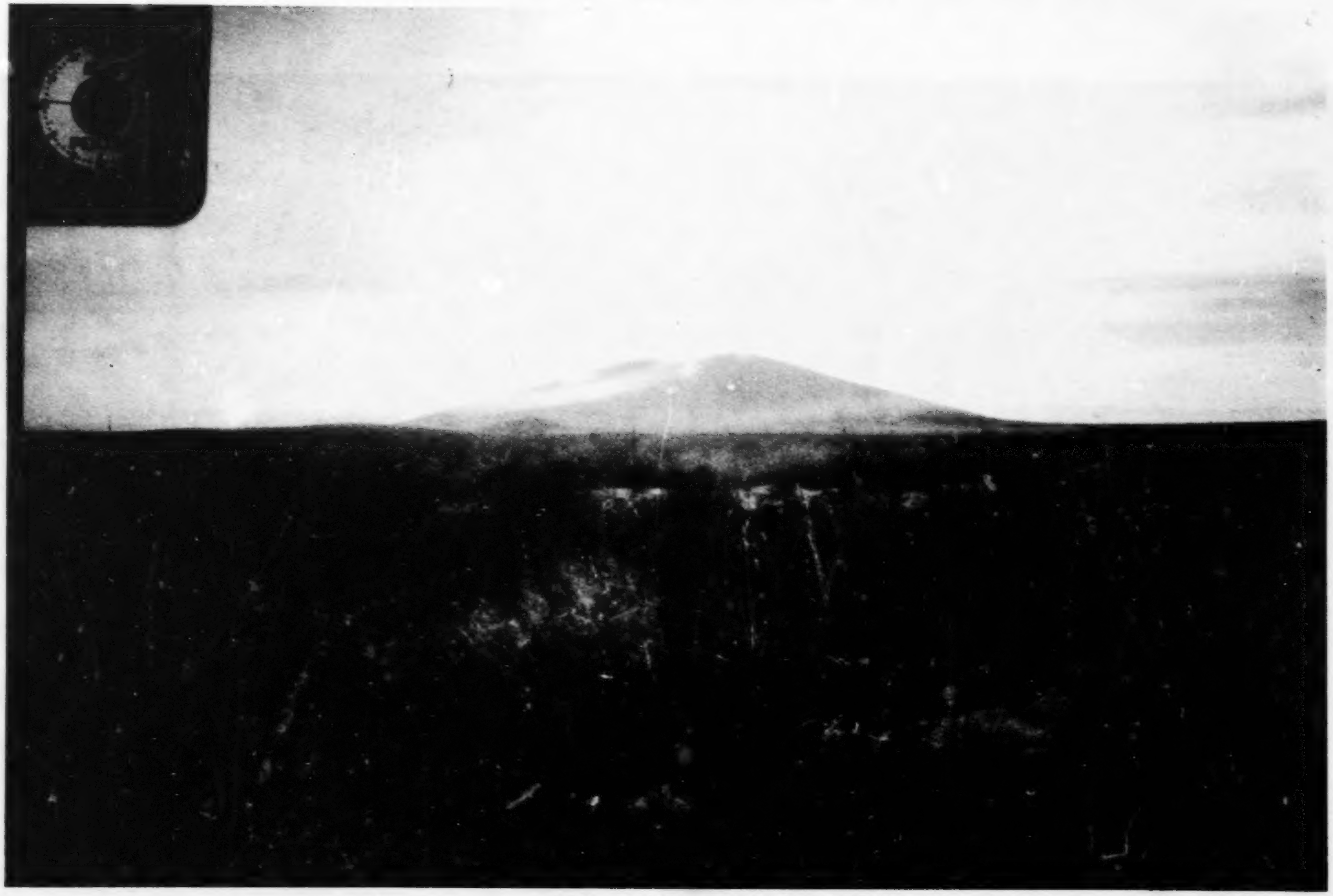

Figure 23. One-minute exposure looking from northeast (Case 206, 0508 MST).

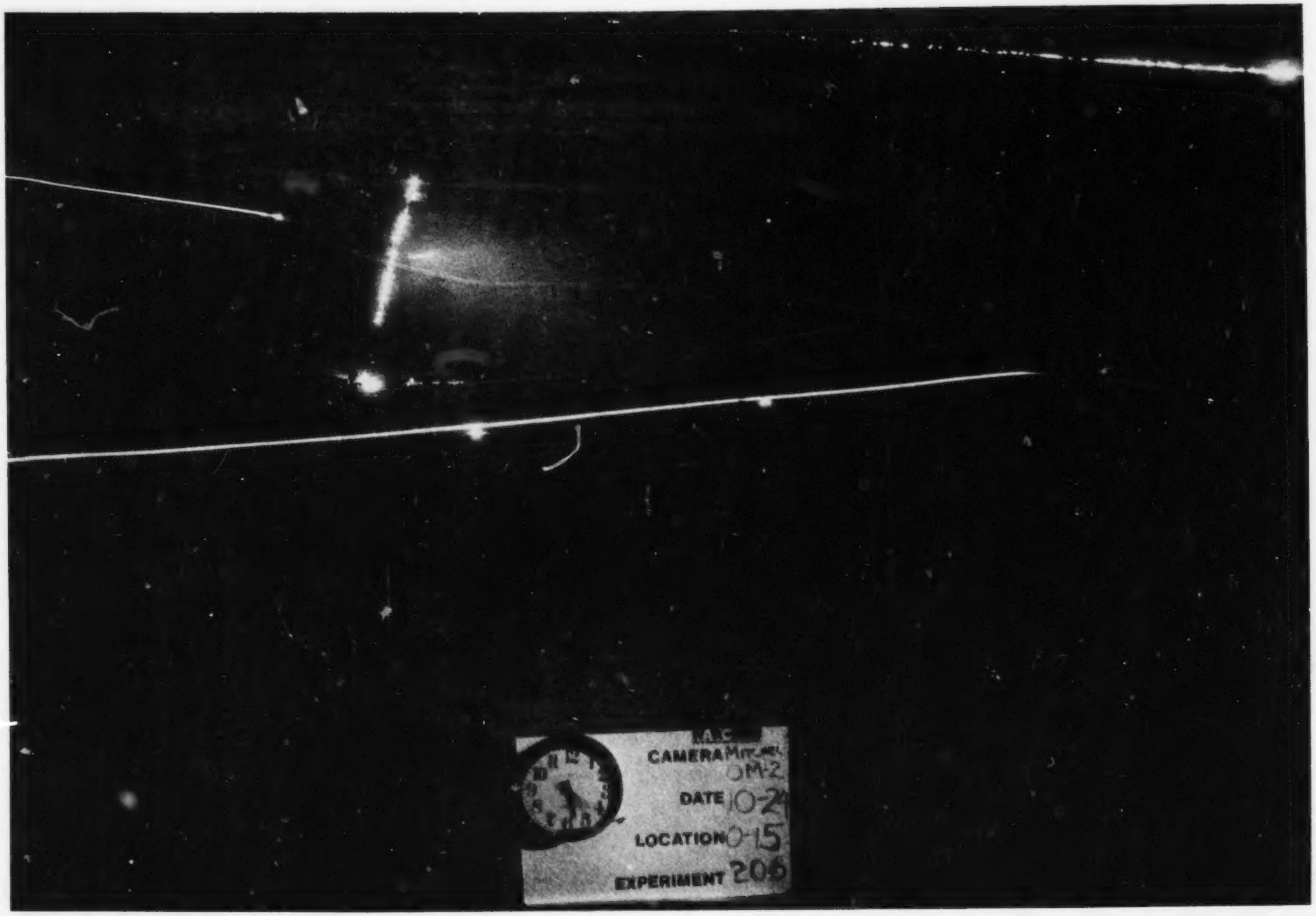
CAMERA OM-2
DATE 10-24
LOCATION O-15
EXPERIMENT 206

Figure 24. Five-minute exposure; camera location O-15 (Case 206, 0530 MST).

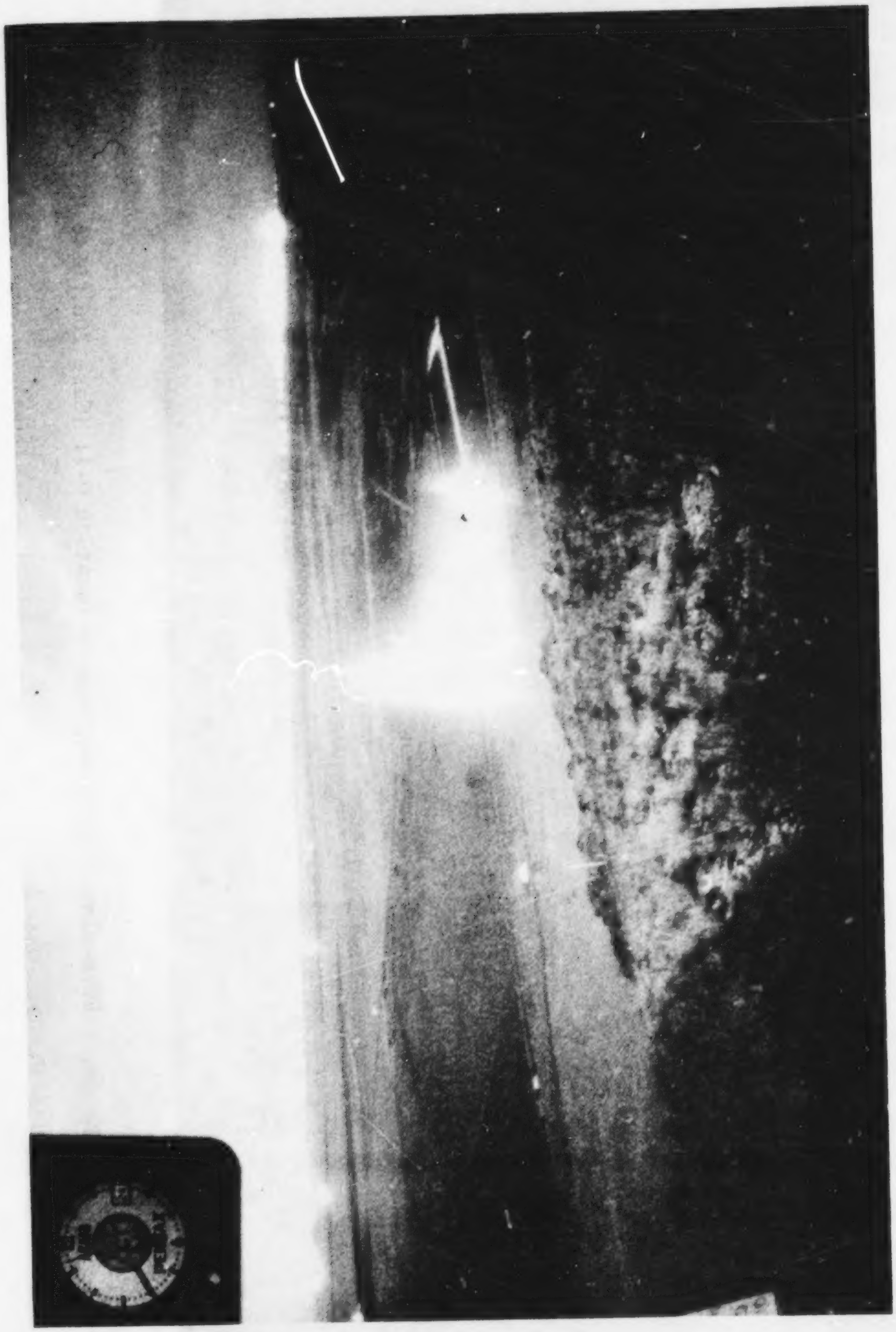

Figure 25. One-minute exposure looking from North Peak (Case 206, 0540 MST).

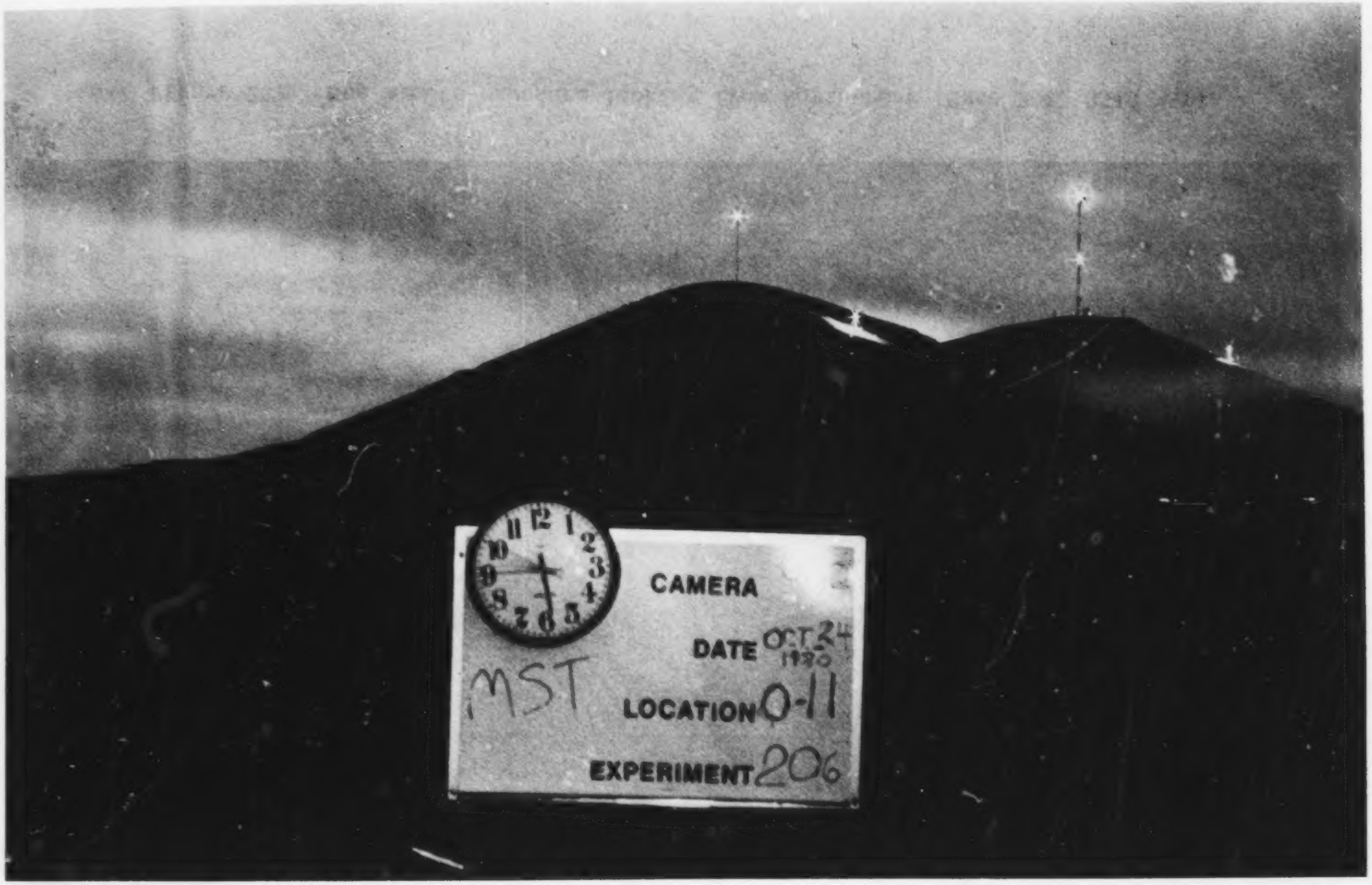
CAMERA
DATE OCT 24 1980
LOCATION O-11
EXPERIMENT 206
MST

Figure 26. Five-minute exposure; camera location O-11 (Case 206, 0546 MST).

released at a local height of 20 m; smoke and CF_3Br were released at 58 m. The average dividing streamline height was 28 m. The Tower A wind direction near the height of the SF_6 source varied from 88° to 165° (5-minute averages) during the hour; the direction near the height of the smoke plume was steadier, ranging from 115° to 142°.

Figures 27 and 28 show plots of the SF_6 and CF_3Br concentration, respectively. The low-level release is below H_{crit} and the resulting SF_6 plume spread all over the hill, with the maximum hourly concentration (2,936 ppt) above the relative release height (i.e., approximately 30 m elevation on CCB compared with a release height of 11 m relative to the 0 m elevation contour). High concentrations were measured throughout an area generally between the 15 m and 35 m contour lines extending from the measured value of 2,936 ppt to values around 1,300 ppt on the northeast slope. SF_6 concentrations above 1,000 ppt were measured in the draw on both the windward and lee sides of CCB. The smoke and CF_3Br plume are transported over the hill, producing essentially zero CF_3Br concentrations on the hill surface. (The two nonzero values are near the detectable limit of CF_3Br.)

Figure 29 shows a photograph of the smoke plume looking from the southwest of 0414. The plume apparently goes up and over CCB with virtually no ground-level impact. As shown in Figure 30 (0435), the plume stays elevated as it is transported over the lee side of CCB.

Case 211 is a good example of plume transport and diffusion when the SF_6 was released below the average dividing streamline height. The SF_6 plume apparently impinged on the hill at levels near and 10-20 m above the relative release height and subsequently spread over and around the hill. The case also shows the difference between releases below and above the dividing streamline. SF_6 released below H_{crit} produced significant ground-level concentrations almost everywhere on CCB whereas the CF_3Br plume, which was emitted well above H_{crit}, went up and over the hill and produced virtually no ground-level concentrations.

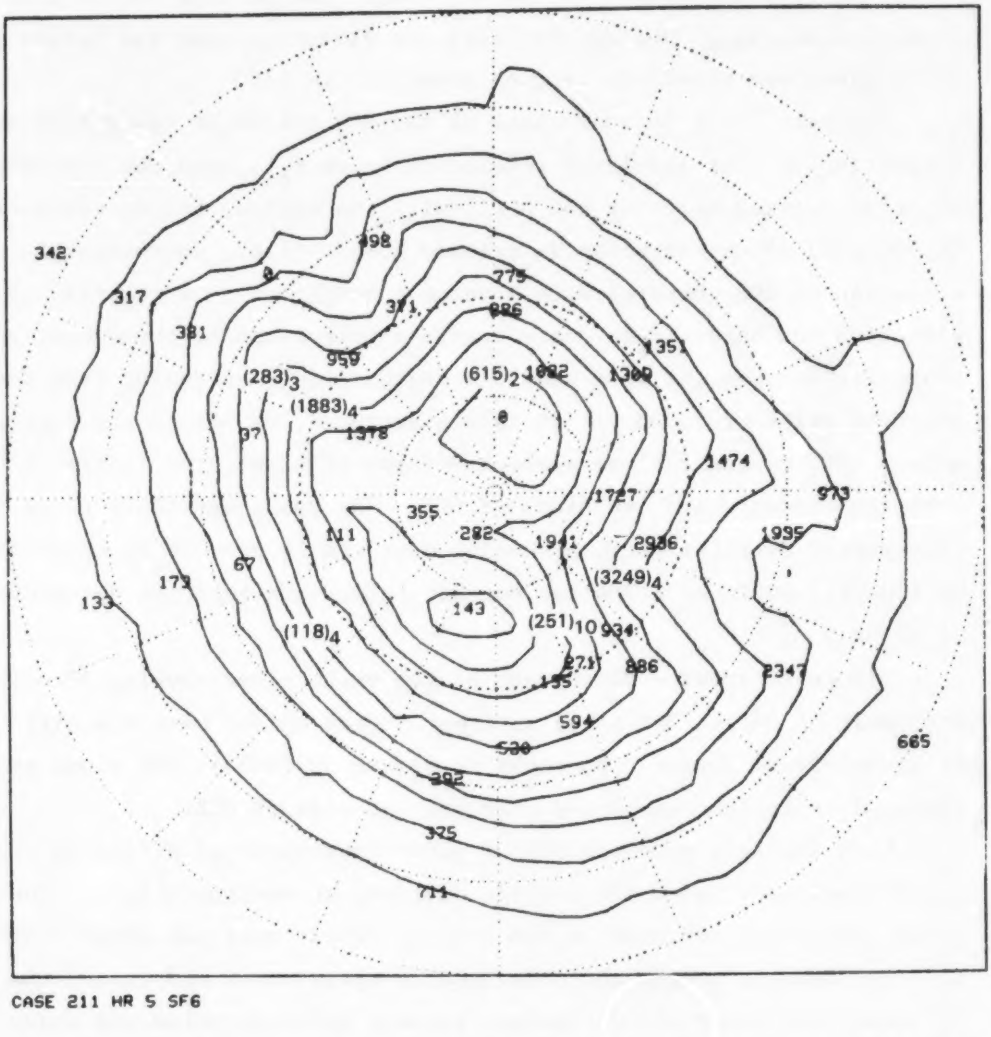

Figure 27. Observed SF_6 concentrations (ppt) for Case 211, 0400-0500. Source: $r = 1156$ m, $\theta = 120.5°$, relative height = 11.1 m, $Q = 0.18$ g/sec.

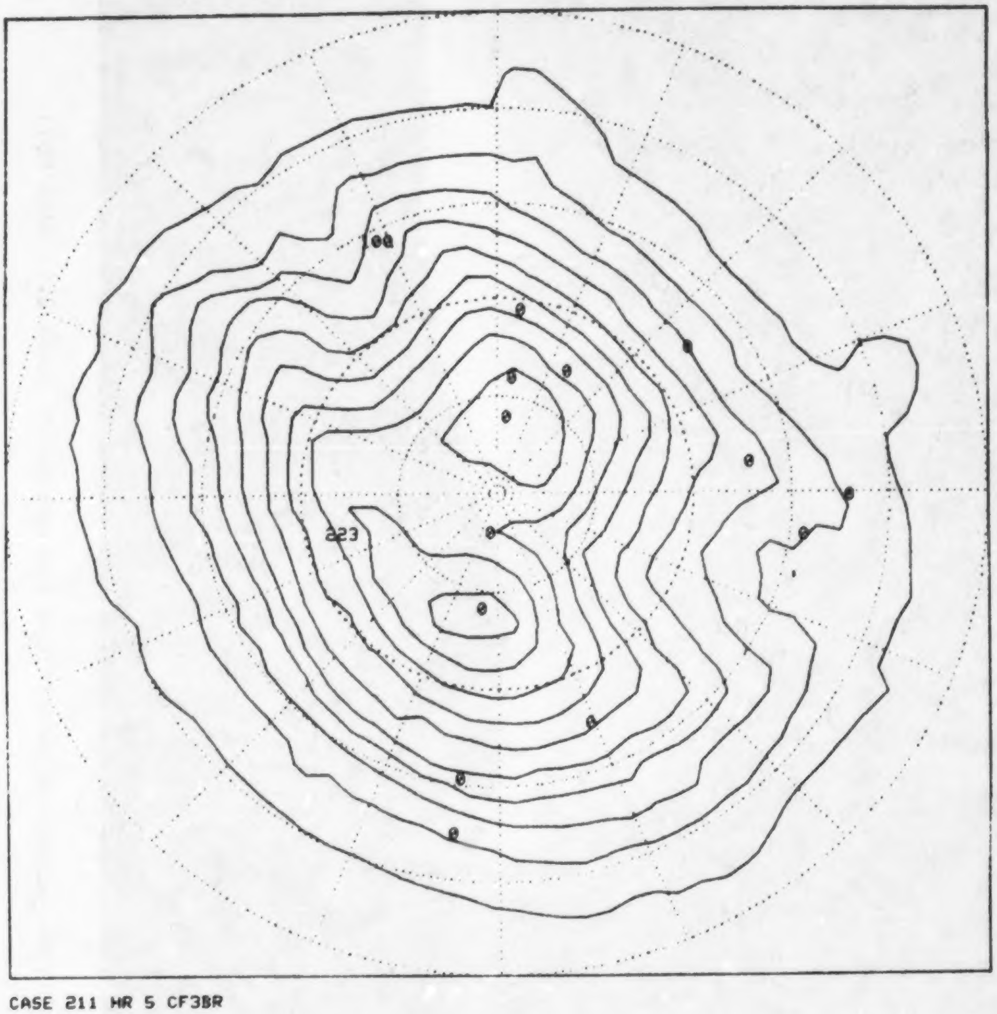

Figure 28. Observed CF_3Br concentrations (ppt) for Case 211, 0400-0500. Source: r = 1156 m, θ = 120.5°, relative height = 49.1 m, Q = 1.02 g/sec.

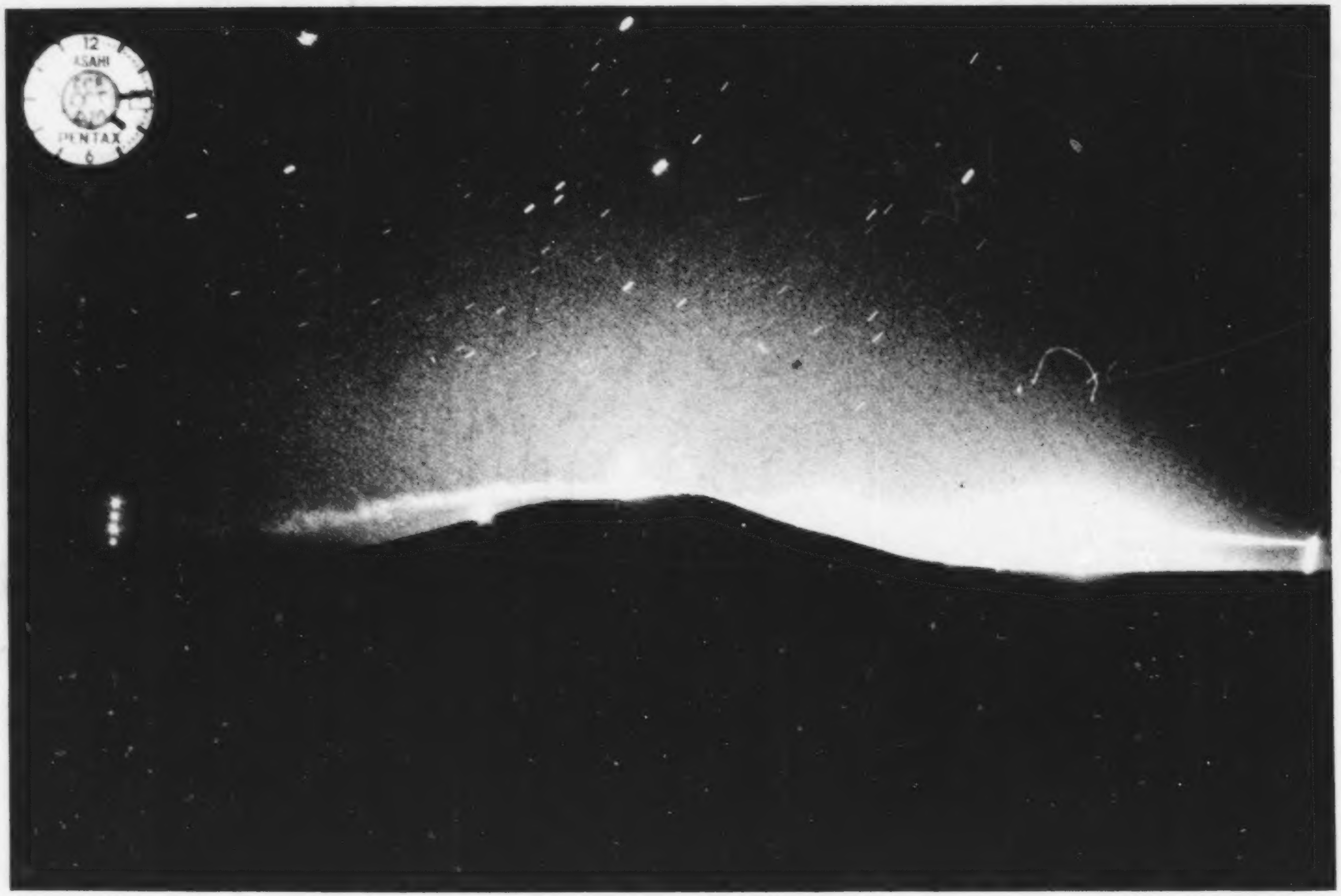
12
ASAHI
PENTAX
6

Figure 29. One-minute exposure from the southwest (Case 211, 0414 MST).

Figure 30. One-minute exposure from lee side of Cinder Cone Butte (Case 211, 0435 MST).

Case 210 (0200-0300)

Both SF_6 and CF_3Br were emitted during this period of stable easterly down-valley winds. The SF_6 and oil-fog were released at 57 m; CF_3Br was emitted at 30 m above the surface. The release crane orientation was 114° with an average wind direction of 110° at 5.5 m/sec (estimated for the SF_6 release height). The wind measured at the 40 m level of Tower A varied from 82° to 132°. The average H_{crit} was 30 m.

As expected, the CF_3Br was transported around the sides (principally the north side) of CCB (see Figure 31), and the SF_6 generally went up and over the hill (see Figure 32). Evidently there was sufficient turbulence in the lee of CCB to diffuse the SF_6 to ground level, thereby producing the highest concentrations on the northwest lee side. Figure 33 shows the plume going up and over the north peak at 0209. Figure 34, which was taken later in the experiment at 0535, illustrates a plume trajectory typical of Case 210.

Case 205 (0400-0500)

This case is presented because it was used to illustrate the model evaluation techniques in Sections 4 and 5. It is representative of a near-neutral, east-southeast (118°) flow with a wind speed of 6.0 m/sec at the SF_6 local release height of 50 m. The release crane was located at an orientation of 120.5° at a distance of 1,156 m from the center of CCB.

Figure 35 presents the sampled ground-level SF_6 concentrations. Values are relatively low; the maximum occurs well below the relative height of the release (41 m). The observed variability of wind direction and concentrations suggest that the plume covers almost the entire hill during the hour.

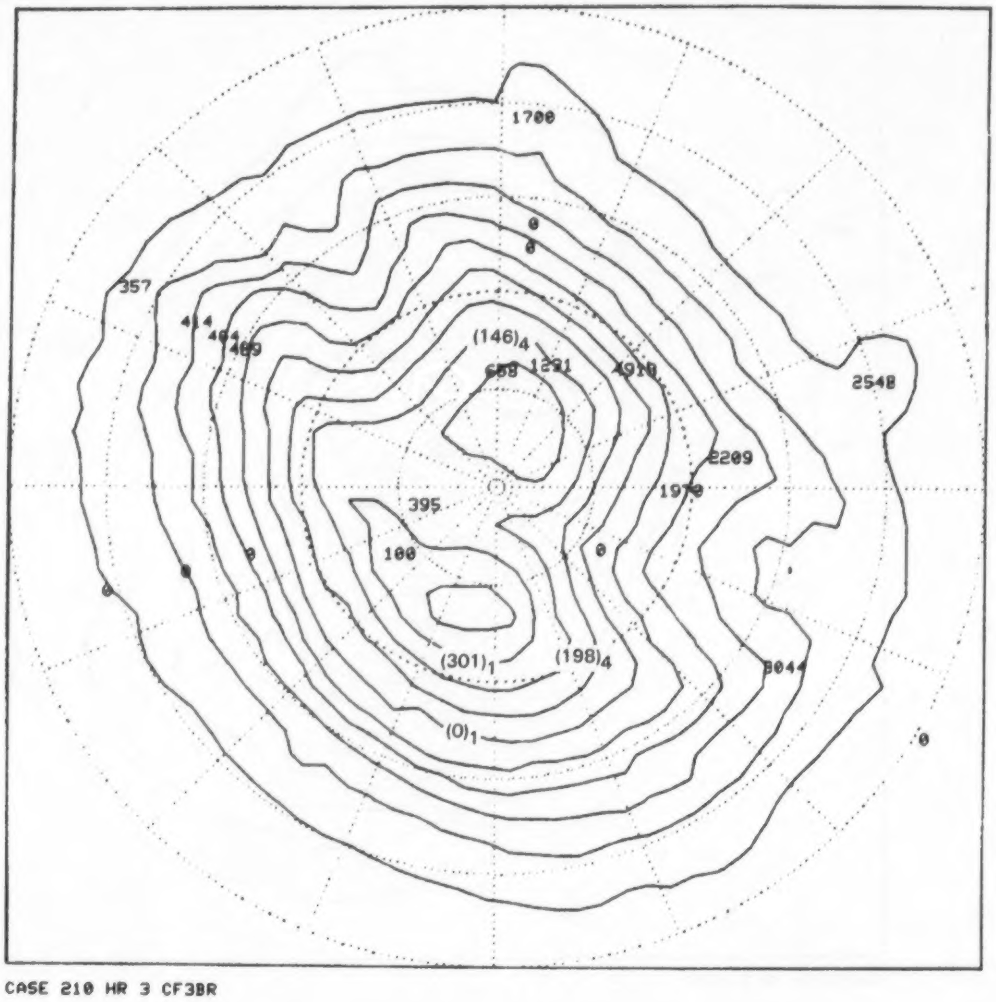

Figure 31. Observed CF_3Br concentrations (ppt) for Case 210, 0200-0300. Source: r = 1085 m, θ = 114.0°, relative height = 22.8 m, Q = 0.95 g/sec.

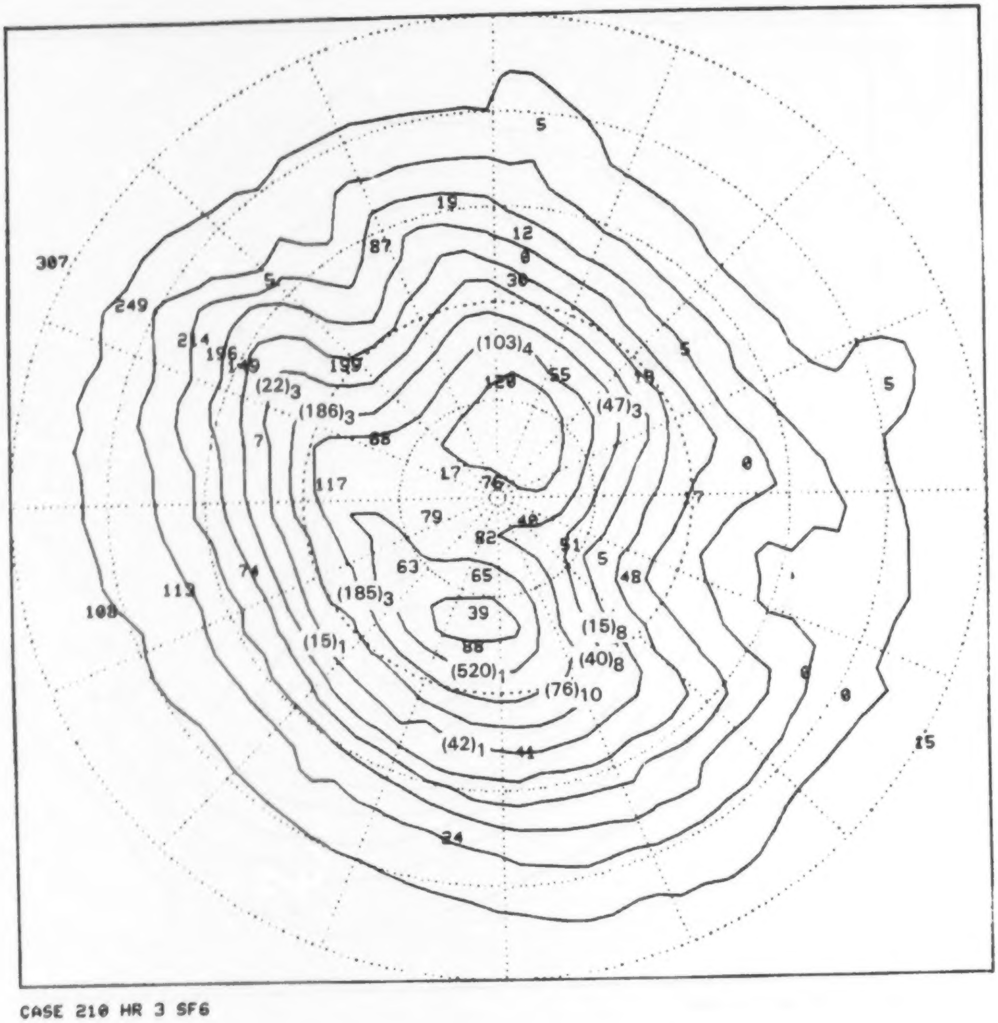

Figure 32. Observed SF_6 concentrations (ppt) for Case 210, 0200-0300. Source: $r = 1085$ m, $\theta = 114.0°$, relative height = 49.8 m, $Q = 0.16$ g/sec.

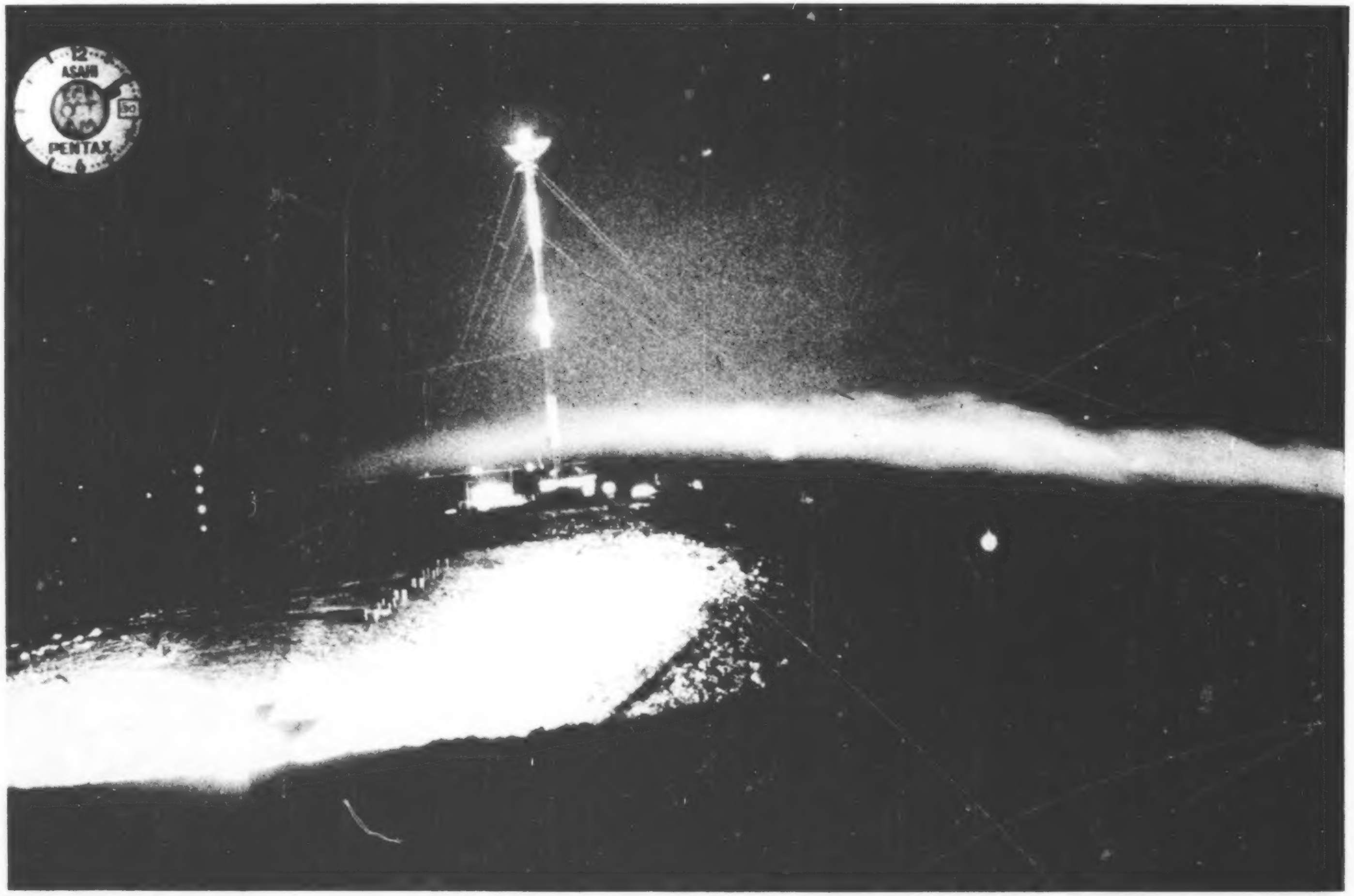

12
ASAHI
50
PENTAX
6

Figure 33. One-minute exposure looking from South Peak (Case 210, 0209 MST).

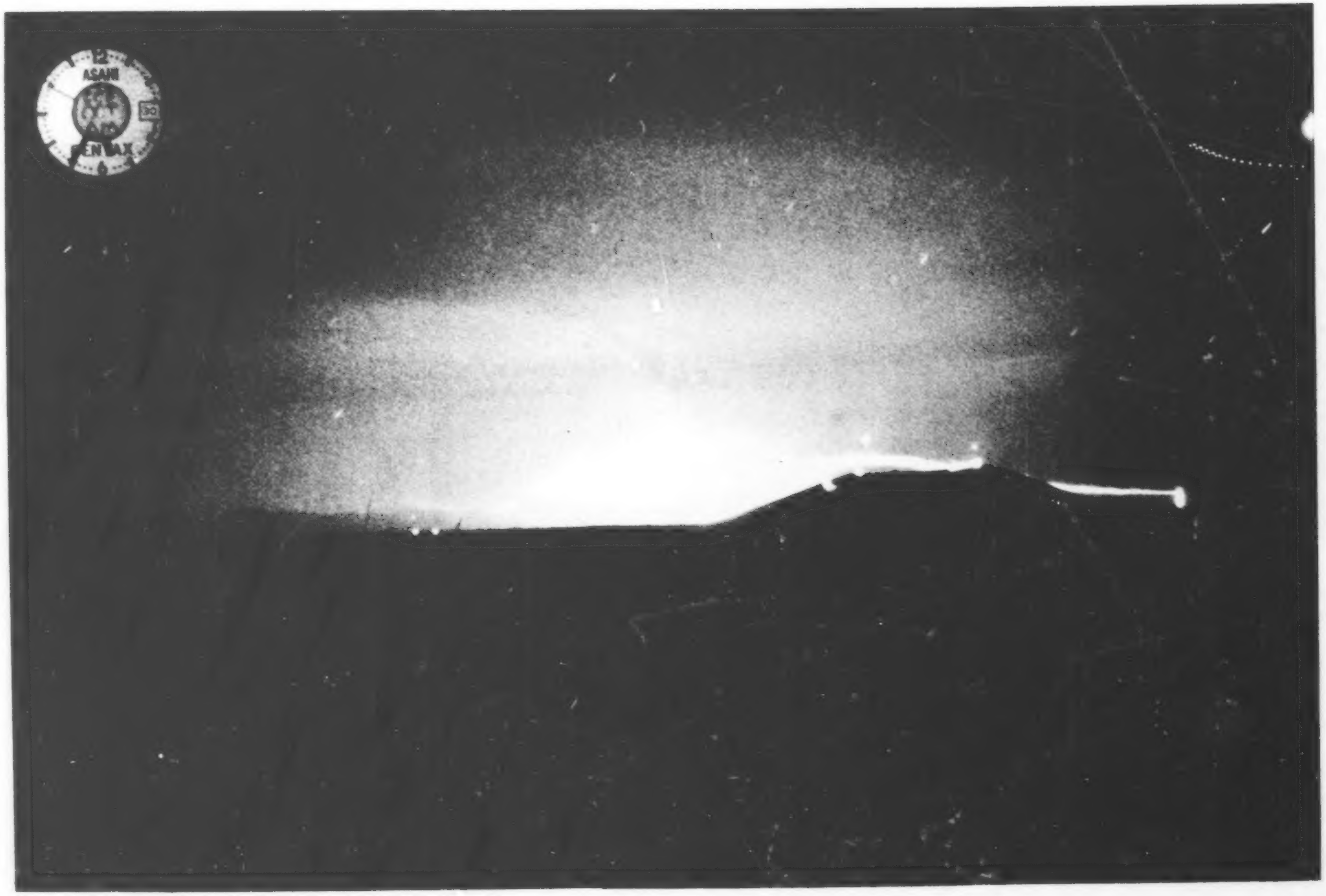
ASAHI
PENTAX

Figure 34. One-minute exposure looking from southwest (Case 210, 0535 MST).

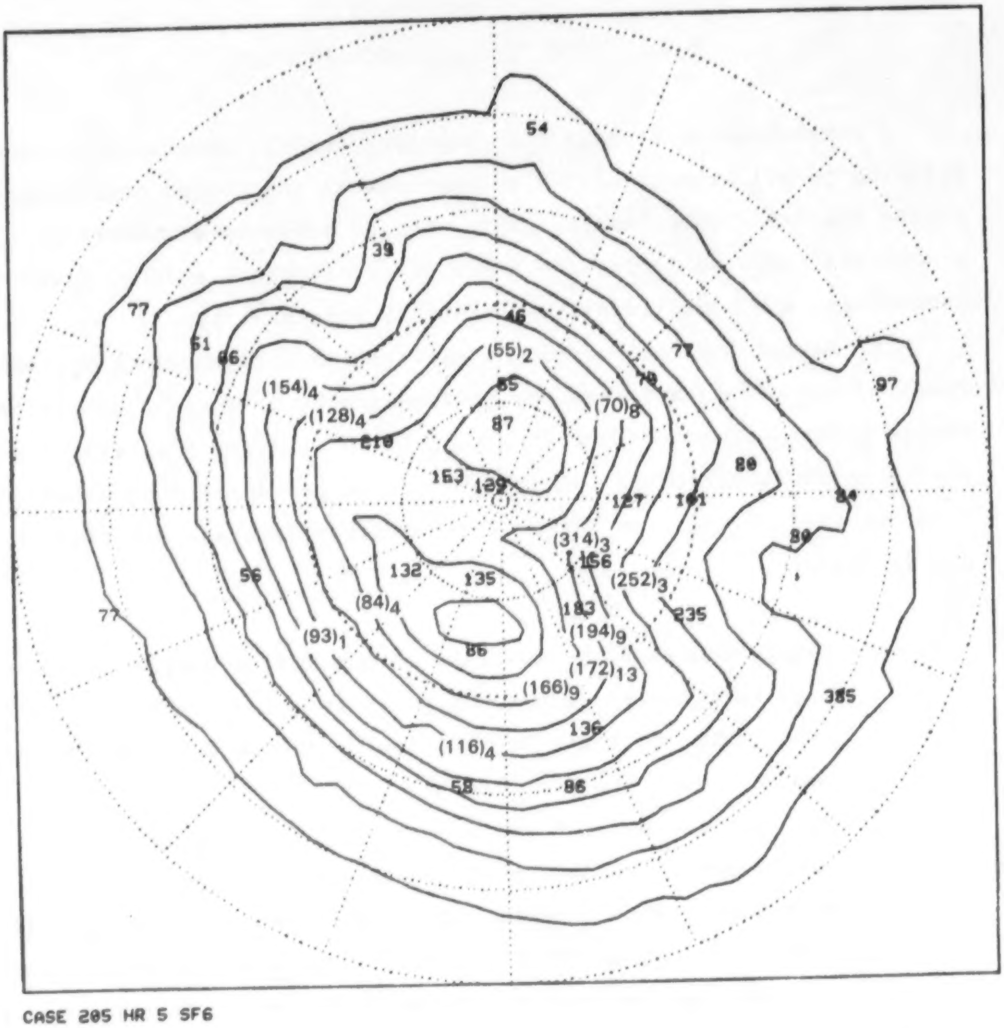

Figure 35. Observed SF_6 concentrations (ppt) for Case 205, 0400-0500. Source: $r = 1156$ m, $\theta = 120.5°$, relative height = 41.1 m, $Q = 0.09$ g/sec.

SECTION 3

QUALITY ASSURANCE PROGRAM

A comprehensive program plan provided quality assurance procedures relating to all aspects of the meteorological and tracer measurements taken during the field experiments. This section presents a summary of the procedures followed during the field study, external audits, data validation procedures, and a preliminary estimate of data quality.

All meteorological instrument calibration data have not yet been received from WSSI, nor have the preformance experiments been performed with sample wind instruments in a wind tunnel. Similarly, the results of some of the tests and experiments relating to tracer gas measurements have not yet been received by ERT from NAWC. These missing data and experiments include the following:

- sample degradation with time in the Tedlar sample bags after the bags were filled with known gases from the calibration cylinders (some data on sample degradation of actual experimental samples, however, are reported here);
- performance tests of the sequential bag samplers in an environmental chamber prior to the tracer experiments;
- experiments with flushing the sample bags with nitrogen to clean them of tracer gas in order to establish an effective procedure for cleaning the bags for reuse in the field experiments; and
- chromatograms from bags exposed to large dosages of particulates from orange smoke candles and smoke generators.

A final quality assurance program report will be produced when the full complement of inputs has been assembled and analyzed.

In general, the meteorological data are of excellent quality. Problems with UVW propellor transmitters seizing, propellors breaking, and communications failure between the data collector and the data stations resulted in a loss of about 18% to 20% of real-time meteorological data during the experiments. (Final data-capture statistics are not yet available.) This estimate of data loss is by measure, not by instrument; the failure of one U or V propellor transmitter results in the loss of all six of the measures that use its input. Pibal, tethersonde, and minisonde data may be used to fill in gaps in the definition of the flow approaching the hill, should a measurement from Tower A be missing or intermediate measurements be required.

The audit of the gas chromatographs by TRC indicates excellent accuracy of the tracer data. All gas chromatograph responses were within ±8% of the designated concentrations specified by the supplier of the audit gases. Nineteen of the 25 gas chromatograph audit points were within the ±5% accuracy range of concentrations specified by the supplier for the audit cylinders.

Preliminary precision information of the tracer measurements is presented in Section 3.2. In general, the precision statistics were very good for both the SF_6 and CF_3Br tracers.

3.1 Meteorological Data

3.1.1 Quality Assurance of Meteorological Data

The basic quality assurance program for meteorological data comprised the following procedures with appropriate documentation:

- performance and calibration checks of the DS-00 microprocessor data stations prior to start-up;
- mechanical checks and calibrations of all instruments at installation and before the tracer experiments;
- calibration checks (and, if necessary, recalibrations) of replacement instruments during the course of the field program;

- two independent audits of instrument accuracy and data system performance;
- calibration checks at system takedown; and
- real-time automated screening by the data collector computer for values out of range.

Although all of these procedures were implemented, some of the documentation has not yet been received by ERT.

The major quality assurance problems with the meteorological data were the result of unforeseen difficulties with equipment. The triaxial propellor (UVW) sensors, of which 48 were deployed in the network, occasionally became unresponsive. Sometimes they would stop turning almost completely, in which case the fault was easy to identify. More frequently, however, the failure was more subtle--a slight "stiffening" of the instrument. This could be identified only by the low ratio of crosswind intensity of turbulence (IY) to downwind intensity of turbulence (IX) if a U or V transmitter failed, or by changes in the relative values of U or V components with respect to an adjacent cup-and-vane wind set in similar flow conditions but separated by one hour or more. When a U or V propellor failed, it affected the values of WS, WD, IX, IY, and IZ.* If a W propellor failed, it affected only IZ. The data have been flagged accordingly.

The second piece of equipment that failed to perform well was the unshielded cable used for transmission of data between the shelters (located on the butte and at Tower A) and the data collector computer (in the operations trailer at Simco Road). Although ERT had specified shielded cable for this purpose, it could not be obtained from vendors in time for system start-up. These failures necessitated an unplanned requirement for detailed value-by-value examination of the measurements taken during the experiments.

---

*Measure codes are listed in Table 2; hourly average measures have the same code as the 5-minute measures with a "1" suffix added.

3.1.2 External Audits

Two independent audits of the real-time meteorological instruments and data system were performed during the first week of November 1980. TRC, under contract to ERT, audited the wind and temperature systems at every level of the six towers using conventional techniques including Haake temperature baths and synchronous motors. Meteorology Research, Inc. (MRI), represented by Thomas J. Lockhart and under contract to EPA, audited an easily accessible subset of temperature and UVW propellor systems using techniques devised by Mr. Lockhart. TRC audited the instruments' performance by checking the voltage output of the translator cards. The calibration of the data stations was audited separately by imposing a fixed, constant voltage on the inputs to the microprocessors for 10 minutes or more and checking the 5-minute averages archived in the data system against the measure values corresponding to the voltage applied. MRI's audit checked the 5-minute averages received by the data collector directly against the audit values. Cup-and-vane wind sets (Climatronics F460) and the orientation of the wind instruments were checked only by TRC.

The results of the audits are shown in Tables 6 through 14. The data for the temperature systems (Table 6) indicate that the errors found in TRC's audit are often of opposite sign from those found in MRI's audit. The largest error found by MRI, +0.40°C (at 2 m on Tower B near the ice point), corresponds to -0.15°C in TRC's audit. Conversely, the largest error found by TRC in a system also audited by MRI was -0.16°C (near the ice point at 2 m on Tower A), for which MRI reported an error of +0.12°C.

The TRC audit results of the nine resistance thermometric device (RTD) temperature systems indicate that the maximum measurement error was 0.20°C in magnitude. The errors at six of the 18 audit points lay within the resolution of the data system. The problem with the auditing of the fast-response bead thermistors at 10 m and 150 m on Tower A has been traced to an error in the color-coding of the wiring diagram supplied by Climatronics. This error was corrected in the actual wiring of the sensors but not on the diagrams in the system documentation left in the shelter. Consequently, the wrong wires were jumpered during the audit. This error

TABLE 6. AUDIT RESULTS: CLIMATRONICS TEMPERATURE SYSTEM

Tower	Level (meters)	Audit Temp. (°C)		Error Response-Audit (°C)	
		TRC	MRI	TRC	MRI
A	2	29.39	32.54	0.08	-0.08
		0.38	0.65	-0.16	0.12
		-	15.89	-	0.04
A	20	29.39	32.54	0.10	0.09
		0.38	0.65	-0.12	-0.14
		-	15.89	-	0.10
A	60	29.39	-	0.13	-
		0.38	-	-0.11	-
A	100	29.39	-	0.10	-
		0.38	-	-0.11	-
A	10	29.39	-	-8.75*	-
		0.38	-	-8.59*	-
	150	29.39	-	-8.64*	-
		0.38	-	-8.49*	-
B	2	30.06	35.41	0.07	-0.16
		-0.01	1.16	-0.15	0.40
		-	19.68	-	0.02
C	2	30.06	-	0.05	-
		-0.01	-	-0.15	-
D	2	30.06	-	0.07	-
		0.02	-	-0.13	-
E	2	30.06	33.15	0.07	-0.14
		-0.01	3.20	-0.13	0.00
		-	18.60	-	0.04
F	2	30.06	-	0.20	-
		0.02	-	-0.07	-

---

*The fast-response bead thermistors were audited incorrectly because of an error in the manufacturer's wiring diagram that had been corrected in the instruments' wiring but not in the diagrams kept in the shelter at Tower A.

TABLE 7. AUDIT RESULTS: CLIMATRONICS DELTA TEMPERATURE SYSTEM

Tower	Level (meters)	Bath Temp. (°C) TRC	Bath Temp. (°C) MRI	Error Response-Audit (°C) TRC	Error Response-Audit (°C) MRI
A	10	29.4	32.54	0.032	0.08
		0.4	0.65	0.024	0.16
		-	15.89	-	0.06
A	40	29.4	0.00	0.032	0.00
		0.4	0.65	0.012	-0.09
		-	15.89	-	0.06
A	80	29.4	-	Not working	
		0.4			
A	150	29.4	-	0.092	-
		0.4	-	0.076	-
B	10	29.6	35.41	0.044	-0.02
		-0.01	1.16	0.000	0.32
			19.68		0.00
B	30	29.6	-	-0.044	-
		-0.01	-	-0.008	-
C	10	29.6	-	-0.012	-
		-0.01	-	-0.004	-
D	10	29.6	-	0.048	-
		0.02	-	-0.012	-
E	10	29.6	33.15	-0.084	-0.13
		-0.01	3.20	-0.080	0.06
		-	18.60	-	0.06
F	10	29.6	-	-0.056	-
		0.02	-	-0.120	-

TABLE 8. AUDIT RESULTS: CLIMATRONICS UVW WIND SYSTEMS

Tower	Level (meters)	Audit Speed (m/sec)		Error Response - Audit (m/sec)					
				U		V		W	
		TRC	MRI	TRC	MRI	TRC	MRI	TRC	MRI
A	2	8.81	-	0.02	-	0.00	-	0.04	-
		-8.81	-	0.09	-	0.09	-	0.02	-
		0.00	0.00	0.09	-0.02	0.07	0.02	0.02	-0.01
		-	-0.15	-	-0.12	-	0.03	-	0.01
A	10	8.81	-	0.06	-	0.02	-	0.04	-
		-8.81	-	0.06	-	0.07	-	0.05	-
		0.00	0.00	0.07	-0.02	0.07	-0.02	0.04	0.01
		-	-0.16	-	-0.02				
A	40	8.81	-	0.03	-	0.09	-	0.09	-
		-8.81	-	0.01	-	0.07	-	-0.03	-
		0.00							
A	80	8.81	-	0.02	-	0.07	-	0.13	-
		-8.81	-	0.08	-	0.03	-	-0.07	-
		0.00							
A	150	8.81	-	-0.05	-	-0.10	-	-0.05	-
		-8.81	-	0.01*	-	-0.06	-	0.01	-
		0.00							
B	2	8.81	-	0.03	-	0.03	-	0.02	-
		-8.81	-	0.02	-	0.01	-	-0.04	-
		0.00	-	0.02	0.02	0.02	0.02	0.00	0.01
		-	-0.16	-	-0.01	-	0.04	-	-0.01
B	10	8.81	-	0.17	-	0.12	-	0.06	-
		-8.81	-	0.07	-	0.00	-	0.02	-
		0.00	-	0.12	0.07			0.06	0.05
			-0.16		0.08			-	0.05
B	30	8.81	-	0.12	-	0.12	-	0.15	-
		-8.81	-	0.02	-	0.01	-	-0.10	-
		0.00	-						

---

*Reading intermittent.

TABLE 8. (continued)

Tower	Level (meters)	Audit Speed (m/sec)		Error Response - Audit (m/sec)					
				U		V		W	
		TRC	MRI	TRC	MRI	TRC	MRI	TRC	MRI
C	2	8.81	-	-0.06	-	-0.01	-	-0.07	-
		-8.81	-	-0.11	-	-0.19	-	-0.01	-
		0.00	-	-0.07	-	-0.08	-	-0.03	-
C	10	8.81	-	0.03	-	0.02	-	-0.03	-
		-8.81	-	0.04	-	0.00	-	-0.01	-
		0.00	-	0.06	-	0.03	-	0.01	-
D	2	8.81	-	0.04	-	0.03	-	0.03	-
		-8.81	-	0.00	-	-0.02	-	-0.08	-
		0.00		0.05	-	0.03	-	0.00	-
D	10	8.81	-	0.06	-	0.00	-	-0.01	-
		-8.81	-	-0.14	-	-0.07	-	-0.05	-
		0.00		0.00	-	-0.01	-	-0.01	-
E	2	8.81	-	0.13	-	-0.62	-	-5.72	-
		-8.81	-	0.01	-	-0.13	-	-0.01	-
		0.00	0.00	0.08	0.12	0.07	0.12	0.03	0.05
		-	-0.16			-	-15.50*	-	0.04
E	10	8.81	-	0.13	-	0.18	-	0.11	-
		-8.81	-	0.06	-	0.05	-	-0.01	-
		0.00		0.11	-	0.12	-	0.04	-
		-	-0.16	-	0.08				
F	2	8.81	-	-0.01	-	-0.02	-	-0.05	-
		-8.81	-	-0.05	-	0.00	-	-0.02	-
		0.00	-	0.02	-	0.02	-	-0.01	-
F	10	8.81	-	-0.04	-	0.02	-	-0.06	-
		-8.81	-	-0.10	-	-0.06	-	0.02	-
		0.00	-	-0.01	-	-0.02	-	0.01	-

---

*Communications error

TABLE 9. AUDIT RESULTS: F460 WIND SPEED SYSTEM

Tower	Level (meters)	Audit Speed (m/sec)	Error Response-Audit (m/sec)
A	2	8.69	0.16
	10	8.69	0.16
	150	8.69	0.15
B	10	8.69	0.15
	30	8.69	0.26
C	10	8.69	-0.16
D	10	8.69	-0.14
E	10	8.69	-0.13
F	10	8.69	-0.15

TABLE 10. AUDIT RESULTS: CLIMAIRONICS F460

WIND DIRECTION ALIGNMENT TO LANDMARK TEST

Tower	Level (meters)	Landmark Used	Audit Direction (degrees)	Error Response-Audit (degrees)
A	2	Tower B	177.0	8
	10	Tower B	177.0	1
	150	Tower B	177.0	1
B	10	Tower A	357.0	0
	30	Tower A	357.0	0
C	10	Tower A	353.0	-2
D	10	Computer trailer	99.8	-1
E	10	Middle of large Butte-West	279.8	-1
F	10	Middle of large Butte-West	279.3	-2

TABLE 11. AUDIT RESULTS: CLIMATRONICS F460 WIND DIRECTION LINEARITY TEST

Tower	Level (meters)	Audit Direction (degrees)	Response (degrees)	Error Response-Audit (degrees)
A	2	356	356	0
		86	85	-1
		176	177	1
		266	266	0
A	10	357	357	0
		87	87	0
		177	179	2
		267	268	1
A	150	359	359	0
		89	88	-1
		179	179	0
		269	270	1
B	10	356	356	0
		86	88	2
		176	178	2
		266	266	0
B	30	359	359	0
		89	90	1
		179	180	1
		269	270	1
C	10	349	349	0
		79	82	3
		169	170	1
		259	260	1
D	10	360	360	0
		90	90	0
		180	182	2
		270	271	1
E	10	359	359	0
		89	91	2
		179	182	3
		269	270	1
F	10	364	364	0
		94	93	-1
		184	184	0
		274	272	-2

TABLE 12. AUDIT RESULTS: ORIENTATION OF V PROPELLOR CROSSARM

Tower	Level	Error Relative to True North
A	2	1°42' West
	10	2°47' East
	30	2°47' East
	80	8°14' East
	150	6°47' East
B	2	2°54' East
	10	1°28' East
	30	2°54' East
C	2	1°58' East
	10	2°22' East
D	2	56' East
	10	14' East
E	2	12' West
	10	19' East
F	2	1°56' East
	10	1°56' East

TABLE 13. AUDIT RESULTS: F460 WIND DIRECTION SYSTEMS ERRORS

Tower	Level	Landmark Orientation	Landmark Alignment	Linearity		Total Error	
				Low	High	Low	High
A	2	0	8	-1	1	7.0	9.0
	10	0	1	0	2	1.0	3.0
	150	1.0	1	-1	1	1.0	3.0
B	10	-1.8	0	0	2	-1.8	0.2
	30	-1.8	0	0	1	-1.8	-0.8
C	10	-0.5	-2	1	3	-1.5	0.5
D	10	Not done	-1	0	2	-1.0	1.0
E	10	0	-1	0	3	-1.0	2.0
F	10	0.7	-2	0	-2	-1.3	3.3

Note: Errors in degrees.

TABLE 14. AUDIT RESULTS: LANDMARK AND NORTH STAKE ORIENTATION ERRORS

		Landmark Orientation Errors		
Tower	Audit Landmark	Audit Measurement	ERT Measurement	Error
A	Tower B	177°3'	177°	-3'
A	Tower C	173°22'	173°24'	2'
B	Tower A	358°46'	357°	-1°46'
C	Tower A	353°50'	353°24'	-26'
D	None done	---	---	---
E	Center of Butte	279°43'	279°48'	5'
F	Tower A	18'	1°	42'

NORTH STAKE ORIENTATION ERRORS

Tower	North Stake Error
A	2°43'
B	1°36'
C	47'
D	1°11'
E	2°11'
F	4°15'

was discovered and duplicated by WSSI technicians after the instruments had been returned to Fort Collins. When properly wired and audited, the bead thermistors gave satisfactory responses. Because these probes were used only to calculate σ_T, however, their actual accuracy is not of primary concern.

The results of the auditing of the RTD ΔT systems are shown in Table 7. (TRC reported the 80 m ΔT to be "not functioning," but the data from Case 213, which began at midnight after the audit, show the 80 m ΔT to be working satisfactorily. In any case, there are no audit data for this instrument.) Twelve of the 18 good audits points taken by TRC on the ΔT systems lay within the performance goal of 0.05°C; ten of the points lay within the PSD guideline criterion of 0.003°C error per meter of vertical separation; and 14 of the points lay within the union of the two goals, that is, the larger of 0.05°C or 0.003°C/m. The only points outside this criterion were the 2-to-10 m ΔT's on Towers E and F.

Again, the TRC results were not generally duplicated by the MRI audit. Eight ΔT audit points, two on each of four different systems, were done at comparable temperatures by both MRI and TRC. Of these, three of MRI's results showed errors of opposite sign to those in the TRC results, one showed no error where TRC had found one, and the largest error (+0.32°C) found by MRI corresponds to an error-free point in TRC's audit.

TRC audited the 48 Climatronics UVW propellors by coupling the propeller shafts to a synchronous motor running at 1,800 rpm (equivalent to 8.81 m/sec wind speed), checking the voltage response of the translator cards, and converting it to meters per second. The propellors were spun in both positive and negative directions. The voltage output of the systems was also checked when the shafts were held stationary. The UVW audit data are shown in Table 8. An accurate but intermittent response was measured from the 150 m U component when it was spun in the negative (easterly) direction. Large negative errors were found in the V and W components at 2 m on Tower E when spun in the positive directions (southerly and upward, respectively); these errors were -0.62 m/sec for V and -5.72 m/sec for W. Other than these anomalous readings, the largest error for any of the propellor instruments was 0.19 m/sec at Tower C's 2 m V component when spun negatively.

According to Climatronics' technical staff, the calibration of a WC-11 propellor sensor and translator is practically linear from the bottom of the signal range at maximum negative speed (-25 m/sec or 0 volts) across the zero speed point (2.5 volts) to maximum positive speed (+25 m/sec or 5 volts.) Consequently, if a large error occurs at a positive speed of 8.8 m/sec and a small error at a negative speed of -8.8 m/sec, there should be a substantial error near zero approximately equal to the mean of the errors at +8.8 and -8.8 m/sec. This was not the case for the audit data from the V and W transmitters at 2 m on Tower E. Furthermore, an error of -5.72 m/sec such as that indicated by TRC for the 2 m W prop on Tower E would be apparent in the data collected as either strongly negative W's or very large IZ's when the propellor changed its direction of rotation. Neither of these discrepancies appears in the data, however.

MRI examined a small sample of the UVW instruments at the 2 and 10 m levels of Towers A and B and the 2 and 10 m levels of Tower E, which ERT's quality assurance officer requested that MRI examine after TRC's anomalous results. MRI spun the propellor shafts with a small motor that gave a low equivalent wind speed of about 0.15 m/sec, which is close to the instrument threshold. The MRI audit did not find the anomaly in the 2 m W component of Tower E when it was spun in the negative direction, the error being +0.04 m/sec at an imposed speed of -0.15 m/sec, but it did turn up an even more extreme anomaly of -15.51 m/sec in the V component when it was spun at -0.16 m/sec. This error was due to a communication problem in which the request for this measure value from the data collector was received by the data station DS-00 as requested for the along-wind intensity of turbulence, which was returned to the data collector in integer form and interpreted as a V-component value. Other than the Tower E 2 m errors, the largest error found by MRI when spinning the transmitters at low speed was -0.12 m/sec at the 2 m U-component of the 150 m tower. This instrument had given a positive error of 0.09 m/sec when spun at -8.81 m/sec by TRC.

Both MRI and TRC checked the instrument output when the UVW shafts were held stationary. Of the 15 transmitters checked by both at this zero wind-speed point, four of the errors were of opposite sign in the two audits; these four errors were also associated with the largest differences in voltage response of the translator cards, the largest such difference being 0.012 volts, or 0.25% of the instrument range of 5 volts. The largest zero offset found by TRC among these 15 instruments was 0.12 m/sec for the 10 m U on Tower B, for which MRI found an offset of 0.07 m/sec; the largest zero offset found by MRI (checking the system all the way through to the data archive) was 0.12 m/sec in the 2 m U-component on Tower E, for which TRC found an offset of 0.08 m/sec.

TRC's audit of the nine F460 wind speed systems (see Table 9) showed a maximum error of 0.26 m/sec at a cup speed corresponding to approximately 8.7 m/sec. The maximum misalignment of the F460 wind vanes with respect to ERT's landmarks (see Table 10) was 2° except for the 2 m level of the 150 m tower, which was mounted on a steel post about 4 m southwest of the tower to keep it somewhat removed from the disruptive effects of the junction box, tower elevator, and structural reinforcements of the tower's bottom end. The boom at this level could be rotated fairly easily by any passerby. The maximum nonlinearity of the F460 vane outputs was 3° (see Table 11). TRC's calculations of the errors in ERT's directions to landmarks and north stakes are tabulated in Table 12, and the total errors of the F460 wind vanes are shown in Table 13. The maximum total error was estimated to be 7° to 9° at the 2 m level of Tower A. All other vane systems were judged to be accurate to within approximately 3°.

The orientation of the UVW systems was audited by TRC by checking the axis of the V-component transmitter with respect to true north (see Table 14). The 80 m and 150 m systems at Tower A were oriented approximately 8° and 7° east of true north, respectively; these misalignments were clear to an observer looking up the tower from the ground. The 16 other UVWs were judged to be aligned within 3° of true north.

Finally, the vertical orientation of the W propellors and the cup-and-vane transmitters was checked by TRC by sighting with a transit from two directions approximately 90° apart. The results of this test were not quantified, but the audit report states that the worst misalignment was less than 2°.

3.1.3 Data Validation Procedures

No changes have been made to the values of the measurements in the data base in response to the results of the audits for several reasons. First, the audits are not generally consistent with each other, so that it is not clear what to do to improve the accuracy of most of the data. Second, the calibration history of all the instrumentation has not been systematically studied for consistency. Third, for those instruments for which an error was demonstrated in an audit, is discernible in the data, and was perhaps even visible to the naked eye (such as the misorientation of the 80 and 150 m UVW sets), it may not be prudent to make adjustments until more information is available.

The direct measures from misaligned propellor sets, for example, are the U and V components and the downwind and crosswind intensities of turbulence IX and IY. On the premise that the wind speeds determined from U and V are independent of wind direction, adjustments could be made to the wind directions and new U and V components resolved. The magnitude of wind speed is dependent upon the wind direction because of the propellor's non-cosine response to the wind stack angle. Errors introduced in U and V, and therefore wind speed and wind direction, by this deviation from cosine response have not yet been examined in detail. When more conclusive information is available, data derived from propellors can be corrected for instrument response, and adjustments for misalignments can then be made.

Data taken during 17 of the 18 tracer experiments of Phase II are being validated according to the procedures described below. (Data from Case 212 have not yet been validated because the tracer plumes never hit the hill.) The 5-minute average data were the basic measurements received by the data collector. All hourly averages except the turbulence intensities and standard deviations of wind direction and temperature were calculated by the data collector from the 5-minute data. Therefore, the major validation effort was directed to the 5-minute data.

The communications problems resulting from the unshielded cable caused two major types of errors. The first type was a miscommunication from a data station to the data collector which was not always picked up by the parity checking on the transmission. Such an error resulted in a value that looked peculiar in the time series of values for the measure affected. From the redundant wind measurements (both cup-and-vane and UVW propellors), errors of this type could be fairly easily verified for wind speed and direction except at the 40 and 80 m levels of Tower A, where the propellors were alone and vertically separated by 30 m or more from the nearest source of data for comparison. Because of the strong thermal layering during many experiments, it was often not feasible to verify a communications "hit" by comparison at these levels, and the determination that a value was suspect or in error depended entirely on whether it was unreasonable or out of place in the time series. Calculated temperatures at 10 m and 150 m could be validated by comparison with the values from the fast-response thermistors at these sites. Temperatures and temperature differences at other heights on Tower A were validated by comparison with the temperatures above and below the height being validated.

Fortunately, few errors of communication from the data stations to the data collector resulted in measure values that were in the range of possible values. Most were recognized as faulty by the data collector and identified as missing by an "M" flag.

A far more common problem of communication occurred in the data requests from the data collector to the data stations. A request for a wind component might be received as a request for a temperature, and the temperature would therefore be returned to the data collector, which would put it into the data base as the wind value. All measure values were transmitted to the data collector as integers (called "counts") between 0 and 1,023 inclusively. The data collector converted them to proper engineering units by interpolation in the range of the measure. A temperature transmitted in error as a wind component would therefore not appear in the data base as the value of the temperature that was sent but rather as the value of the wind component appropriate to the number of counts corresponding to the temperature. Consequently one could look through all the data for the 5-minute scan in which the suspect value occurred for another measure value that had the same associated counts. If such a measure was found, the suspect value was regarded as bad.

Typically, the same error in transmission of data requests to the data stations occurred more than once during the course of an experiment, and this recurrence confirmed the fault. The data collector sometimes recognized that an error of this sort had occurred and flagged the measure value in the subsequent scan with an "M." The data base therefore contained good values flagged "M" as well as bad values with no error flag.

To expedite the time-consuming error check through all the measurements taken during the experiments, the 5-minute data were retrieved from the data base in time-series files for each experiment. In general, each of these files included all the 5-minute measures for one measurement height on a tower; there are 19 files per experiment in this "edit" format. The program quality assurance officer drew up a series of guidelines for editing these files and a set of data flags for identifying the quality of the data. The flags are the following:

" " (blank): Both the editor and the data system concur that the value is valid.

"M" (missing): Both the editor and the data system concur that the value is invalid.

"U" (unavailable): The value is unavailable because of data collector or data station failure.

"B" (bad): The editor believes the value is invalid but the data system did not catch the error; this flag is therefore associated either with instrument malfunction or communications problems.

"R" (restored): The editor believes the value is valid, although the data system had flagged it "M."

"C" (calculated): The editor calculated a derived measure (WD, WS, SP, DR, TC), usually from "R" values.

"S" (suspect): The editor believes the data are somewhat in error but cannot confirm either an instrument malfunction or communications failure.

"L" (at limit): The measure is at the upper limit of its range and the "true" value exceeds that shown. The instrument ranges were not themselves exceeded during the experiments, and this flag is necessary only for the turbulence data (IX, IY, IZ, SD) in very light and variable winds.

No data have been estimated and inserted into the data base.

The program quality assurance officer personally conducted a final quality check on all of the real-time meteorological values before they were released to the EPA. In this final editing, he tried to maintain a balance between the premise that all data are potentially valid and the premise that no data are above suspicion. Consequently, if no instrument failure or communications error could be verified, a value was regarded as valid unless it appeared to be unreasonable with respect to comparable values adjoining it in time or space. This is generally not a difficult judgment to make, but in some situations a value may look peculiar but not completely unreasonable and might indicate a significant phenomenon. Such data were left unflagged if they were not misleading or were flagged "S" if they were sufficiently removed from the general trend to substantially influence an hourly average.

The different characteristics of propellor wind sets and cup-and-vane systems are well demonstrated in the CCB data. In general, the vector resultant wind speed from propellors was less than the vector resultant wind speed from a cup-and-vane set at the same location. The ratio of WS to SP decreases from 0.8 to 0.9 in high-speed, smooth flows down to 0.5 or less in light and variable winds. In near-calm conditions, the props were observed to be more responsive to gentle puffs than the vanes, so that a 5-minute wind direction and wind speed resolved from the props might be 175° at 0.2 m/sec whereas the corresponding cup-and-vane direction and speed might be 245° at 0.5 m/sec. Both these pairs of wind measurements might appear in the data without any error flag because there was no indication of instrument malfunction or communications error. The differences between the measurements are thus attributable to the differences in the instruments.

Similarly, the response of propellor sensors is somewhat direction-dependent. Often the difference between WD and DR at a site changed markedly when WD passed through a cardinal direction such as 0°, 45°, 90°, or 135°. Again, the measures were both retained as valid in the data base. The users of the data should be aware of these instrumental characteristics. To invalidate the data from the propellors would require that WS, WD, IX, IY, and IZ all be flagged "B" or "S." Such a requirement would decrease the utility of the data enormously.

The differences between the speeds and directions from the two kinds of instruments show quite general consistency with the differences anticipated as a result of the departure from the cosine response curve. Furthermore, the horizontal intensities of turbulence IX and IY tend to become more nearly equal when the average angle of attack of the wind is approximately equal on both propellers (i.e., directions near 45°, 135°, 225°, 315°), whereas IX tends to exceed IY when the average angles of attack are substantially different (i.e., directions near 0°, 90°, 180°, 270°). This consistency suggests that the quality of the UVW data might significantly improve if corrections were applied similar to those described by Horst (1973), which were derived from comparisons of propellor data and sonic anemometer data. ERT has been unable to find any similar comparative analysis of data for the Climatronics system.

The procedures for data validation were based on common sense, comparison between neighboring sensors, searching for measures whose contemporaneous values were associated with the same "counts" as a suspect measure, reports of malfunctions in the field logs by the instrument technicians and others, and by a learned feeling for how instruments track one another when they are working correctly. Examples of an as-taken file and its edited version are given in Figures 36 and 37.

When editing and flagging of the 5-minute data were completed, hour-averages of the direct measures other than the turbulence measures were calculated by computer from the 5-minute values; hour-averages of the derived measures were in turn calculated from these. A set of classification criteria and data quality flags has been established for the hour-averages; it is shown in Table 15.

```
  YR JDY HR  SEC     AL1T    AL2TD    AL2TC     AL3T    AL4TD    AL4TC     AL5T    AL6TD    AL6TC     AL7T    AL8TD    AL8TC
1980 305  0    0      811    2 331     000M    4 643    5 890    6 701    8 631    9 115    9 927    9 961    9 643     000M
1980 305  0  300      731    2 742    3 475   5 347M    7 160    7 893    9 413  -5 000M     000M    9 961    9 545   10 435
1980 305  0  600      890    1 979     000M    5 582    7 023    7 913    9 022    8 920    9 809    9 883    9 213     000M
1980 305  0  900      811    1 784    2 595    5 582    6 750     000M    9 257    9 096     000M -30 000M    9 154     000M
1980 305  0 1200      342    2 742     000M    4 252    6 241    6 505    8 944  -5 000M     000M -30 000M    9 409     000M
1980 305  0 1500      420    2 937    3 436    4 878  -5 000M     000M -30 000M    8 900    9 399 -30 000M    9 252    9 751
1980 305  0 1800 -30 000M    1 368    4 179    5 816    5 733    6 544    8 084    8 275    9 086    9 413    8 744    9 555
1980 305  0 2100      577  5 000M     000M    5 894    6 457    6 955    8 475    8 744    9 242    9 492    9 154    9 653
1980 305  0 2700    - 362    2 077    1 716    4 956    6 437    5 997 -30 000M    9 233    8 793    9 101    9 800     000M
1980 305  0 3000 -30 000M    2 429    2 458    5 816  -5 000M     000M    7 849  -5 000M     000M -30 000M    9 154    9 340
1980 305  0 3300 -30 000M    1 354    2 243    5 425    6 515    7 170    8 084    4 873    5 528 -30 000M    8 627    9 282
1980 305  1    0 -30 000M    1 667     000M -30 000M  -5 000M     000M -30 000M  -5 000M     000M -30 000M    8 959    9 457
1980 305  1  300 -30 000M  5 000M     000M    6 285  -5 000M     000M -30 000M   8 842M     000M -30 000M    9 096    9 438
1980 305  1  600    - 127  5 000M     000M    5 347  -5 000M     000M    7 771    8 685    8 558    9 101    9 389     000M
1980 305  1  900    - 362    1 413     000M    5 425    7 219    6 857    7 458  -5 000M     000M -30 000M    9 467    9 106
1980 305  1 1200    - 203    3 035     000M    6 207    7 219    6 935    7 849    8 939    8 656    9 022    9 370    9 086
1980 305  1 1500 -30 000M    5 479     000M    6 833    7 610    7 248    8 162  -5 000M     000M    9 101    9 897     000M
1980 305  1 1800    - 909    7 845     000M    7 380    8 431    7 522    7 849    9 526    8 617 -30 000M   10 406    9 497
1980 305  1 2100   -1 378    6 887     000M   25 914    8 705    7 326    7 458    9 780    8 402    8 866   10 464     000M
1980 305  1 2400 -30 000M    3 426    1 813    3 236  -5 000M     000M    7 693   10 093    8 480    8 866   10 367     000M
1980 305  1 2700    - 987    3 739    2 752    4 252    8 157    7 170 -30 000M    9 780     000M    8 866    9 995    9 086
1980 305  1 3000    - 362    4 169    3 807    6 285    7 630    7 268    8 397   -5 000     000M    8 866    9 370    9 242
1980 305  1 3300      029    5 029     000M    6 129  -5 000M     000M   8 788M   8 939M     000M    8 788    8 959     000M
1980 305  2    0   -1 691    5 518     000M    5 191    8 666    6 818    8 397  -5 000M     000M    8 710   10 875    9 027
1980 305  2  300  -2 395M    5 420     000M    4 330    8 490    6 017    7 615   11 012    8 539    8 710   11 364    8 891
1980 305  2  600 -30 000M  5 000M     000M    4 487    8 705    6 075    7 615   11 344    8 715 -30 000M   11 794    9 164
1980 305  2  900   -2 786    6 867     000M    4 956  -5 000M     000M    7 693      826   -1 960    8 710   11 970    9 027
1980 305  2 1200   -2 551    6 730     000M    5 425  -5 000M     000M -30 000M  11 149M     000M    8 788   12 028     000M
1980 305  2 1500   -2 864    7 219    4 198    5 738   10 093    7 072    8 397   11 755    8 734 -30 000M   13 514     000M
1980 305  2 1800   -1 177    7 082    3 905    5 816   10 601    7 424   8 006M  -5 000M     000M    8 553   14 668   11 491
1980 305  2 2100   -3 490    5 850    2 361    4 721    9 858    6 369    7 224  -5 000M     000M    8 162   14 629   11 139
1980 305  2 2400   -3 333  5 000M     000M    2 688    8 803    5 469    6 442  -5 000M     000M -30 000M   13 006    9 673
1980 305  2 2700   -1 691  5 000M     000M   32 639  -5 000M     000M    6 520    8 822    7 131 -30 000M   11 403     000M
1980 305  2 3000   -1 222    4 091     000M    4 643    7 180    5 958    6 598  -5 000M     000M -30 000M   11 383   10 161
1980 305  2 3300   -1 222  5 000M     000M    4 878    6 984    5 762    6 442    8 177    6 955    7 380   11 559   10 259
1980 305  3    0   -1 378    4 619    3 240    4 330    6 750    5 371    6 207  -5 000M     000M -30 000M   11 931     000M
1980 305  3  300   -3 099    6 535     000M    4 330    8 724     000M    6 285   10 152    7 053    6 911   13 866   10 767
1980 305  3  600   -4 272    6 300    2 028    3 939    9 311    5 039    5 973   10 671    6 349    6 520   14 159    9 888
1980 305  3  900 -30 000M    5 870    2 067    3 157    8 236    4 433    5 660    4 638      445    6 598   13 729     000M
1980 305  3 1200   -3 021  5 000M     000M    3 470    7 473    4 453    5 582   9 506M     000M    7 771   13 221   10 275
1980 305  3 1500   -3 490    5 127     000M    3 236    7 923    4 433    5 503   10 171    6 681    8 240   13 925   10 200
1980 305  3 1800   -4 115    4 775      660 -30 000M    8 275    4 159    5 503   11 108    7 053 -30 000M    4 482      288
1980 305  3 2100   -4 037    4 232      894    2 688  -5 000M     000M    5 816   11 285    7 248    8 162   13 045    9 164
1980 305  3 2400   -3 959    5 293    1 090 -30 000M    8 079    4 120    5 660   11 149    7 190    7 849   12 771     000M
1980 305  3 2700 -30 000M    5 870    1 989    3 001    7 884    4 003    5 660   10 953     000M    7 537   12 713    8 910
1980 305  3 3000 -30 000M   5 870M     000M    3 236    8 118    4 550    5 894   10 586     000M -30 000M   12 361    8 793
1980 305  3 3300    3 724  5 000M     000M    2 923    8 509    4 785    6 051   10 894    7 170    7 537   12 322    8 597
1980 305  4    0 -30 000M  5 000M     000M    2 766  -5 000M     000M    5 582    5 244     000M    6 833   11 657    7 933
1980 305  4  300   -4 272    4 130     000M    2 297    8 275     000M    5 503  10 797M     000M    6 364   11 989    7 561
1980 305  4  600   -4 506    4 247    - 181    1 984    9 330     000M -30 000M   10 621    6 193    6 051   11 012    6 584
1980 305  4  900 -30 000M    3 974    - 533   32 639  -5 000M     000M    5 816   10 347     000M    5 738   10 914     000M
1980 305  4 1200 -30 000M    4 971      152    2 923  10 327M     000M    5 738   10 562     000M    5 582   11 188    6 369
1980 305  4 1500   -4 585  5 000M     000M    1 906    9 019    5 391    5 582   10 054    5 626 -30 000M   10 152    5 723
1980 305  4 1800    4 194  5 000M     000M    2 375  -5 000M     000M    5 347    9 448    5 330    5 112    9 761    5 645
1980 305  4 2100    4 037  5 000M     000M    4 157    9 076    4 883    5 112    9 174    5 137 -30 000M    9 663    5 626
1980 305  4 2400 -30 000M    5 342     000M    4 018    9 467    5 112    5 191    9 761    5 567    5 269   10 327     000M
1980 305  4 2700    4 741    5 907    1 168    4 096    9 839     000M    5 347   -2 322     000M    5 503   10 758    6 017
1980 305  4 3000 -30 000M    6 167    1 891    4 174  -5 000M     000M    5 660  -5 000M     000M    5 660   10 523    6 251
1980 305  4 3300 -30 000M    5 987     000M    4 409    8 744    5 098 -30 000M  -5 000M     000M    5 738    9 897    6 251
1980 305  5    0   -3 803    6 163    1 970    4 018  -5 000M     000M    5 347  -5 000M     000M -30 000M   10 152    6 349
1980 305  5  300   -4 037    5 831     000M    3 783    8 920    4 883 -30 000M  -5 000M     000M -30 000M   10 582    6 544
1980 305  5  600    3 333  -5 000M     000M    4 018    8 333    5 000    5 503   9 154M     000M -30 000M   10 073     000M
1980 305  5  900 -30 000M    4 326    1 696    3 705    7 688    4 746    5 503    8 803    6 173    6 285    9 800     000M
1980 305  5 1200   -2 473    4 365    1 891    3 627    7 278     000M    5 660    8 744    6 271    6 364    9 487    7 014
1980 305  5 1500   -1 535    4 013    2 478    3 861    6 789    5 254    5 894  -5 000M     000M    6 520    8 685    7 151
1980 305  5 1800    1 378    4 326     000M    4 330    7 043    5 665    6 129    7 805    6 114    6 676    9 037     000M
1980 305  5 2100   -2 004    4 150     000M    4 252    7 551    5 547    6 207  -5 000M     000M    6 833    9 956     000M
1980 305  5 2400   -1 300    3 152    1 852    4 174    6 554     000M    5 816    7 336    6 036    6 442    9 604    8 460
1980 305  5 2700    - 907    2 586    1 598    3 314    5 596    4 609    5 269    6 554    5 567    5 660    3 915     000M
1980 305  5 3000  30 000M    2 077    1 891    2 610    3 974    3 768    4 643  -5 000M     000M    5 503    7 669     000M
1980 305  5 3300 -30 000M    2 351    2 302    2 766    3 622    3 573    4 487    5 166     000M    5 973    7 727    7 913
1980 305  6    0    1 202    1 393    2 595    2 845    2 449     000M    4 800    4 285    5 567 -30 000M    6 867     000M
1980 305  6  300 -30 000M    1 158    2 517    2 845    2 566    3 925    5 034    4 384     000M    6 364    6 593    7 952
1980 305  6  600    1 281    1 178     000M    2 923    3 035    4 238    5 112    4 638     000M    6 676    6 730     000M
1980 305  6  900    1 124    1 530    2 654    3 392    3 289    4 413 -30 000M    4 619    5 743    6 364    6 105    7 229
1980 305  6 1200    1 202    1 784    2 986    3 470    3 231     000M -30 000M  -5 000M     000M -30 000M    5 987    7 190
1980 305  6 1500 -30 000M    1 549    2 986    3 392    2 996    4 433    4 878    3 915    5 352    5 973    6 574     000M
1980 305  6 1800    1 359    1 588    2 947    3 392    3 016    4 374    4 878    4 071    5 430    5 894    7 532     000M
1980 305  6 2100    1 359    1 647    3 006    3 627    3 152    4 511    5 034    4 286     000M    5 973    8 627    9 985
1980 305  6 2400    1 359    1 510     000M    3 627    3 152    4 511    5 034    4 150     000M    5 582    7 473    8 832
1980 305  6 2700    1 124  -5 000M     000M    7 693    3 035    4 159    4 721  -5 000M     000M -30 000M    5 362     000M
1980 305  6 3000    1 046  -5 000M     000M    3 627   2 996M     000M    4 409    3 661    4 707 -30 000M    4 795    5 841
1980 305  6 3300      420  -5 000M     000M    3 548  -5 000M     000M    4 330  -5 000M     000M    4 800    5 186    5 606
1980 305  7    0    - 362  -5 000M     000M    3 314  -5 000M     000M    4 096    4 580    4 218    4 565    5 440    5 156
1980 305  7  300   -1 691    3 055    1 598    2 532    4 619     000M -30 000M  -5 000M     000M -30 000M    6 476    4 394
1980 305  7  600 -30 000M    4 599    1 109    1 828    6 359    2 869 -30 000M    7 317    3 827    4 018    7 903    4 335
1980 305  7  900  -3 881M  5 000M     000M    2 141    7 121    2 928    3 783    7 903    4 022    4 096    8 470    4 511
1980 305  7 1200   -4 115    5 440    1 325    1 906  -5 000M     000M    3 705    8 040    3 925    4 018    8 548    4 433
1980 305  7 1500   -4 037    5 674    1 657    2 219    7 297     000M    3 705    7 942    3 827 -30 000M   -4 902     000M
1980 305  7 1800   -3 959    6 065    2 107    2 845    7 395     000M    3 705    7 884    4 081    4 096   8 333M     000M
1980 305  7 2100 -30 000M    6 046    2 634    3 236    7 121     000M    3 939    7 669    4 257 -30 000M    8 548    5 137
1980 305  7 2400 -30 000M    6 046    2 634    3 236    6 965    3 710 -30 000M    7 649     000M    4 487    8 314     000M
1980 305  7 2700   -2 786    3 641    1 090    1 906    5 557    3 006    3 627    6 769    4 218    4 330    7 493    4 941
1980 305  7 3000   -1 222  -5 000M     000M    - 987  -5 000M     000M    3 548    5 264    4 277    4 643    6 496    5 508
1980 305  7 3300    - 596    2 116    1 676   2 532M  -5 000M     000M    3 939  -5 000M     000M -30 000M    6 320    5 802
1980 305  8    0    - 127  5 000M     000M    2 610    3 270    3 299    4 018    4 482     000M -30 000M    5 381     000M
```

Reproduced from
best available copy.

Figure 36. Example of a data file.

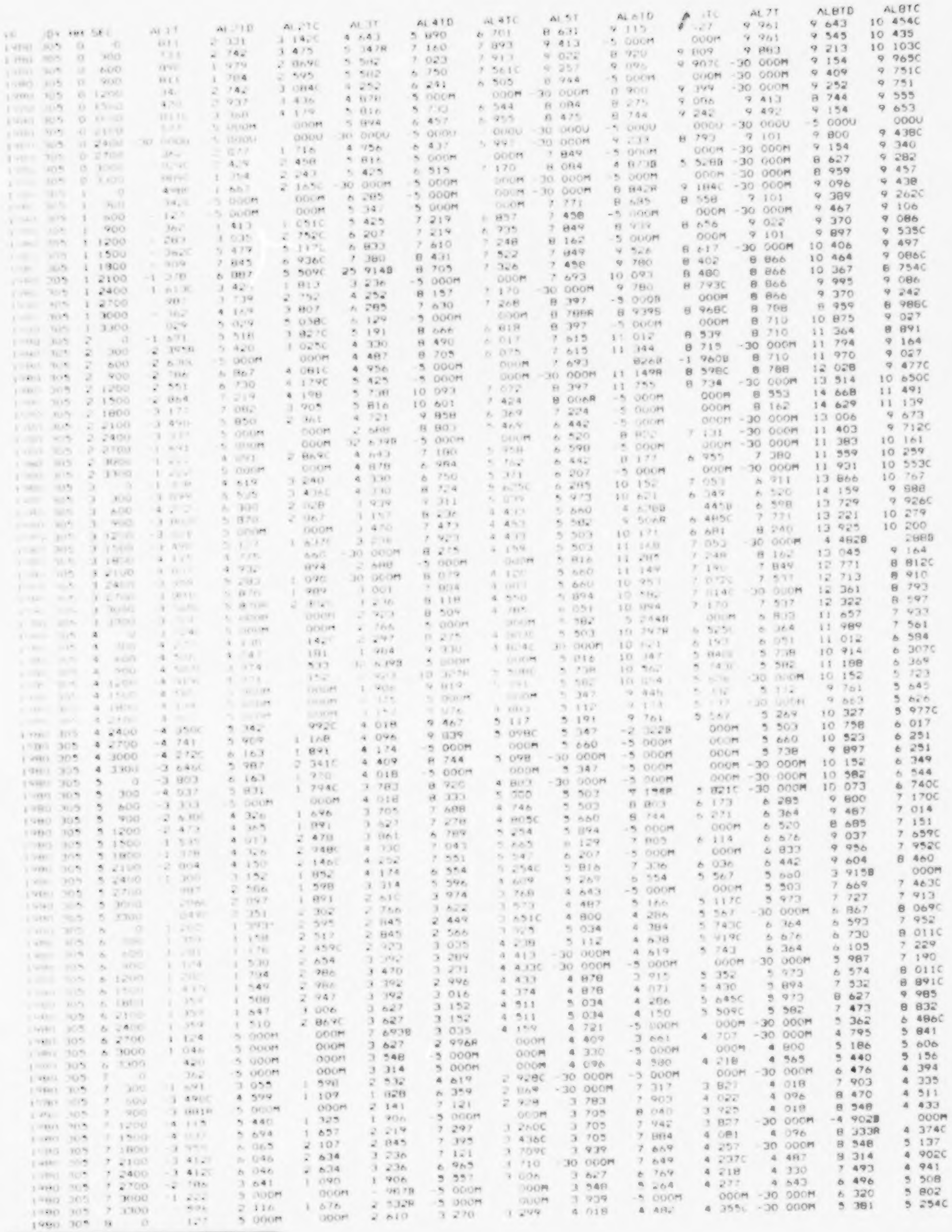

Reproduced from best available copy.

Figure 37. Example of an edited data file.

TABLE 15. CLASSIFICATION CRITERIA AND DATA QUALITY FLAGS FOR HOUR-AVERAGES PRODUCED FROM 5-MINUTE DATA

Definitions:

- Invalid 5-minute data are those flagged either M (Missing), B (Bad), or U (Unavailable).
- Valid 5-minute data are those flagged either " " (Good), C (Calculated) or R (Restored).
- Doubtful 5-minute data are those flagged either S (Suspect) or L (at Limit).

MB = Number of missing and bad 5-minute values
U = Number of unavailable values
GCR = Number of good, calculated, or restored values
SL = Number of suspect or at-limit values

Cases

I. $MB + U = 12$

1) $U < MB$ Hr-avg = -999.0; Flag = M
2) $U \geq MB$ Hr-avg = -999.0; Flag = U

II. $6 < MB + U < 12$

1) $U < MB$ Hr-avg = $\frac{\sum \text{valid} + \sum \text{doubtful}}{GCR + SL}$; Flag = M

2) $U > MB$ Hr-avg = Same ; Flag = U

III. $MB + U \leq 6$

1) $GCR > 10$ Hr-avg = $\frac{\sum \text{valid}}{GCR}$; Flag = " "

2) $7 < GCR$ Hr-avg = $\frac{\sum \text{valid}}{GCR}$; Flag = I (Incomplete)

3) $GCR < 6$ and $SL = 1$ Hr-avg = $\frac{\sum \text{valid} + \text{doubtful}}{GCR + SL}$; Flag = S

4) $GCR < 6$ and $SL > 1$

   1) $S > L$ 1 Hr-avg = $\frac{\sum \text{valid} + \text{doubtful}}{GCR + SL}$; Flag = S

   2) $S < L$ Hr-avg = Same ; Flag = L

3.2 Tracer Data

3.2.1 Quality Assurance Procedures During Field Study

Strict quality assurance procedures were followed during every phase of the tracer sampling and analysis field program. These procedures included:

- multipoint calibrations of every gas chromatograph at the start and finish of each analysis day;
- span checks every four hours on every gas chromatograph;
- recounts (samples analyzed twice on different gas chromatographs) on 5% of the total samples;
- background air samples upwind of the tracer release in every experiment;
- pairs of co-located samplers set up at two locations in every experiment;
- testing of sample degradation with time in the sample bags up to 42 hours;
- an independent audit on the accuracy of the SF_6 analysis system.

Each of these quality assurance procedures is discussed below in more detail.

Calibrations were performed on each gas chromatograph at the start and finish of each analysis day. However, because a typical analysis day was 16 hours long, a span check with one calibration gas (usually 100 ppt SF_6) was performed every four hours on every chromatograph to check any response drift with time. If the span check showed a greater than 5% difference from the most recent calibration, that chromatograph was completely recalibrated with all of the calibration gases. On the average, one extra calibration during the analysis day was performed for each chromatograph because of failure to pass a span check.

Roughly 5% of the samples analyzed in each test were analyzed again, usually on a different gas chromatograph.* The results of these recounts are summarized in Table 16. The results are segregated into low and high SF_6 and CF_3Br concentrations because of the higher imprecision inherent in concentrations near the lower detection limit. The recount statistics on the higher SF_6 and CF_3Br concentrations were very good, with 89% of the SF_6 recounts greater than 50 ppt within ±15%, and 95% of the CF_3Br recounts greater than 1,000 ppt within ±10%. The CF_3Br recount statistics were somewhat better than the SF_6 recounts, possibly because all CF_3Br samples were analyzed on one gas chromatograph.

Background air samples taken upwind of the tracer release system consistently recorded zero concentrations for both SF_6 and CF_3Br. Therefore, contamination from sources other than the release was not a problem. Perhaps the best documentation of the lack of background air contamination was Case 212, in which the tracer plume missed the hill for the entire 8-hour experiment. No concentrations higher than 5 ppt SF_6 (the detection limit of the gas chromatographs) were recorded during this 8-hour experiment, indicating no background contamination nor any residual contamination in the sampler or the sample bags from previous experiments.

At two locations during each experiment, two samplers were placed side by side and set to sample air during the same time periods. These co-located samplers were used to assess the variability in the sampling technique. The results are shown in Table 17. Because of random sampler failure, the co-located data capture was relatively poor. The co-located statistics were somewhat poorer than the recount statistics, with only 50% of the SF_6 co-located samples (greater than 50 ppt) within ±15%. One reason for this relatively poor comparison may have been the intermittent pump sampling; because the samplers took in air for only one second every 15 seconds, they were not sampling the same air parcels because the samplers were driven by separate timers.

---

*All CF_3Br analyses were done on gas chromatograph No. 8, the AID instrument, since this was the only one that could separate SF_6 and CF_3Br. Hence, all recounts for CF_3Br were also done on this gas chromatograph.

TABLE 16. RECOUNT STATISTICS

Percent Difference	No. SF_6 Samples		No. CF_3Br Samples	
	≤50 ppt	>50 ppt	≤1000 ppt	>1000 ppt
0-5	221	140	11	17
5-10	26	65	9	2
10-15	28	42	2	0
15-20	13	16	2	1
20-25	11	5	0	0
25-30	15	5	1	0
>30	57	4	1	0
Total	371	277	26	20

TABLE 17. CO-LOCATED SAMPLER STATISTICS

Percent Difference	No. SF_6 Samples		No. CF_3Br Samples	
	≤50 ppt	>50 ppt	≤1000 ppt	>1000 ppt
0-5	28	3	7	0
5-10	0	3	1	0
10-15	0	3	1	0
15-20	1	1	0	0
20-25	0	1	1	2
25-30	1	1	0	0
>30	17	6	3	0
Total	47	18	13	2

During most experiments, all samples were analyzed within 24 hours; the longest time period between sampling and analysis for any experiment was 48 hours. A test was made to determine if any sample degradation took place in the Tedlar bags by analyzing five test samples immediately and at various times up to 42 hours later. The results are shown in Table 18. As shown, no sample degradation was apparent for any of the samples; the concentration variability was well within that demonstrated by the recounts.

3.2.2 External Audits

Under subcontract to ERT, Edmund J. Burke, manager of quality assurance at TRC Environmental Consultants, supervised an independent performance audit of the four chromatographs that were operational in the Boise laboratory on the audit day. The results, shown in Table 19, indicate that 15 of the 20 audit samples were within the ±5% limit of accuracy given by the supplier (±3% for Gas 3), and all samples were within ±8%.

Because the calibration gases used by NAWC and the audit gases used by TRC were all supplied by Scott-Marrin, Inc., of Riverside, California, the audit gases were subsequently analyzed by C. Ray Dickson at the NOAA Air Resources Laboratory (ARL) in Idaho Falls to check the concentrations (and hence the calibrations of the GCs in Boise) against standards other than Scott-Marrin's. The results of these replicated analyses are also listed in Table 19. If the results for Gas 5 are disregarded because the concentration was outside the range of calibration of the ARL system, the mean analysis for each of the other four audit gases was within 6% of the concentration indicated by Scott-Marrin.

3.2.3 Data Validation Procedures

As discussed in Section 2.3, all sampler and analysis data were entered into the ERT computer during the field study, and concentrations were then calculated on the basis of the two closest calibrations before and after the analysis time. Because of the time constraints during the experiment, it was not possible to double check the data entry process during the field study. All tracer data files were therefore validated after the field experiment was over.

TABLE 18. SAMPLE DEGRADATION TEST

Sample	Time in Bag (hr)	SF_6 (ppt)	CF_3Br (ppt)
1	0	11	490
	6	9	510
	11	13	480
	18	15	420
	42	9	450
2	0	23	2,970
	6	21	3,030
	11	22	3,250
	18	22	3,090
	42	21	3,130
3	0	24	5,530
	6	21	5,550
	11	24	5,670
	18	24	5,520
	42	22	5,630
4	0	45	6,270
	6	46	6,330
	11	51	6,340
	18	47	6,400
	42	48	6,500
5	0	68	4,100
	6	67	4,110
	11	66	4,160
	18	72	4,110
	42	66	4,100

TABLE 19. RESULTS OF ANALYSES OF TRC'S SF_6 AUDIT GASES

(concentrations in ppt)

Concentration Analysis	SF_6 Audit Gases				
	Gas 1	Gas 2	Gas 3	Gas 4	Gas 5
Supplier's Analysis*	99	247	505	1,000	10,300
GC No. (Make)					
5 (S^3)	105	260	518	1,000	10,100
6 (S^3)	101	244	483	954	10,400
7 (S^3)	96	241	465	958	10,500
7 (S^3)**	96	234	471	950	10,300
8 (AID)	99	264	510	989	10,700
Avg/Std Dev	100/3.8	252/11.4	494/24.5	975/22.7	10,400/250
ARL/NOAA Analysis	95	235	484	1,060	7,990$^+$
Std Dev (No. of pts)	2.5(22)	2.6(19)	5.1(19)	11.6(10)	15.6(10)
Percent Differences					
GC 5 - Supplier	6.1	5.3	2.6	0.0	-1.9
GC 6 - Supplier	2.0	-1.2	-4.4	-4.6	1.0
GC 7 - Supplier	-3.0	-2.4	-7.9	-4.2	1.9
GC 8 - Supplier	0.0	6.9	1.0	-1.1	3.9
Average	1.3	2.2	-2.2	-2.5	1.2
GC 5 - ARL	10.5	10.6	7.0	-5.7	--$^+$
GC 6 - ARL	6.3	3.8	-0.2	-10.0	--
GC 7 - ARL	1.1	2.6	-3.9	-9.6	--
GC 8 - ARL	4.2	12.3	5.4	-6.7	--
Average	5.5	7.3	2.1	-8.0	--
ARL - Supplier	-4.0	-4.9	-4.2	6.0	--

Mean Absolute Percent Differences

NAWC GCs - Supplier	3.1%	Avg NAWC GCs - Supplier	1.7%
NAWC GCs - ARL	6.2%	Avg NAWC GCs - ARL	5.6%
ARL - Supplier	4.8%		

---

*Gas supplier certified Gas 3 to ±3%, other gases to ±5%.

**This audit of GC 7 was done with audit gases first injected into Tedlar sampler bags and then into the GC; results were not used in the remainder of this table.

+ARL's GC was not calibrated for SF_6 concentraitons as high as Gas 5 and gave a low response.

The entire tracer data base (over 14,000 data points) was methodically checked line-by-line against the original data sheets. This validation process revealed numerous simple data entry errors, primarily in the sampler on-off times, which were relatively easy to correct. Other discrepancies, such as uncertain sampler locations, were resolved using best judgment. Questionable data that could not be resolved satisfactorily (such as unknown sampler times) were deleted from the data base. Questionable tracer concentrations, which conceivably could be resolved by reviewing the original recorder strip charts and integrator tapes, were indicated by a "Q" in the tracer data files. These questionable data consisted mainly of recounts and co-located samples that differed by more than ±30%, in addition to other probable errors in transcription from the integrator tapes to the data sheets.

The systematic line-by-line check of the original data sheets was complemented by a number of computer tests on the data base. These quality assurance computer checks included:

- A printout of any sampler on-off times outside the time window of the experiment and any times indicating other than 10-minute or hourly averages. In many of the tracer tests, some samples were actually taken after the experiment had concluded; these data have been kept in the tracer data base for possible use in following the tracer decay with time after the release was stopped.
- A printout of all tracer data indicating the same location and on-off times. This check revealed a number of duplicate and erroneous entries, as well as the correct co-located sampler data.
- A comparison of all recount data (bags that were analyzed twice on a different gas chromatograph). The recounts are tabulated in the data base by the fictitious "75Z" sampler location.
- A printout of all SF_6 concentrations higher than 1,000 ppt and all CF_3Br concentrations higher than 10,000 ppt. These high tracer concentrations were then checked again for accuracy against the original data sheets.
- A printout of any sampler locations other than those used in the field experiments.

All obvious discrepancies found by the computer checks were corrected. The data sheet verification and computer checking validation procedures necessitated corrections in roughly 10% of the total number of data points.

The tracer data files now contain four different alphabetic codes for each sample:

- G - good sample
- B - bad sample (a bag half-full or less but which could still be analyzed)
- R - recount
- Q - questionable concentration (generally, recounts and co-located samples that differed by more than ± 30%)

It may be possible to resolve the questionable concentrations by reviewing the original recorder strip charts and integrator tapes. In the evaluation and testing of the various air quality models in Sections 4 and 5, only those tracer concentrations considered good were used in the analyses.

SECTION 4

AIR QUALITY MODELS EVALUATED

4.1 Introduction

One key objective for this phase of the program was to evaluate existing complex terrain models against the CCB field data. The performance of the Valley model is of special interest because it is the only complex terrain screening model recommended for regulatory use by the EPA. Comparisons of Valley estimates of the peak hourly concentrations with observed peak hourly concentrations not only test the model's ability to estimate the peak tracer concentration during the field study but also offer references of model performance against which to evaluate other complex terrain models. Other models chosen with the concurrence of the EPA Project Officer for evaluation against the CCB observations were COMPLEX I, COMPLEX II, and PFM. Two new experimental algorithms--one for flow over the crest of the hill (Neutral model), the other for stable flow around the hill (Impingement model)--were developed in this phase of the program.

None of these more refined models has been validated or accepted for regulatory use. COMPLEX I and COMPLEX II have been issued by EPA only for public testing and evaluation. PFM may be made available soon (for the same purpose) as a modeling system (called COMPLEX/PFM) similar to the COMPLEX models. The two new experimental models are very preliminary, contain many partly tested algorithms, and have no regulatory status. The following subsections briefly describe each model and its application to the CCB data.

4.2 Valley Model

4.2.1 Description

The Valley model (Burt 1977) is recommended by EPA for screening analyses in support of regulatory decisions (Budney 1977). Valley is designed to provide an estimate of the maximum 24-hour pollutant concentration expected to occur on elevated terrain near a point source of air pollution in any one-year period. This concentration is computed with a steady-state, univariate Gaussian plume dispersion equation, modified to provide a uniform crosswind distribution over a 22.5° sector, using assumed worst-case meteorology.

The model assumes that the plume travels toward nearby terrain with no vertical deflection until the centerline of the plume comes to within 10 m of the local terrain surface. (Thereafter, the centerline is deflected to maintain a stand-off distance of 10 m from the terrain surface.) The plume is considered to impinge upon the terrain at points where terrain height equals the plume height, and the impingement point used in the calculation of maximum plume impact is the nearest such topographic point as viewed from the source, independent of hourly wind direction.

Worst-case meteorology is that combination of wind speed and Pasquill-Gifford (PG) dispersion stability class leading to the highest concentration at the impingement point. For most large sources of air pollution, a stack-top wind speed of 2.5 m/sec and PG stability class F are recommended for the vertical growth of the plume under inversion conditions at night when plume impingement is most likely.

The model estimate is implied to be a 1-hour average concentration. The 24-hour average concentration is estimated by dividing this 1-hour average concentration by four, on the premise that the plume may affect a specific point for no more than six hours in any 24-hour period.

It should be stressed that because neither the tracer source release heights, crane locations, nor meteorology were equivalently "persistent" from hour to hour during the actual experiment, the CCB data base is not appropriate for testing the Valley model as it is used in regulatory applications. (The CCB field experiment was not intended specifically to validate or invalidate the Valley model but rather to assemble a data base that will support the development and refinement of progressively better modeling approaches for plume interactions with complex terrain.)

4.2.2 Application Procedures

The longest steady averaging period for tracer releases and concentrations in the CCB field study was four hours. Most steady averaging periods were between one and two hours. Consequently, only 1-hour Valley estimates were compared with maximum observed hourly tracer concentrations.

Release crane positions during the experiments ranged from a distance of 538 m to a distance of 1,452 m from the center of the hill. The local release heights of the nonbuoyant tracer gas varied from 15 m to 60 m. The distance to the nearest point of impingement was obtained from a contour map of the hill for each hour of the 45 case hours modeled. (Section 5.1 lists those experiment case hours included in the model evaluation.) These distances ranged from 213 m to 867 m. In each instance, the difference between the local elevation at the crane position and the zero height contour on the hill was taken into account to maintain the level plume geometry of the model. The local elevation at each release location was interpolated from the nearest survey points and the shape of the local hill contours.

Concentration estimates scaled by the emission rate were computed by:

$$\frac{C}{Q} = \frac{(2.03)(10^6)}{\sigma_z ux} \exp(-0.5\ (H/\sigma_z)^2), \tag{7}$$

which is derived from Equation 2-1 of the Valley User's Guide (Burt 1977). C is in units of $\mu g/m^3$, and Q is in units of g/sec.

The standard deviation of the vertical pollutant distribution (σ_z) is calculated from:

$$\sigma_z = 0.362\ x^{0.55} - 2.7 \tag{8}$$

The constants in this equation are taken from Table 2-1 of the Valley User's Guide. They are applicable for PG stability class F over a range of x between 100 and 1,000 m, which includes all of the impingement distances developed for the 45 test case hours.

The wind speed was set to 2.5 m/sec, and the stand-off distance (H) was fixed at 10 m to be consistent with the regulatory applications of Valley. However, because the 10 m value is not based on any theoretical analysis, it may not be an appropriate scale for the narrow plume configuration of the tracer experiments (compared to plume sizes encountered with large pollutant sources). Therefore, parallel computations are also presented for the centerline (i.e., center of the plume) concentration at the impingement point, not including a surface reflection contribution.

4.3 COMPLEX I and COMPLEX II Models

4.3.1 Description

COMPLEX I and COMPLEX II are sequential complex terrain models designed to estimate 1-hour, 3-hour, 24-hour, and annual pollutant concentrations resulting from emissions from many point sources. Concentrations are estimated at many receptors using hour-by-hour meteorological data.

Several terrain treatment options (formulated by the Complex Terrain Team at the February 1980 Chicago Workshop on Air Quality Models) are available in the COMPLEX models. The standard option for PG stability classes E and F simulates the plume behavior contained in the Valley model. This was the option selected for comparison with the CCB field data. (The COMPLEX models also contain a buoyancy-induced dispersion option, but this feature was not used in this modeling because the tracer releases are not buoyant.)

COMPLEX I is a univariate Gaussian plume model with 22.5° sector averaging in the horizontal. It uses the PG stability class system. COMPLEX II differs from COMPLEX I only in its representation of crosswind plume spread. Whereas COMPLEX I assumes a 22.5° horizontal sector averaging, COMPLEX II assumes the familiar crosswind Gaussian profile. (In all other respects, the two models are identical.)

COMPLEX I is essentially an extension of the direct-impingement Valley model to hourly averaged wind speed, wind direction, and stability class instead of the assumed worst-case meteorology; and COMPLEX II merely replaces Valley's 22.5° horizontal sector averaging with a Gaussian crosswind profile. For neutral or unstable conditions, COMPLEX I and COMPLEX II permit different (nonimpingement) terrain assumptions. For stability classes A through D, the terrain treatment allows the plume centerline to rise over terrain features but at a height less than its initial height over flat terrain. Its actual height at any point is computed from its initial height, the local terrain height, and a plume path coefficient.

4.3.2 Application Procedures

With the concurrence of the EPA Project Officer, it was decided that for efficiency, the evaluations of COMPLEX I and COMPLEX II with the CCB data base would actually be carried out by embedding the essential computational algorithms of these two models within a flexible, research-oriented computer code. The COMPLEX algorithms are invoked by selecting specific options for plume path coefficients, dispersion parameters, sector averaging, and surface reflection treatment. The flexibility inherent in this code structure will allow the testing of various permutations of the COMPLEX modeling assumptions in future analyses.

In addition, because this modeling svstem was developed by ERT specifically for the CCB field experiment, it can access any portion of the CCB data archive. It retrieves such information as the locations, elevations, and validated concentrations of all samples recorded, hourly average winds, and other field data for a given hour. The predictive segment of the code is set up for real-time application via an interactive terminal. It also allows a wide choice of user input and data override options, control over postprocessing, data archiving and file management, and statistical and graphical displays.

Input data for the models consist of hourly average wind speed and direction, source location, source height, stability class, receptor location, and receptor height. Receptor information is provided for all potential (93) sampling locations. Although the samplers were designed to measure tracer concentrations no closer to the surface than 1 m, no receptor height offset was used in the modeling because the overall model resolution is no more accurate than 1 m. Source locations are input to the nearest meter and nearest 0.5 degree (polar coordinates referenced to the center of the hill). Release heights relative to the zero height contour on the hill are input to the nearest 0.1 m. Average wind speed is input to the nearest 0.5 m/sec, and the wind direction is input to the nearest whole degree. Data used in the modeling are summarized in Section 5.2.

Stability classes used in the modeling required special treatment. No attempt was made before the fact to select only the one PG stability class that is most appropriate for a given hour. Instead, both models were run three times for each hour, assuming (in turn) stability classes D, E, and F. Thus, for each hour of observational data, six model predictions were generated--three for COMPLEX I, three for COMPLEX II--with the following rationale.

The PG stability classification scheme, in conjunction with the PG dispersion coefficients, is strictly applicable only to near-surface releases; its use to characterize dispersion of plumes at elevations of 30 m to 40 m in a very stable, layered flow is less justified. It was therefore prudent to run COMPLEX I and COMPLEX II with the same range of stability classes for all of the case hours and compare observed and predicted concentrations for each hour to judge whether the PG classification scheme was appropriate.

We made no attempt to compare COMPLEX I and COMPLEX II to the CCB data in terms of 3-hour or 24-hour averages because the source position or release height was often changed during a field experiment. The CCB field experiment does not provide a basis for evaluating the multiple-hour (running average) performance of these models; only the 1-hour averages may be legitimately compared.

4.4 Potential Flow Model (PFM)

4.4.1 Description

The PFM was developed and refined by ERT under EPA Contract 68-02-2759 (Isaacs et al. 1980; Bass et al. 1981; Strimaitis et al. 1981). Grounded in both empirical evidence and theoretical arguments, PFM takes as its starting point the fact that as air flows over and around terrain features, an embedded plume will experience regions of acceleration and distortion along its trajectory. For flow situations in which vertical density gradients are unimportant and surface boundary layer effects can be ignored, inviscid potential flow theory provides an analytical tool for approximating velocity fields, streamline trajectories, and plume deformation in the presence of simple, isolated terrain features.

The model calculations of terrain-modified plume dispersion coefficients and surface concentrations are based largely on work by Hunt and Mulhearn (1973) and Hunt and Snyder (1978) on the theory of turbulent, Gaussian-like plumes embedded within potential flow fields. Strimaitis et al. (1981) describe additional modifications made to incorporate more general isolated terrain features. They present a method for incorporating PFM computations within the framework of sequential complex terrain models (such as COMPLEX).

PFM has recently undergone final revisions allowing it to operate within the framework of the COMPLEX models--specifically, a version called COMPLEX/PFM (Strimaitis et al. 1981). The version of PFM used in comparisons against the CCB field data is fully equivalent to the PFM algorithm in COMPLEX/PFM. However, more data analysis is required in running PFM separately, as some required input data are computed within COMPLEX/PFM.

The PFM code is used to generate a potential flow streamline that defines the path of a plume in neutral flow about an isolated hill or ridge (modeled as either an ellipsoid or a bluff). The code then alters the path and velocity along the path to approximate changes introduced by stratification as measured by the hill Froude number. Line integrals from the source then determine cumulative distortions in the plume sigmas.

Output from PFM includes a file containing the coordinates of the plume trajectory and a file containing modification factors (for σ_y, σ_z, plume elevation, and centerline concentration) that connect flat terrain values to values consistent with the computed flow field.

Other subroutines within COMPLEX/PFM use this information in computing concentrations at all receptors. A postprocessor performs this function in a similar way here. The postprocessor evaluates plume-receptor geometry, computes modified plume σ_y and σ_z values based on Turner workbook coefficients (although other functions may be substituted easily), and uses the hourly emission rate and wind speed to calculate the field of concentration estimates in a format consistent with the requirements of the statistical analysis software.

4.4.2 Application Procedures

PFM requires the following information:

- hill shape: along-wind and crosswind aspect ratios,
- effective hill height,
- distance from source to hill center,
- effective source height,
- wind angle (zero degrees takes the plume over the hill center),
- effective Froude number, and
- downwind receptor resolution.

The CCB-specific postprocessor requires the following information:

- local source height,
- absolute hill height,
- height of the critical dividing streamline (H_{crit}),
- actual wind speed and direction,
- emission rate,
- PG stability class, and
- sampler positions and heights.

Although some of these quantities are needed to run other models (wind speed, direction, source height and location, and emission rates are presented in Section 5.2), several are specific to the PFM computations. These are highlighted below:

Hill Height and Shape - CCB is taken to be an axisymmetric ellipsoid. The aspect ratios are therefore equal and are derived by dividing the mean radius of the hill at the 40 m contour by the total hill height (the 40 m contour is about halfway up the hill). The highest labeled contour on the hill is 95 m on the south peak; the highest contour that virtually spans the saddle between the peaks is 85 m. The 90 m contour, which spans much of both peaks, is taken to represent the top of the hill for modeling purposes. The base of the hill is taken to be the -5 m contour height. (The contour heights on the hill are referenced to the 945 m (3,100 ft) height contour above sea level.) Thus, the total hill height is taken as 95 m. The average radius at the 40 m height contour is 244 m, which gives a hill aspect ratio of 2.6.

H_{crit} - The concept of the dividing streamline height was presented in Section 1.2. H_{crit} values are computed with a hill height of 95 m for each case hour.

Effective Source and Hill Heights - The potential flow is assumed to take place only above a surface defined by the effective value of H_{crit}, as shown in Figure 38. The region below H_{crit} is considered "dead" insofar as interaction with the plume is concerned. The hill height is just that portion of the hill above H_{crit}--that is (in cross-section), the arc AB. The model approximates this upper portion of the hill with an equivalent ellipsoid of the same semimajor axes b and c used to define the entire hill shape. (The dashed curve represents this equivalent ellipsoid, exaggerated for illustration.) Similarly, the effective source height is the local source height minus H_{crit}. (This definition implies that the dividing streamline of the flow is assumed to follow the small undulations of the terrain up to the base of the hill.) If any release heights lie below H_{crit}, no PFM computation is performed. This does not mean that the

8104203

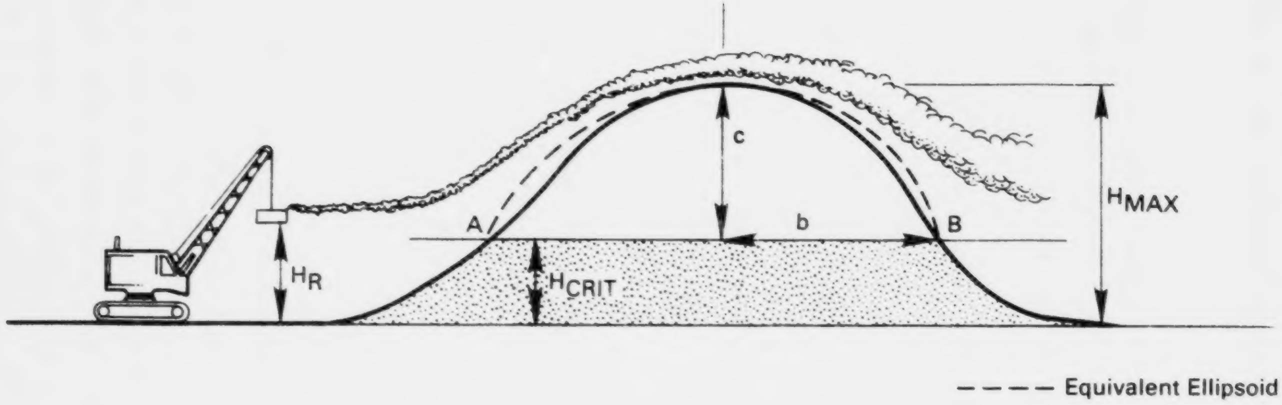
c
A
b
B
H_R
H_{CRIT}
H_{MAX}
---- Equivalent Ellipsoid

Figure 38a. PFM geometry for Cinder Cone Butte calculations.

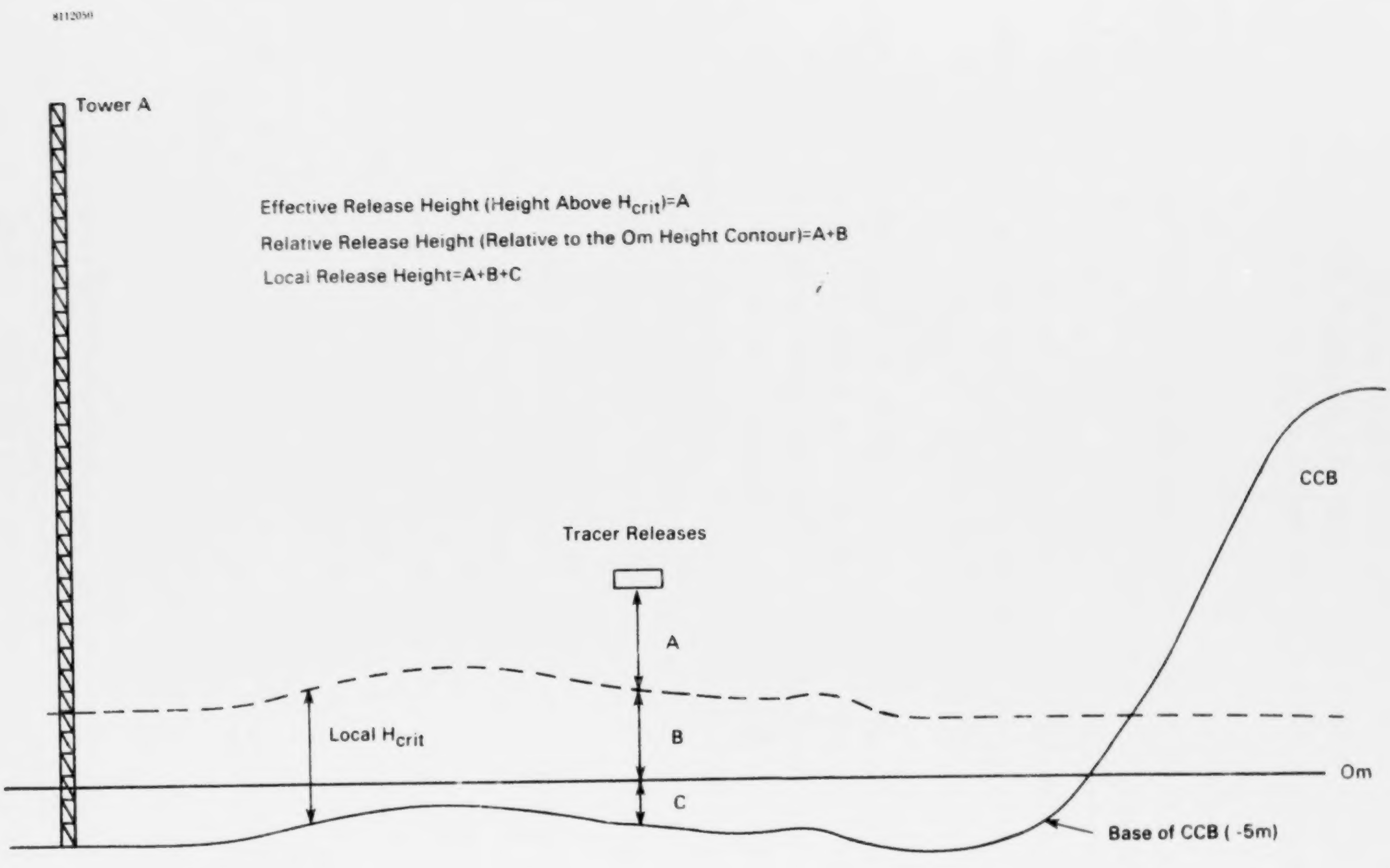
8112050
Tower A
Effective Release Height (Height Above H_{crit})=A
Relative Release Height (Relative to the Om Height Contour)=A+B
Local Release Height=A+B+C
Tracer Releases
A
B
C
Local H_{crit}
CCB
Om
Base of CCB (-5m)

Figure 38b. Illustration of the relationship between the tracer release height and important reference surfaces at CCB.

plume will impinge somewhere on the hill; it means only that the flow is likely to move around the hill with more horizontal than vertical deflection and that PFM in its present configuration is not applicable. Within the COMPLEX/PFM system, a COMPLEX I computation would be performed under these circumstances.

Effective Froude Number - The Froude number (Fr) used with PFM is a bulk Froude number defined over the layer extending from H_{crit} to 150 m (the top measurement level on Tower A). It is assumed that H_{crit} caps a surface layer of large ΔT so that above H_{crit} the temperature gradients vary slowly; hence, a simple bulk value will suffice for the Froude number. One Froude number is computed for each hour.

Receptor Resolution - PFM is run for receptors spaced evenly along the trajectory from the source to a point near the downwind base of CCB. The resolution varies from 25 m to 36 m along the direction from the source through the center of the hill. The end receptor is located 600 m beyond the hill center. Once the PFM computations are made, the postprocessor converts the plume trajectory and the plume deformation factors to a field of tracer concentrations for various choices of stability class.

Following a rationale such as that used to run the COMPLEX models with different stability classes, the PFM model was run for each hour with stability classes D and E to form two estimates at each receptor for each hour. (Class F computations have not been made, as the class D and E comparisons are thought to form an adequate base for comparing the relative performance of PFM with the other models.)

4.5 New Experimental Models

4.5.1 Overview

This section describes initial progress in the development of new models to explain 1-hour average concentration patterns observed on CCB during the field study conducted in the fall of 1980. It must be emphasized that these models are preliminary and subject to change as this study proceeds.

A complicated plume dispersion problem such as that presented by CCB involves a large number of physical processes that together constitute the relevant physical system. It is desirable to identify a small number of essential variables that may control the behavior of the system. One way of doing this is to construct a simple model with empirical parameterization of important effects.* Testing this type of model against observations can lead to an understanding of the relative importance of the controlling physical variables. This approach to modeling, adopted to guide new model development, relies heavily on the analysis of concentration observations.

Two preliminary models are proposed. One model, the Impingement model, corresponds to low Froude-number flows in which the plume remains horizontal as it flows around the hill. The other model, the Neutral model, corresponds to moderate or large Froude-number flows and allows the plume to go over the top of the hill. The simplicity of these models is deliberate; it will encourage applications in situations for which input information for the model is minimal.

4.5.2 Impingement Model for Low Froude Number Flows

This preliminary model development effort focused on 1-hour average concentrations and meteorology to parallel the regulatory use of existing models. Visual plume observations made during the field study indicate that when the flow was stably stratified, there was often considerable meander of the horizontal wind. Moreover, horizontal turbulent intensities averaged over an hour were typically around 20% of the mean vector average wind speed. Under these circumstances, it is not physically realistic to assume that the mean flow can be separated from much smaller scale turbulence. This assumption of separability is central to the theories of Hunt and others (see, for example, Hunt and Mulhearn 1973). To be consistent with observations, a distribution of streamlines about a

---

*This approach to modeling should be contrasted to that which relies on prior assumptions about the relevant physics of the problem in order to assemble the model by combining detailed mechanistic submodels.

"mean" streamline corresponding to the hourly average wind is postulated. Next, the concentration at a receptor is determined by the probability (the fraction of time) that the wind blows in the direction of the streamline that passes close to the receptor.

Figure 39 is a schematic of the physical situation being considered. The figure shows that the stagnation streamline is the only one that hugs the hill. If the dispersion caused by small-scale motion (turbulence) is small compared to the horizontal meandering of the instantaneous plume, the hill concentration is determined by the probability that the wind blows along the stagnation streamline. For a hill with a circular cross section, the maximum concentration will occur at stagnation point A. The instantaneous concentration C_i at A can be written as

$$C_i = Q/(\sqrt{2\pi} u_s \sigma_z \theta_s d) \tag{9}$$

where θ_s is the instantaneous angular spread (in radians) of the plume and d is the distance of the source to the receptor. The mass per unit length of the plume is Q/u_s where Q is the emission rate and u_s is the mean wind speed at the source. We can compute u_s if we assume that the flow around the obstacle is described by potential theory. Then,

$$u_s = \left|\frac{dw}{dz}\right|; \; z = x + iy \tag{10}$$

where w is the complex velocity potential with the argument z given by

$$w = \left(U\ z + \frac{a^2}{z}\right) \tag{11}$$

and U is the mean wind speed far upwind of the hill (Milne-Thompson 1968). It is assumed that the concentration distribution is Gaussian in the vertical.

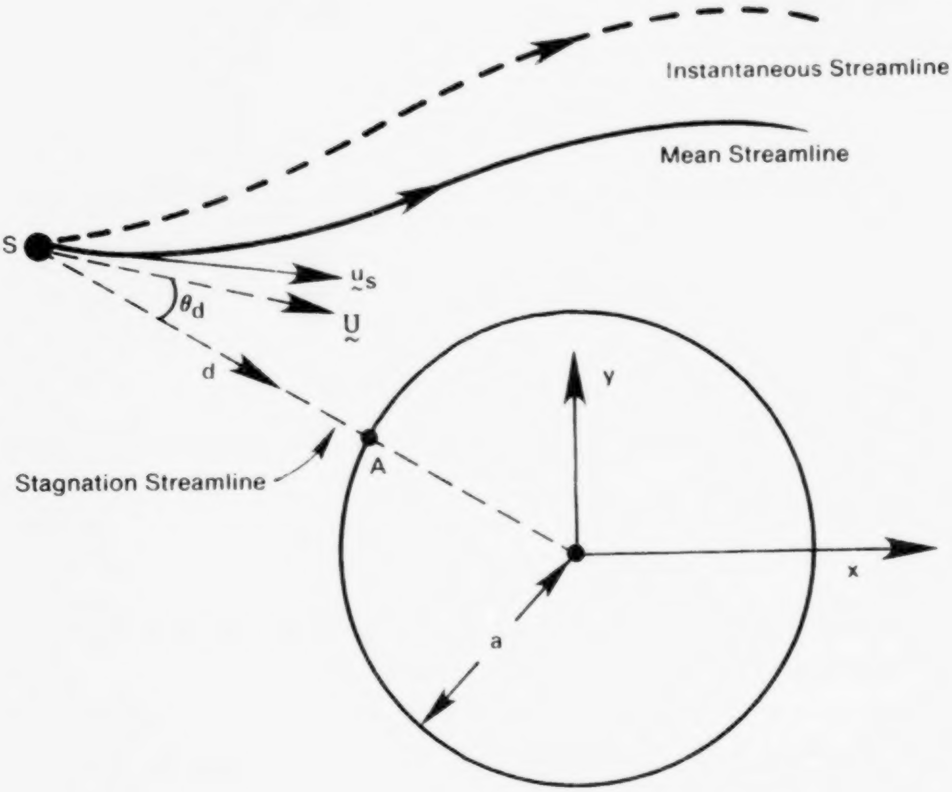
Instantaneous Streamline
Mean Streamline
S
$\underset{\sim}{u}_s$
θ_d
$\underset{\sim}{U}$
d
y
Stagnation Streamline
A
x
a

Figure 39. Geometry used in formulating Impingement model for low Froude number flows.

The maximum hourly averaged concentrations, C_{max} at A, can be written as

$$C_{max} \simeq C_i \int_{\theta_s} P(\theta)d\theta \qquad (12)$$

where $P(\theta)d\theta$ is the probability that the wind blows in the interval $(\theta - d\theta/2, \theta + d\theta/2)$ during the hour. By assumption, $\sigma_\theta >> \theta_s$ and Equation 12 can be written as

$$C_{max} = C_i P(\theta_d)\theta_s \qquad (13)$$

where σ_θ is the hourly average standard deviation of the horizontal wind direction and θ_d is the angle between the stagnation streamline and U.

With Equation 9, Equation 13 becomes

$$C_{max} = \frac{Q\ P(\theta_d)}{\sqrt{2\pi}\ u_s \sigma_z d} \qquad (14)$$

The distribution of $P(\theta_d)$ is assumed to be Gaussian, so that Equation 14 can be written as

$$C_{max} = \frac{Q}{2\pi u_s \sigma_z \sigma_\theta d} \quad \exp\ [-\theta_d^{\ 2}/2\sigma_\theta^{\ 2}] \qquad (15)$$

Note that in Equation 15, θ_d is used instead of the angular difference between u_s and the direction of the stagnation streamline. This is because $P(\theta_d)$ is determined by the upstream flow field rather than the distorted flow close to the obstacle. In order to use Equation 15, a formulation for σ_z is needed; the suggested expression for σ_z is presented in Section 4.5.4.

4.5.3 Neutral Model For Moderate to High Froude-Number Flows

Figure 40 is a schematic of a plume embedded in a neutral flow (that is, a flow that can be considered to be a potential flow based upon the hill Froude number). For convenience, an axisymmetric flow is considered. The lower figure shows, in cross section, the plume heading towards the hill. As the plume goes over the hill, it is distorted in the vertical and horizontal directions and its height (the height of the plume centerline above the hill surface) varies with the distance along the plume. These effects must be parameterized in a dispersion model. Based on the model of Egan (1975), the following formulation for the concentration on the hill surface is proposed:

$$C(x,y) = \frac{2Q}{(2\pi u \sigma_y \sigma_z)_f D_y D_z} \exp -\left[\left(\frac{\eta}{\zeta}\right)^2 \frac{{z_r}^2}{2D_z^2\,\sigma_{zf}^2}\right] \exp\left[-\frac{(\beta y)^2}{2D_y^2\,\sigma_{yf}^2}\right] \qquad (16)$$

where the subscript f denotes values in the absence of the hill (e.g., σ_{yf} is the unperturbed horizontal plume spread, and σ_y is the plume spread perturbed by the hill). The other terms in Equation 16 are defined as follows:

$$\eta = n_o/z_r \qquad \text{(See Figure 40)} \qquad (17)$$

$$\zeta = (\partial\psi/\partial z)_o/(\partial\psi/\partial z) \qquad (18)$$

$$D_y = \sigma_y/\sigma_{yf};\ D_z = \sigma_z/\sigma_{zf} \qquad (19)$$

In Equation 18, ψ is the stream function. The factor ζ is the ratio of the streamline spacing at the position of the source to that at a given distance. It accounts for the vertical deformation of the plume. The justification for using local stream function gradients to account for the vertical distortion of σ_z relies on the fact that σ_z is relatively small when the flow is stably stratified (that is, when $\partial\theta/\partial z$ is large).

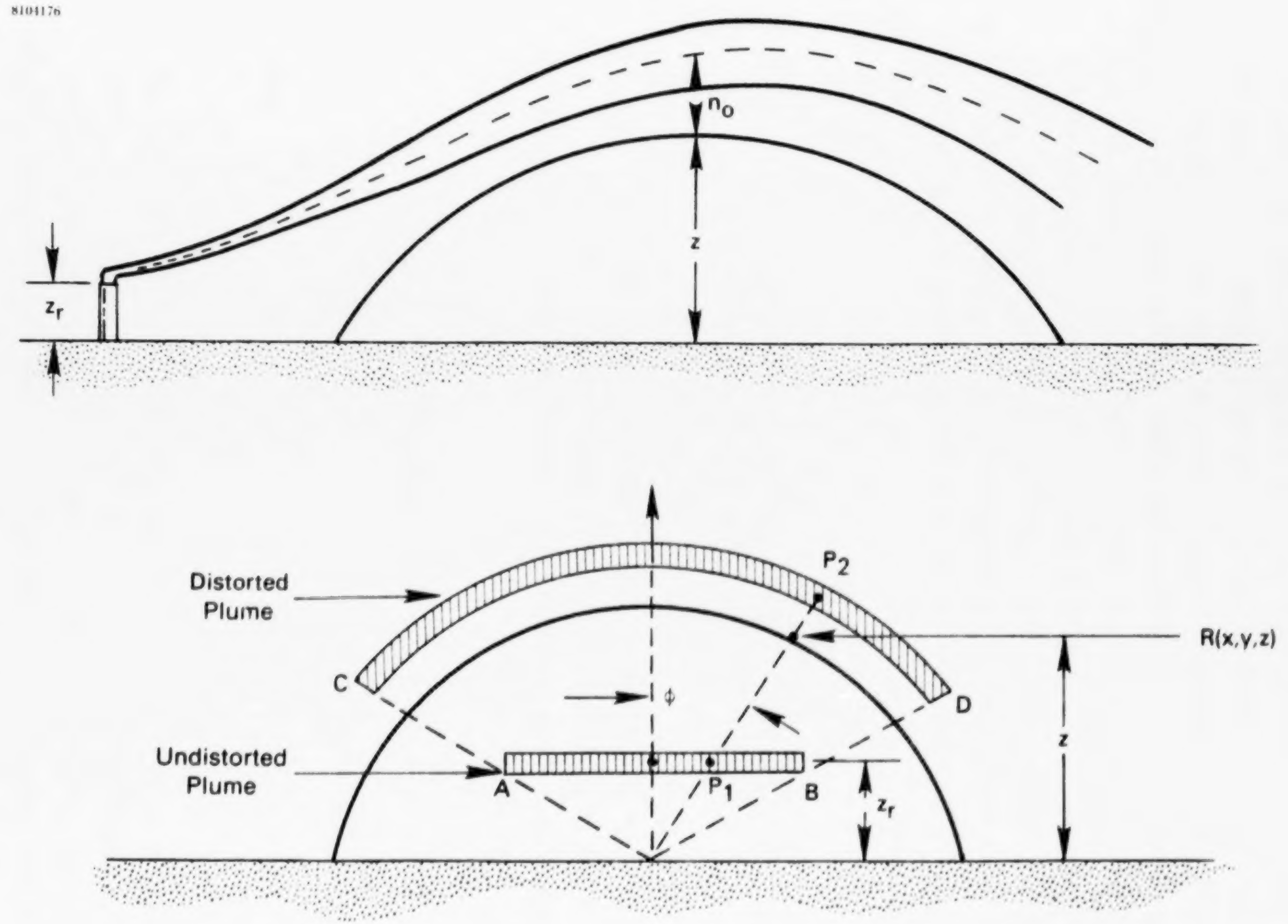
8104176
z_r
n_o
z
Distorted Plume
Undistorted Plume
P_2
P_1
A
B
C
D
ϕ
R(x,y,z)
z
z_r

Figure 40. Geometry used in formulating Neutral model for high Froude number flows.

Note: The plume goes over the hill as it undergoes distortion in the vertical and horizontal directions.

Because of horizontal meandering of the wind, the same assumption cannot be made to estimate the horizontal distortion factor β. To estimate β we use the fact that in axisymmetric flow the angle ϕ (see Figure 40) remains a constant along a streamline. We next assume that horizontal plume distortion is uncoupled from turbulent plume spread and occurs after the plume has spread because of turbulence. In other words, the segment AB (in Figure 40), which would describe the plume spread at a downwind distance x from the source in the absence of the hill, becomes the plume segment CD at the same downwind distance in the presence of the hill. In effect, the point P_2 maps onto the point P_1 on the "flat terrain" plume. For a plume directed towards the center of the hill, simple geometry shows that $\beta = z_r/z$.* As a first approximation, it is also assumed that $D_y = D_z = 1.0$.

A hill factor, f_h, can be defined as:

$$f_h = \eta/\zeta \tag{20}$$

Using potential flow theory, Egan (1975) shows that for two-dimensional flow, $f_h \sim 1$. On the other hand, f_h is usually smaller than unity for three-dimensional flows. The minimum value is close to 1/2. In the absence of detailed flow computations, a simple formulation that interpolates between these two values is suggested:

$$\begin{aligned} f_h &= 1 - z/2z_r ; \quad z \leq z_r \\ &= 1/2 \quad ; \quad z > z_r \end{aligned} \tag{21}$$

When the receptor is not located on elevated terrain ($z = 0$), $f_h = 1.0$ as expected. (Note that Equation 21 does not allow f_h to be smaller than 1/2.)

---

*When the plume direction is not along the radius of the hill, the expression for β is slightly less straightforward, although the concept behind its derivation is still very simple.

4.5.4 Dispersion Parameters

Dispersion in stable flows is far from being fully understood, although some progress has been made in modeling the behavior of surface releases (see Van Ulden 1978). At the present time, the analysis of lidar data collected during the small hill experiment is not complete. Because of this lack of adequate theory and data, the suggested expressions for sigmas should be considered very tentative.

The horizontal meandering of the wind suggests that σ_y can be expressed as

$$\sigma_y = \sigma_\theta x \tag{22}$$

where σ_θ is measured at source height. This equation has not yet been fully tested.

For elevated releases in the stable boundary layer, the vertical length scale of turbulence, ℓ_w, can be expressed as

$$\ell_w \sim \sigma_w / N \tag{23}$$

where σ_w is the standard deviation of vertical velocity fluctuations and N is the Brunt-Vaisala frequency. The Lagrangian integral timescale, t_ℓ, should be on the order of 1/N. A typical value of N measured at source height during the CCB experiment is 0.05 s^{-1}, which translates to a t_ℓ of about 20 s. With a typical wind speed of 5 ms^{-1}, it is expected that σ_z will approach the large travel time behavior beyond 200 m from the source. Because the source receptor distance was usually more than 400 m, the following equation is tentatively proposed for σ_z:

$$\sigma_z^2 = 2 \frac{\sigma_w^2 x}{uN} \tag{24}$$

where all of the variables in Equation 24 refer to source height.

A preliminary test of Equation 24 for σ_z has been made using lidar data from 15 case hours. In the course of reducing the raw lidar data, the Wave Propagation Laboratory (WPL) has computed standard deviations of the inferred smoke plume density. These values apply to the nearly instantaneous distribution of oil fog material in one of several sampling planes. Sampling planes lie along rays originating at the lidar location. Therefore, calculated σ_z values usually apply to a plane that is not a perpendicular slice through the plume.

An estimate of 1-hour plume sigmas is obtained from these lidar data by assuming that the effective 1-hour sigma is a combination of the average instantaneous sigma and the standard deviation of the positions of the instantaneous centroid of the distribution. For example, during hour 2 of Case 202, the plume was sampled five times in a plane approximately 210 m downwind of the source. The mean instantaneous sigma ($<\sigma_z>$) was 8.6 m. This average is formed as follows:

$$<\sigma_z> = \left(\frac{1}{N} \sum_{i=1}^{N} \sigma_i^2\right)^{1/2} \qquad (25)$$

The standard deviation of the height of the centroid (σ_H) using N - 1 weighting is 0.9 m. An effective 1-hour σ_z is formed according to

$$\sigma_{ze} = \sqrt{<\sigma_z>^2 + \sigma_H^2} \qquad (26)$$

Using the data from Case 202, hour 2, $\sigma_{ze} = 8.6$ m.

All 1-hour estimates of plume sigmas formed in this way from the lidar should be viewed as crude estimates only. Many planes are sampled no more than three times in an hour, and these may be grouped in the first half-hour during some hours. The results are presented mainly to see if the distance function proposed in Equation 24 is a reasonable description of plume development upwind of the hill and if the magnitudes of the predicted sigmas are comparable to the observed values.

Table 20 summarizes the results of the sigma comparisons. In the table, "R" is the approximate distance of the sampling plane from the center of the hill. Any distances less than 300 m are likely to be close enough to the hill to produce significant distortion in the instantaneous plume. "Calculated σ_z" is the value of σ_z computed from Equation 24. Undoubtedly, interpolating measured intensities of turbulence to the release height contributes to the imprecision of the estimate.

There is generally good agreement between the lidar-derived σ_z values and those calculated using Equation 24 in 12 of the 15 case hours analyzed. The mean percentage error (absolute value of the difference divided by lidar-derived σ_z), assuming all of the error is contained in the predicted σ_z values, is 22% with a standard deviation of 17%.

Agreement was much poorer for the remaining three case hours. The worst comparison is with Case 209, hour 8. The calculated σ_z is about one-third the size of the lidar σ_z. Calculated σ_z for the other two hours differ from the lidar sigmas by about a factor of two (100% error).

Figure 41 summarizes the behavior of the lidar-derived σ_z as a function of downwind distance. Distance is scaled by the length scale u/N, and σ_z is scaled by the vertical length scale of turbulence in the stable boundary layer, σ_w/N. Although scatter is certainly evident, there appears to be a significant growth of σ_z with distance. The curve of σ_z values calculated with Equation 24 is also displayed in the figure. Its square root growth assumption appears to be reasonable.

Case 209, hour 8, is plotted separately in Figure 41. It is the case hour with the worst correpondence between lidar observations and predicted values. Four of the five sampling planes show nearly equal plume spread. This hour, which has the lowest value of σ_w/N, may represent a case in which the density stratification inhibits continued plume growth with distance.

PG σ_z values are also compared with the lidar observations in Table 20. In seven of the 15 case hours, the best stability class (based on σ_z alone) is class F; class E appears best in three of the hours. If the same hours are classified by the Turner scheme, 13 hours are classified class F, one hour class E, and one hour class D. These latter two designations agree with those inferred from the lidar observations.

TABLE 20. COMPARISON OF σ_z DERIVED FROM LIDAR OBSERVATIONS WITH PREDICTED σ_z

Case	Hour	Downwind Distance	R	No. of Lidar Scans	Lidar Derived $\langle\sigma_z\rangle$	Lidar Derived σ_H	Lidar Derived σ_{ze}	Calculated σ_z	$\sigma_{w/N}$	Pasquill-Gifford $\sigma_z(D)$	Pasquill-Gifford $\sigma_z(E)$	Pasquill-Gifford $\sigma_z(F)$
202	1	200	820	3	7.8	2.5	8.2	15.0	18.6	8.5	6.2	4.1
		520	500	4	12.9	7.9	15.1	24.2	18.6	18.9	13.2	8.7
202	2	210	810	5	8.6	0.9	8.6	9.0	7.6	8.9	6.5	4.3
		480	535	6	11.0	3.2	11.4	13.5	7.6	17.7	12.4	8.1
204	1	225	810	2	3.8	1.8	4.2	4.1	1.2	9.4	6.9	4.5
		450	585	3	3.4	2.6	4.3	5.8	1.2	16.8	11.8	7.7
		660	375	3	5.1	6.3	8.1	7.0	1.2	22.9	15.8	10.4
204	8	130	830	2	7.4	3.5	8.2	7.5	2.1	5.8	4.4	2.9
		360	600	1	20.3	-	(20.3)	12.5	2.1	14.0	10.0	6.5
		580	380	1	16.6	-	(16.6)	15.8	2.1	20.6	14.3	9.4
205	4	555	600	3	8.2	2.6	8.6	7.7	2.6	19.9	13.9	9.1
		780	375	3	7.4	1.1	7.5	9.1	2.6	26.2	17.9	11.8
		865	290	2	6.9	8.7	11.1	9.6	2.6	28.5	19.4	12.6
205	5	350	805	1	3.2	-	(3.2)	9.2	3.7	13.7	9.8	6.3
		555	600	3	8.1	4.6	9.3	11.5	3.7	19.9	13.9	9.1
		785	370	2	8.8	2.6	9.2	13.7	3.7	26.4	18.0	11.8
205	6	350	805	1	4.8	-	(4.8)	5.6	2.2	13.7	9.8	6.3
		545	610	3	6.6	0.8	6.6	7.0	2.2	19.6	13.7	9.0
		690	465	2	5.8	3.5	6.8	7.9	2.2	23.8	16.3	10.8
		800	355	1	5.5	-	(5.5)	8.5	2.2	26.8	18.3	12.0
206	4	215	380	5	3.2	0.8	3.3	4.4	2.0	9.1	6.6	6.8
		425	170	4	5.2	4.1	6.6	6.2	2.0	16.0	11.3	7.4
206	6	225	370	3	7.9	5.8	9.8	10.9	3.7	9.4	6.9	4.5
209	1	215	775	3	8.1	3.0	8.6	10.1	6.7	9.1	6.6	4.3
		385	600	2	11.2	8.6	14.1	13.5	6.7	14.8	10.5	6.8
209	3	485	505	9	8.9	11.9	14.9	6.6	1.2	17.9	12.5	8.2
		350	640	2	7.5	1.2	7.6	5.6	1.2	13.7	9.8	6.3
		195	795	2	7.4	7.4	10.5	4.2	1.2	8.3	6.1	4.0
209	8	95	905	2	8.2	5.0	9.6	1.7	0.6	4.4	3.4	2.2
		190	810	2	9.2	5.0	10.5	2.4	0.6	8.1	6.0	3.9
		295	705	3	8.6	7.5	11.4	3.0	0.6	11.9	8.6	5.6
		510	490	4	8.0	6.6	10.4	3.9	0.6	18.6	13.0	8.5
		605	395	3	6.9	2.2	7.2	4.3	0.6	21.4	14.8	9.7
210	3	200	885	1	4.3	-	(4.3)	2.3	1.3	8.5	6.2	4.1
		295	790	4	3.9	1.0	4.0	2.7	1.3	11.9	8.6	5.6
		565	520	5	6.5	1.8	6.7	3.8	1.3	20.2	14.0	9.2
		785	302	10	7.2	4.2	8.3	4.5	1.3	26.4	18.0	11.8
211	1	210	790	2	9.9	0.8	9.9	8.7	1.9	8.9	6.5	4.3
		385	615	2	8.7	0.6	8.7	11.8	1.9	14.8	10.5	6.8
		470	530	7	10.6	8.2	13.4	13.0	1.9	17.4	12.2	8.0
211	4	445	710	3	4.2	6.1	7.4	14.0	2.8	16.6	11.7	7.7
		645	510	3	5.6	3.1	6.4	16.9	2.8	22.5	15.5	10.3
		885	270	9	5.9	9.0	10.8	19.8	2.8	29.0	19.7	12.8

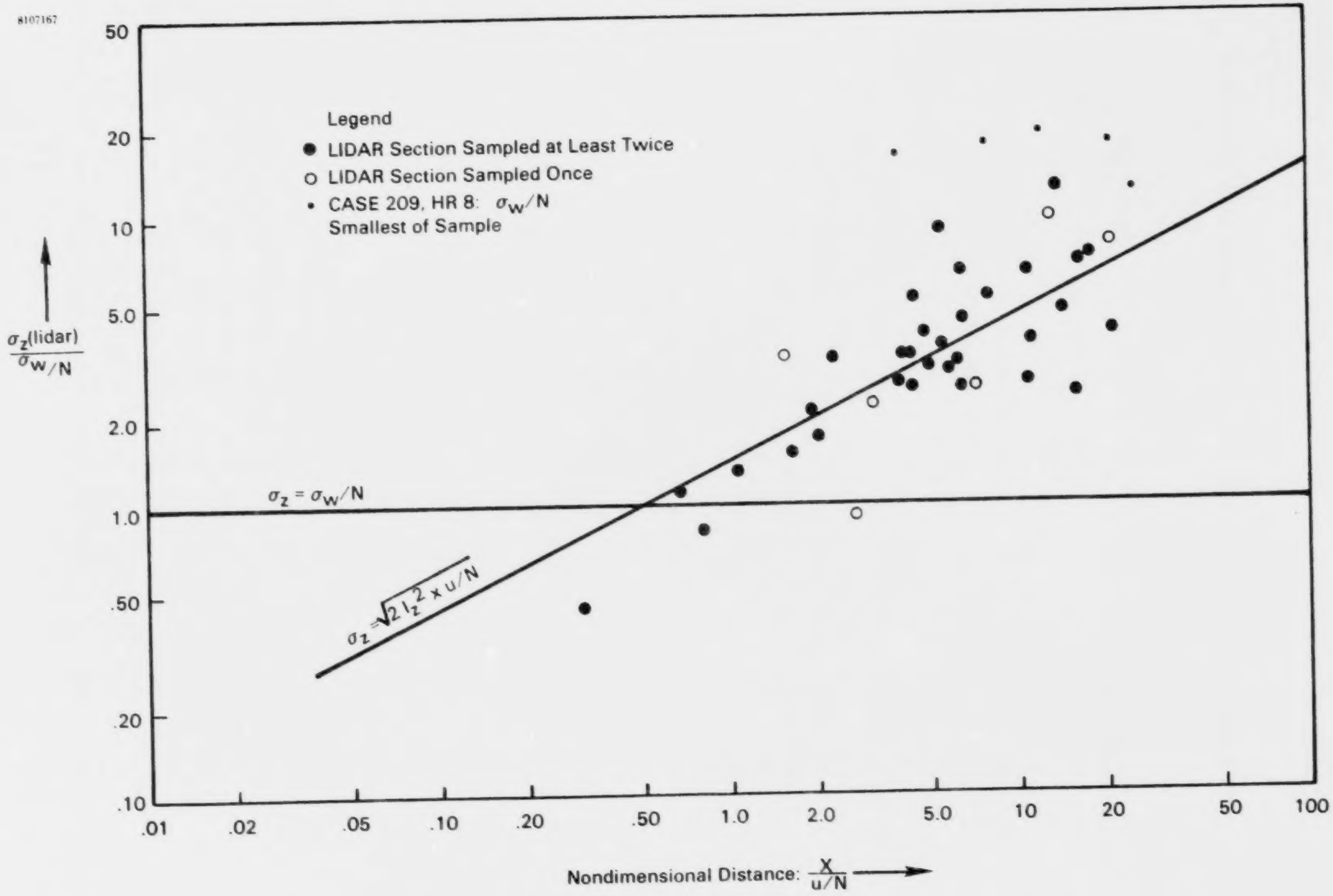

Figure 41. Dependence of lidar-derived σ_z on downwind distance for 15 case hours.

4.5.5 Application Procedures

The Neutral model was run in much the same way as the COMPLEX models. The relationship between the source and the receptors on the hill is the same. However, several additional meteorological variables are needed: N (Brunt-Vaisala frequency) and IX, IY, and IZ (turbulence intensities). N is calculated at release height from the local temperature gradient. The intensities of turbulence are linearly interpolated to the release height. Section 5.2 summarizes these data.

The Impingement model computes a maximum concentration on the hill rather than an entire concentration field. This maximum occurs at the theoretical stagnation point for a wind flow directed from the source to the hill center. The location of this point is approximated in the following way.

An average radius for each height contour between 10 m and 60 m is obtained from a map of the hill. The contours are evaluated for each 10 m height change. Averages are computed from actual north-south and east-west dimensions. These radii are then fit with a function of the form

$$R = A\ H^{B} \tag{27}$$

where H is the height in meters above the zero height contour, and the constants A and B are then found to be 970 and -0.38, respectively. This function is now included in the modeling system so that the Impingement model operates from the same input file used to run the Neutral model.

SECTION 5

MODEL PERFORMANCE USING CINDER CONE BUTTE FIELD DATA

5.1 Case Hours Selected for Model Evaluations

To select case hours for model evaluation, all 120 hours of experimental data for Cases 201-215 were examined.* In 21 of these hours, no SF_6 had been released. From the remaining 99 hours, 54 were identified as having reasonably good SF_6 sampling data (i.e., more than trace amounts of SF_6 were measured at many samplers on the hill). These 54 hours are distributed among Cases 201, 202, 204-211, and 213-215. Some of the hours removed will be analyzed at a later date, as they are still considered useful in the model development and evaluation tasks.

The final number of case hours selected for model evaluation in this report was reduced to 45 by removing Cases 207, 208, 213, and 215 from consideration at this time because quality assurance evaluations of the meteorological data had not been completed. The final selection of 45 representative hours was made among Cases 201-202, 204-206, 209-211, and 214.

Each of the models was evaluated using these 45 case hours except PFM, which was applied only for hours in which the release height exceeded the critical dividing streamline height (H_{crit}) by at least 5 m. The choice of a 5 m margin of error in H_{crit} was included to ensure that the model would be applied in cases where the plume was higher than the theoretical dividing streamline height. A total of 23 of the 45 hours were selected for the PFM evaluation. The 45 case hours chosen for the evaluations are described in more detail in Section 5.2.5.

---

*Case hour data for Cases 216-218 were not yet fully reduced to be included in the comparisons made in this report.

5.2 Data Preparation

5.2.1 Tracer Release Data

Release logs maintained during the field experiment at CCB contain information on the release crane position, the time and duration of tracer releases, the change in weight of the tracer container as the material is released, and the height of the tracer release above the local surface. When used in conjunction with survey data, this information defines the location of the release point in the hill polar coordinate system (r, θ, z) and the tracer emission rate.

The emission rate was computed directly from the weight change entries for the tracer gas cylinders. The weight of the cylinders was recorded several times during each hour and whenever the tracer was started or stopped. Emission rates were computed for each hour and tabulated to the nearest 0.01 g/sec for modeling. Over the course of the experiment, characteristic SF_6 emission rates varied from 0.06 g/sec to 0.20 g/sec.

Release positions were denoted by distances from known markers along the major roads. Primary markers were surveyed for position as well as height with respect to the zero height of the hill coordinate system (945 m [3,100 feet] above sea level). Secondary markers were set out by the tracer release crew and were not surveyed; the positions of these secondary markers were plotted on the survey map of the hill. Release locations were described by the distance and direction to the nearest marker. The coordinates of these release points were then measured directly on the map and recorded to the nearest meter from the hill center and to the nearest 0.1°. The angular coordinate was later rounded to the nearest 0.5° for input to the models.

The local elevation of the release point was not directly measured but rather interpolated from the elevations of the closest primary markers and the general shape of the height contours. In most cases, bracketing primary markers existed and the height at an intermediate point could be linearly interpolated. When there was only one primary marker near the release point, the shape of the nearest height contours was used as a guide. The local elevation was recorded to the nearest 0.1 m when warranted by the proximity of the primary markers. Otherwise, the elevation was recorded to the nearest 0.5 m.

Release height above the local surface was measured by a calibrated rope hanging from the release system (see Section 2.3.3). This height was reported to the nearest meter on the release logs.

5.2.2 Wind Data

Wind speeds and directions derived primarily from Tower A data (the 150 m tower north of the hill) were used in the modeling to represent conditions at the release point. Meteorology at the release height was assumed to be equivalent to the meteorology at Tower A for the same height above the local surface. If this height corresponded to a measurement level on the tower, the measurements were used directly; if the release height fell between two instrumented levels, a linear interpolation was used to estimate the meteorology at the release height.

At times, additional guidance was needed from photographs, tracer concentration maps, tethersonde data, and data from the instrumented 30 m tower on top of CCB (Tower B). This need arose in cases in which one of the propeller anemometers at the 40 m level of Tower A had seized up or when there was considerable directional wind shear between the instrumented levels. When one propeller malfunctioned at 40 m, the wind at that level was usually reconstructed from the good wind component at 40 m and the mean wind speeds at the adjacent levels (10 m and 80 m). A reasonable interpolation of wind speed at 40 m could usually be corroborated by the derived wind direction (consistent with the good wind component and the inferred mean wind speed) and other supporting evidence (photos, SF_6, and maps). This was not always possible, however; therefore, the inferred wind speed at 40 m was computed to be consistent with the most reasonable wind direction in these cases.

For modeling purposes, wind speeds were rounded to the nearest 0.5 m/sec although they are probably less certain in many cases. Wind directions were rounded to the nearest 1.0° but the accuracy may be more like ±2°. Subjective choices, where they were made, were based mainly on 1-hour average data. Later analyses of the 5-minute average meteorology may suggest alternate methods for inferring reasonable wind data for the release height.

Another source of uncertainty in wind data was the problem of interpreting the 1-hour vector-averaged wind data taken from the propeller anemometers. The response of a propeller is less sensitive at large attack angles. This loss of sensitivity could be responsible for some underestimation of wind speed or for several degrees of error in wind direction, the error magnitudes depending upon both speed and direction.

Data used in the modeling have not yet been modified for this effect; moreover, 1-hour vector averages themselves are usually an underestimation of actual wind speeds during the hour. A complete analysis of model sensitivity to possible underestimation of the wind speed has not been made.*

5.2.3 Turbulence Intensities

The 1-hour intensities of turbulence were measured at 2, 10, 40, 80, and 150 m on Tower A. Linear interpolation was used when the release height did not coincide with one of these instrumented levels.

Some horizontal turbulence intensity data were not available because of a seizing propeller anemometer at 40 m. In such cases, the interpolation was carried out across the 10 m to 80 m interval. The vertical turbulence intensity at 40 m could be corrected in these instances because the vertical propeller data were good, but the mean horizontal wind was underestimated. The correction factor was approximately the ratio of the speed from the good horizontal wind component to the inferred wind speed (see Section 5.2.2).

5.2.4 Dividing Streamline Height (H_{crit})

Computation of H_{crit} is based on wind speed and temperature data from Tower A and the height of CCB. The effective height of CCB is taken to be

---

*Concentrations from models like COMPLEX, which use the wind speed only for dilution, are inversely proportional to changes in the wind speed.

95 m (base at -5 m; "top" at the 90 m contour). The computation of H_{crit} was made from 1-hour averaged data.

Where valid 1-hour average data were available on Tower A, H_{crit} was computed from the data base directly. In cases where one 40 m wind component malfunctioned, however, the computation made use of the inferred wind speed calculated for that height (see Section 5.2.2).

5.2.5 Summary of Model Input Data

All of the data used as input to the models evaluated in this report are listed in Table 21. The time and date of each of the 45 test case hours is followed by the SF_6 emission rate (Q), the relative release height above the hill zero contour (not the base of the hill), the local release height, the local height of the critical dividing streamline (H_{crit}), the release location, the hourly average wind speed and direction, the turbulence intensities (IX, IY, IZ), the Brunt-Vaisala frequency (N), and the bulk Froude number (Fr) of the flow above H_{crit}. See Figure 38b for a depiction of the relationship between H_{crit}, release heights, and the hill coordinate system.

5.3 Model Evaluation Methods

The statistical evaluation measures adopted for this report follow the recommendations of the Woods Hole Workshop on Dispersion Model Performance (Fox 1981). Of the broad set of difference measures suggested in the Workshop report, a subset was judged appropriate for the observed and modeled concentration data sets. We routinely calculated and tabulated the following difference measures:

- the average of the residuals, $\overline{C_o - C_p}$ (called "the bias" in the Workshop report);
- the average of the absolute residuals, $\overline{|C_o - C_p|}$ (the "absolute gross error");
- the variance of the residual, $\sigma^2(C_o - C_p)$ (the "noise"); and
- the variance of the absolute residual, $\sigma^2|C_o - C_p|$.

TABLE 21. DATA ESTIMATED AT SOURCE HEIGHT FOR CASE HOURS SELECTED FOR MODEL COMPARISONS

Experiment Day (Date)	Case Hour	End Time	SF_6 Emission (g/s)	Relative Source Height(m)	Local Source Height(m)	H_{crit} (m)	Source Location r (m)	Source Location θ(°)	Average Wind Speed (ms^{-1})	Average Wind Direction(°)	N(s^{-1})	Fr*	Turbulence Intensities IX	Turbulence Intensities IY	Turbulence Intensities IZ
201(10/16)	1	18:00	.09	23.0	30	0	994	317.0	5.5	315	.0129	3.9	.120	.100	.040
201	2	19:00	.10	23.0	30	11	994	317.0	4.0	310	.0348	2.4	.080	.080	.015
201	4	21:00	.09	23.0	30	27	941	312.0	3.0	312	.0512	-	.270	.180	.025
201	5	22:00	.09	23.0	30	30	941	312.0	3.0	311	.0578	-	.150	.140	.020
201	6	23:00	.08	23.0	30	35	941	312.0	2.5	313	.0594	-	.230	.220	.015
202(10/17)	1	18:00	.08	43.0	50	0	1017	319.5	8.0	317	.0129	5.8	.080	.080	.030
202	2	19:00	.08	43.0	50	0	1017	319.5	8.0	321	.0262	3.1	.070	.050	.025
202	3	20:00	.08	13.0	20	0	1017	319.5	6.0	321	.0322	2.7	.110	.075	.030
202	4	21:00	.08	13.0	20	4	1017	319.5	6.0	326	.0372	2.5	.105	.060	.025
202	5	22:00	.09	23.0	30	9	1017	319.5	6.5	329	.0475	2.3	.145	.060	.020
202	6	23:00	.09	33.0	40	9	1017	319.5	8.0	326	.0604	2.1	.135	.045	.001
204(10/21)	1	1:00	.10	23.2	30	63	1036	4.5	2.0	360	.0511	-	.230	.290	.030
204	2	2:00	.09	23.2	30	82	1036	4.5	1.0	36	.0477	-	.445	.390	.050
204	5	5:00	.09	20.7	30	49	960	130.5	1.0	126	.0578	-	.560	.520	.110
204	6	6:00	.09	20.7	30	44	960	130.5	1.5	130	.0478	-	.340	.350	.040
204	7	7:00	.08	20.7	30	48	960	130.5	1.0	130	.0477	-	.510	.560	.095
204	8	8:00	.09	20.7	30	54	960	130.5	1.0	124	.0374	-	.700	.330	.080
205(10/23)	4	4:00	.09	31.1	40	18	1156	120.5	5.5	116	.0423	2.6	.200	.090	.020
205	5	5:00	.09	41.1	50	25	1156	120.5	6.0	118	.0481	2.6	.340	.170	.030
205	6	6:00	.09	21.1	30	17	1156	120.5	5.0	126	.0463	2.5	.290	.170	.020
206(10/24)	4	4:00	.04	29.5	35	24	595	123.5	4.0	130	.0443	2.0	.195	.150	.020
206	5	5:00	.06	29.5	35	24	595	123.5	4.0	143	.0401	2.2	.330	.170	.025
206	6	6:00	.06	29.5	35	40	595	123.5	2.0	126	.0354	-	.440	.180	.065
206	7	7:00	.06	29.5	35	26	595	123.5	3.0	136	.0378	2.5	.330	.280	.050
206	8	8:00	.06	29.5	35	36	595	123.5	2.5	140	.0401	-	.410	.520	.075
209(10/28)	1	18:00	.15	33.0	40	7	988	316.5	3.5	311	.0184	2.3	.140	.115	.035
209	2	19:00	.17	33.0	40	23	988	316.5	2.5	307	.0372	2.0	.230	.110	.030
209	3	20:00	.18	33.0	40	37	988	316.5	2.0	333	.0576	-	.290	.125	.035
209	7	00:00	.16	35.3	40	60	999	101.0	2.0	102	.0942	-	.260	.110	.025
209	8	1:00	.16	35.3	40	54	999	101.0	2.0	103	.0854	-	.275	.075	.025
210(10/30)	3	3:00	.16	49.8	57	30	1085	114.0	5.5	110	.0439	2.0	.130	.150	.010
210	4	4:00	.17	49.8	57	23	1085	114.0	6.5	121	.0398	2.3	.120	.080	.015
210	6	6:00	.19	49.8	58	12	1089	122.5	6.0	115	.0230	2.3	.100	.050	.010
210	7	7:00	.16	49.8	58	16	1089	122.5	6.5	123	.0352	2.4	.200	.145	.040
210	8	8:00	.13	31.8	40	17	1089	122.5	5.0	128	.0462	2.4	.170	.095	.015
211(10/31)	1	1:00	.18	25.3	30	48	1003	101.5	1.5	105	.0577	-	.415	.590	.075
211	2	2:00	.18	25.3	30	34	1003	101.5	3.0	110	.0529	-	.265	.205	.065
211	3	3:00	.18	25.3	30	34	1003	101.5	3.0	120	.0546	-	.640	.225	.040
211	4	4:00	.18	11.1	20	39	1156	120.5	3.0	120	.0753	-	.395	.350	.070
211	5	5:00	.18	11.1	20	28	1156	120.5	2.0	119	.0922	-	.360	.410	.060
211	6	6:00	.17	11.1	20	22	1156	120.5	3.0	122	.0753	-	.370	.230	.045
214(11/5)	3	5:00	.17	14.8	24	45	788	143.0	1.5	111	.0636	-	.345	.620	.090
214	4	6:00	.17	14.8	24	26	891	134.5	3.0	135	.0606	-	.290	.290	.080
214	7	9:00	.16	22.0	24	18	538	113.0	2.0	122	.0264	2.6	.275	.210	.080
214	8	10:00	.16	18.5	24	0	598	124.0	2.0	136	-.0026**	3.0	.280	.285	.140

---

*Bulk Froude number for layer above H_{crit}; computed only where local release height exceeds H_{crit}.

**+.0026 used.

In addition, because it is sometimes asserted that observed concentrations are lognormally distributed, the following relative difference measures, although not expressly recommended in the Workshop, were routinely calculated as well:

- the arithmetic and geometric means of the ratio (C_p/C_o) (for nonzero observed concentrations) and
- the corresponding variances.

Data pairings also follow the priority recommendations of the Workshop. For each data hour, the 1-hour average observed and modeled concentrations are paired as follows:

- The peak observed concentration is paired with the concurrent modeled concentration at the same location.
- The peak observed concentration is paired with the concurrent peak modeled concentration independent of location.
- All observed concentrations are paired with the concurrent modeled concentrations at the same locations.

Next, to examine and compare their respective distribution functions, the concurrent observed concentrations, modeled concentrations, residuals, and absolute residuals are routinely sorted into frequency histograms so as to emphasize any gross biases or asymmetries in the distributions.

In accord with the Workshop recommendations for graphical displays, concurrent sets of observed and modeled concentrations were also compared in scatterplots of C_p versus C_o. Scatterplots of C_p/C_o versus the ratio of release height to critical dividing streamline height (z_r/H_{crit}) were also generated. These were done to flag any systematic or clear-cut differences in how the models performed in the limiting cases of stable (impingement-type) flow ($z_r \ll H_{crit}$) or neutral flow ($z_r \gg H_{crit}$). The form of the scatterplots was chosen to emphasize model relative performance--for example, to show how many of the 1-hour average model predictions fall within a factor of 2 (or more) of the observed concentrations.

Table 22 summarizes the descriptive statistics (including graphical displays) used for this report. In this table, "paired concentrations" means sets of 1-hour average observations for the same case hour. The nomenclature for "peak values" follows the Workshop report:

- $C_o(l_n,t_n)$ = peak value observed at time t_n and location l_n.
- $C_p(l_n,t_n)$ = the corresponding modeled value for the same time period at the location of observed peak value.
- $C_p(l_j,t_n)$ = the peak modeled value for the time t_n, irrespective of location.

Finally, in order to compare the overall relative performance of the different models, statistics for each individual case hour were aggregated and summarized for the ensemble of 45 case study hours. Evaluating and interpreting overall model performance on the basis of these statistics requires a clear understanding of the relationship between modeled and observed concentrations. This relationship is described below.

Time-averaged concentrations at a single point are governed by complex phenomena with wide ranges of space and time scales. Models characteristically use parametric descriptions of many of these phenomena in order to simplify or reduce the input information and number of computations required. Such simplifications introduce many sources of uncertainty and, therefore, model estimates will usually not agree precisely with observed concentrations.

These differences between modeled and observed concentrations result both from the input data and from the model formulation. Any discrete set of model input data is necessarily an incomplete description of the actual flow field. Many Gaussian plume models in use today characterize the flow field by hourly averages of wind speed and direction measured at one point. This information is insufficient to resolve the detailed spatial and temporal structures of the flow field. Any number of different flow fields may be described by the same average data, and each distinct realization of the flow field may produce a different observed concentration at a particular point. The incomplete model inputs, therefore, lead to an infinite set of possible

TABLE 22. DESCRIPTIVE STATISTICS AND ASSOCIATED ANALYSES

Paired Concentrations	Means	Variances	Distributions	Scatter-plots	Tabular Data
C_o	X	X	X		X
C_p	X	X	X	vs. C_o	X
C_o-C_p	X	X	X		X
$\lvert C_o-C_p \rvert$	X	X	X	vs. C_p	X
C_p/C_o	X	X		vs. C_p	X
Peak Values					
$C_o(l_n, t_n)-C_p(l_n, t_n)$	X	X	X		X
$\lvert C_o(l_n, t_n)-C_p(l_n, t_n) \rvert$	X	X			X
$C_o(l_n, t_n)-C_p(l_j, t_n)$	X	X	X		X
$\lvert C_o(l_n, t_n)-C_p(l_j, t_n) \rvert$	X	X			X
$\frac{C_o(l_n, t_n)}{C_p(l_j, t_n)}$	X	X		vs. Zr/H_{crit} vs. C_p	X

observed concentrations for each set of input data; or, in other words, the input data set itself describes an ensemble of possible observed concentrations.

The Venn diagram in Figure 42 illustrates the ensembles of observed concentrations corresponding to two distinct input data sets. Each input data set contains the same variables, but their values are different in the two sets. In principle, if many more events are observed for the same two sets of input data, more concentration measurements will be associated with one or the other of these two data sets. Eventually, an ensemble of possible observed concentrations might be described for each set of input data values. Ensembles associated with different input data sets may overlap, and the range of each ensemble will depend, among other things, upon how fully the input data describes the wind flow's influence on measured concentrations.

If the input data and concentration measurements contain no measurement errors, then for a particular input data set the difference between modeled and observed concentrations will depend upon the standard deviation of the distribution of possible observed concentrations within the ensemble, and the difference between the mean of the ensemble and the model estimate. A highly accurate model may closely estimate the mean of the ensemble, and may incorporate enough information so that the standard deviation of the distribution is a small fraction of the mean concentration in the ensemble.

A less accurate model that incorporates less input data might also closely reproduce all ensemble means but with larger standard deviation. The performance of these two models will differ because the second model will be estimating the means of ensembles with broader distributions of possible observed concentrations.

Figure 43 illustrates the difference between the two models. Denote the less accurate model as model A, with input data set A, and ensemble standard deviation σ_A. Model B is the more accurate model. Suppose an observed concentration, C_o, lies in the region in which the two ensembles overlap. Model A's estimate of the ensemble mean concentration, C_A, might not be useful if σ_A is large compared to the range of C_o over all data sets. Model B's estimate of the ensemble mean concentration, that is, C_B, provides a more useful estimate of C_o because σ_B is smaller.

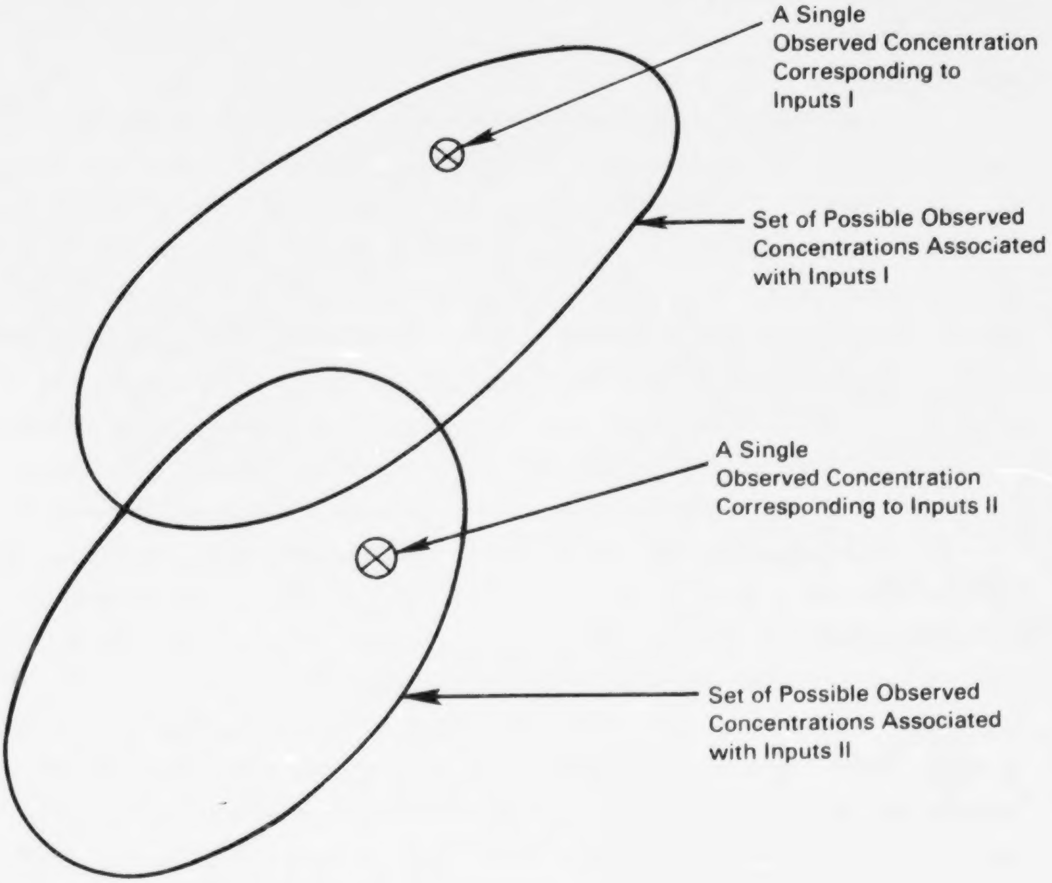
A Single Observed Concentration Corresponding to Inputs I
Set of Possible Observed Concentrations Associated with Inputs I
A Single Observed Concentration Corresponding to Inputs II
Set of Possible Observed Concentrations Associated with Inputs II

Figure 42. Relationship between model inputs, single concentration observations, and the set of possible concentrations associated with model inputs.

8107123

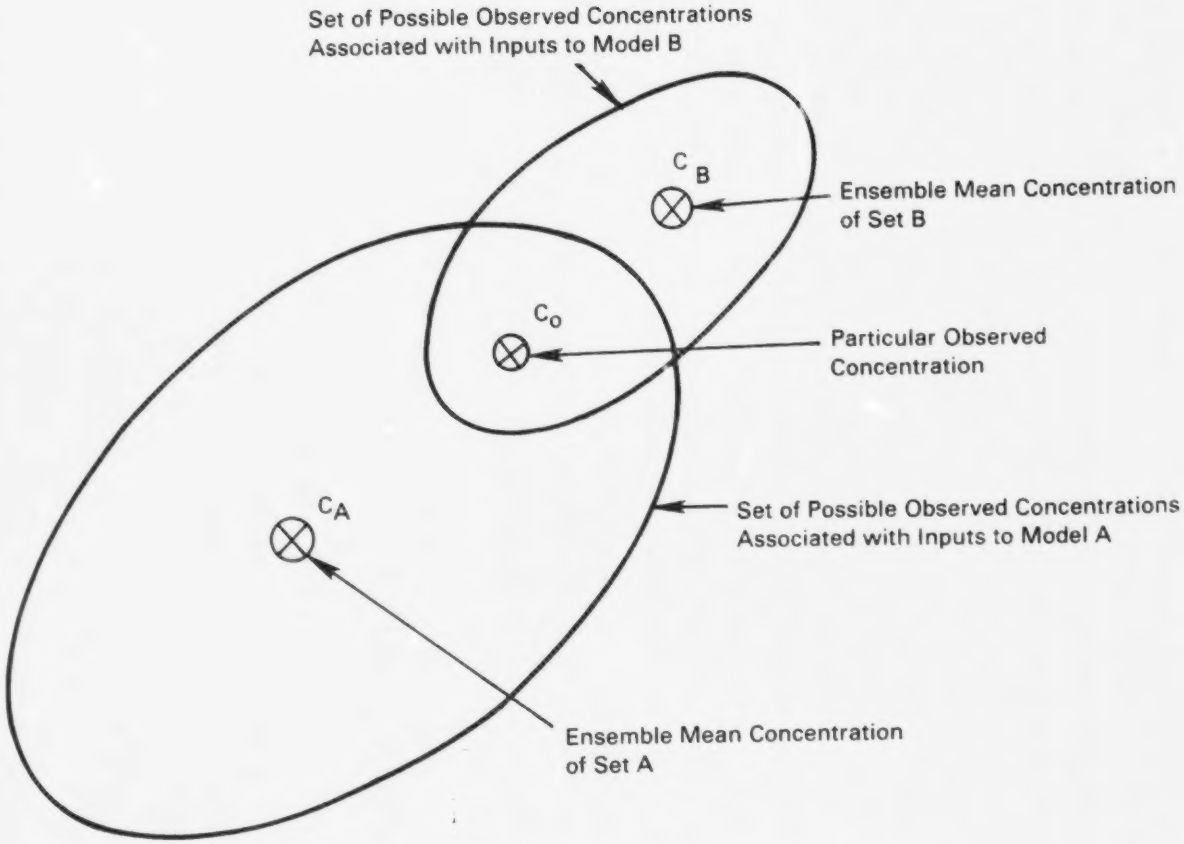
Set of Possible Observed Concentrations
Associated with Inputs to Model B
C_B
Ensemble Mean Concentration
of Set B
C_o
Particular Observed
Concentration
C_A
Set of Possible Observed Concentrations
Associated with Inputs to Model A
Ensemble Mean Concentration
of Set A

Figure 43. Relationship between an observed concentration and estimates of this concentration from models A and B when these models accurately simulate the ensemble mean concentration.

This way of looking at the relationship between model estimates and observed concentrations suggests that the performance of a model is ultimately limited by the amount of input information available. A good model will extract and correctly interpret this information so that the residual between modeled and observed concentrations is reduced to a random variable. The observed concentration should actually be treated as a random variable (Papoulis 1965) because it embodies everything that is "unknown" in the model. If two or more models use the same input information, then a comparison of residuals for each model will show which model is most successful in interpreting the input data. Similarly, a comparison of residuals for models that are formulated in nearly the same way, but that use different input information, will show the value of incorporating more information. The costs of providing more input data and the unavoidable measurement errors are likely to constrain the benefits of more complicated, data-intensive models. Careful analyses of residuals should help in defining the technical benefits associated with increased modeling costs.

We will now recast in mathematical terms the approach to model comparison.

Observed Concentration

Inputs to an air quality model constitute only part of the information required to explain concentrations. If the set of model inputs (the "known" variables) are denoted by x_1, the concentration C at a specific location can be expressed as

$$C = f(x_1, x_2) \tag{28}$$

where $f(x_1, x_2)$ is some function of known variables (the set x_1), and unknown variables (the set x_2). Because the set x_2 can take any values for given x_1, the concentration C can also assume any of a broad range of values. Therefore, the model inputs x_1 define an infinitely large ensemble of concentrations.

An observed concentration $C_o(x_1)$ belonging to this ensemble can be written as the sum of the mean of the ensemble and a random variable ε:

$$C_o\ (x_1,\ x_2) = \langle C_o(x_1,\ x_2)\rangle + \varepsilon(x_1,\ x_2) \tag{29}$$

where $\langle\varepsilon(x_1,\ x_2)\rangle \equiv 0$. In Equation 29, the angle brackets denote an ensemble average obtained by keeping x_1 fixed. Therefore, the ensemble mean is independent of x_2. If C_p is the average over the ensemble of concentrations defined by the x_1, then $\langle C_o\ (x_1,\ x_2)\rangle \equiv C_p\ (x_1)$.

The Modeled Concentration

Equation 29 may be rewritten as:

$$C_o(x_1,\ x_2) \ = \ C_p(x_1) + \varepsilon(x_1,\ x_2) \tag{30}$$

In this equation only x_1 is known, so the best a model can do is estimate $C_p(x_1)$. Because x_2 is unknown, we expect any single observation corresponding to x_1 to deviate from the ideal model prediction $C_p(x_1)$. The magnitude of this deviation is determined by $\langle\varepsilon^2\rangle = \sigma_\varepsilon^2$.

Because ε is a random variable, x_1 should be chosen so that σ_ε is as small as possible. Also, in order to use a model it is necessary to know how σ_ε varies with x_1. This means that an air quality model should ideally consist of a submodel for C_p as well as a submodel for the stochastic term ε. While physical principles can help in constructing the model for C_p, we have to rely on trial-and-error empirical methods to infer σ_ε. To simplify the modeling of ε, it is convenient to choose the model inputs x_1 (and the model itself) so that ε is not a function of the inputs x_1. Equation 30 can then be written as

$$C_o = C_p(x_1) + \varepsilon(x_2) \tag{31}$$

Equation 31 then represents the "ideal" relationship between model calculation and observation. As described by Box, Hunter, and Hunter (1978), such a model produces ϵ's that have zero mean and constant variance (independent of x_1), and are distributed independently of one another. The characteristics of an adequate model can then be described in terms of the residual $\epsilon = C_o - C_p$. With a series of observations and calculations we can calculate the following statistics:

$$\bar{\epsilon} = \frac{1}{N} \sum_i (C_{oi} - C_{pi}) \tag{32}$$

$$\sigma_\epsilon = \left[\frac{1}{N} \sum_i (\epsilon_i - \bar{\epsilon})^2 \right]^{1/2} \tag{33}$$

Then, for an adequate model, $\bar{\epsilon}$ should be near zero (i.e., the model should be accurate) and σ_ϵ should be small (i.e., the model should be precise).

Model Improvement

The previous discussion shows that a model can be improved by reducing σ_ϵ. This process is equivalent to expanding x_1 to include as much of x_2 as possible. If x_1 included all of x_2, a model could in principle calculate the observed concentration C_o precisely. Because this is impossible in practice, the observed concentration must be treated as a random variable. The formulation of an improved model is subject to several limitations. The uncertainty associated with formulating a model to incorporate added information can lead to errors. Also, inevitable errors in model inputs may degrade the utility of increasing the complexity of a model.

A Method to Test Models

The previous discussion provides the framework for a method to test models. We have seen that for an adequate model, the residuals $(C_o - C_p)$ have the following properties:

- $\overline{\varepsilon} \simeq 0$,
- σ_ε should be small, and
- ε should be unrelated to C_p or x_1.

The first step in examining a model is to plot ε against C_p or x_1. The plot should show a band-like structure in which ε is uncorrelated with C_p. Also ε should be randomly distributed about zero. This visual examination provides an easy check on residual behavior. It also indicates the range of C over which the model can be used. Clearly, one would like to have as large a range of C_p as possible in which the model behavior is acceptable.

To use the statistics of ε, it is desirable to transform C_o and C_p so that ε is normally distributed. This knowledge of the distribution of ε allows us to estimate confidence intervals for the model prediction. This procedure is illustrated in Appendix C.

The relationship between the transformed observation C_o' and the transformed prediction C_p' can be written as

$$C_o' = C_p' + \varepsilon \qquad (34)$$

where ε is normally distributed with zero mean and variance σ_ε^2. At the present time, our analysis of the data has not yet allowed us to choose the appropriate transformation for the concentrations. Therefore, the residual statistics will be based on two possible forms for C'

$$C' = C \text{ or}$$
$$C' = \ln C \qquad (35)$$

A convenient way of representing the performance of a model is to plot $\overline{\varepsilon}$ against σ_ε. This is shown in Figure 44. Recall that the ideal values of $\overline{\varepsilon}$ and σ_ε are zero. If we accept the hypothesis that the sample of residuals available to us is drawn from a normal population whose mean is zero, the length of the vector $\overline{\varepsilon^2}$ drawn from the "perfect" prediction point (0,0) to the point $(\overline{\varepsilon}, \sigma_\varepsilon)$ is a measure of the uncertainty in the model calculation.

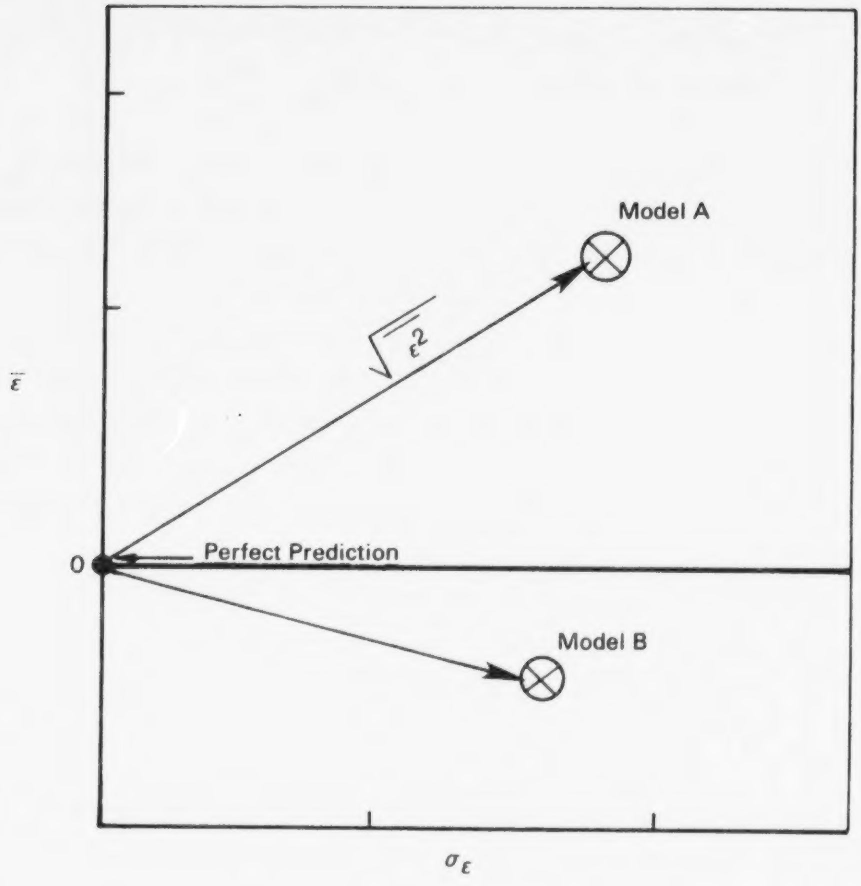
Model A
$\sqrt{\overline{\varepsilon^2}}$
$\bar{\varepsilon}$
0
Perfect Prediction
Model B
σ_ε

8107123

Figure 44. The relative performance of different models.

For the transformation $C' = \ln C$, it is convenient to plot the logarithmic mean m_g against the logarithmic standard deviation s_g, where m_g and s_g are defined as follows:

$$m_g = \exp \bar{\varepsilon} = \exp \overline{\ln (C_o/C_p)} \qquad (36)$$

$$s_g = \exp (\sigma_\varepsilon) = \exp \sigma(\ln(C_o/C_p)) \qquad (37)$$

When plotted on double log paper, m_g and s_g figures are equivalent to $\bar{\varepsilon}$ and σ_ε figures. This labeling allows one to interpret model performance in terms of multiplicative factors. For example, an m_g of 0.5 implies a tendency to overestimate by factor of 2.

5.4 Sample Case Study Results - Case 205, Hour 5

This section provides a representative case study to illustrate the kinds of analyses available for use in evaluating model performance on an hour-by-hour basis. Spatial characteristics of calculated and observed concentration fields must be used if we want to know why one model may estimate the highest observed concentrations better than another. This sample case study hour (Case 205, hour 5) has already been described in Section 2.4.2. The following discussion presents a synopsis of the meteorological conditions and the observed distribution of 1-hour average SF_6 concentrations.

Case 205, hour 5 was an hour with persistent southeast winds averaging 6.0 m/sec at the release height. The flow regime was observed to be neutral (flow up the east draw and over the top of CCB) with respect to plume behavior, although the Turner scheme for estimating dispersion stability class indicated that class F was appropriate for this hour (1.3 m/sec hourly average wind speed at 10 m). The local release height was 50 m, and the computed dividing streamline height was 25 m. The observed 1-hour SF_6 concentration distribution for this hour, shown in Figure 45, confirms the considerable spatial extent to which the plume contacted the surface of CCB, although concentrations are relatively low.

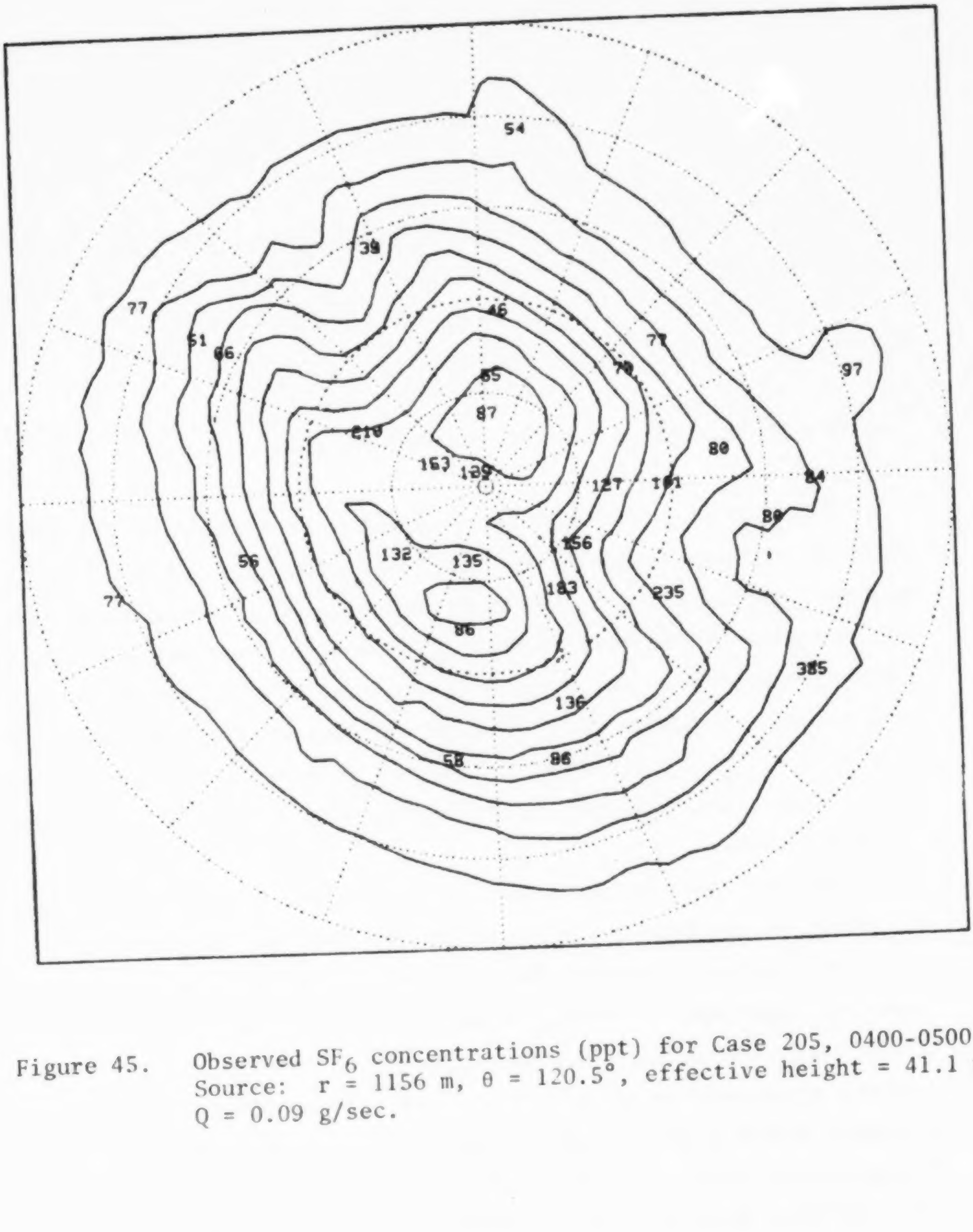

Figure 45. Observed SF_6 concentrations (ppt) for Case 205, 0400-0500. Source: $r = 1156$ m, $\theta = 120.5°$, effective height = 41.1 m, $Q = 0.09$ g/sec.

The model evaluation products for this case hour are presented for COMPLEX I and II, PFM, and the Neutral model only. Estimates from Valley and the Impingement models are deferred until Section 5.5, as these models produce an estimate of the maximum concentration only.

5.4.1 COMPLEX I and COMPLEX II

The first step in the model evaluation is a quantitative comparison of the distribution of measured and calculated concentrations. The 1-hour average ground-level SF_6 concentrations calculated by COMPLEX I and COMPLEX II for stability classes D, E, and F, respectively, are shown in Figures 46 through 51. (For stability class D, COMPLEX I and COMPLEX II use plume path coefficient = 0.5; for stability classes E and F, both models use plume path coefficient = 0.) The calculated concentrations are given as parts per trillion (ppt). The model calculations were made at each of the 93 possible sample locations shown earlier in Figure 12.

Only in the COMPLEX II runs for E and F stability is the peak concentration (385 ppt, observed at the base of the southeast draw) equaled or exceeded elsewhere on the hill. Qualitatively, though, the spatial distribution pattern shown in the COMPLEX II runs is too narrow in the crosswind direction (compared to the observed concentrations).

If the peak concentration at the base of the hill is ignored for the moment*, then COMPLEX II estimates using stability class D dispersion coefficients show a better agreement with the observations. It nonetheless appears that the calculations across the top of the hill and out to the sides would improve further if the model plume were broader.

The COMPLEX I results, by comparison, show a horizontal spread that appears too large, especially with respect to the concentrations on the south side of the hill. Nonetheless, if we focus on the higher concentrations near

---

*These locally large concentrations at the base of the hill were observed on several occasions during the experiments; they are tentatively attributed to downslope flows driven by horse-shoe vortices or drainage. None of the models addresses this effect, but the model statistics reflect these large measured concentrations nonetheless.

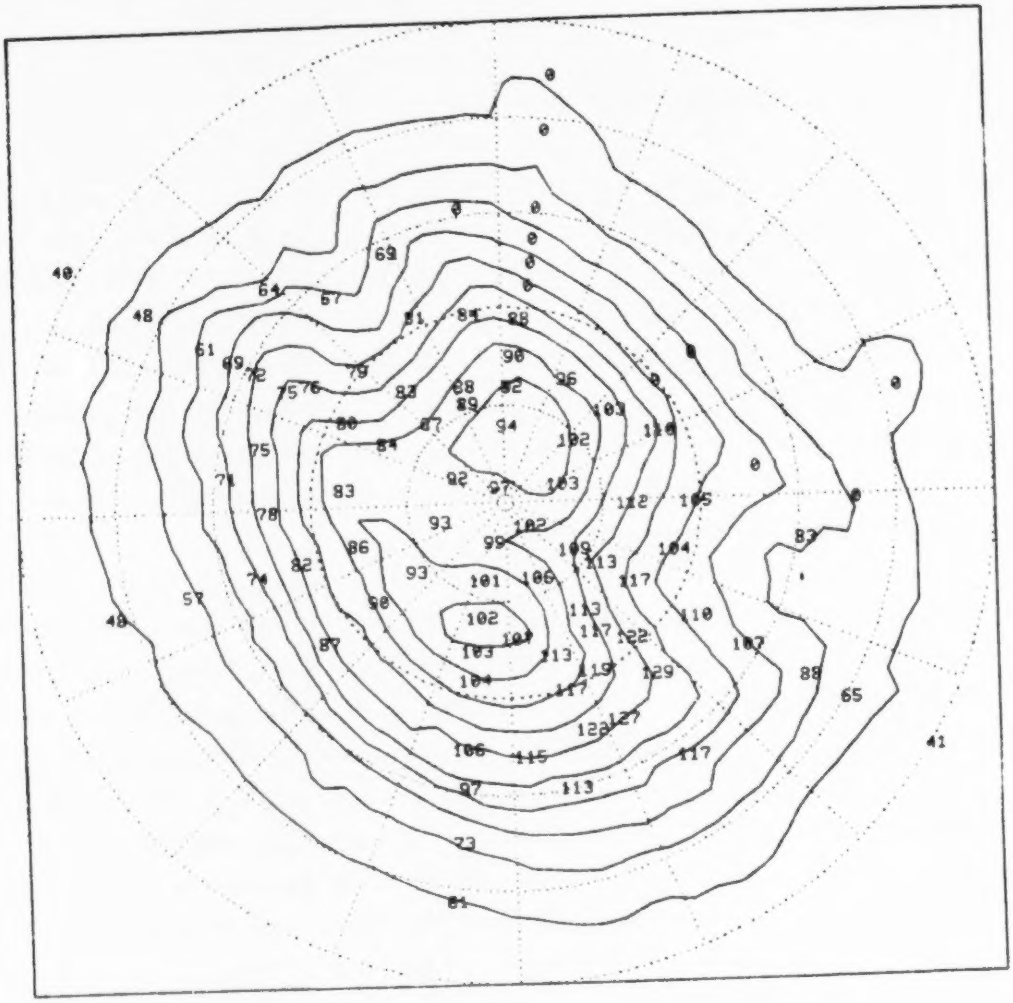

Figure 46. Complex I: calculated SF_6 concentrations (ppt) for Case 205, Hour 5, Stability Class D.

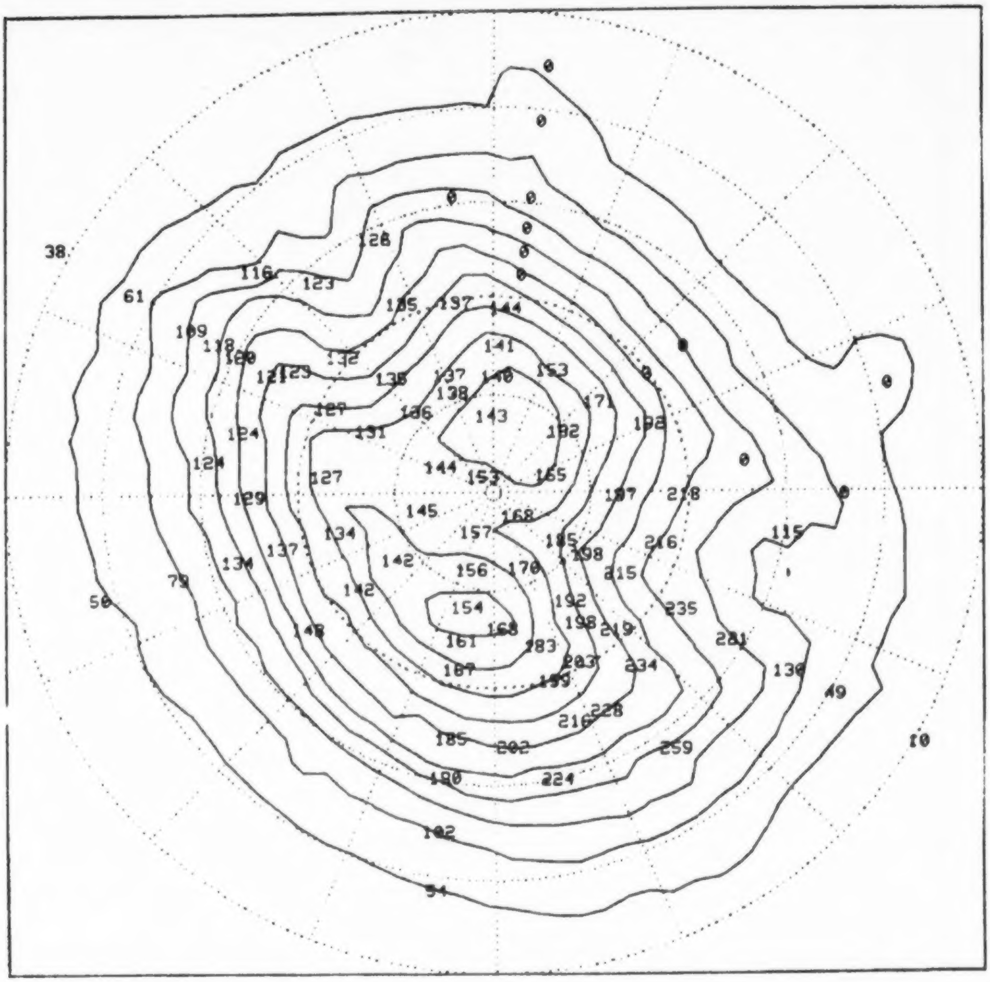

Figure 47. Complex I: calculated SF_6 concentrations (ppt) for Case 205, Hour 5, Stability Class E.

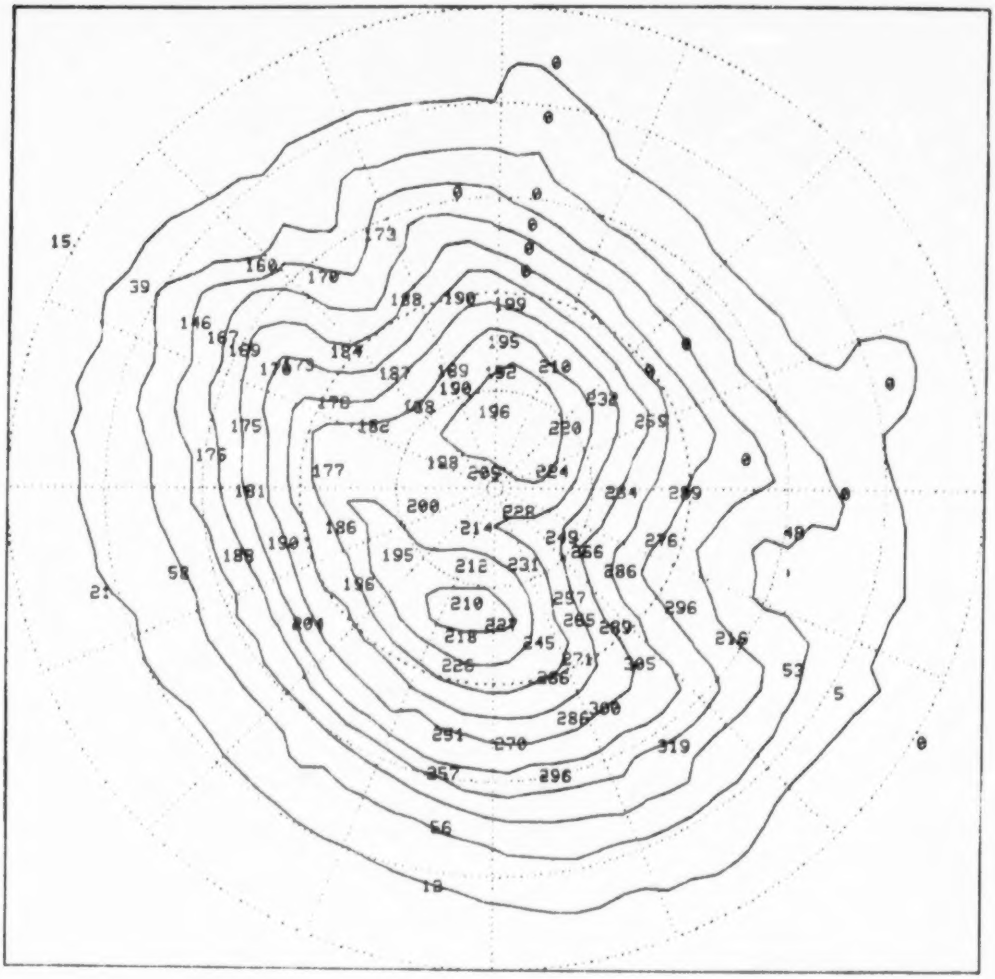

Figure 48. Complex I: calculated SF_6 concentrations (ppt) for Case 205, Hour 5, Stability Class F.

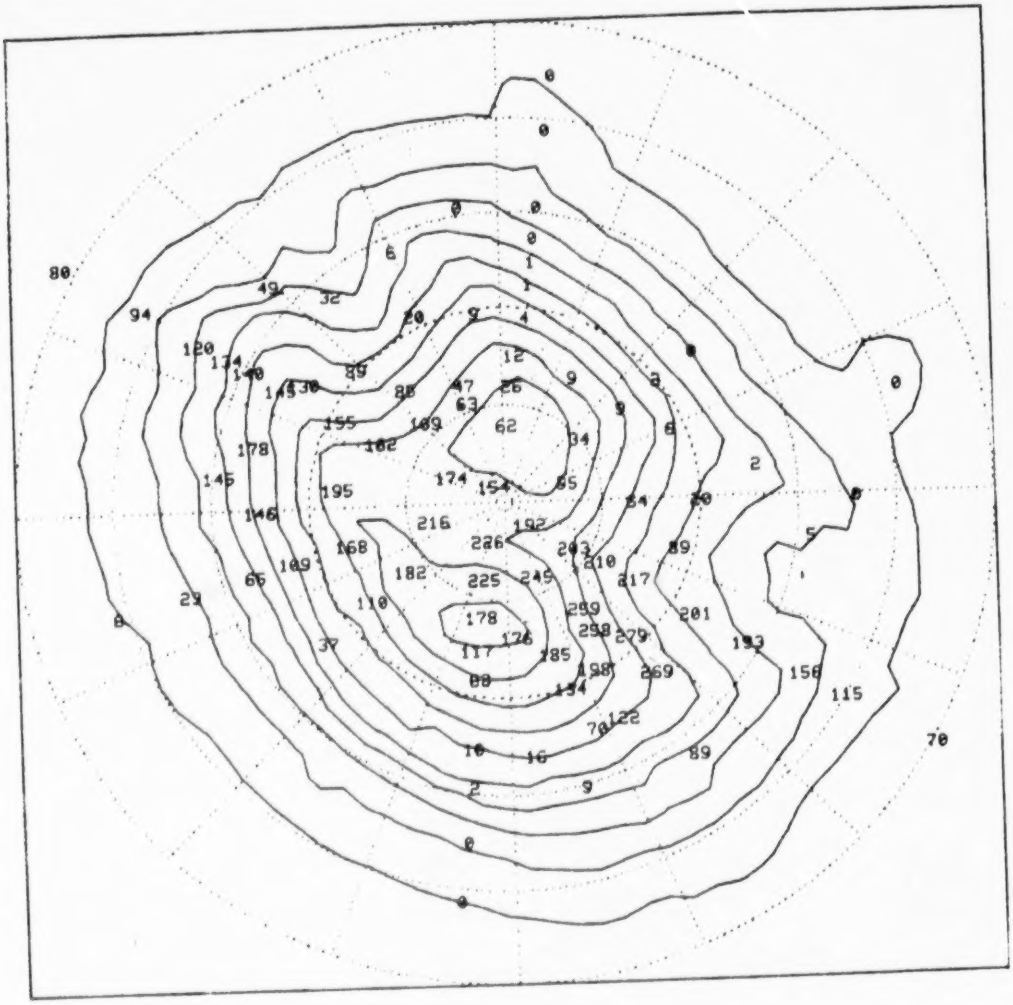

Figure 49. Complex II: calculated SF_6 concentrations (ppt) for Case 205, Hour 5, Stability Class D.

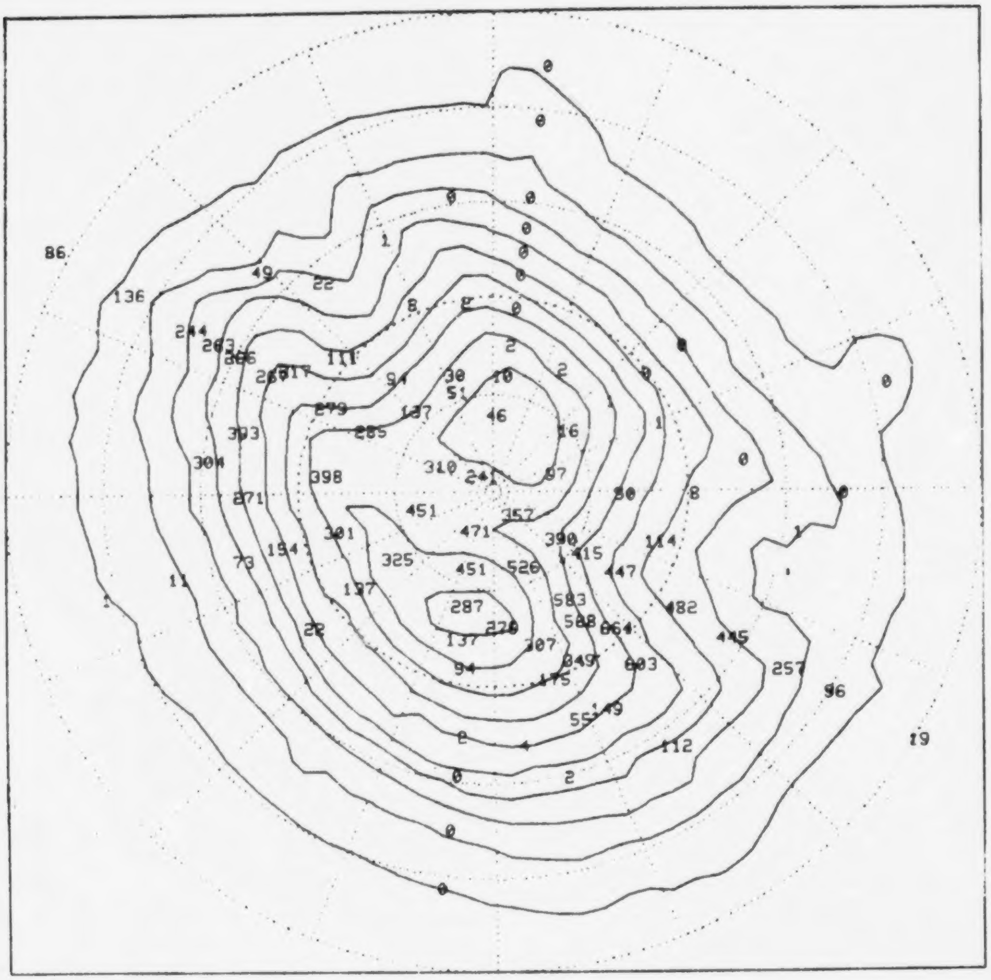

Figure 50. Complex II: calculated SF_6 concentrations (ppt) for Case 205, Hour 5, Stability Class E.

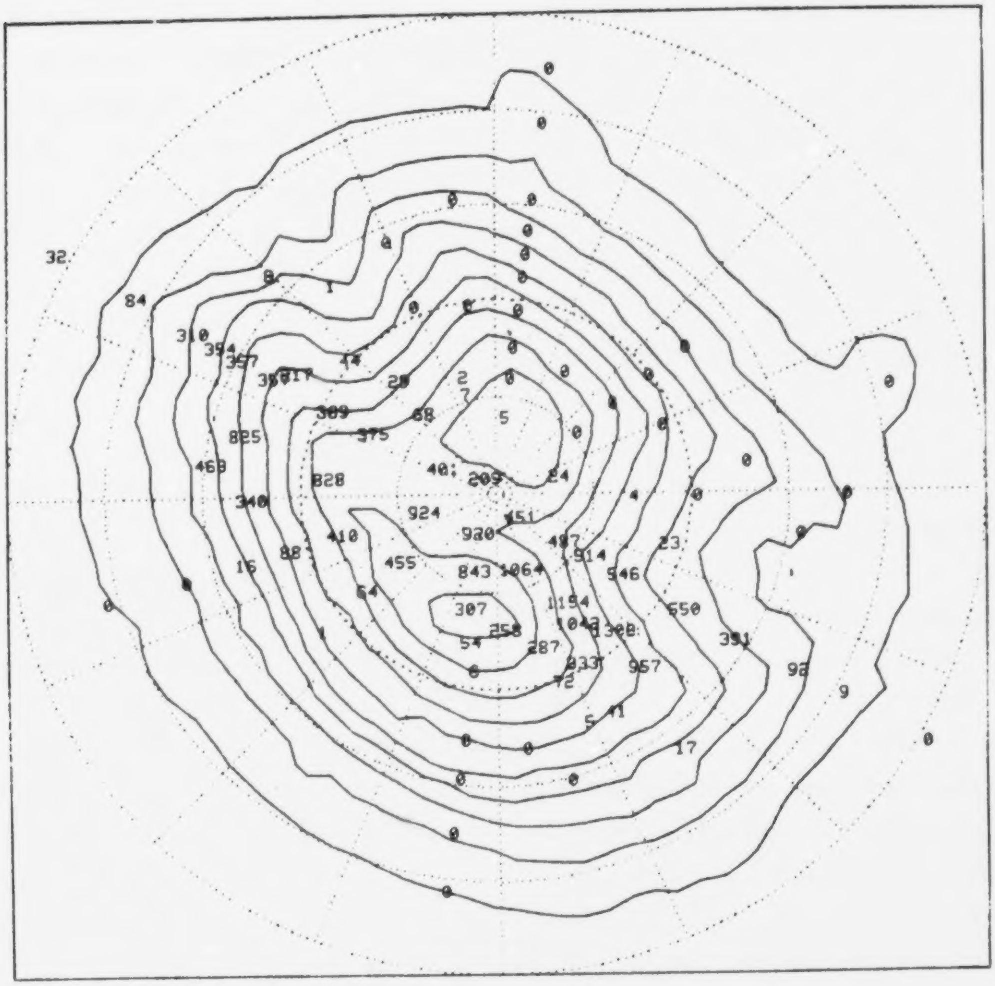

Figure 51. Complex II: calculated SF_6 concentrations (ppt) for Case 205, Hour 5, Stability Class F.

the top of the hill, COMPLEX I with class E dispersion coefficients does a fair job of estimating those concentrations.

A better quantitative idea of the performance of each of the models is obtained by looking at scatterplots of modeled versus observed concentrations. In Figures 52, 53, and 54, the solid triangles indicate COMPLEX II results and the open squares indicate COMPLEX I results. For potential regulatory application, of course, the chief interest is to gauge how extensively and consistently the models may overestimate or underestimate concentrations, especially the highest observed concentrations. Scatterplots are extremely helpful in identifying such gross tendencies. As shown in the second of these scatterplots, for example, the COMPLEX I model run with E stability tends to overestimate the lower observed concentrations ($C_o <$ 80 ppt) but to underestimate the higher concentrations. By comparison, the COMPLEX II model both overestimates and underestimates the lower observed concentrations by much wider margins than COMPLEX I. COMPLEX II underestimates the peak observed concentration but overestimates the second highest, in each case by substantial margins.

Tables 23 through 25 display frequency histograms for the observed concentrations, for the concentrations modeled with COMPLEX I and COMPLEX II, and for the residuals. (As before, the model calculations are shown successively for stability classes D, E, and F.) For example, as Table 24 for class E shows, the COMPLEX I results span a narrow range similar to the observed concentrations; whereas the COMPLEX II results are broadly distributed. From the histograms of the residuals, it can readily be seen that the COMPLEX II paired results are on average skewed slightly toward overestimation; that the COMPLEX I results are skewed (very weakly) toward overestimation; and that for either model most of the residuals are less than 160 ppt.

The next level of analysis uses the descriptive statistics calculated from all paired concentrations for the case study hour. Tables 26 through 31 show these calculations for the six previous combinations of model and stability class. The column "ID" refers to individual sampler locations shown previously in Figure 12. (For this data hour, a total of 31 valid, nonzero, full-hour average SF_6 concentration samples was obtained.) The other table entries are self-explanatory.

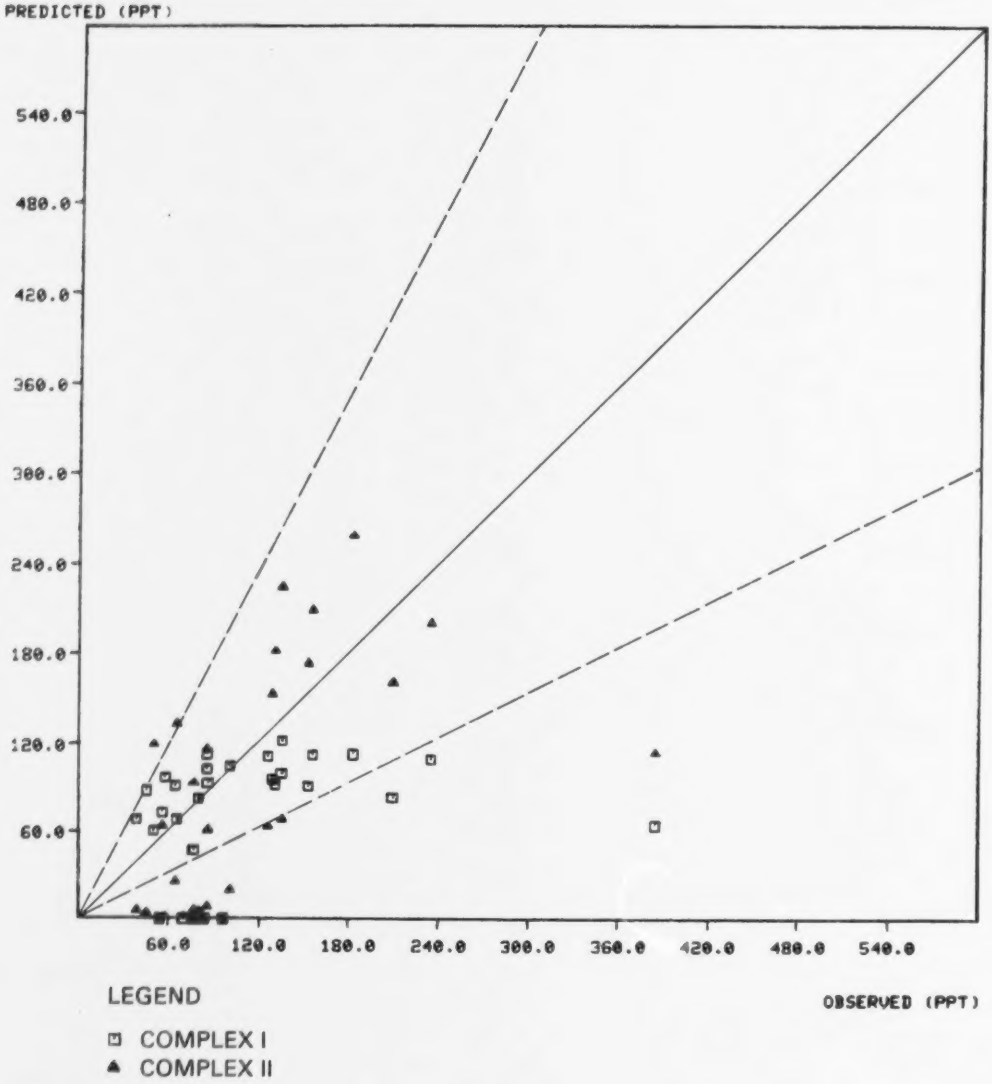

Figure 52. Complex I and II: calculated SF_6 concentrations versus observed SF_6 concentrations for Case 205, Hour 5, Stability Class D.

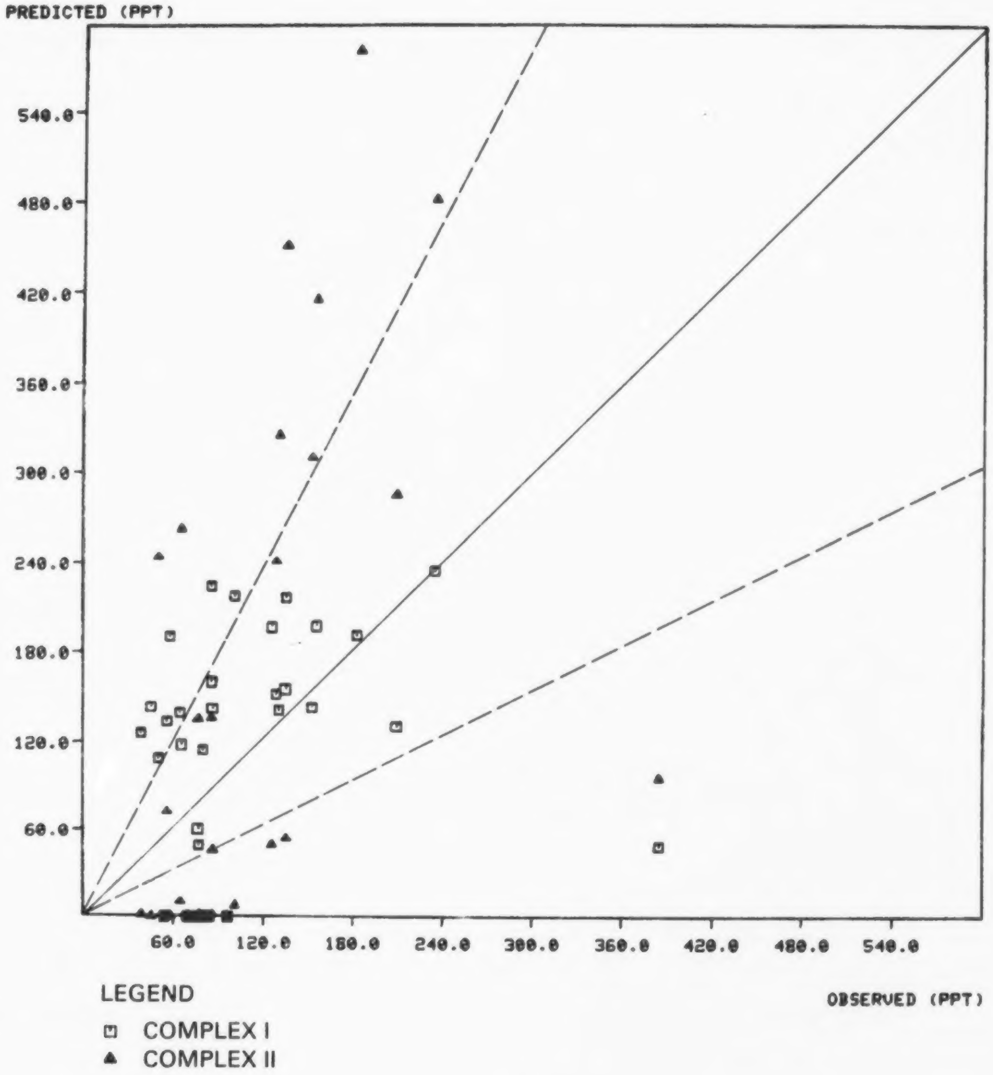

Figure 53. Complex I and II: calculated SF_6 concentrations versus observed SF_6 concentrations for Case 205, Hour 5, Stability Class E.

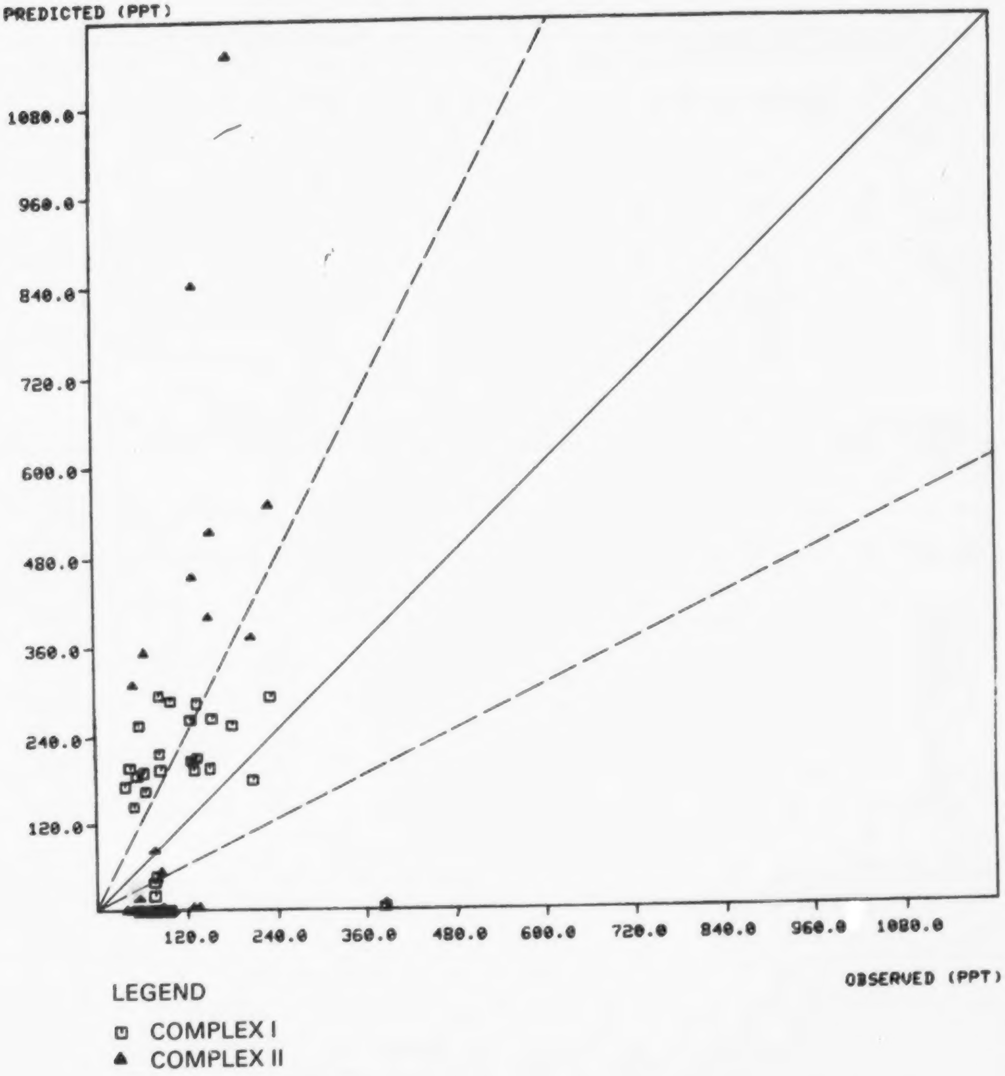

Figure 54. Complex I and II: calculated SF_6 concentrations versus observed SF_6 concentrations for Case 205, Hour 5, Stability Class F.

TABLE 23. FREQUENCY DISTRIBUTIONS OF SF_6 CONCENTRATIONS (ppt)
FOR COMPLEX I AND II MODELS
(CASE 205, HOUR 5, STABILITY CLASS D)

CLASS INTERVAL	OBSERVED	COMPLEX I	COMPLEX II
0. - 5.	0	6	8
5. - 10.	0	0	4
10. - 60.	6	2	2
60. - 110.	14	17	5
110. - 160.	7	6	5
160. - 210.	2	0	5
210. - 260.	1	0	2
260. - 310.	0	0	0
310. - 360.	0	0	0
360. - 410.	1	0	0

RESIDUALS (CO-CP)

CLASS INTERVAL	COMPLEX I	COMPLEX II
-400. - -320.	0	0
-320. - -240.	0	0
-240. - -160.	0	0
-160. - -80.	0	1
-80. - 0.	12	10
0. - 80	13	16
80. - 160	5	3
160. - 240.	0	0
240. - 320.	1	1
320. - 400.	0	0

ABSOLUTE RESIDUALS |CO-CP|

CLASS INTERVAL	COMPLEX I	COMPLEX II
0. - 40.	18	9
40. - 80.	7	17
80. - 120.	3	4
120. - 160.	2	0
160. - 200.	0	0
200. - 240.	0	0
240. - 280.	0	1
280. - 320.	1	0
320. - 360.	0	0
360. - 400.	0	0

TABLE 24. FREQUENCY DISTRIBUTIONS OF SF_6 CONCENTRATIONS (ppt) FOR COMPLEX I AND II MODELS (CASE 205, HOUR 5, STABILITY CLASS E)

CLASS INTERVAL	OBSERVED	COMPLEX I	COMPLEX II
0. - 5.	0	6	12
5. - 10.	0	0	1
10. - 90.	18	3	5
90. - 170.	9	14	3
170. - 250.	3	8	2
250. - 330.	0	0	4
330. - 410.	1	0	0
410. - 490.	0	0	3
490. - 570.	0	0	0
570. - 650.	0	0	1

RESIDUALS (CO-CP)

CLASS INTERVAL	COMPLEX I	COMPLEX II
-400. - -320.	0	1
-320. - -240.	0	3
-240. - -160.	0	3
-160. - -80.	6	2
-80. - 0.	14	4
0. - 80	7	11
80. - 160	3	6
160 - 240.	0	0
240. - 320	0	1
320. - 400	1	0

ABSOLUTE RESIDUALS |CO-CP|

CLASS INTERVAL	COMPLEX I	COMPLEX II
0. - 40.	9	2
40. - 80.	12	13
80. - 120.	7	7
120. - 160.	2	1
160. - 200.	0	3
200. - 240.	0	0
240. - 280.	0	2
280. - 320.	0	2
320. - 360.	1	0
360. - 400.	0	1

TABLE 25. FREQUENCY DISTRIBUTIONS OF SF_6 CONCENTRATIONS (ppt) FOR COMPLEX I AND II MODELS (CASE 205, HOUR 5, STABILITY CLASS F)

CLASS INTERVAL	OBSERVED	COMPLEX I	COMPLEX II
0. - 5.	0	6	16
5. - 10.	0	1	2
10. - 160.	27	4	3
160. - 310.	3	20	1
310. - 460.	1	0	5
460. - 610.	0	0	2
610. - 760.	0	0	0
760. - 910.	0	0	1
910. - 1060.	0	0	0
1060. - 1210.	0	0	1

RESIDUALS (CO-CP)			ABSOLUTE RESIDUALS |CO-CP|		
CLASS INTERVAL	COMPLEX I	COMPLEX II	CLASS INTERVAL	COMPLEX I	COMPLEX II
-1000. - -800.	0	1	0. - 100.	17	18
-800. - -600.	0	1	100. - 200.	12	4
-600. - -400.	0	0	200. - 300.	1	3
-400. - -200.	1	6	300. - 400.	1	4
-200. - 0.	19	3	400. - 500.	0	0
0. - 200.	10	19	500. - 600.	0	0
200. - 400.	1	1	600. - 700.	0	0
400. - 600.	0	0	700. - 800.	0	1
600. - 800.	0	0	800. - 900.	0	0
800. - 1000.	0	0	900. - 1000.	0	1

TABLE 26. OBSERVED VERSUS COMPLEX I PAIRED CONCENTRATIONS
(CASE 205, HOUR 5, STABILITY CLASS D)

ID	CO (PPT)	CP (PPT)	CO-CP (PPT)	CP/CO
26C	84.3	.0	84.3	.00
26E	101.3	105.1	-3.8	1.04
26F	126.7	112.3	14.4	.89
27C	80.2	.0	80.2	.00
28Z	96.7	.0	96.7	.00
31E	76.5	.0	76.5	.00
31G	70.1	.0	70.1	.00
37C	54.4	.0	54.4	.00
37K	64.8	91.9	-27.1	1.42
37L	86.6	93.8	-7.2	1.08
37T	45.9	88.5	-42.6	1.93
37Z	128.9	96.6	32.3	.75
39E	58.4	97.4	-39.0	1.67
39R	85.8	103.4	-17.6	1.20
39T	135.4	100.7	34.7	.74
45X	131.5	92.8	38.7	.71
48B	77.0	47.8	29.2	.62
48E	55.9	73.5	-17.6	1.32
54D	85.9	113.5	-27.6	1.32
55E	136.1	122.2	13.9	.90
57Z	182.8	113.4	69.4	.62
60B	384.6	65.3	319.3	.17
60V	234.6	110.1	124.5	.47
60X	155.9	112.8	43.1	.72
63C	80.3	82.9	-2.6	1.03
67B	76.8	47.9	28.9	.62
67D	50.6	61.4	-10.8	1.21
67E	66.0	68.8	-2.8	1.04
67Y	209.6	84.4	125.2	.40
67Z	153.0	91.7	61.3	.60
72W	39.0	68.7	-29.7	1.76

```
MEAN OBSERVED CONC. =      110.2 PPT   VAR. =   4747.3 PPT**2   STD. DEV. =  68.9 PPT
MEAN PREDICTED CONC. =      72.5 PPT   VAR. =   1597.7 PPT**2   STD. DEV. =  40.0 PPT
MEAN CO-CP CONC. =          37.7 PPT   VAR. =   4788.7 PPT**2   STD. DEV. =  69.2 PPT
MEAN !CO-CP! CONC. =        52.4 PPT   VAR. =   3461.4 PPT**2   STD. DEV. =  58.8 PPT
```

TABLE 27. OBSERVED VERSUS COMPLEX I PAIRED CONCENTRATIONS
(CASE 205, HOUR 5, STABILITY CLASS E)

ID	CO (PPT)	CP (PPT)	CO-CP (PPT)	CP/CO
26C	84.3	.0	84.3	.00
26E	101.3	218.0	-116.7	2.15
26F	126.7	197.0	-70.3	1.55
27C	80.2	.0	80.2	.00
28Z	96.7	.0	96.7	.00
31E	76.5	.0	76.5	.00
31G	70.1	.0	70.1	.00
37C	54.4	.0	54.4	.00
37K	64.8	139.9	-75.1	2.16
37L	86.6	142.8	-56.2	1.65
37T	45.9	143.8	-97.9	3.13
37Z	128.9	152.7	-23.8	1.18
39E	58.4	190.5	-132.1	3.26
39R	85.8	160.6	-74.8	1.87
39T	135.4	155.7	-20.3	1.15
45X	131.5	141.8	-10.3	1.08
48B	77.0	49.6	27.4	.64
48E	55.9	134.5	-78.6	2.41
54D	85.9	224.4	-138.5	2.61
55E	136.1	216.5	-80.4	1.59
57Z	182.8	191.7	-8.9	1.05
60B	384.6	49.4	335.2	.13
60V	234.6	235.0	-.4	1.00
60X	155.9	198.1	-42.2	1.27
63C	80.3	114.7	-34.4	1.43
67B	76.8	60.5	16.3	.79
67D	50.6	109.4	-58.8	2.16
67E	66.0	118.2	-52.2	1.79
67Y	209.6	131.1	78.5	.63
67Z	153.0	143.8	9.2	.94
72W	39.0	126.1	-87.1	3.23

MEAN OBSERVED CONC. = 110.2 PPT VAR. = 4747.3 PPT**2 STD. DEV. = 68.9 PPT
MEAN PREDICTED CONC. = 120.8 PPT VAR. = 5549.6 PPT**2 STD. DEV. = 74.5 PPT
MEAN CO-CP CONC. = -10.6 PPT VAR. = 8463.9 PPT**2 STD. DEV. = 92.0 PPT
MEAN !CO-CP! CONC. = 70.6 PPT VAR. = 3597.7 PPT**2 STD. DEV. = 60.0 PPT

TABLE 28. OBSERVED VERSUS COMPLEX I PAIRED CONCENTRATIONS (CASE 205, HOUR 5, STABILITY CLASS F)

ID	CO (PPT)	CP (PPT)	CO-CP (PPT)	CP/CO
26C	84. 3	. 0	84. 3	. 00
26E	101. 3	289. 4	-188. 1	2. 86
26F	126. 7	264. 4	-137. 7	2. 09
27C	80. 2	. 0	80. 2	. 00
28Z	96. 7	. 0	96. 7	. 00
31E	76. 5	. 0	76. 5	. 00
31G	70. 1	. 0	70. 1	. 00
37C	54. 4	. 0	54. 4	. 00
37K	64. 8	192. 5	-127. 7	2. 97
37L	86. 6	196. 1	-109. 5	2. 26
37T	45. 9	198. 8	-152. 9	4. 33
37Z	128. 9	209. 0	-80. 1	1. 62
39E	58. 4	257. 3	-198. 9	4. 41
39R	85. 8	217. 9	-132. 1	2. 54
39T	135. 4	212. 0	-76. 6	1. 57
45X	131. 5	194. 9	-63. 4	1. 48
48B	77. 0	21. 1	55. 9	. 27
48E	55. 9	187. 9	-132. 0	3. 36
54D	85. 9	296. 4	-210. 5	3. 45
55E	136. 1	286. 4	-150. 3	2. 10
57Z	182. 8	256. 9	-74. 1	1. 41
60B	384. 6	5. 1	379. 5	. 01
60V	234. 6	295. 6	-61. 0	1. 26
60X	155. 9	265. 8	-109. 9	1. 70
63C	80. 3	48. 3	32. 0	. 60
67B	76. 8	39. 3	37. 5	. 51
67D	50. 6	145. 7	-95. 1	2. 88
67E	66. 0	166. 9	-100. 9	2. 53
67Y	209. 6	182. 0	27. 6	. 87
67Z	153. 0	198. 0	-45. 0	1. 29
72W	39. 0	173. 1	-134. 1	4. 44

MEAN OBSERVED CONC. = 110. 2 PPT VAR. = 4747. 3 PPT**2 STD. DEV. = 68. 9 PPT
MEAN PREDICTED CONC. = 154. 9 PPT VAR. = 11304. 5 PPT**2 STD. DEV. = 106. 3 PPT
MEAN CO-CP CONC. = -44. 7 PPT VAR. = 14491. 8 PPT**2 STD. DEV. = 120. 4 PPT
MEAN ¦CO-CP¦ CONC. = 108. 9 PPT VAR. = 4638. 0 PPT**2 STD. DEV. = 68. 1 PPT

TABLE 29. OBSERVED VERSUS COMPLEX II PAIRED CONCENTRATIONS
(CASE 205, HOUR 5, STABILITY CLASS D)

ID	CO (PPT)	CP (PPT)	CO-CP (PPT)	CP/CO
26C	84.3	.1	84.2	.00
26E	101.3	20.2	81.1	.20
26F	126.7	64.3	62.4	.51
27C	80.2	2.1	78.1	.03
28Z	96.7	.0	96.7	.00
31E	76.5	.1	76.4	.00
31G	70.1	1.5	68.6	.02
37C	54.4	.0	54.4	.00
37K	64.8	26.2	38.6	.40
37L	86.6	61.9	24.7	.72
37T	45.9	3.8	42.1	.08
37Z	128.9	153.9	-25.0	1.19
39E	58.4	1.9	56.5	.03
39R	85.8	116.5	-30.7	1.36
39T	135.4	224.9	-89.5	1.66
45X	131.5	182.5	-51.0	1.39
48B	77.0	6.5	70.5	.08
48E	55.9	64.8	-8.9	1.16
54D	85.9	8.7	77.2	.10
55E	136.1	69.5	66.6	.51
57Z	182.8	259.4	-76.6	1.42
60B	384.6	115.0	269.6	.30
60V	234.6	201.2	33.4	.86
60X	155.9	209.8	-53.9	1.35
63C	80.3	5.4	74.9	.07
67B	76.8	94.0	-17.2	1.22
67D	50.6	119.9	-69.3	2.37
67E	66.0	134.0	-68.0	2 03
67Y	209.6	161.8	47.8	.77
67Z	153.0	174.3	-21.3	1.14
72W	39.0	6.1	32.9	.16

MEAN OBSERVED CONC. = 110.2 PPT VAR. = 4747.3 PPT**2 STD. DEV. = 68.9 PPT
MEAN PREDICTED CONC. = 80.3 PPT VAR. = 6519.0 PPT**2 STD. DEV. = 80.7 PPT
MEAN CO-CP CONC. = 29.8 PPT VAR. = 5008.9 PPT**2 STD. DEV. = 70.8 PPT
MEAN !CO-CP! CONC. = 62.8 PPT VAR. = 1951.4 PPT**2 STD. DEV. = 44.2 PPT

TABLE 30. OBSERVED VERSUS COMPLEX II PAIRED CONCENTRATIONS
(CASE 205, HOUR 5, STABILITY CLASS E)

ID	CO (PPT)	CP (PPT)	CO-CP (PPT)	CP/CO
26C	84. 3	. 0	84. 3	. 00
26E	101. 3	7. 9	93. 4	. 08
26F	126. 7	50. 1	76. 6	. 40
27C	80. 2	. 1	80. 1	. 00
28Z	96. 7	. 0	96. 7	. 00
31E	76. 5	. 0	76. 5	. 00
31G	70. 1	. 1	70. 1	. 00
37C	54. 4	. 0	54. 4	. 00
37K	64. 8	10. 1	54. 7	. 16
37L	86. 6	46. 3	40. 3	. 54
37T	45. 9	. 3	45. 6	. 01
37Z	128. 9	240. 8	-111. 9	1. 87
39E	58. 4	. 1	58. 3	. 00
39R	85. 8	136. 7	-50. 9	1. 59
39T	135. 4	450. 8	-315. 3	3. 33
45X	131. 5	325. 2	-193. 7	2. 47
48B	77. 0	. 9	76. 1	. 01
48E	55. 9	72. 6	-16. 7	1. 30
54D	85. 9	1. 6	84. 3	. 02
55E	136. 1	54. 6	81. 5	. 40
57Z	182. 8	582. 7	-399. 9	3. 19
60B	384. 6	96. 3	288. 3	. 25
60V	234. 6	481. 9	-247. 3	2. 05
60X	155. 9	415. 5	-259. 6	2. 66
63C	80. 3	. 6	79. 7	. 01
67B	76. 8	135. 7	-58. 9	1. 77
67D	50. 6	243. 9	-193. 3	4. 82
67E	66. 0	262. 7	-196. 7	3. 98
67Y	209. 6	285. 5	-75. 9	1. 36
67Z	153. 0	310. 2	-157. 2	2. 03
72W	39. 0	1. 1	37. 9	. 03

MEAN OBSERVED CONC. = 110. 2 PPT VAR. = 4747. 3 PPT**2 STD. DEV. = 68. 9 PPT
MEAN PREDICTED CONC. = 135. 9 PPT VAR. = 29162. 2 PPT**2 STD. DEV. = 170. 8 PPT
MEAN CO-CP CONC. = -25. 8 PPT VAR. = 22643. 3 PPT**2 STD. DEV. = 150. 5 PPT
MEAN !CO-CP! CONC. = 121. 2 PPT VAR. = 8627. 0 PPT**2 STD. DEV. = 92. 9 PPT

TABLE 31. OBSERVED VERSUS COMPLEX II PAIRED CONCENTRATIONS
(CASE 205, HOUR 5, STABILITY CLASS F)

ID	CO (PPT)	CP (PPT)	CO-CP (PPT)	CP/CO
26C	84.3	.0	84.3	.00
26E	101.3	.1	101.2	.00
26F	126.7	4.3	122.4	.03
27C	80.2	.0	80.2	.00
28Z	96.7	.0	96.7	.00
31E	76.5	.0	76.5	.00
31G	70.1	.0	70.1	.00
37C	54.4	.0	54.4	.00
37K	64.8	.2	64.6	.00
37L	86.6	5.5	81.1	.06
37T	45.9	.0	45.9	.00
37Z	128.9	209.3	-80.4	1.62
39E	58.4	.0	58.4	.00
39R	85.8	54.3	31.5	.63
39T	135.4	843.4	-708.0	6.23
45X	131.5	454.7	-323.2	3.46
48B	77.0	.0	77.0	.00
48E	55.9	16.4	39.5	.29
54D	85.9	.0	85.9	.00
55E	136.1	4.6	131.5	.03
57Z	182.8	1153.7	-970.9	6.31
60B	384.6	8.7	375.9	.02
60V	234.6	550.1	-315.5	2.34
60X	155.9	514.2	-358.3	3.30
63C	80.3	.0	80.3	.00
67B	76.8	84.4	-7.6	1.10
67D	50.6	310.4	-259.8	6.13
67E	66.0	354.0	-288.0	5.36
67Y	209.6	374.5	-164.9	1.79
67Z	153.0	401.2	-248.2	2.62
72W	39.0	.0	39.0	.00

MEAN OBSERVED CONC. =	110.2 PPT	VAR. =	4747.3 PPT**2	STD. DEV. =	68.9 PPT
MEAN PREDICTED CONC. =	172.4 PPT	VAR. =	79747.1 PPT**2	STD. DEV. =	282.4 PPT
MEAN CO-CP CONC. =	-62.2 PPT	VAR. =	69765.7 PPT**2	STD. DEV. =	264.1 PPT
MEAN !CO-CP! CONC. =	178.1 PPT	VAR. =	41910.6 PPT**2	STD. DEV. =	204.7 PPT

To determine which of these six model/stability class combinations best matches the observed concentrations during Case 205, hour 5, the respective statistics shown at the bottom of each table should be compared. Table 32 lists these for side-by-side comparisons. If all criteria were given equal weight, the descriptive statistics would seem to suggest that of these six choices of model and stability class, the COMPLEX I model with E stability is preferred (note that the maximum is estimated better by two other choices):

- the mean modeled value agrees most closely with the mean observed value and is somewhat larger (slightly conservative),
- the mean residual error is smallest (least bias),
- the standard deviation of the residual error is not much larger than the standard deviation of the observed concentrations, and
- the standard deviation of the modeled concentrations is only marginally greater than that of the observed concentrations.

5.4.2 PFM

A similar set of plots, tables, and figures is presented below for the PFM simulation of Case 205, hour 5. Stability classes D and E were both used in running PFM so that comparisons could be made with the best-performing versions of the COMPLEX computations.

The 1-hour average ground-level SF_6 concentrations calculated by PFM are shown in Figures 55 and 56. The distribution of modeled concentrations is qualitatively similar to that calculated by the COMPLEX II model for the same stability classes because they use similar horizontal distribution functions. The magnitudes, however, are different.

PFM with stability class E produces concentrations in excess of the observed maximum but tends to overestimate all of the concentrations on the central part of the hill. If the observed maximum (located at the base of the windward side of the hill) is ignored, PFM with stability class D does better; still, there appears to be too little plume spread to match the observations.

TABLE 32. SUMMARY STATISTICS FOR COMPLEX I AND COMPLEX II

(Case 205, Hour 5)

		COMPLEX I Stability Class			COMPLEX II Stability Class		
	OBSERVED	D	E	F	D	E	F
Number of Points	31	-	-	-	-	-	-
$\overline{C}_o$	110	-	-	-	-	-	-
$\sigma(C_o)$	69	-	-	-	-	-	-
$\max(C_o)$	385	-	-	-	-	-	-
$\overline{C}_p$	-	73	121	155	80	136	172
$\sigma(C_p)$	-	40	75	106	81	171	282
$\max(C_p)$	-	122	235	296	259	583	1,154
$\overline{C_o - C_p}$	-	38	-11	-45	30	-26	-62
$\sigma(C_o - C_p)$	-	69	92	120	71	151	264
$\max\lvert C_o - C_p\rvert$	-	319	335	380	270	400	971
$\overline{\lvert C_o - C_p\rvert}$	-	52	71	109	63	121	178
$\sigma(\lvert C_o - C_p\rvert)$	-	59	60	68	44	93	205

Note: SF_6 concentrations are in ppt.

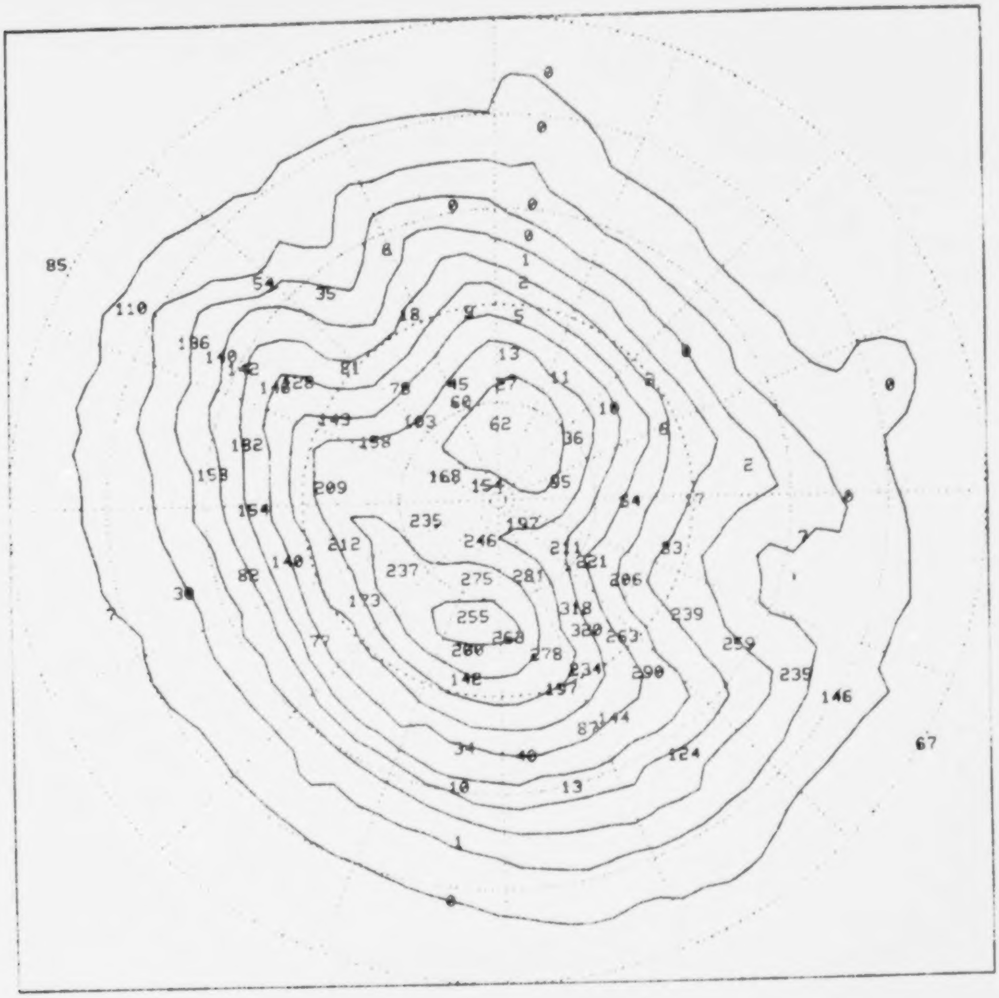

Figure 55. PFM: calculated SF_6 concentrations for Case 205, Hour 5, Stability Class D.

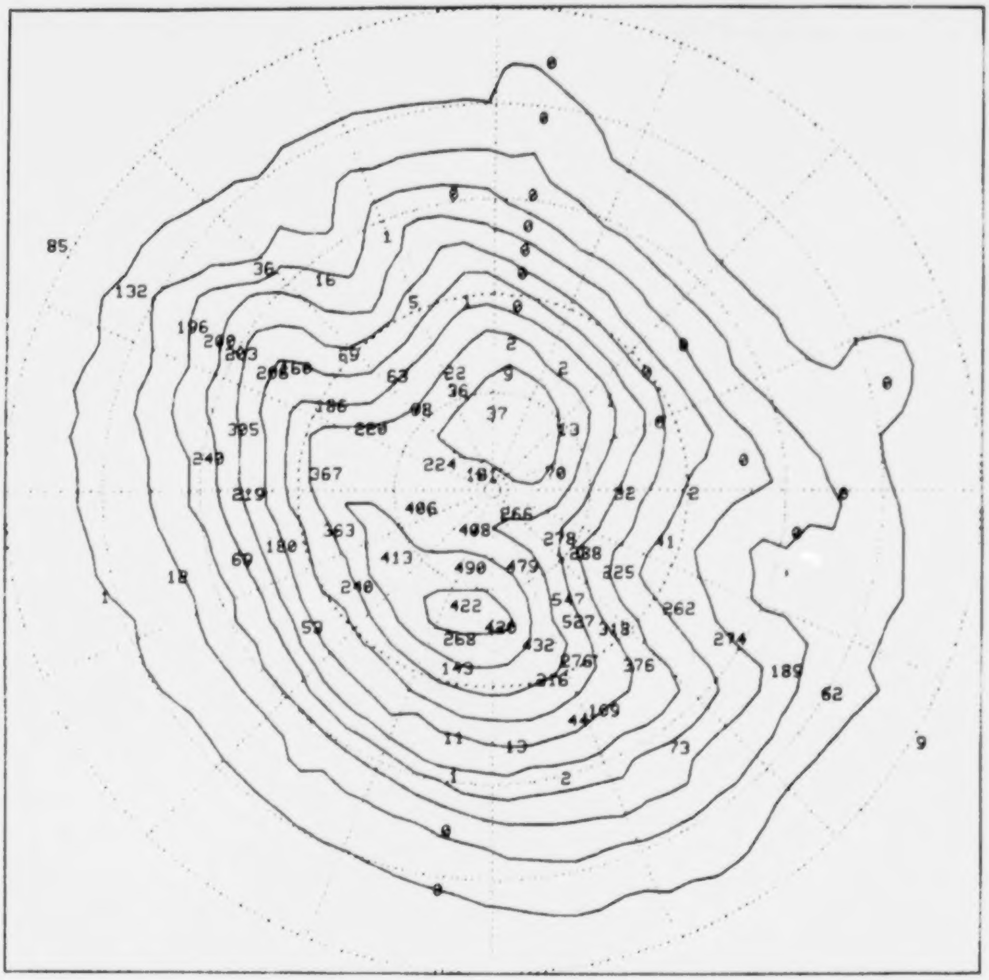

Figure 56. PFM: calculated SF_6 concentrations for Case 205, Hour 5, Stability Class E.

Scatterplots of modeled versus observed concentrations presented in Figures 57 and 58 show evident similarities with the scatterplots for COMPLEX II with stability classes D and E. Many low concentrations away from the hill center are underestimated, and most of the concentrations above 60 ppt are overestimated (especially for stability class E). Frequency distributions presented in Tables 33 and 34 show that although many similarities between PFM and COMPLEX II concentrations exist, PFM tends to produce higher concentrations. This tendency increases the range in the distribution of residuals.

Finally, paired concentrations and a summary table of the PFM statistics for this case hour are presented in Tables 35 through 37. The stability class for which PFM performs better (on the basis of summary statistics) appears to be class D, even though the mean statistics and the peak concentration show a tendency toward underestimation. A comparison of PFM and COMPLEX summary statistics shows that PFM performs as well as any of the COMPLEX models for the case hour.

5.4.3 New Experimental Models

Figure 59 displays the distribution of concentrations calculated by the Neutral model (see Section 4.5.3) for Case 205, hour 5. Concentrations are presented only at those samplers with good SF_6 data. The spread of concentrations over the hill appears to be reproduced fairly well, but most concentrations are underestimated.

These features are evident in the scatterplot of modeled versus observed concentrations as well (see Figure 60). The lower concentra- tions are just as likely to be either over- or underestimated, but few concentrations are calculated to be less than 5 ppt. The higher concentrations (>120 ppt) are underestimated.

Frequency distributions (see Table 38) and the statistics of paired concentrations (see Tables 39 and 40) reinforce this description. Modeled concentrations populate lower class intervals, and the distribution of residuals is biased toward underestimation. One half of the calculations lie within 40 ppt of the corresponding observations. The mean of all calculations is slightly greater than half the mean of all observed

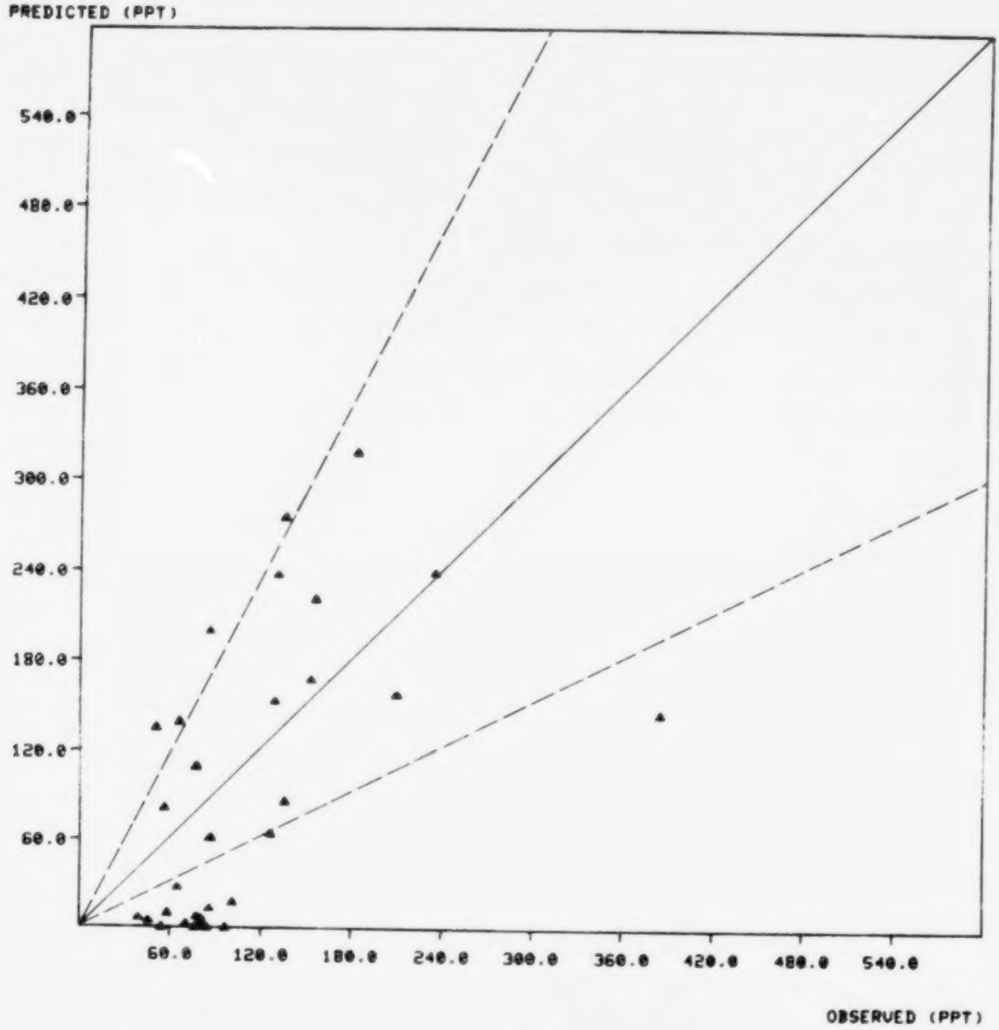

Figure 57. PFM: calculated SF_6 concentrations versus observed SF_6 concentrations for Case 205, Hour 5, Stability Class D.

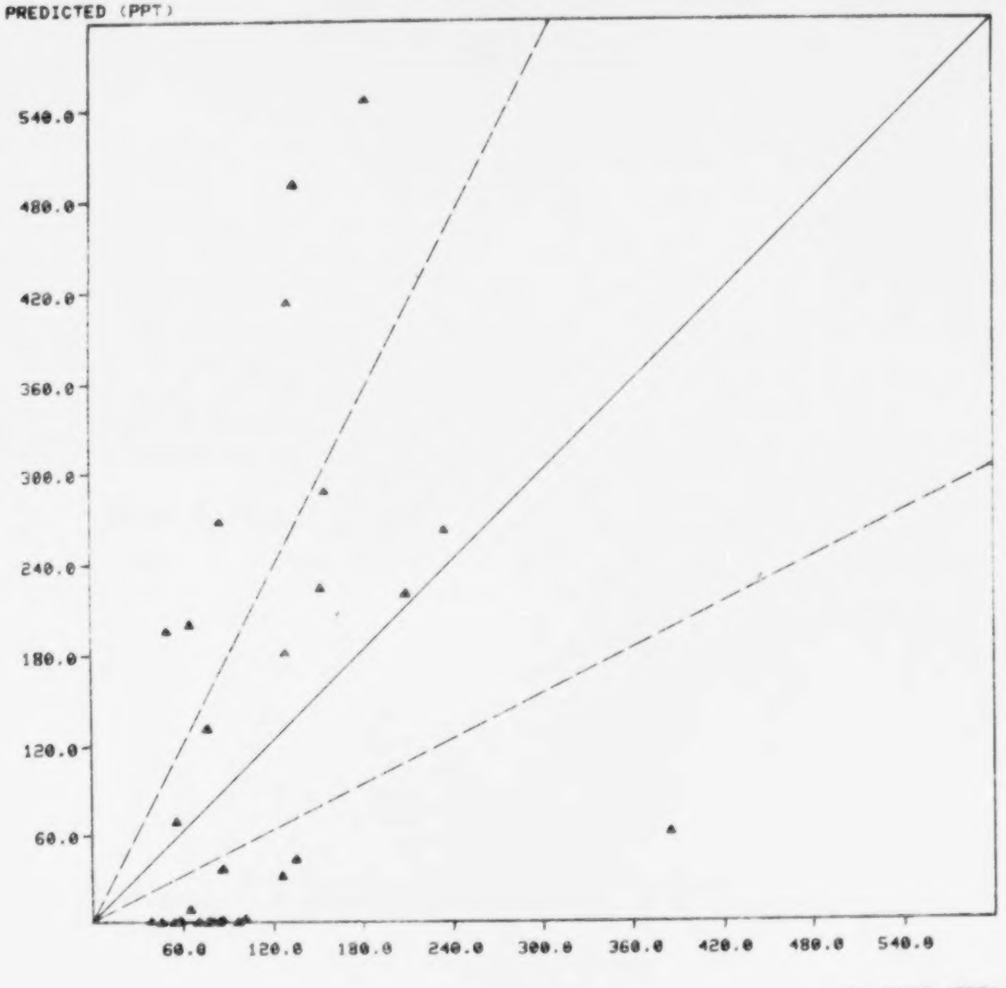

Figure 58. PFM: calculated SF_6 concentrations versus observed SF_6 concentrations for Case 205, Hour 5, Stability Class E.

TABLE 33. FREQUENCY DISTRIBUTIONS OF SF_6 CONCENTRATIONS (ppt) FOR PFM (CASE 205, HOUR 5, STABILITY CLASS D)

CLASS INTERVAL	OBSERVED	PFM
0. - 5.	0	7
5. - 10.	0	3
10. - 60.	6	4
60. - 110.	14	5
110. - 160.	7	5
160. - 210.	2	2
210. - 260.	1	3
260. - 310.	0	1
310. - 360.	0	1
360. - 410.	1	0

RESIDUALS (CO-CP)

CLASS INTERVAL	PFM
-300. - -240.	0
-240. - -180.	0
-180. - -120.	2
-120. - -60.	5
-60. - 0.	5
0. - 60.	8
60. - 120.	10
120. - 180.	0
180. - 240.	1
240. - 300.	0

ABSOLUTE RESIDUALS |CO-CP|

CLASS INTERVAL	PFM
0. - 30.	5
30. - 60.	8
60. - 90.	12
90. - 120.	3
120. - 150.	2
150. - 180.	0
180. - 210.	0
210. - 240.	1
240. - 270.	0
270. - 300.	0

TABLE 34. FREQUENCY DISTRIBUTIONS OF SF_6 CONCENTRATIONS (ppt)
FOR PFM (CASE 205, HOUR 5, STABILITY CLASS E)

```
*******************************************************
*******************************************************

      CLASS INTERVAL          OBSERVED        PFM

          0.  -     5.
          5.  -    10.            0           13
         10.  -    80.            0            1
         80.  -   150.           12            5
        150.  -   220.           13            1
        220.  -   290.            4            3
        290.  -   360.            1            5
        360.  -   430.            0            0
        430.  -   500.            1            1
        500.  -   570.            0            1
                                  0            1

*******************************************************
*******************************************************

      RESIDUALS (CO-CP)          ABSOLUTE RESIDUALS |CO-CP|

  CLASS INTERVAL       PFM       CLASS INTERVAL       PFM

  -400.  -   -320       2
  -320.  -   -240.      1           0.  -    40.        4
  -240.  -   -160.      1          40   -    80.       12
  -160.  -    -80.      3          80.  -   120.        7
   -80   -      0.      6         120   -   160.        3
     0.  -     80       10        160.  -   200.        1
    80.  -    160.      7         200.  -   240         0
   160.  -    240.      0         240.  -   280.        0
   240.  -    320.      0         280.  -   320.        1
   320.  -    400.      1         320.  -   360         2
                                  360.  -   400         1

*******************************************************
*******************************************************
```

TABLE 35. OBSERVED VERSUS PFM PAIRED CONCENTRATIONS (CASE 205, HOUR 5, STABILITY CLASS D)

ID	CO (PPT)	CP (PPT)	CO-CP (PPT)	CP/CO
26C	84.3	.2	84.1	.00
26E	101.3	17.3	84.0	.17
26F	126.7	64.5	62.2	.51
27C	80.2	2.0	78.2	.02
28Z	96.7	.0	96.7	.00
31E	76.5	.3	76.2	.00
31G	70.1	2.0	68.2	.03
37C	54.4	.0	54.4	.00
37K	64.8	27.4	37.4	.42
37L	86.6	61.8	24.8	.71
37T	45.9	4.7	41.2	.10
37Z	128.9	153.6	-24.7	1.19
39E	58.4	10.0	48.4	.17
39R	85.8	199.7	-113.9	2.33
39T	135.4	274.8	-139.4	2.03
45X	131.5	237.2	-105.7	1.80
48B	77.0	7.2	69.8	.09
48E	55.9	81.7	-25.8	1.46
54D	85.9	13.2	72.7	.15
55E	136.1	86.6	49.5	.64
57Z	182.8	318.4	-135.6	1.74
60B	384.6	146.4	238.2	.38
60V	234.6	238.9	-4.3	1.02
60X	155.9	221.2	-65.3	1.42
63C	80.3	6.7	73.6	.08
67B	76.9	109.6	-32.8	1.43
67D	50.6	135.9	-85.3	2.69
67E	66.0	139.5	-73.5	2.11
67Y	209.6	158.0	51.6	.75
67Z	153.0	167.9	-14.9	1.10
72W	39.0	6.4	32.6	.16

MEAN OBSERVED CONC. = 110.2 PPT VAR. = 4747.3 PPT**2 STD. DEV. = 68.9 PPT
MEAN PREDICTED CONC. = 93.3 PPT VAR. = 9060.5 PPT**2 STD. DEV. = 95.2 PPT
MEAN CO-CP CONC. = 16.9 PPT VAR. = 6585.8 PPT**2 STD. DEV. = 81.2 PPT
MEAN !CO-CP! CONC. = 69.8 PPT VAR. = 1991.3 PPT**2 STD. DEV. = 44.6 PPT

TABLE 36. OBSERVED VERSUS PFM PAIRED CONCENTRATIONS
(CASE 205, HOUR 5, STABILITY CLASS E)

ID	CO (PPT)	CP (PPT)	CO-CP (PPT)	CP/CO
26C	84.3	.0	84.3	.00
26E	101.3	2.4	98.9	.02
26F	126.7	31.7	95.0	.25
27C	80.2	.1	80.1	.00
28Z	96.7	.0	96.7	.00
31E	76.5	.0	76.5	.00
31G	70.1	.1	70.1	.00
37C	54.4	.0	54.4	.00
37K	64.8	8.7	56.1	.13
37L	86.6	36.5	50.1	.42
37T	45.9	.4	45.5	.01
37Z	128.9	181.2	-52.3	1.41
39E	58.4	1.2	57.2	.02
39R	85.8	267.6	-181.8	3.12
39T	135.4	490.5	-355.1	3.62
45X	131.5	412.9	-281.4	3.14
48B	77.0	.9	76.1	.01
48E	55.9	69.1	-13.2	1.24
54D	85.9	1.5	84.4	.02
55E	136.1	43.5	92.6	.32
57Z	182.8	546.7	-363.9	2.99
60B	384.6	61.6	323.0	.16
60V	234.6	262.2	-27.6	1.12
60X	155.9	288.2	-132.3	1.85
63C	80.3	.4	79.9	.00
67B	76.8	132.0	-55.2	1.72
67D	50.6	195.6	-145.0	3.87
67E	66.0	199.9	-133.9	3.03
67Y	209.6	220.1	-10.5	1.05
67Z	153.0	224.0	-71.0	1.46
72W	39.0	.7	38.3	.02

MEAN OBSERVED CONC. = 110.2 PPT VAR. = 4747.3 PPT**2 STD. DEV. = 68.9 PPT
MEAN PREDICTED CONC. = 118.7 PPT VAR. = 23759.5 PPT**2 STD. DEV. = 154.1 PPT
MEAN CO-CP CONC. = -8.5 PPT VAR. = 20545.4 PPT**2 STD. DEV. = 143.3 PPT
MEAN |CO-CP| CONC. = 109.1 PPT VAR. = 8713.3 PPT**2 STD. DEV. = 93.3 PPT

TABLE 37. SUMMARY STATISTICS FOR PFM

(Case 205, Hour 5)

	OBSERVED	PFM Stability Class D	PFM Stability Class E
Number of Points	31	-	-
$\overline{C}_o$	110	-	-
$\sigma(C_o)$	69	-	-
max (C_o)	385	-	-
$\overline{C}_p$	-	93	119
$\sigma(C_p)$	-	95	154
max (C_p)	-	318	547
$\overline{C_o - C_p}$	-	17	-9
$\sigma(C_o - C_p)$	-	81	143
max $\lvert C_o - C_p \rvert$	-	238	355
$\overline{\lvert C_o - C_p \rvert}$	-	70	109
$\sigma(\lvert C_o - C_p \rvert)$	-	45	93

Note: SF_6 concentrations are in ppt.

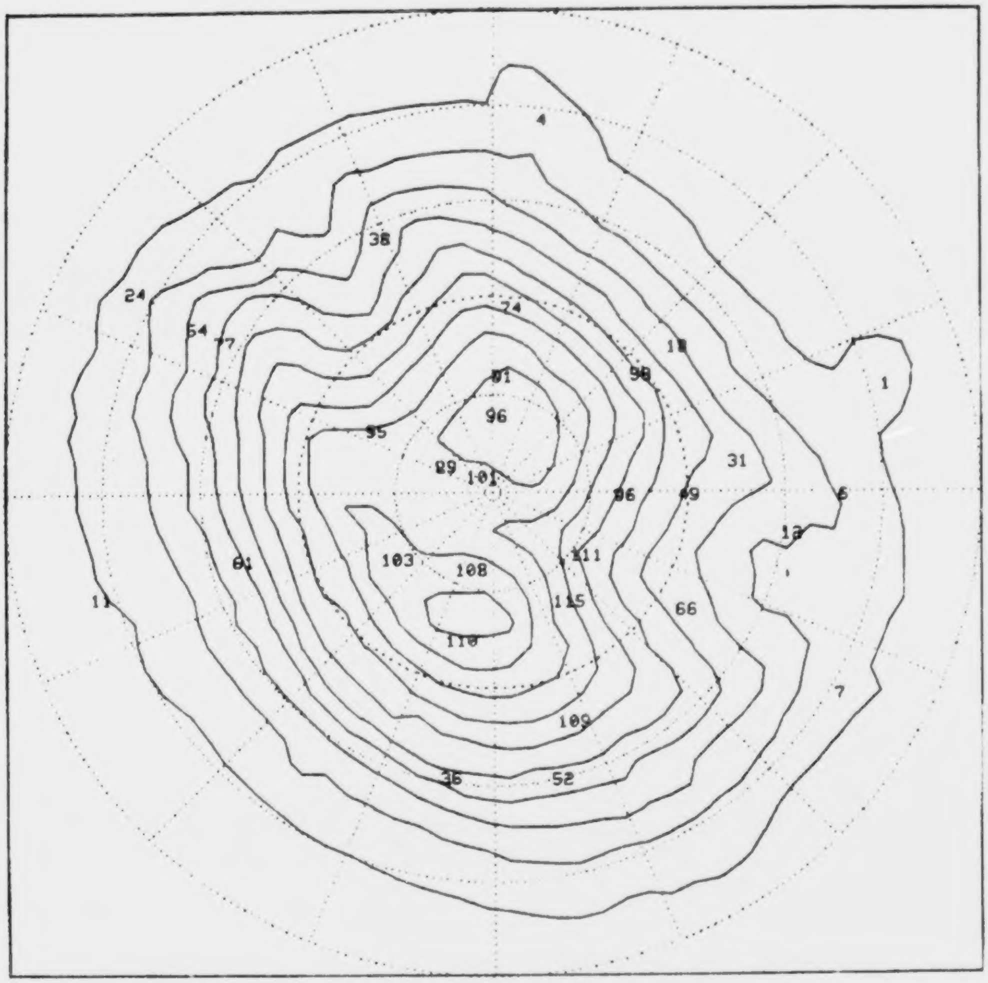

Figure 59. Neutral model: calculated SF_6 concentrations (ppt) for Case 205, Hour 5.

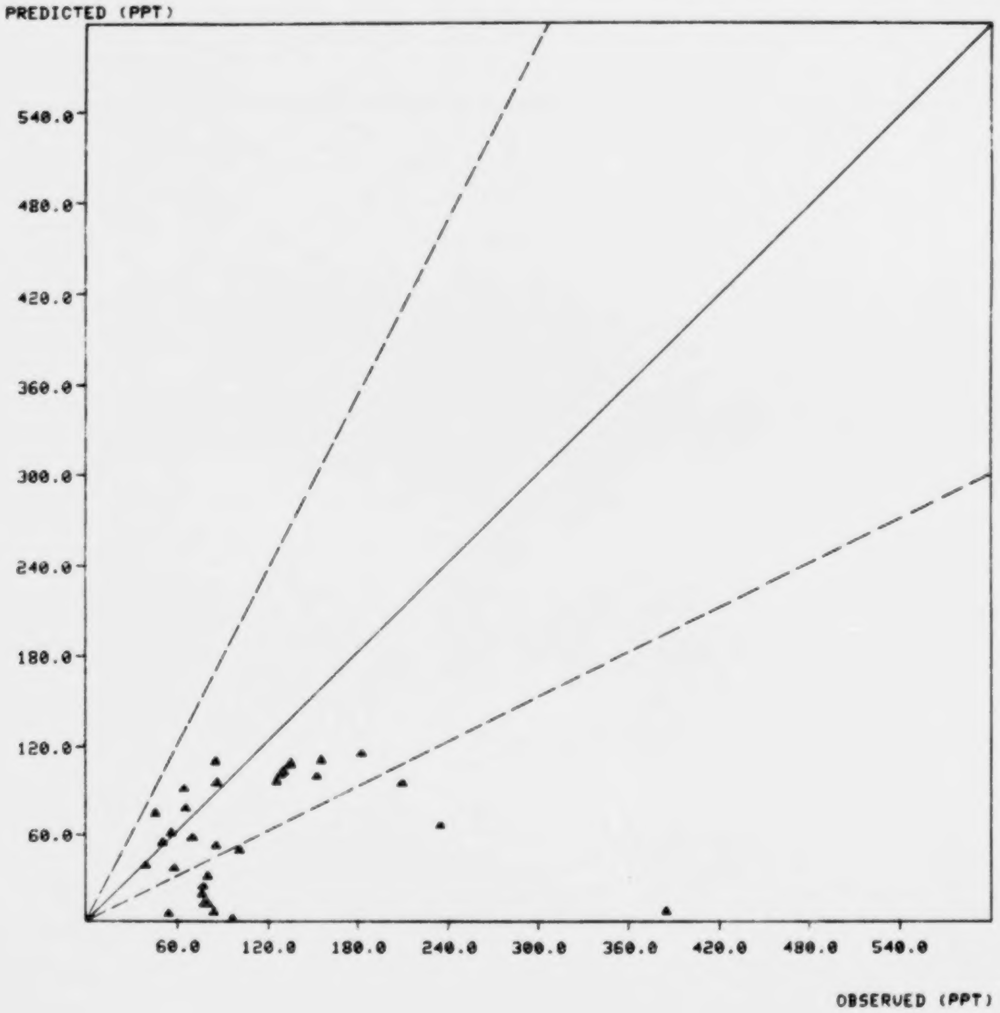

Figure 60. Neutral model: calculated SF_6 concentrations versus observed SF_6 concentrations for Case 205, Hour 5.

TABLE 38. FREQUENCY DISTRIBUTIONS OF SF_6 CONCENTRATIONS (ppt)
FOR NEUTRAL MODEL (CASE 205, HOUR 5)

```
********************************************************
********************************************************

       CLASS INTERVAL          OBSERVED   NEUTRAL MODEL


          0.  -     5.             0            2
          5.  -    10.             0            2
         10.  -    60.             6           11
         60.  -   110.            14           14
        110.  -   160.             7            2
        160.  -   210.             2            0
        210.  -   260.             1            0
        260.  -   310.             0            0
        310.  -   360.             0            0
        360.  -   410.             1            0

********************************************************
********************************************************


       RESIDUALS (CO-CP)         ABSOLUTE RESIDUALS :CO-CP!

  CLASS INTERVAL    NEUTRAL      CLASS INTERVAL    NEUTRAL


  -400.  -   -320.     0            0.  -    40.     16
  -320.  -   -240.     0           40.  -    80.     11
  -240.  -   -160.     0           80.  -   120.      2
  -160.  -    -80.     0          120.  -   160.      0
   -80.  -      0.     7          160.  -   200.      1
    0.   -     80.    20          200.  -   240.      0
   80.   -    160.     2          240.  -   280.      0
  160.   -    240.     1          280.  -   320.      0
  240.   -    320.     0          320.  -   360.      0
  320.   -    400.     1          360.  -   400.      1

********************************************************
********************************************************
```

TABLE 39. OBSERVED VERSUS NEUTRAL PAIRED CONCENTRATIONS
(CASE 205, HOUR 5)

ID	CO (PPT)	CP (PPT)	CO-CP (PPT)	CP/CO
26C	84.3	5.8	78.5	.07
26E	101.3	49.0	52.3	.48
26F	126.7	96.0	30.7	.76
27C	80.2	31.1	49.1	.39
28Z	96.7	.9	95.8	.01
31E	76.5	18.3	58.2	.24
31G	70.1	57.6	12.6	.82
37C	54.4	4.3	50.1	.08
37K	64.8	91.1	-26.3	1.41
37L	86.6	95.5	-8.9	1.10
37T	45.9	74.4	-28.5	1.62
37Z	128.9	101.1	27.8	.78
39E	58.4	36.3	22.1	.62
39R	85.8	109.6	-23.8	1.28
39T	135.4	107.7	27.7	.80
45X	131.5	103.2	28.3	.79
48B	77.0	11.4	65.6	.15
48E	55.9	60.8	-4.9	1.09
54D	85.9	52.1	33.8	.61
55E	136.1	108.6	27.5	.80
57Z	182.8	115.0	67.8	.63
60B	384.6	7.1	377.5	.02
60V	234.6	66.0	168.6	.28
60X	155.9	110.8	45.1	.71
63C	80.3	11.6	68.7	.14
67B	76.8	23.5	53.3	.31
67D	50.6	54.0	-3.4	1.07
67E	66.0	77.3	-11.3	1.17
67Y	209.6	94.9	114.7	.45
67Z	153.0	99.5	53.5	.65
72W	39.0	38.2	.8	.98

```
MEAN OBSERVED CONC. =       110.2 PPT    VAR. =    4747.3 PPT**2    STD. DEV. =    68.9 PPT
MEAN PREDICTED CONC. =       61.7 PPT    VAR. =    1458.5 PPT**2    STD. DEV. =    38.2 PPT
MEAN CO-CP CONC. =           48.5 PPT    VAR. =    5391.6 PPT**2    STD. DEV. =    73.4 PPT
MEAN !CO-CP! CONC. =         55.4 PPT    VAR. =    4673.0 PPT**2    STD. DEV. =    68.4 PPT
```

TABLE 40. SUMMARY STATISTICS FOR NEUTRAL FLOW MODEL

(Case 205, Hour 5)

	OBSERVED	NEUTRAL MODEL
Number of Points	31	-
$\overline{C}_o$	110	-
$\sigma(C_o)$	69	-
max (C_o)	385	-
$\overline{C}_p$	-	62
$\sigma(C_p)$	-	38
max (C_p)	-	115
$\overline{C_o - C_p}$	-	49
$\sigma(C_o - C_p)$	-	73
max $C_o - C_p$	-	378
$\overline{\lvert C_o - C_p \rvert}$	-	55
$\sigma(\lvert C_o - C_p \rvert)$	-	68

Note: SF_6 concentrations are in ppt.

concentrations, and the maximum calculated concentration is about one-third of the maximum observed.

5.5 Summary of Model Performance

5.5.1 Model Performance Statistics

Valley

Valley model estimates of the maximum 1-hour average tracer concentrations (scaled by the emission rate) are presented in Table 41 for each of the 45 case hours. The concentrations are scaled by the emission rate to facilitate comparisons. Also included are the associated centerline concentrations (zero stand-off distance, no surface reflection), observed concentrations, and ratios of the hourly calculated to observed concentrations.

The Valley estimates of C/Q depend only on the distance from the source to the nearest possible point of impingement. With Valley, predicted C/Q values* range from 53 to 105. The maximum possible C/Q from the Valley model occurs at a distance of 366 m. This value is about 107, so the calculated value of 105 is virtually the greatest C/Q possible from Valley.

Valley appreciably underestimated peak observed concentrations in the four test case hours with the highest observed scaled peak concentrations (C/Q), and estimated the fifth and sixth highest scaled peak concentrations to within 1%. All peak concentrations in the remaining 39 case hours were overestimated by Valley. Of the four hours in which Valley underestimated observed concentrations, one was a nonimpingement case in that the plume was released above the critical dividing streamline. This case hour occurred in the early morning as the sun was rising, and the release was very close to the hill (213 m); so the class F dispersion rate for σ_z apparently underestimated the size of the plume. Wind speeds for the other three

---

*Units of 10^{-6} sec m^{-3}; 1 $\mu g/m^{-3}$ = 167.5 ppt for SF_6.

TABLE 41. SUMMARY C/Q STATISTICS FOR VALLEY AND CENTERLINE VALLEY CALCULATIONS

Exp	Case Hour	Max Co	Max Cp	Max Cp/ Max Co	Max CL	Max CL/ Max Co
201	1	32.2	79.5	2.47	67.5	2.10
201	2	25.1	79.5	3.17	67.5	2.69
201	4	18.6	86.2	4.63	78.5	4.22
201	5	34.6	86.2	2.49	78.5	2.27
201	6	18.7	86.2	4.61	78.5	4.20
202	1	18.0	68.2	3.79	52.4	2.91
202	2	33.6	68.2	2.03	52.4	1.56
202	3	67.2	81.4	1.21	70.3	1.05
202	4	81.6	81.4	1.00	70.3	.86
202	5	49.2	76.7	1.56	63.4	1.29
202	6	11.8	71.9	6.09	57.0	4.83
204	1	14.5	68.9	4.75	53.2	3.67
204	2	11.3	68.9	6.10	53.2	4.71
204	5	4.8	81.3	16.94	70.3	14.64
204	6	17.6	81.3	4.62	70.3	3.99
204	7	9.6	81.3	8.47	70.3	7.32
204	8	16.1	81.3	5.05	70.3	4.37
205	4	15.4	56.5	3.67	39.9	2.59
205	5	25.5	54.8	2.15	38.2	1.50
205	6	15.5	60.9	3.93	44.3	2.86
206	4	56.7	92.2	1.63	279.0	4.92
206	5	41.2	92.2	2.24	279.0	6.77
206	6	124.2	92.2	0.74	279.0	2.25
206	7	92.8	92.2	0.99	279.0	3.01
206	8	154.6	92.2	0.60	279.0	1.81
209	1	3.8	75.6	19.89	61.8	16.27
209	2	5.0	75.6	15.12	61.8	12.36
209	3	5.6	75.6	13.50	61.8	11.04
209	7	7.6	60.8	8.00	44.2	5.82
209	8	20.3	60.8	3.00	44.2	2.18
210	3	11.5	55.3	4.81	38.7	3.37
210	4	4.6	55.3	12.02	38.7	8.42
210	6	4.4	58.1	13.20	41.5	9.43
210	7	8.1	58.1	7.17	41.5	5.13
210	8	17.9	64.1	3.58	47.8	2.67
211	1	11.5	69.6	6.05	54.2	4.71
211	2	6.4	69.6	10.88	54.2	8.46
211	3	3.9	69.6	17.85	54.2	13.89
211	4	33.0	62.6	1.90	46.2	1.40
211	5	97.4	62.6	0.64	46.2	.48
211	6	53.1	62.6	1.18	46.2	.87
214	3	77.6	105.1	1.35	139.7	1.80
214	4	54.4	93.4	1.72	93.7	1.72
214	7	119.1	53.4	0.45	454.5	3.82
214	8	31.7	70.1	2.21	376.4	11.88

hours were between 2 and 2.5 m/sec (Case 206, hours 5 and 8; Case 211, hour 5). In fact, the highest observed C/Q of 155 occurred with a wind speed of 2.5 m/sec and PG class F (Case 206, hour 8).

One possible cause of Valley's failure to estimate the highest observed hourly SF_6 concentrations at CCB may be related to the assumed 10 m "miss distance." Although this distance may be appropriate for large pollutant sources in complex terrain where plume σ_z values are considerably larger than 10 m, it may be too large for the scale of the experiment at CCB. Reducing the miss distance to 8.4 m would be sufficient to reproduce the maximum observed C/Q ratio in Case 206, hours 6 and 8. However, it would not be sufficient to reproduce the maximum concentration of 97 ppt observed in Case 211, hour 5. If the average wind speed for this hour were used (2.0 m/sec instead of 2.5 m/sec), then a C/Q in excess of 97 would be produced with a miss distance of 6.5 m. The use of a lower wind speed as well as a smaller miss distance at CCB may be justified again by the scale of the experiment: tracer plumes are much closer to the ground, much closer to terrain, and much narrower than typical plumes from large sources.

Figures 61 and 62 are scatterplots of modeled to observed concentration ratios versus modeled concentrations for both Valley and Valley centerline SF_6 concentrations. It is seen that about one-third of the 45 observed concentrations are within a factor of 2 of the hourly Valley calculations, whereas about one-fourth are within a factor of 2 of the Valley centerline calculations. (Note that in these scatterplots some data points fell on top of one another within the resolution of the plotter, and some values fell below the bottom of the plot when modeled values were very small. Therefore, the number of points distinguishable on the plots may not be as large as the number of sample points in the data set plotted.)

COMPLEX I and COMPLEX II

A complete set of statistical and graphical analyses of COMPLEX model calculations, like those illustrated for the example case study hour, was assembled for each of the 45 case hours. (The complete set of analyses is available from the EPA Project Office upon request.) Most of the key statistical results are summarized in Tables 42 and 43. The asterisks that

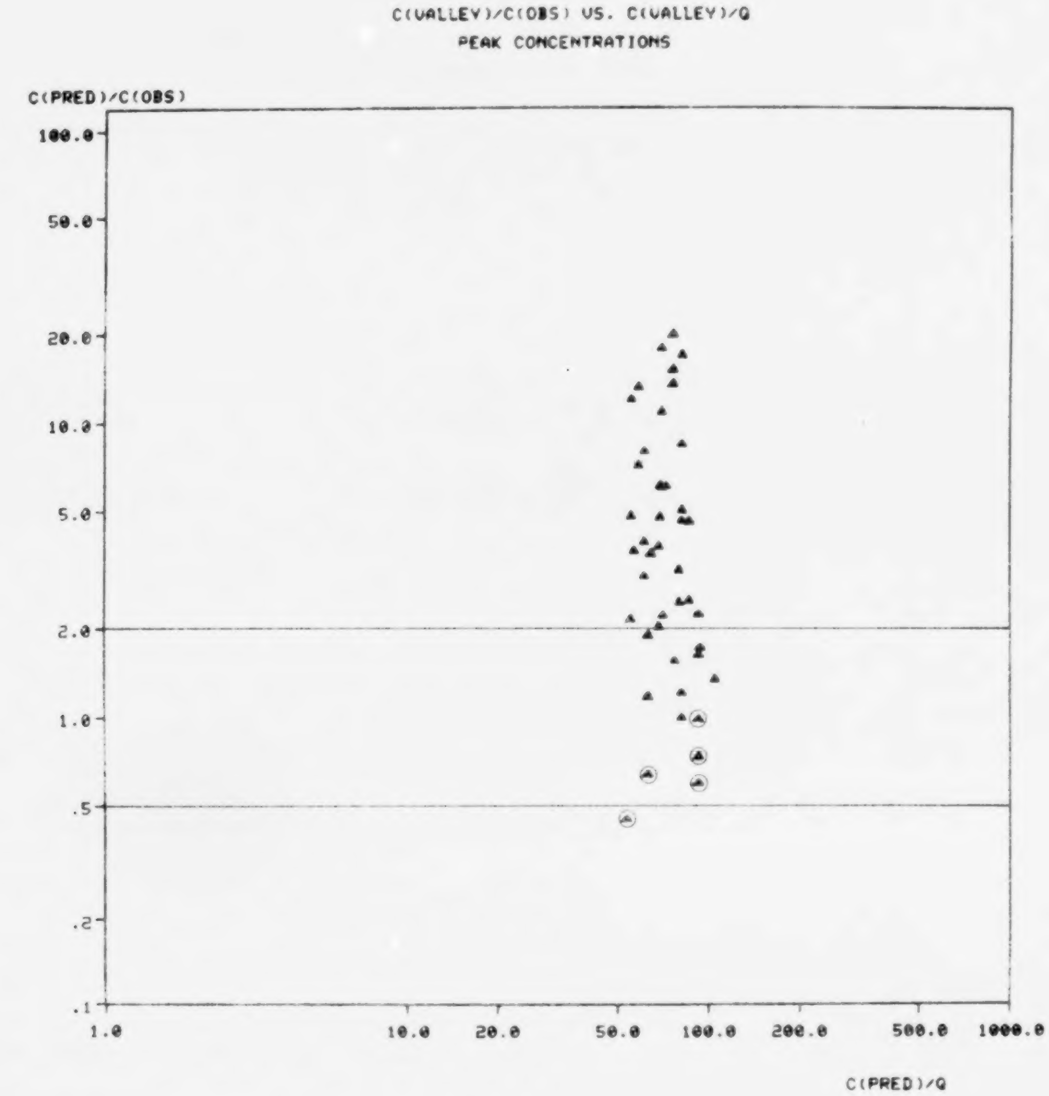

Figure 61. Variation of modeled-to-observed ratios of maximum hourly SF_6 concentrations with modeled concentrations calculated by Valley. Circles identify the five highest observed SF_6 concentrations (C/Q).

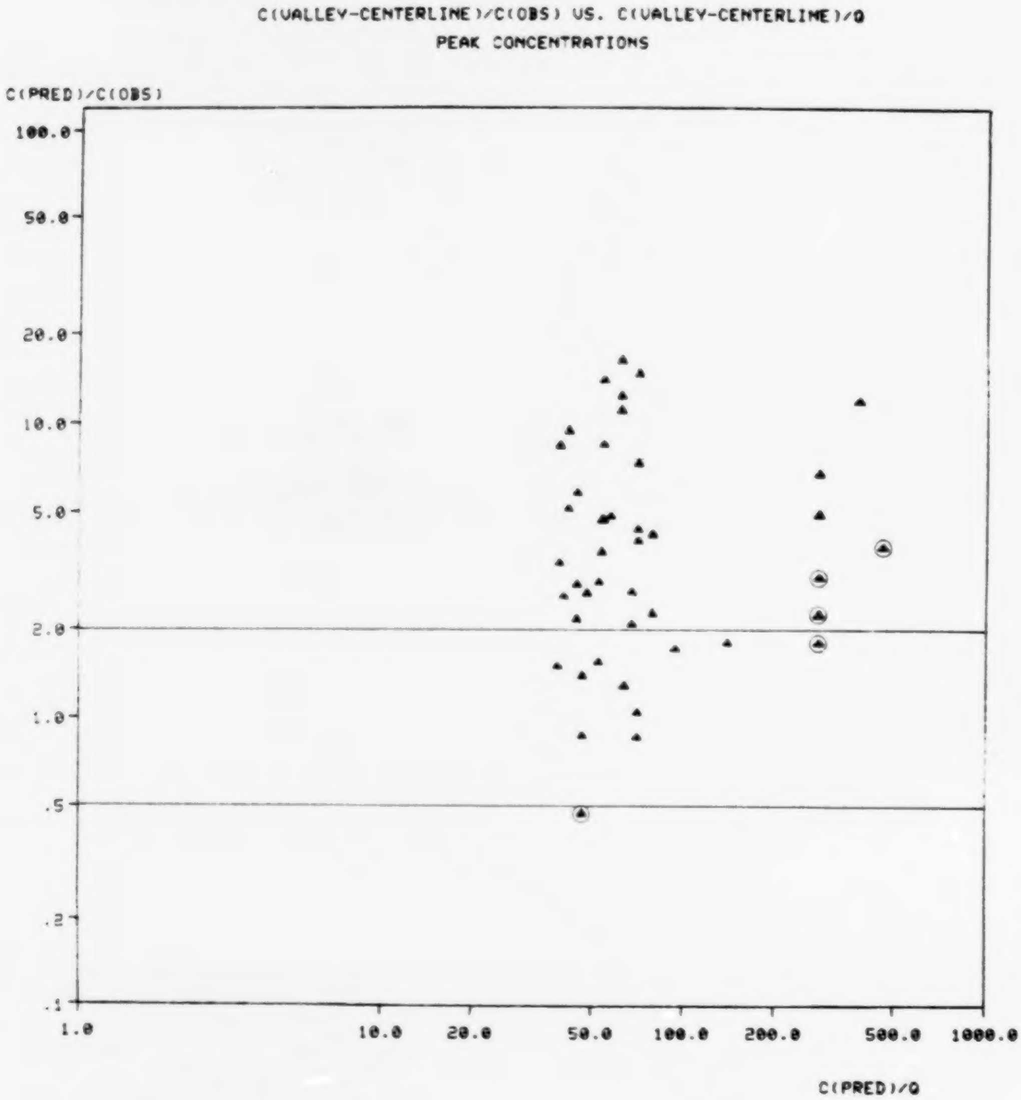

Figure 62. Variation of modeled-to-observed ratios of maximum hourly SF_6 concentrations with modeled concentrations calculated by Valley (centerline). Circles identify the five highest observed SF_6 concentrations (C/Q).

TABLE 42. SUMMARY C/Q STATISTICS FOR COMPLEX I CALCULATIONS

			Observed			Stability Class D						Stability Class E						Stability Class F					
Exp	Case Hour	N	$\overline{Co}$	σ(Co)	Max Co	$\overline{Cp}$	σ(Cp)	Max Cp	Max Cp/ Max Co	$\overline{Co-Cp}$	σ(Co-Cp)	$\overline{Cp}$	σ(Cp)	Max Cp	Max Cp/ Max Co	$\overline{Co-Cp}$	σ(Co-Cp)	$\overline{Cp}$	σ(Cp)	Max Cp	Max Cp/ Max Co	$\overline{Co-Cp}$	σ(Co-Cp)
201	1	16	13.1	8.4	32.2	9.9	6.2	19.3	.60	3.2	5.0	13.1*	8.5	28.0	.87	0	5.0	16.5	10.4	32.9	1.02	-3.5	6.0
201	2	16	8.3	8.1	25.1	12.1	8.7	26.5	1.06	-3.8	8.0	16.4	12.1	38.4	1.53	-8.1	10.2	21.0*	15.0	45.2	1.80	-12.7	12.2
201	4	16	6.4	5.6	18.6	16.4	13.5	39.8	2.13	-10.0	16.3	21.7	18.3	57.7	3.09	-15.4	20.9	27.1*	22.1	65.6	3.51	-20.7	24.7
201	5	10	11.2	10.1	34.6	15.2	10.9	28.8	.83	-4.0	16.8	20.4	14.2	37.5	1.09	-9.2	22.0	26.4*	18.0	46.3	1.34	-15.2	25.6
201	6	11	7.9	5.7	18.7	23.8	16.0	47.8	2.56	-15.9	16.4	31.7	21.9	69.2	3.71	-23.8	21.8	39.1*	26.0	78.7	4.22	-31.2	26.0
202	1	26	4.0	4.9	18.0	4.1*	2.9	7.8	.43	-.1	4.2	7.2	5.2	14.7	.81	-3.2	5.1	9.1	6.6	18.3	1.01	-5.1	6.0
202	2	32	8.4	6.8	33.6	4.1	2.8	7.8	.23	4.4	6.5	7.2*	5.3	14.7	.44	1.3	6.9	9.0	6.8	18.3	.54	-.6	8.2
202	3	28	8.6	16.9	67.2	7.9*	5.8	20.5	.30	.6	16.3	10.0	7.3	27.8	.41	-1.5	16.2	12.9	8.9	32.1	.48	-4.4	16.9
202	4	24	7.8	17.8	81.6	7.6	6.2	20.5	.25	.2	14.9	9.4*	7.9	27.8	.34	-1.6	13.9	12.0	9.6	32.1	.39	-4.3	14.2
202	5	24	5.2	11.1	49.2	4.7	5.1	15.2	.31	.5	8.7	6.4*	7.3	22.1	.45	-1.3	7.8	7.9	8.7	26.5	.54	-2.7	9.2
202	6	21	3.1	3.2	11.8	4.0	3.7	9.7	.82	-.9	3.0	6.2*	5.9	18.1	1.54	-3.1	4.9	7.6	7.5	21.7	1.84	-4.6	6.6
204	1	37	1.7	2.7	14.5	22.7	12.5	45.8	3.16	-21.1	13.6	31.0	17.7	77.3	5.33	-29.3	18.7	40.7*	21.9	83.0	5.73	-39.0	22.9
204	2	36	2.0	2.9	11.3	1.5	9.0	54.8	4.84	.4	7.8	2.3	13.7	83.1	7.34	-.3	12.3	2.6*	15.2	92.3	8.15	-.6	13.8
204	5	30	1.1	1.0	4.8	56.4	29.6	112.2	23.55	-55.3	29.0	76.8	41.2	161.4	33.89	-75.7	40.6	97.8*	49.4	187.0	39.27	-96.7	48.9
204	6	34	2.1	3.4	17.6	35.8	19.7	74.8	4.26	-33.7	17.9	48.6	27.8	107.6	6.13	-46.6	25.8	62.2*	33.3	124.7	7.10	-60.2	31.5
204	7	32	2.5	2.4	9.6	60.6	24.9	106.0	11.06	-58.1	24.7	82.3	35.8	154.4	16.14	-79.7	35.4	102.9*	40.0	181.6	18.98	-100.4	40.0
204	8	33	6.6	4.3	16.1	45.7	36.4	112.2	6.96	-39.2	36.6	62.3	50.5	161.4	10.02	-55.7	50.5	79.2*	61.9	187.0	11.61	-72.6	62.0
205	4	33	5.2	4.4	15.4	6.4	3.5	11.6	.75	-1.1	4.2	9.5	5.4	19.3	1.26	-4.2	5.4	12.3*	7.4	24.8	1.61	-7.1	6.6
205	5	31	7.3	4.6	25.5	4.8	2.7	8.1	.32	2.5	4.6	8.0	4.9	15.6	.61	-.7	6.1	10.3*	7.1	19.7	.77	-3.0	8.0
205	6	37	5.3	3.6	15.5	9.2	2.8	14.4	.93	-3.9	4.2	12.8	4.3	21.2	1.37	-7.5	5.1	16.9*	5.1	27.1	1.75	-11.6	6.2
206	4	35	13.6	16.1	56.7	26.1	12.2	49.1	.87	-12.5	22.6	41.4	24.2	101.0	1.78	-27.9	33.1	41.7*	17.7	67.5	1.19	-28.2	26.2
206	5	30	5.7	9.5	41.2	25.7	12.8	49.1	1.19	-20.0	16.9	39.7	23.0	99.1	2.40	-34.0	26.3	40.7*	18.2	67.5	1.64	-35.0	21.4
206	6	28	35.4	31.5	124.2	49.1	27.2	84.0	.68	-13.7	41.2	76.0	48.6	201.9	1.63	-40.6	52.1	77.0*	42.1	127.9	1.03	-41.6	51.0
206	7	33	21.6	25.5	92.8	38.6	14.8	65.5	.71	-16.9	28.0	62.1	30.7	134.6	1.45	-40.4	36.6	61.4*	20.5	90.0	.97	-39.8	30.0
206	8	70	38.6	35.3	154.6	45.7	16.9	78.6	.51	-7.1	33.9	73.5	35.7	161.5	1.04	-35.0	35.8	71.4*	26.1	108.0	.70	-32.8	36.5
209	1	47	.4	.6	3.8	9.1	8.4	24.6	6.54	-8.7	8.4	14.0	13.5	45.2	12.02	-13.6	13.5	17.7*	17.1	53.0	14.08	-17.3	17.1
209	2	46	.9	1.3	5.0	12.7	11.9	34.5	6.84	-11.7	12.0	20.0	19.3	63.3	12.57	-19.0	19.4	25.2*	24.3	74.1	14.72	-24.3	24.4
209	3	48	2.1	1.2	5.6	9.0	14.0	43.1	7.70	-6.9	14.4	13.5	21.7	73.0	13.06	-11.4	22.1	15.7*	26.8	87.1	15.57	-13.6	27.1
209	7	46	1.6	2.0	7.6	17.2	11.6	35.5	4.67	-15.6	11.4	26.4	19.0	69.4	9.13	-24.8	18.9	32.7*	24.9	84.0	11.05	-31.1	24.6
209	8	40	3.2	4.9	20.3	18.8	11.0	35.5	1.75	-15.6	8.9	29.1	18.8	69.4	3.42	-25.9	15.6	37.7*	24.5	84.0	4.14	-34.5	21.4
210	3	45	2.4	2.7	11.5	3.9	3.8	8.1	.71	-1.5	3.6	6.8	5.9	17.4	1.52	-4.4	6.1	8.4*	8.1	22.8	1.99	-6.0	8.3
210	4	39	1.6	1.3	4.6	4.6	1.8	7.0	1.53	-3.0	1.9	8.2	3.6	14.8	3.23	-6.6	3.7	10.0*	5.6	19.3	4.22	-8.5	5.5
210	6	40	.5	1.0	4.4	3.8	3.0	8.1	1.86	-3.3	2.9	6.9	6.1	17.5	4.00	-6.4	6.0	8.6*	8.2	22.5	5.13	-8.2	8.1
210	7	45	.8	1.5	8.1	4.3	2.1	7.3	.90	-3.5	2.6	7.7	4.5	15.4	1.91	-6.9	4.8	9.6*	6.5	19.9	2.47	-8.8	6.7
210	8	15	3.3	5.4	17.9	8.5	3.1	13.2	.74	-5.2	6.7	12.9	5.6	24.3	1.36	-9.6	8.1	16.3*	7.5	30.2	1.69	-13.0	9.2
211	1	43	4.3	2.8	11.5	27.0	20.0	62.5	5.45	-22.7	19.3	38.3	30.3	104.0	9.07	-34.0	29.4	48.8*	36.7	122.3	10.67	-44.4	35.9
211	2	36	2.3	1.4	6.4	17.5	8.0	31.3	4.89	-15.2	7.7	24.5	12.2	49.2	7.71	-22.2	11.9	31.2*	14.5	55.9	8.75	-28.9	14.1
211	3	34	.5	.8	3.9	19.0	7.4	31.3	8.05	-18.5	7.4	26.8	12.2	52.0	13.40	-26.3	12.1	33.9*	14.3	61.1	15.76	-33.3	14.2
211	4	36	8.7	9.2	33.0	16.1	7.6	35.3	1.07	-7.3	9.1	20.8	10.3	46.2	1.40	-12.1	10.2	27.4*	11.9	54.1	1.64	-18.7	12.4
211	5	40	24.6	23.0	97.4	23.4	10.4	52.9	.54	1.2	21.6	30.2	13.6	69.3	.71	-5.6	21.8	40.1*	15.8	74.8	.77	-15.5	22.3
211	6	37	12.3	12.2	53.1	15.5	6.7	35.3	.66	-3.2	10.8	20.0	9.0	46.2	.87	-7.7	11.0	26.5*	10.1	54.1	1.02	-14.2	11.6
214	3	41	5.0	14.9	77.6	5.9	21.2	91.8	1.18	-.9	12.3	7.9	28.8	124.8	1.61	-2.9	19.6	7.4*	29.2	139.1	1.79	-2.4	22.8
214	4	37	16.7	13.8	54.4	20.0	12.2	44.4	.82	-3.3	13.2	25.6	15.4	58.3	1.07	-8.9	16.6	31.9*	18.3	65.9	1.21	-15.2	19.5
214	7	43	25.0	31.7	119.1	62.5*	52.1	202.9	1.70	-37.4	54.7	76.9	66.2	224.9	1.89	-51.9	67.4	66.8	46.2	132.3	1.11	-41.7	48.2
214	8	46	9.0	8.4	31.7	60.0*	42.3	169.7	5.35	-51.0	38.1	73.5	50.9	227.8	7.18	-64.5	46.9	71.8	38.7	127.3	4.01	-62.9	35.1

TABLE 43. SUMMARY C/Q STATISTICS FOR COMPLEX II CALCULATIONS

			Observed			Stability Class D						Stability Class E						Stability Class F					
Exp	Case Hour	N	$\overline{Co}$	σ(Co)	Max Co	$\overline{Cp}$	σ(Cp)	Max Cp	Max Cp/ Max Co	$\overline{Co-Cp}$	σ(Co-Cp)	$\overline{Cp}$	σ(Cp)	Max Cp	Max Cp/ Max Co	$\overline{Co-Cp}$	σ(Co-Cp)	$\overline{Cp}$	σ(Cp)	Max Cp	Max Cp/ Max Co	$\overline{Co-Cp}$	σ(Co-Cp)
201	1	16	13.1	8.4	32.2	9.4	10.3	32.8	1.02	3.7	7.9	12.3	17.5	51.3	1.59	.7	14.3	16.3	28.1	77.2	2.40	-3.3	25.4
201	2	16	8.3	8.1	25.1	11.4	14.3	42.2	1.68	-3.1	11.9	15.4	24.1	73.2	2.91	-7.1	21.3	20.4	39.5	120.2	4.78	-12.1	37.3
201	4	16	6.4	5.6	18.6	19.4	23.6	81.5	4.37	-13.0	27.2	27.6	41.6	148.7	7.97	-21.2	44.8	36.3	64.1	214.6	11.49	-29.9	67.3
201	5	10	11.2	10.1	34.6	15.0	18.9	48.6	1.41	-3.8	25.3	21.4	32.1	82.8	2.40	-10.2	37.6	34.5	61.3	162.9	4.72	-23.3	65.8
201	6	11	7.9	5.7	18.7	34.5	31.5	86.3	4.63	-26.6	32.1	50.9	52.9	142.6	7.64	-43.0	53.1	63.6	76.2	206.0	11.04	-55.7	76.9
202	1	26	4.0	4.9	18.0	5.5	5.2	14.7	.82	-1.5	5.1	10.2	11.0	32.5	1.81	-6.2	10.2	14.4	19.9	59.2	3.29	-10.4	19.5
202	2	32	8.4	6.8	33.6	3.3	4.7	16.8	.50	5.2	7.1	5.7	10.6	42.6	1.27	2.8	11.2	7.4	18.1	79.8	2.38	1.0	18.4
202	3	28	8.6	16.9	67.2	6.7	7.2	24.6	.37	1.9	18.3	7.2	10.1	37.6	.56	1.4	19.2	7.3	16.2	73.7	1.10	1.3	22.4
202	4	24	7.8	17.8	81.6	8.5	10.8	33.7	.41	-.7	17.5	10.9	16.1	53.6	.66	-3.2	21.3	15.2	26.7	98.5	1.21	-7.4	31.5
202	5	24	5.2	11.1	49.2	4.7	8.8	33.9	.69	.4	6.7	7.2	15.9	65.9	1.34	-2.1	10.3	9.4	26.0	118.4	2.41	-4.3	22.1
202	6	21	3.1	3.2	11.8	4.2	6.2	20.4	1.73	-1.2	5.2	6.8	12.4	42.4	3.59	-3.7	11.5	9.3	20.7	78.0	6.61	-6.3	20.0
204	1	37	1.7	2.7	14.5	28.7	23.5	85.3	5.89	-27.0	24.6	40.2	42.0	168.3	11.61	-38.6	42.8	51.0	70.5	231.0	15.93	-49.4	71.3
204	2	36	2.0	2.9	11.3	.1	.4	2.6	.23	1.9	2.7	.0	.0	.2	.02	2.0	2.9	.0	.0	.0	.00	2.0	2.9
204	5	30	1.1	1.0	4.8	62.0	61.7	225.0	47.25	-61.0	61.1	89.0	106.2	400.7	84.13	-87.9	105.6	117.6	166.5	558.3	117.22	-116.6	166.1
204	6	34	2.1	3.4	17.6	45.0	34.2	107.5	6.13	-43.0	33.8	63.9	58.3	177.5	10.11	-61.8	58.3	84.6	100.9	291.4	16.60	-82.5	101.5
204	7	32	2.5	2.4	9.6	75.3	55.7	194.8	20.36	-72.7	56.9	109.1	99.1	333.2	34.83	-106.6	100.2	152.3	173.5	499.4	52.20	-149.8	174.4
204	8	33	6.6	4.3	16.1	40.7	54.9	248.0	15.40	-34.1	55.0	51.1	96.9	477.0	29.62	-44.5	96.6	59.4	164.7	828.9	51.46	-52.8	163.8
205	4	33	5.2	4.4	15.4	6.8	6.7	24.1	1.57	-1.6	6.6	9.7	12.5	50.1	3.26	-4.5	12.4	11.6	23.5	97.9	6.37	-6.3	23.8
205	5	31	7.3	4.6	25.5	5.3	5.4	17.2	.67	2.0	4.7	9.0	11.3	38.7	1.52	-1.7	10.0	11.4	18.7	76.5	3.00	-4.1	17.5
205	6	37	5.3	3.6	15.5	7.5	7.5	26.4	1.70	-2.2	6.9	9.6	13.1	50.7	3.27	-4.3	12.5	12.1	24.8	97.9	6.31	-6.8	24.5
206	4	35	13.6	16.1	56.7	20.3	24.4	81.3	1.43	-6.8	24.6	33.5	51.2	181.0	3.19	-20.0	50.7	30.3	57.4	204.6	3.60	-16.8	53.9
206	5	30	5.7	9.5	41.2	15.1	22.4	78.7	1.91	-9.4	18.7	23.2	42.4	167.7	4.07	-17.6	38.2	29.0	65.4	251.8	6.11	-23.4	61.5
206	6	28	35.4	31.5	124.2	38.9	51.3	167.1	1.35	-3.5	44.3	71.3	128.9	536.6	4.32	-35.9	114.5	70.6	140.4	482.6	3.89	-35.2	128.4
206	7	33	21.6	25.5	92.8	19.1	29.2	92.7	1.00	2.6	24.8	30.2	52.6	180.2	1.94	-8.5	43.0	31.5	62.2	225.1	2.42	-9.8	53.8
206	8	70	38.6	35.3	154.6	15.1	28.5	131.5	.85	23.4	35.8	21.3	55.7	291.7	1.89	17.3	54.6	19.4	68.4	369.1	2.39	19.1	67.2
209	1	47	.4	.6	3.8	10.9	12.9	39.2	10.41	-10.5	12.9	16.7	23.9	77.8	20.68	-16.3	23.9	21.1	39.6	137.6	36.57	-20.7	39.7
209	2	46	.9	1.3	5.0	12.7	18.4	65.5	13.02	-11.8	18.4	20.9	36.4	150.1	29.80	-19.9	36.4	26.8	59.2	244.1	48.47	-25.9	59.2
209	3	48	2.1	1.3	5.6	6.0	13.3	62.9	11.25	-3.9	13.7	7.8	22.5	127.0	22.71	-5.6	22.7	6.3	28.8	194.7	34.81	-4.1	29.0
209	7	46	1.6	2.0	7.6	18.1	19.6	72.1	9.49	-16.6	19.6	26.5	37.7	151.0	19.87	-24.9	37.7	30.8	64.5	277.1	36.46	-29.2	64.4
209	8	40	3.2	4.9	20.3	20.9	20.5	75.0	3.70	-17.7	20.0	32.9	41.5	174.3	8.59	-29.6	40.7	44.1	73.9	310.4	15.31	-40.9	73.1
210	3	45	2.4	2.7	11.5	5.1	5.4	16.7	1.46	-2.7	6.0	9.1	12.0	38.9	3.40	-6.7	12.4	10.8	19.3	78.9	6.90	-8.4	19.6
210	4	39	1.6	1.3	4.6	3.8	4.0	13.0	2.85	-2.2	3.8	6.6	9.7	30.3	6.64	-5.1	9.5	8.0	16.8	61.1	13.38	-6.4	16.6
210	6	40	.5	1.0	4.4	3.9	5.3	18.4	4.21	-3.4	4.9	7.6	13.4	53.0	12.09	-7.1	12.9	11.1	24.4	101.7	23.21	-10.6	23.9
210	7	45	.8	1.5	8.1	5.4	5.0	15.4	1.92	-4.6	5.4	10.9	12.6	42.1	5.23	-10.1	12.9	16.7	24.7	83.4	10.36	-15.9	24.9
210	8	15	3.3	5.4	17.9	4.9	5.9	15.4	.86	-1.7	6.1	7.1	10.4	29.2	1.63	-3.9	9.4	6.5	13.4	49.7	2.78	-3.2	11.0
211	1	43	4.3	2.8	11.5	30.3	35.4	120.7	10.53	-25.9	35.0	47.4	65.8	233.6	20.37	-43.0	65.4	65.4	106.5	430.5	37.55	-61.0	106.3
211	2	36	2.3	1.4	6.4	14.2	17.0	56.9	8.91	-11.9	17.1	21.0	31.1	112.2	17.57	-18.7	31.3	27.2	48.9	156.4	24.50	-24.9	49.0
211	3	34	.5	.8	3.9	1.5	3.7	16.5	4.25	-.9	3.8	.9	2.7	12.5	3.23	-.3	2.8	.1	.3	1.6	.41	.4	.9
211	4	36	8.7	9.2	33.0	21.7	21.7	76.3	2.31	-13.0	20.5	33.3	38.8	131.1	3.98	-24.6	36.4	55.8	70.0	226.3	6.86	-47.0	67.6
211	5	40	24.6	23.0	97.4	24.9	26.4	105.1	1.08	-.2	31.3	34.1	43.3	169.0	1.74	-9.5	44.9	47.7	69.4	231.8	2.38	-23.1	69.6
211	6	37	12.3	12.2	53.1	22.8	18.6	75.3	1.42	-10.5	18.4	34.1	32.8	128.2	2.41	-21.8	31.0	52.0	54.6	202.0	3.80	-39.7	52.4
214	3	41	5.0	14.9	77.6	5.3	25.1	159.4	2.06	-.2	19.3	7.9	46.6	302.4	3.90	-2.9	40.7	9.0	56.8	367.9	4.74	-4.0	50.9
214	4	37	16.7	13.8	54.4	18.0	22.9	78.9	1.45	-1.3	27.0	23.4	35.5	130.9	2.41	-6.7	38.7	29.1	57.0	228.1	4.19	-12.4	59.7
214	7	43	25.0	31.7	119.1	20.2	47.5	240.4	2.02	4.8	43.5	21.2	64.8	365.3	3.07	3.8	61.9	17.6	71.6	442.7	3.72	7.4	72.3
214	8	46	9.0	8.4	31.7	24.2	47.4	168.4	5.31	-15.3	48.5	28.7	62.6	226.9	7.15	-19.8	63.9	22.6	63.3	287.9	9.07	-13.6	65.1

appear in Table 42 denote the stability class for each case hour according to the Turner scheme for nighttime stability using the observed 10 m wind speed (assuming no cloud cover, which generally agreed with net radiometer measurements). For a given case hour, the appropriate stability class is signaled by an asterisk in one of the three C_p columns. For example, at the entries for Case 205, hour 5, the asterisk appears in the C_p column corresponding to stability class F; for this hour, class F stability was the most appropriate choice according to the Turner scheme because the mean 10 m wind speed was 1.3 m/s and clear skies prevailed.

Figures 63 through 70 are scatterplots of modeled maximum-to-observed maximum concentration ratios versus modeled maximum concentrations. These concentrations have been scaled by the emission rate (Q) to facilitate comparisons from one case hour to the next. About one-half of the points lie in the range $0.5 \leq C_p/C_o \leq 2$ (at least in the COMPLEX I results), and the other half lie significantly above this range (indicating overestimation). As the stability class changes from D to F, both COMPLEX I and COMPLEX II tend to overestimate more. Figures 66 and 70 illustrate the performance of COMPLEX I and COMPLEX II when the stability class is selected be the Turner scheme. These figures show that COMPLEX I would be preferable to COMPLEX II for use at CCB.

Each of these scatterplots may be interpreted as a plot of the residual between the modeled and observed concentration versus the modeled concentration, if the observed concentration is assumed to be lognormally distributed about the modeled concentration (see Section 5.3). An excellent model should produce a scatterplot with the residuals tightly clustered about zero ($C_p/C_o = 1$) for all C_p, and the scatter about zero should be equal throughout the range of C_p.

Figures 63 through 70 show that the residuals based on maximum concentrations (for all variants of the COMPLEX models tested) do not exhibit these characteristics. The scatter is large at all C_p, and the mean increases with C_p.

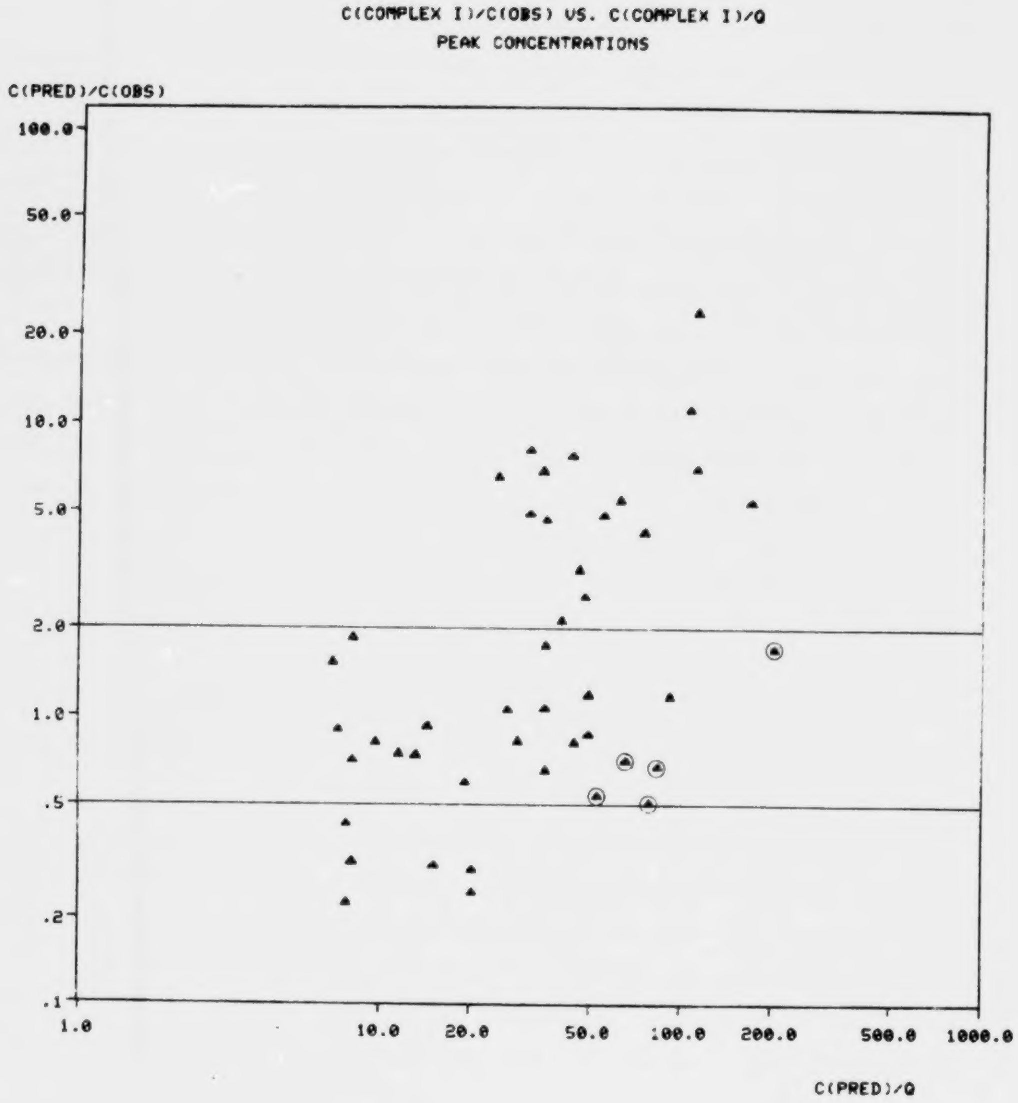

Figure 63. Variation of modeled-to-observed ratios of maximum hourly SF_6 concentrations with modeled concentrations calculated by Complex I (Stability Class D). Circles identify the five highest observed SF_6 concentrations (C/Q).

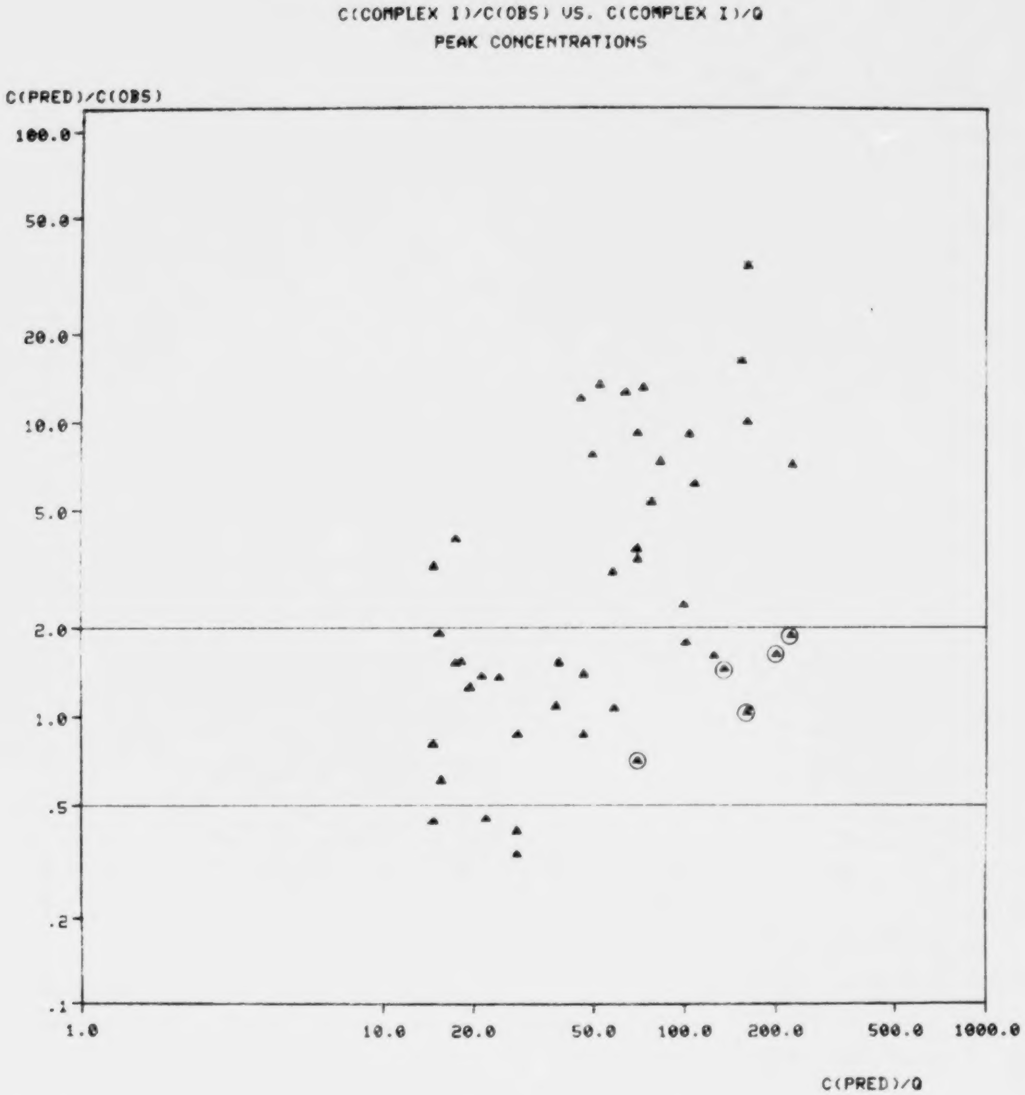

Figure 64. Variation of modeled-to-observed ratios of maximum hourly SF_6 concentrations with modeled concentrations calculated by Complex I (Stability Class E). Circles identify the five highest observed SF_6 concentrations (C/Q).

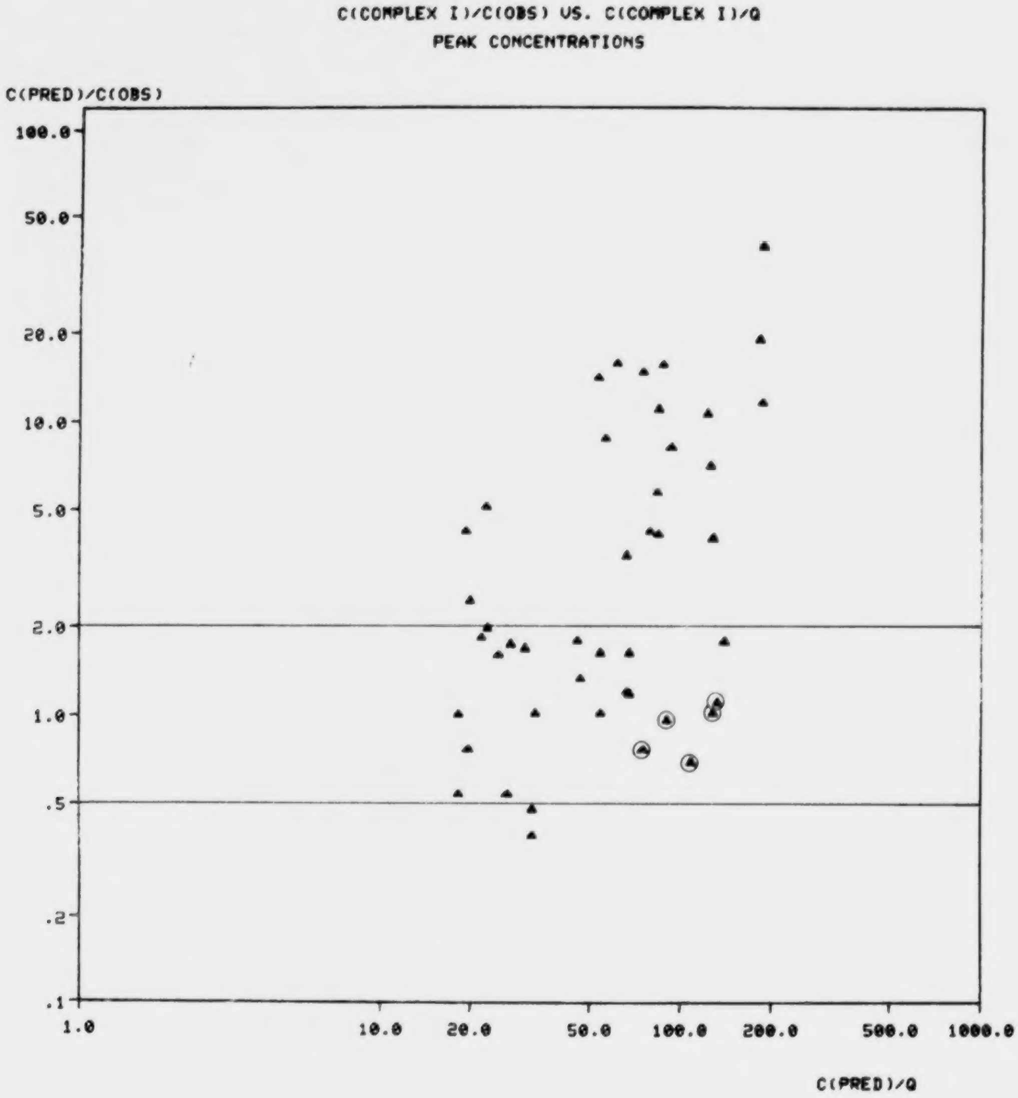

Figure 65. Variation of modeled-to-observed ratios of maximum hourly SF_6 concentrations with modeled concentrations calculated by Complex I (Stability Class F). Circles identify the five highest observed SF_6 concentrations (C/Q).

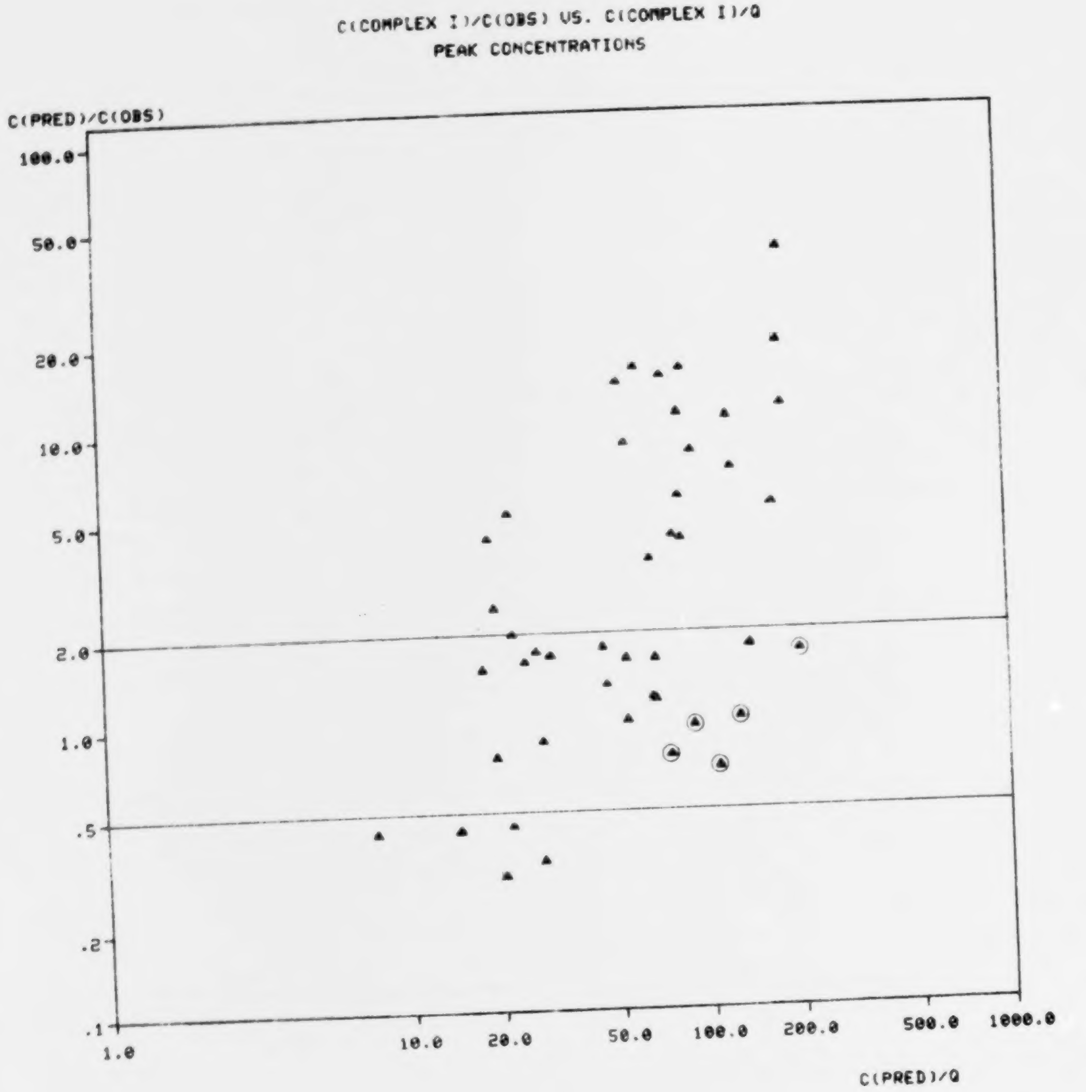

Figure 66. Variation of modeled-to-observed ratios of maximum hourly SF_6 concentrations with modeled concentrations calculated by Complex I (appropriate stability class - Turner scheme). Circles identify the five highest observed SF_6 concentrations (C/Q).

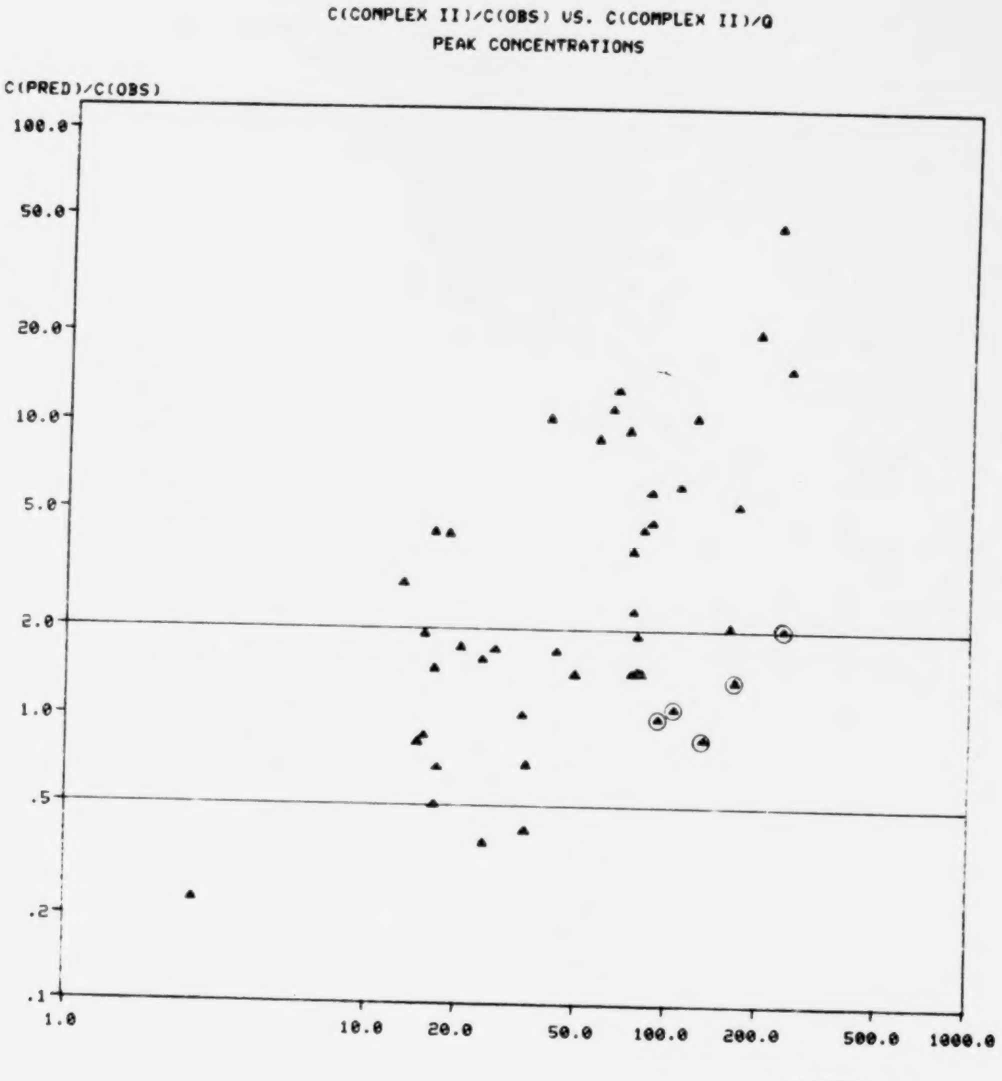

Figure 67. Variation of modeled-to-observed ratios of maximum hourly SF_6 concentrations with modeled concentrations calculated by Complex II (Stability Class D). Circles identify the five highest observed SF_6 concentrations (C/Q).

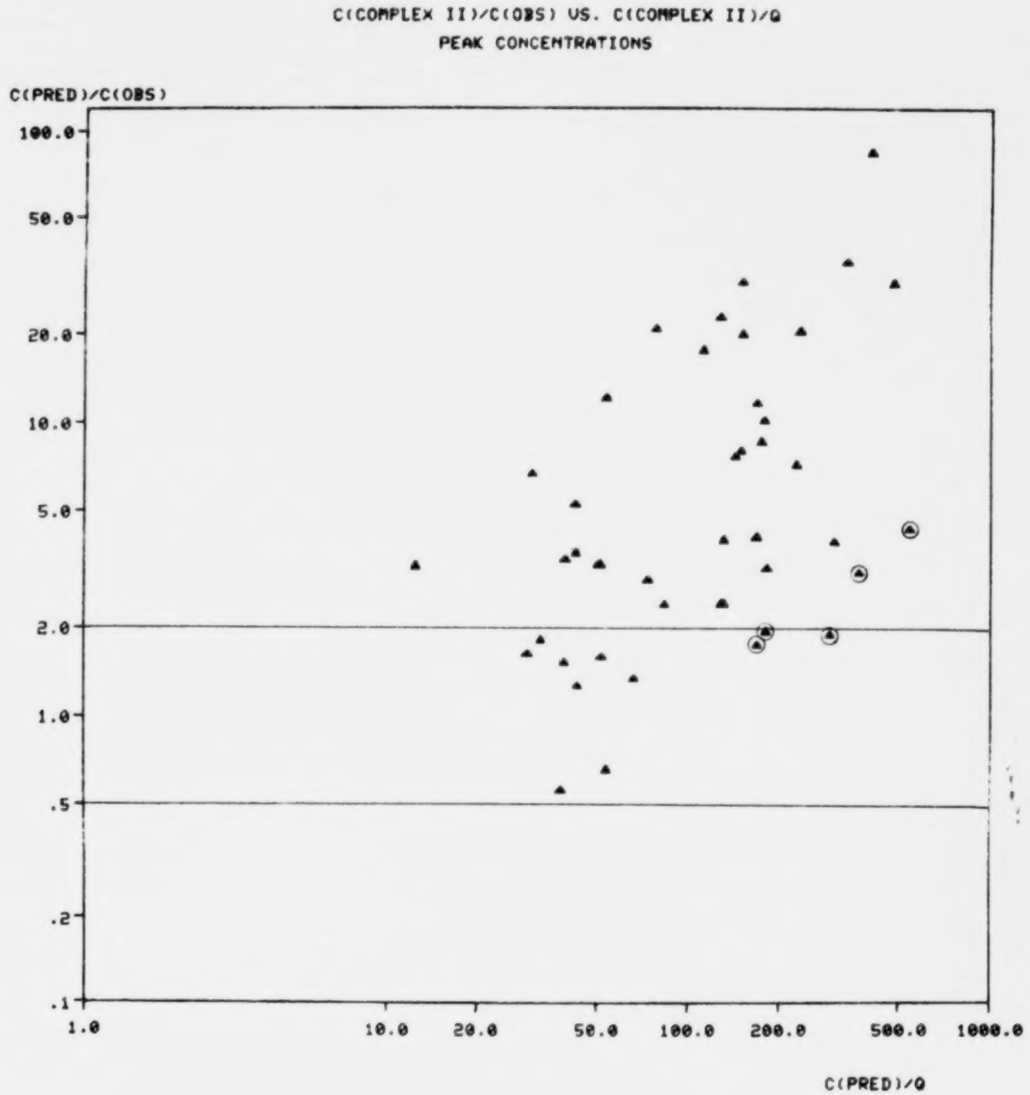

Figure 68. Variation of modeled-to-observed ratios of maximum hourly SF_6 concentrations with modeled concentrations calculated by Complex II (Stability Class E). Circles identify the five highest observed SF_6 concentrations (C/Q).

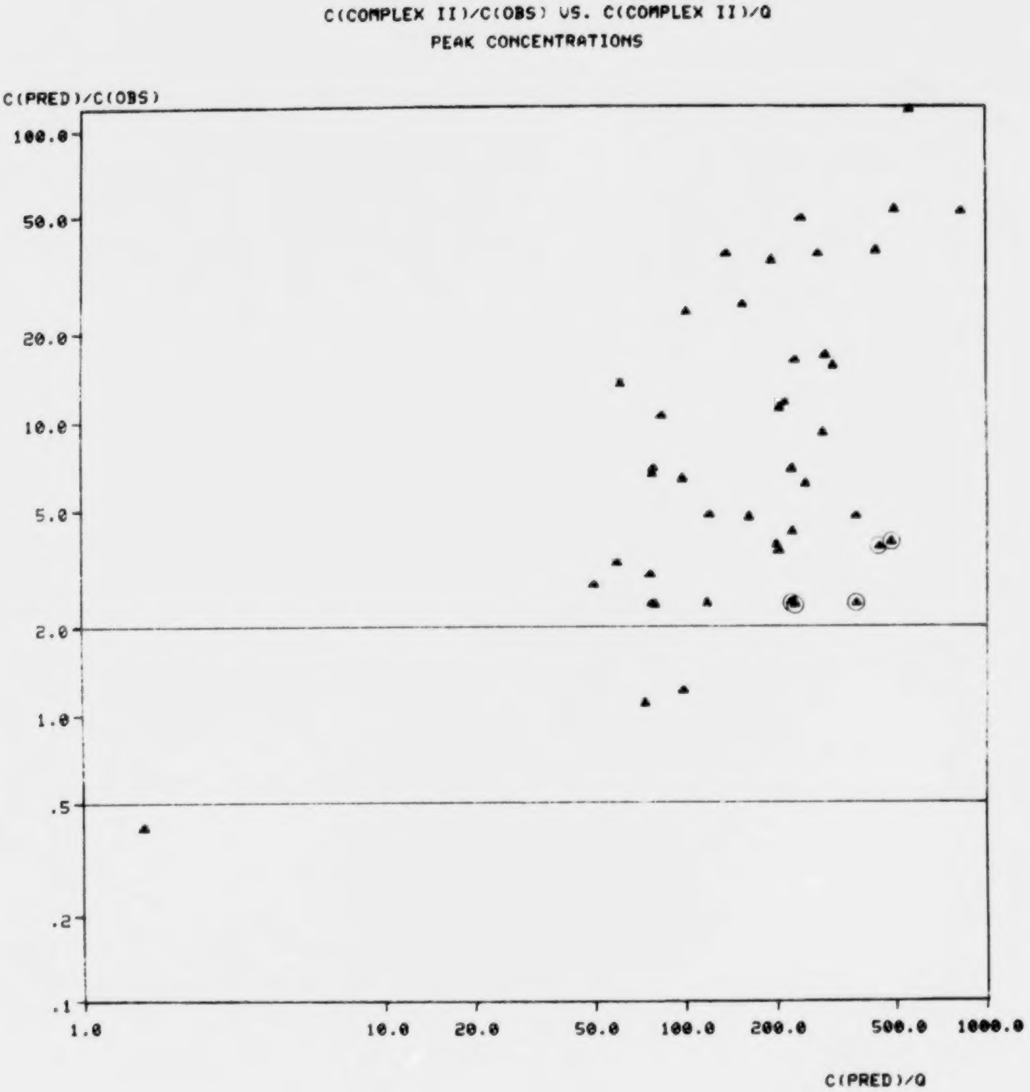

Figure 69. Variation of modeled-to-observed ratios of maximum hourly SF_6 concentrations with modeled concentrations calculated by Complex II (Stability Class F). Circles identify the five highest observed SF_6 concentrations (C/Q).

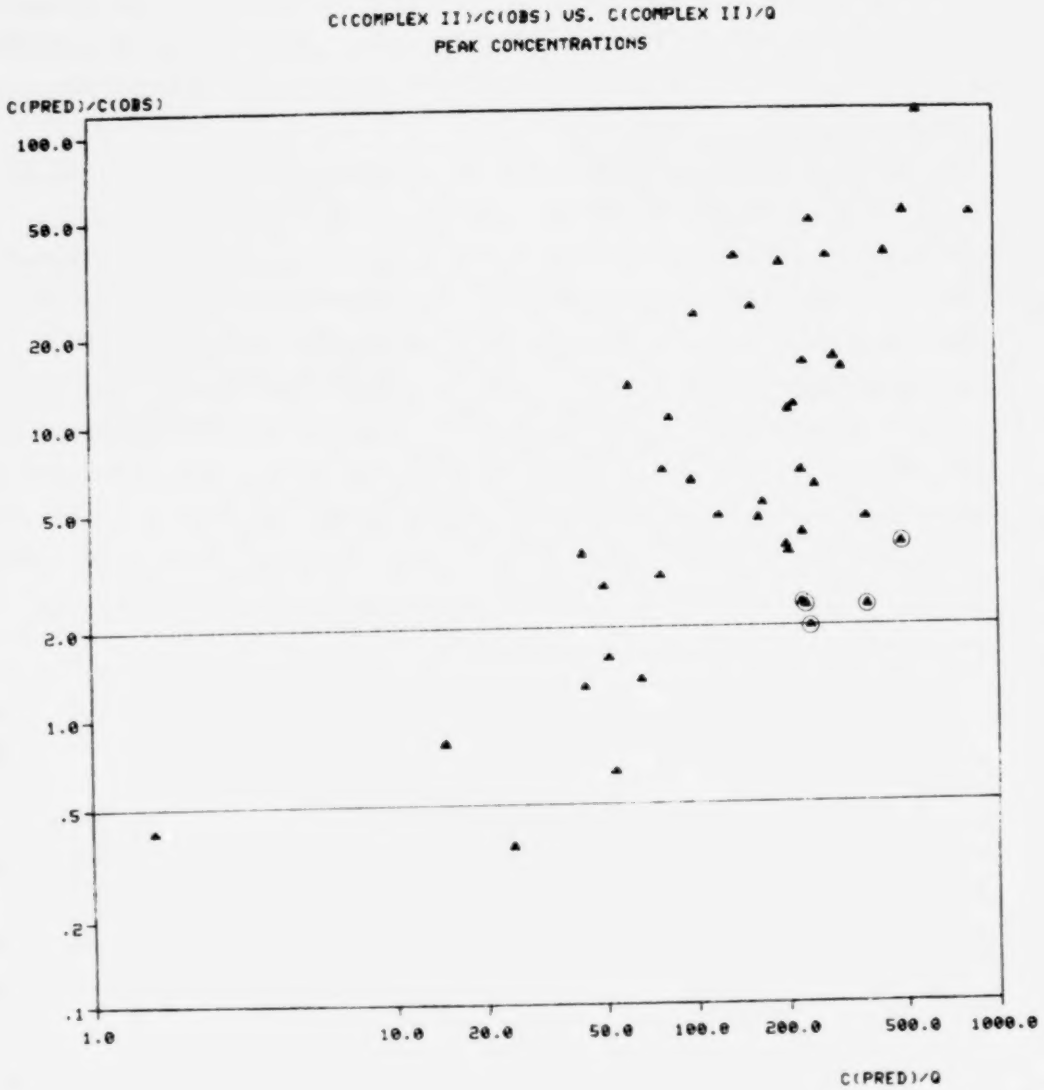

Figure 70. Variation of modeled-to-observed ratios of maximum hourly SF_6 concentrations with modeled concentrations calculated by Complex II (appropriate stability class - Turner scheme). Circles identify the five highest observed SF_6 concentrations (C/Q).

PFM

The analysis of PFM model calculations followed the same procedures used in preparing results from the COMPLEX models. Differences in tabular data summaries arise only from the fewer case hours used and the fewer stability classes tested.

Table 44 summarizes PFM model performance statistics for the 23 hours in which the SF_6 release height exceeded H_{crit} by 5 m or more. All concentrations have again been scaled by the emission rate. Figures 71 and 72 present scatterplots of peak calculated concentration ratios. The distribution of data in these figures shows some tendency toward overestimation, and this overestimation increases in going from class D to class E dispersion rates. However, in comparing the PFM scatterplots with the COMPLEX model scatterplots, there appears to be less of a trend toward increasing the magnitude of the residuals with C_p. This is apparently more a function of the case hours selected than the model. The relationship between model performance and data classification by H_{crit} will be discussed further in Section 5.5.2.

Impingement Model

Impingement model calculations are similar to those of Valley--a maximum concentration is calculated for each hour. Unlike Valley, however, the Impingement model simulates the maximum concentrations using actual meteorological conditions observed during a particular hour. The Impingement model should better account for the hour-to-hour variability in the observed maximum concentrations because it uses dispersion parameters calculated from observed turbulence intensities (see Section 4.5.4). Table 45 summarizes the analysis of the calculated concentrations (scaled by the emission rate) for each of the 45 hours.

Two consecutive case hours (Case 209, hours 7 and 8) show conspicuously large overestimates, apparently because of differences in the σ_z calculated by the model and the σ_z estimated from lidar data (see Section 4.5.4). In particular, for Case 209, hour 8, the proposed equation for σ_z seriously underestimates the size of the σ_z derived for this

TABLE 44. SUMMARY C/Q STATISTICS FOR PFM CALCULATIONS

			Observed			Stability Class D						Stability Class E					
Exp	Case Hour	N	$\overline{Co}$	σ(Co)	Max Co	$\overline{Cp}$	σ(Cp)	Max Cp	Max Cp/ Max Co	$\overline{Co-Cp}$	σ(Co-Cp)	$\overline{Cp}$	σ(Cp)	Max Cp	Max Cp/ Max Co	$\overline{Co-Cp}$	σ(Co-Cp)
201	1	16	13.1	8.4	32.2	8.6	8.8	26.8	.83	4.4	8.9	9.6	13.1	41.5	1.29	3.4	13.4
201	2	16	8.3	8.1	25.1	9.3	12.1	38.8	1.54	-1.0	10.2	10.7	18.5	63.9	2.54	-2.4	17.0
202	1	26	4.0	4.9	18.0	4.4	4.2	11.6	.64	-.4	4.2	3.8	4.2	11.2	.62	.2	4.5
202	2	32	8.4	6.8	33.6	2.6	3.6	12.1	.36	5.8	6.9	1.8	3.2	10.7	.32	6.6	6.9
202	3	28	8.6	16.9	67.2	6.7	7.7	28.6	.43	1.8	18.6	8.4	12.6	48.8	.73	.1	20.9
202	4	24	7.8	17.8	81.6	6.5	8.9	31.6	.39	1.3	14.9	7.6	11.8	42.8	.52	.1	16.8
202	5	24	5.2	11.1	49.2	3.7	7.8	27.8	.57	1.4	5.5	3.9	9.0	34.6	.70	1.3	6.5
202	6	21	3.1	3.2	11.8	4.3	6.4	19.8	1.68	-1.2	5.0	4.8	8.4	26.8	2.27	-1.8	6.8
205	4	33	5.2	4.4	15.4	6.4	6.7	22.9	1.49	-1.1	7.5	7.3	10.6	35.7	2.32	-2.0	11.5
205	5	31	7.3	4.6	25.5	6.2	6.3	21.1	.83	1.1	5.4	7.9	10.2	36.3	1.42	-.6	9.5
205	6	37	5.3	3.6	15.5	6.5	7.1	25.7	1.65	-1.2	6.8	7.6	11.1	41.4	2.67	-2.3	11.0
206	4	35	13.6	16.1	56.7	29.6	40.2	142.6	2.51	-16.1	40.5	38.7	56.3	203.0	3.57	-25.2	56.0
206	5	30	5.7	9.5	41.2	13.0	21.2	79.3	1.92	-7.3	17.9	13.8	25.9	77.5	1.88	-8.1	21.0
206	7	33	21.6	25.5	92.8	16.1	32.0	156.6	1.69	5.5	26.9	18.7	47.2	226.7	2.44	2.9	40.9
209	1	47	.4	.6	3.8	9.2	11.3	40.1	10.66	-8.8	11.3	9.5	14.7	52.4	13.94	-9.1	14.7
209	2	46	.9	1.3	5.0	12.0	18.7	70.5	14.00	-11.1	18.8	13.9	24.8	94.9	18.84	-12.9	24.9
210	3	45	2.4	2.7	11.5	5.7	6.2	20.6	1.80	-3.3	6.8	6.2	9.0	33.9	2.97	-3.8	9.5
210	4	39	1.6	1.3	4.6	3.3	3.6	12.0	2.64	-1.7	3.7	2.5	3.5	11.6	2.54	-.9	3.6
210	6	40	.5	1.0	4.4	1.6	2.4	9.7	2.22	-1.2	1.9	.7	1.5	7.2	1.65	-.2	1.1
210	7	45	.8	1.5	8.1	5.7	5.1	16.6	2.06	-4.9	5.4	6.1	6.8	21.0	2.61	-5.3	7.1
210	8	15	3.3	5.4	17.9	5.8	6.8	20.4	1.14	-2.5	6.7	6.0	7.8	23.2	1.30	-2.7	6.6
214	-	43	25.0	31.7	119.1	13.1	27.4	124.2	1.04	11.9	36.6	12.3	40.3	191.7	1.61	12.7	49.8
214	8	46	9.0	8.4	31.7	12.0	24.5	81.5	2.57	-3.0	25.7	10.5	27.8	111.1	3.50	-1.6	28.9

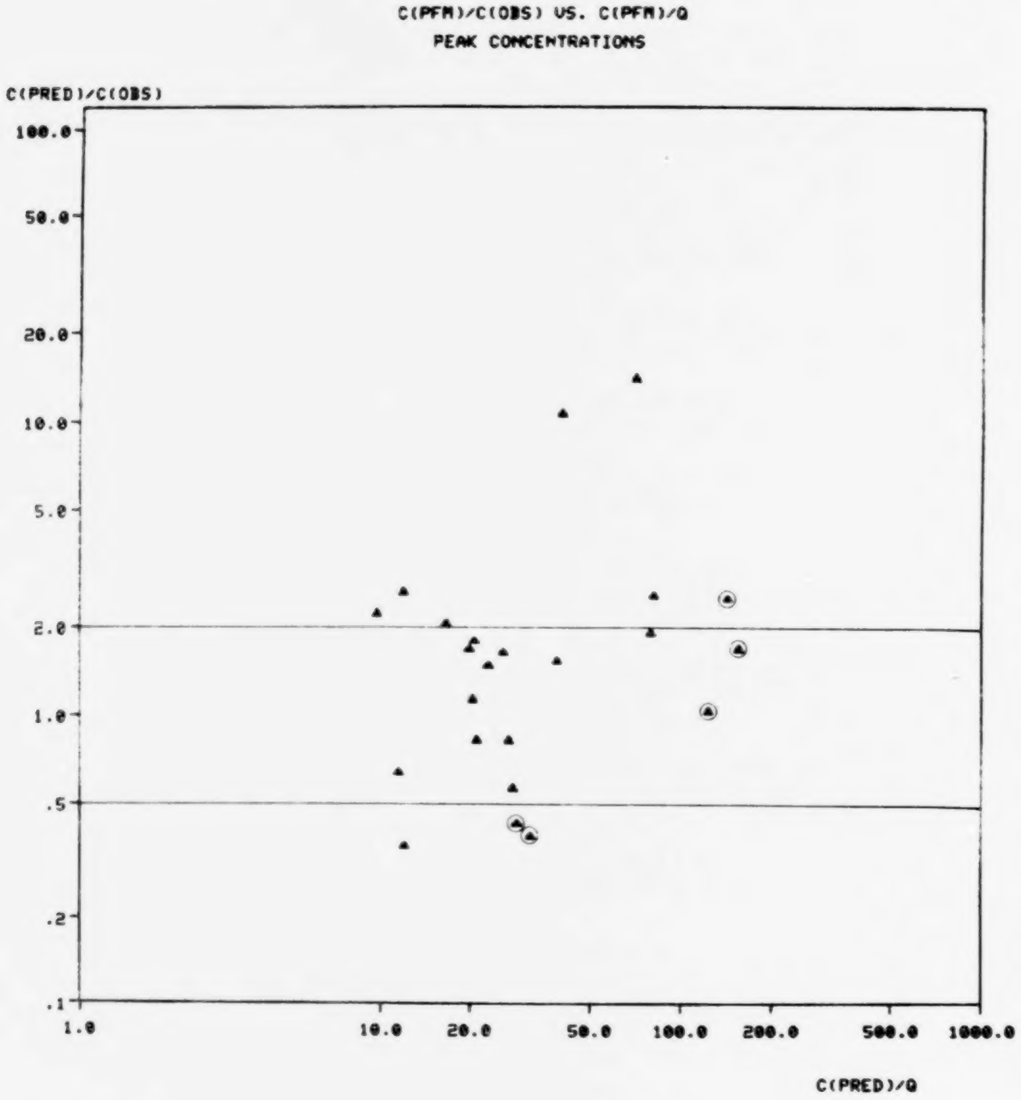

Figure 71. Variation of modeled-to-observed ratios of maximum hourly SF_6 concentrations with modeled concentrations calculated by PFM (Stability Class D). Circles identify the five highest observed SF_6 concentrations (C/Q).

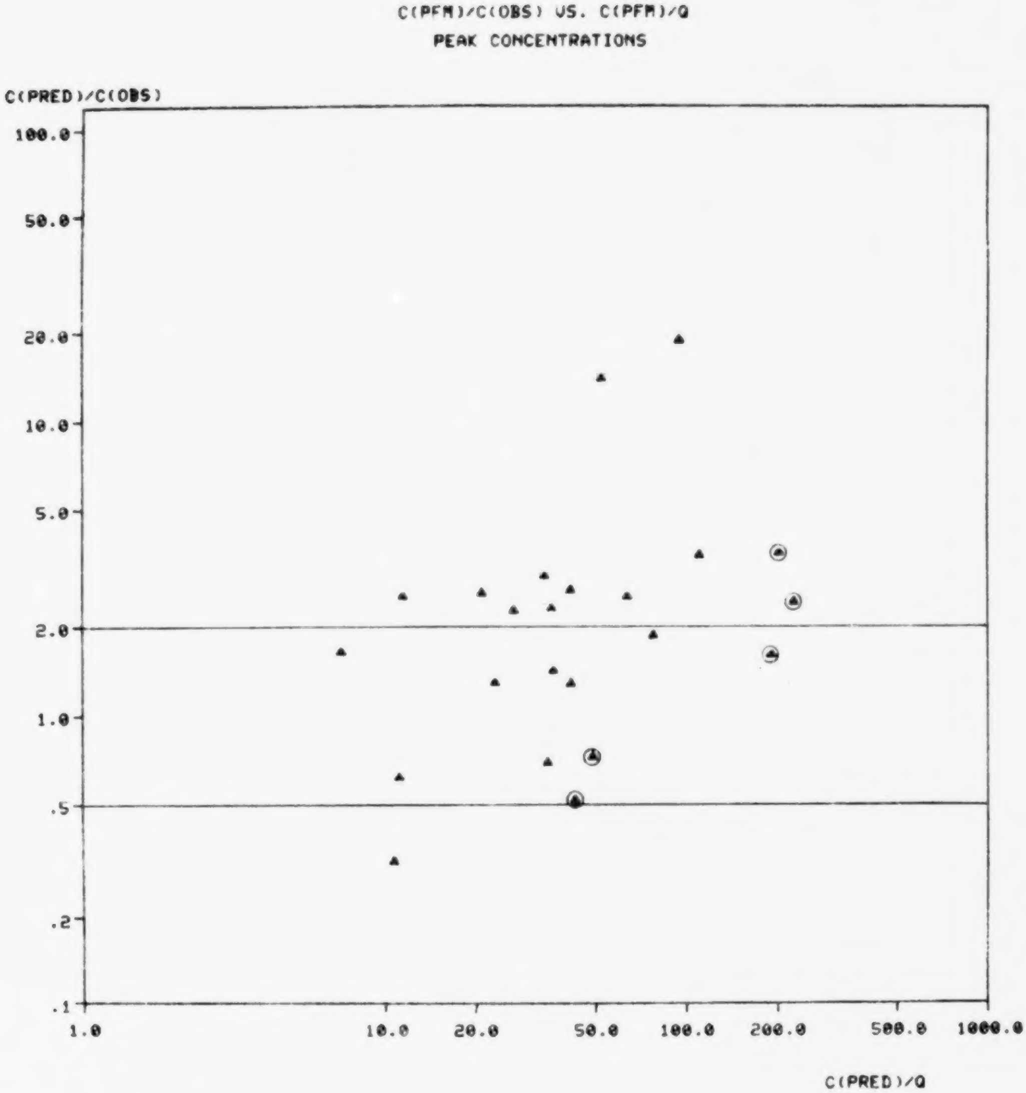

Figure 72. Variation of modeled-to-observed ratios of maximum hourly SF_6 concentrations with modeled concentrations calculated by PFM (Stability Class E). Circles identify the five highest observed SF_6 concentrations (C/Q).

TABLE 45. SUMMARY C/Q STATISTICS FOR IMPINGEMENT MODEL CALCULATIONS

			Observed					
Exp.	Case Hour	N	$\overline{Co}$	$\sigma(\overline{Co})$	Max Co	Max Cp	Max Cp/ Max Co	Co-Cp
201	1	16	13.1	8.4	32.2	14.1	.44	18.0
201	2	16	8.3	8.1	25.1	41.8	1.66	-16.7
201	4	16	6.4	5.6	18.6	71.4	3.83	-52.8
201	5	10	11.2	10.1	34.6	126.5	3.66	-91.9
201	6	11	7.9	5.7	18.7	137.8	7.39	-119.2
202	1	26	4.0	4.9	18.0	9.9	.55	8.1
202	2	32	8.4	6.8	33.6	27.4	.82	6.2
202	3	28	8.6	16.9	67.2	41.8	.62	25.3
202	4	24	7.8	17.8	81.6	12.1	.15	69.6
202	5	24	5.2	11.1	49.2	1.6	.03	47.6
202	6	21	3.1	3.2	11.8	58.6	4.96	-46.8
204	1	37	1.7	2.7	14.5	50.6	3.49	-36.1
204	2	36	2.0	2.9	11.3	18.5	1.63	-7.2
204	5	30	1.1	1.0	4.8	23.2	4.88	-18.5
204	6	34	2.1	3.4	17.6	57.1	3.25	-39.5
204	7	32	2.5	2.4	9.6	23.0	2.41	-13.5
204	8	33	6.6	4.3	16.1	38.4	2.39	-22.3
205	4	33	5.2	4.4	15.4	26.6	1.73	-11.2
205	5	31	7.3	4.6	25.5	11.0	.43	14.6
205	6	37	5.3	3.6	15.5	22.4	1.44	-6.9
206	4	35	13.6	16.1	56.7	169.1	2.98	-112.3
206	5	30	5.7	9.5	41.2	89.9	2.18	-48.6
206	6	28	35.4	31.5	124.2	126.3	1.02	-2.1
206	7	33	21.6	25.5	92.8	47.4	.51	45.4
206	8	70	38.6	35.3	154.6	23.7	.15	131.0
209	1	47	.4	.6	3.8	22.4	5.94	-18.6
209	2	46	.9	1.3	5.0	28.7	5.69	-23.6
209	3	48	2.1	1.3	5.6	8.1	1.45	-2.5
209	7	46	1.6	2.0	7.6	221.7	29.17	-214.1
209	8	40	3.2	4.9	20.3	281.1	13.86	-260.8
210	3	45	2.4	2.7	11.5	44.2	3.87	-32.8
210	4	39	1.6	1.3	4.6	14.4	3.16	-9.9
210	6	40	.5	1.0	4.4	3.1	.71	1.3
210	7	45	.8	1.5	8.1	8.7	1.08	-.6
210	8	15	3.3	5.4	17.9	40.5	2.26	-22.6
211	1	43	4.3	2.8	11.5	14.2	1.23	-2.7
211	2	36	2.3	1.4	6.4	15.6	2.45	-9.2
211	3	34	.5	.8	3.9	9.1	2.34	-5.2
211	4	36	8.7	9.2	33.0	11.3	.34	21.7
211	5	40	24.6	23.0	97.4	22.6	.23	74.8
211	6	37	12.3	12.2	53.1	28.1	.53	25.0
214	3	41	5.0	14.9	77.6	24.2	.31	53.4
214	4	37	16.7	13.8	54.4	55.0	1.01	-.6
214	7	43	25.0	31.7	119.1	128.5	1.08	-9.5
214	8	46	9.0	8.4	31.7	12.8	.40	19.0

hour from the lidar data. No other case hour showed so large a discrepancy. If the turbulent plume spread during the preceding hour was also underestimated to the same extent, then the consecutive hours of overestimation are not surprising. (Hour 7 lidar data are currently unavailable because only selected hours of lidar data have been processed to date.) It is not known if the turbulence measurements, the temperature measurements, or the functional form for σ_z are responsible for these discrepancies.

A scatterplot of the Impingement model calculated-to-observed concentration ratios versus calculated concentrations (scaled by the emission rate) is presented in Figure 73. It shows a general tendency for overestimation of concentration peaks, although many observations are underestimated. The scatter in the residuals is very large, especially for the lower two-thirds of the data points (as ordered by C_p).

Neutral Model

Neutral model calculations are summarized and the overall statistics are presented in Table 46. A scatterplot of calculated-to-observed concentration ratios versus calculated concentrations is presented in Figure 74.

The Neutral model calculations underestimated the concentrations observed during the two case hours singled out above (Case 209, hours 7 and 8). A third hour (Case 202, hour 6) stands out because the model predicted no SF_6 anywhere on the hill. This clearly results from the magnitude of the vertical intensity of turbulence (IZ) used to compute σ_z. IZ for this hour was extremely small compared to all other hours tested. Although the magnitude of IZ is unusual, the variation of IZ and IW throughout the hour (5-minute averages) indicates that the propellor anemometer was probably not seizing.

The scatterplot for the Neutral model shows a wide variability in model performance, with cases of overestimation and underestimation of the hourly maximum concentration. However, no strong increase in the residual with C_p is evident. The Neutral model may thus have a mean residual close to zero, but it is far from being a good model for estimating maximum hourly

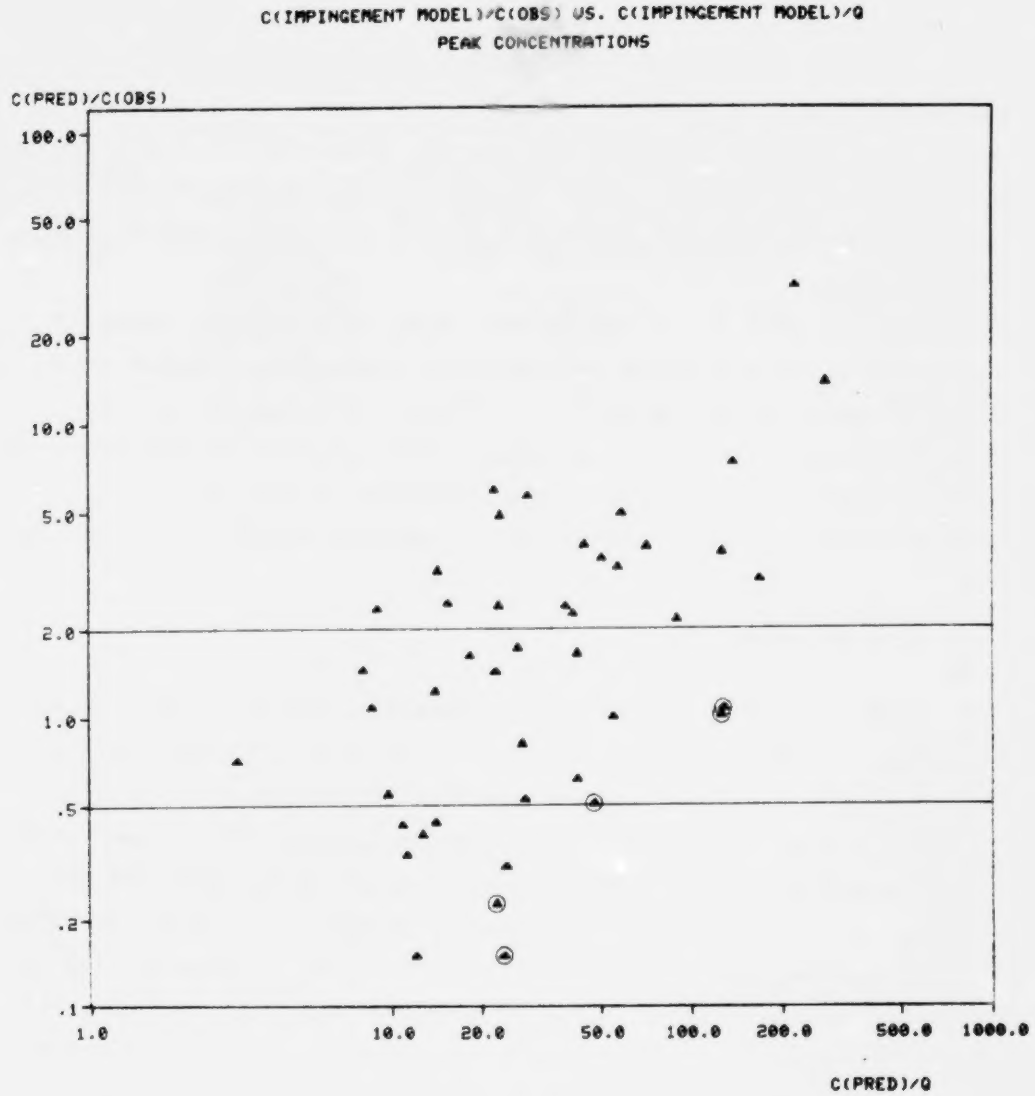

Figure 73. Variation of modeled-to-observed ratios of maximum hourly SF_6 concentrations with modeled concentrations calculated by the Impingement model. Circles identify the five highest observed SF_6 concentrations (C/Q).

TABLE 46. SUMMARY C/Q STATISTICS FOR NEUTRAL MODEL CALCULATIONS

			Observed								
Exp	Case Hour	N	$\overline{Co}$	σ(Co)	Max Co	$\overline{Cp}$	σ(Cp)	Max Cp	Max Cp/ Max Co	$\overline{Co-Cp}$	σ(Co-Cp)
201	1	16	13.1	8.4	32.2	12.4	6.2	22.8	.71	.6	5.2
201	2	16	8.3	8.1	25.1	10.0	8.6	26.0	1.03	-1.7	7.2
201	4	16	6.4	5.6	18.6	22.0	10.7	32.4	1.74	-15.6	12.9
201	5	10	11.2	10.1	34.6	17.0	7.2	23.8	.69	-5.8	13.6
201	6	11	7.9	5.7	18.7	2.4	1.2	4.9	.26	5.5	6.1
202	1	26	4.0	4.9	18.0	6.4	5.1	13.4	.75	-2.4	4.4
202	2	32	8.4	6.8	33.6	4.9	7.7	25.5	.76	3.5	8.9
202	3	28	8.6	16.9	67.2	22.2	15.0	50.4	.75	-13.6	22.9
202	4	24	7.8	17.8	81.6	11.5	14.5	58.0	.71	-3.8	15.1
202	5	24	5.2	11.1	49.2	4.9	12.0	44.5	.90	.2	10.6
202	6	21	3.1	3.2	11.8	.0	.0	0	.00	3.1	3.2
204	1	37	1.7	2.7	14.5	20.6	5.8	25.7	1.78	-18.9	7.3
204	2	36	2.0	2.9	11.3	8.7	5.9	27.4	2.42	-6.7	4.9
204	5	30	1.1	1.0	4.8	21.0	6.3	34.9	7.32	-20.0	5.8
204	6	34	2.1	3.4	17.6	30.9	8.9	46.6	2.65	-28.9	7.5
204	7	32	2.5	2.4	9.6	20.4	5.5	31.7	3.32	-17.9	4.7
204	8	33	6.6	4.3	16.1	33.0	9.8	57.4	3.56	-26.4	9.1
205	4	33	5.2	4.4	15.4	8.7	5.6	18.0	1.17	-3.4	4.8
205	5	31	7.3	4.6	25.5	4.1	2.5	7.6	.30	3.2	4.9
205	6	37	5.3	3.6	15.5	12.7	4.7	20.7	1.33	-7.4	5.4
206	4	35	13.6	16.1	56.7	6.4	4.2	13.2	.23	7.1	13.4
206	5	30	5.7	9.5	41.2	10.2	6.3	19.6	.48	-4.6	8.4
206	6	28	35.4	31.5	124.2	42.6	21.2	85.6	.69	-7.2	28.6
206	7	33	21.6	25.5	92.8	17.9	7.2	32.4	.35	3.8	22.5
206	8	70	38.6	35.3	154.6	11.4	4.2	22.6	.15	27.2	32.4
209	1	47	.4	.6	3.8	13.6	9.7	33.2	8.83	-13.2	9.7
209	2	46	.9	1.3	5.0	9.7	9.4	35.2	6.98	-8.8	9.4
209	3	48	2.1	1.3	5.6	2.9	5.1	26.3	4.70	-.7	5.4
209	7	46	1.6	2.0	7.6	.5	.6	2.1	.27	1.1	1.9
209	8	40	3.2	4.9	20.3	1.3	1.4	4.4	.22	1.9	5.3
210	3	45	2.4	2.7	11.5	1.0	1.1	3.6	.31	1.4	2.7
210	4	39	1.6	1.3	4.6	2.9	3.0	10.7	2.35	-1.4	2.6
210	6	40	.5	1.0	4.4	.7	1.5	8.9	2.04	-.2	.9
210	7	45	.8	1.5	8.1	3.8	2.1	7.4	.92	-3.0	2.6
210	8	15	3.3	5.4	17.9	8.2	4.7	16.6	.93	-5.0	4.9
211	1	43	4.3	2.8	11.5	11.1	3.2	17.6	1.53	-6.8	3.2
211	2	36	2.3	1.4	6.4	13.3	5.0	25.4	3.98	-10.9	4.9
211	3	34	.5	.8	3.9	6.6	3.8	18.5	4.76	-6.1	4.0
211	4	36	8.7	9.2	33.0	10.5	3.2	18.7	.57	-1.7	7.0
211	5	40	24.6	23.0	97.4	19.0	5.4	32.1	.33	5.6	20.4
211	6	37	12.3	12.2	53.1	21.5	7.1	37.8	.71	-9.2	10.4
214	3	41	5.0	14.9	77.6	11.9	4.5	24.8	.32	-6.9	13.2
214	4	37	16.7	13.8	54.4	25.7	10.2	44.6	.82	-9.0	14.9
214	7	43	25.0	31.7	119.1	29.9	20.8	84.8	.71	-4.9	26.2
214	8	46	9.0	8.4	31.7	7.1	11.8	76.9	2.42	1.8	14.7

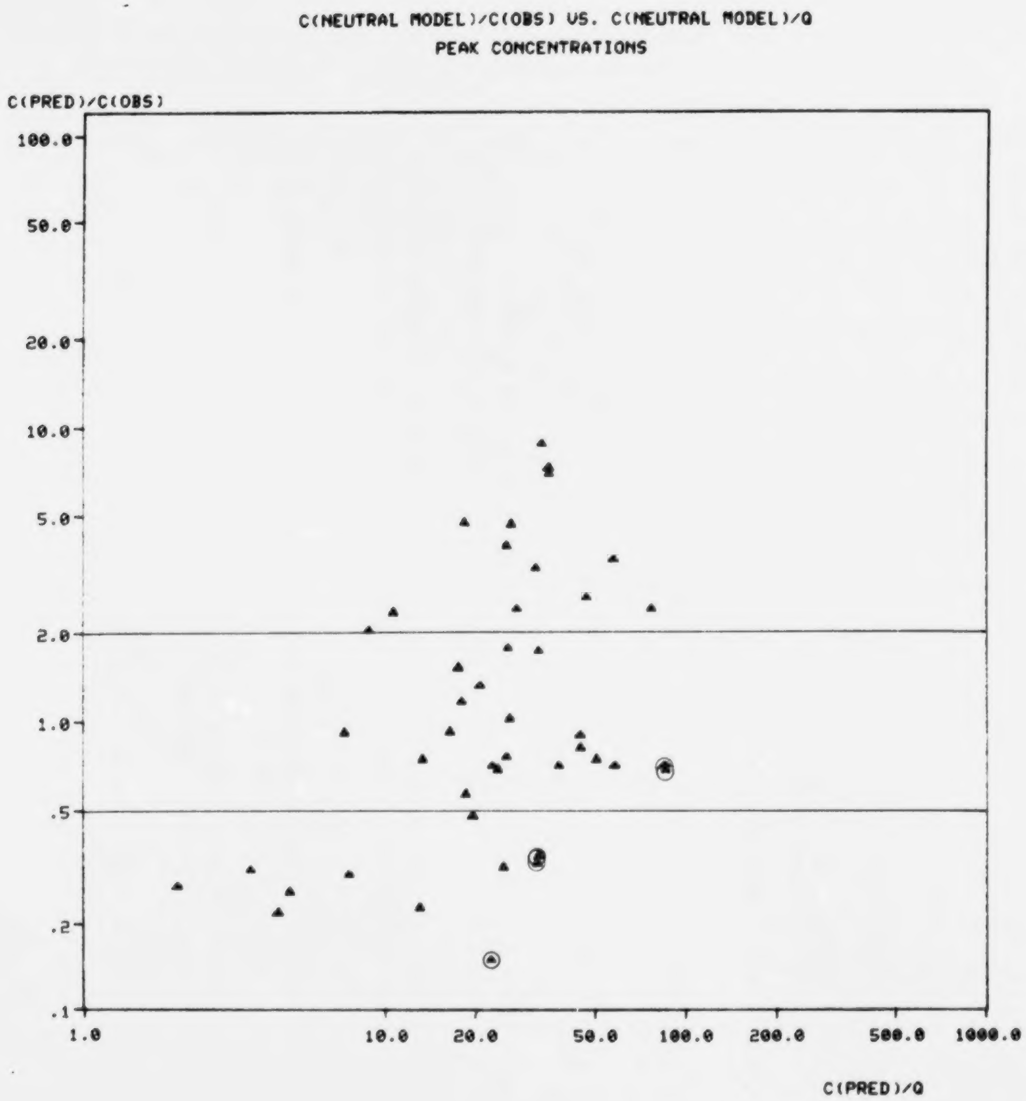

Figure 74. Variation of modeled-to-observed ratios of maximum hourly SF_6 concentrations with modeled concentrations calculated by the Neutral model. Circles identify the five highest observed SF_6 concentrations (C/Q).

concentrations at CCB because of the scatter in the residuals and because it underestimates the highest observations.

5.5.2 Performance Evaluation

Overall model error statistics for Valley, COMPLEX I, COMPLEX II, PFM, and the new experimental models have been assembled in Table 47 for the following measures related to $\bar{\epsilon}$ and σ_{ϵ}:

- m_g, s_g: lognormal statistics (geometric mean and geometric standard deviation) of the residual errors in maximum computed and maximum observed concentrations.
- $\overline{\text{Max } C_o - \text{Max } C_p}$, $\sigma(\text{Max } C_o - \text{Max } C_p)$: statistics of the residuals in maximum computed and maximum observed concentrations.
- $\overline{C_o - C_p}$, $\sigma(C_o - C_p)$: statistics of the residuals in computed and observed concentrations paired by sampling location.

The first two sets of statistics summarize the errors in estimating 1-hour maximum concentrations, regardless of location, over the hours included in this analysis. The third set summarizes the mean errors in estimating observed concentrations at all sampling points. Plots of $\bar{\epsilon}$ versus σ_{ϵ} based on the data in Table 47 are displayed in Figures 75 through 77.

Not all model statistics summarized in Table 47 are based on 45 case hours. The geometric statistics include only those hours with maximum estimated concentrations greater than zero. Several models produced an estimate of zero for one hour, and so the geometric statistics for these are based on 44 hours. Furthermore, PFM was run for only those 23 hours in which the release height exceeded the calculated dividing streamline height by 5 m.

Table 47 also contains statistics for a "hybrid" model made up of Neutral and Impingement model estimates. Neutral model results are taken for those 23 cases where the release height exceeds H_{crit} by 5 m or more and the Impingement model results are taken for the remaining 22 hours. However, geometric statistics for this Neutral-Impingement combination model are based on only 44 case hours because one of the 23 Neutral model estimates is zero.

TABLE 47. SUMMARY OF ANALYSIS OF C/Q RESIDUALS - ALL CASE HOURS

Model	N	$\underline{m}_g$	$\underline{s}_g$	$\overline{\text{Max } C_o - \text{Max } C_p}$	$\sigma(\text{Max } C_o - \text{Max } C_p)$	$\overline{C_o - C_p}$	$\sigma(C_o - C_p)$
Valley	45	0.29	2.64	-38.9	33.2	-	-
Valley (CL)	45	0.28	2.27	-64.9	80.0	-	-
COMPLEX I D	45	0.66	3.10	-11.5	43.4	-12.0	18.9
COMPLEX I E	45	0.40	3.09	-37.8	52.6	-20.2	24.5
COMPLEX I F	45	0.37	3.18	-36.1	53.2	-24.8	25.1
COMPLEX I T*	45	0.39	3.37	-37.6	55.9	-24.0	25.5
COMPLEX II D	45	0.41	3.16	-40.9	60.8	-9.3	26.0
COMPLEX II E	45	0.23	3.87	-109.9	113.3	-17.3	45.5
COMPLEX II F	44	0.13	3.29	-178.9	158.4	-23.7	68.5
COMPLEX II T*	44	0.16	3.85	-165.3	162.8	-23.2	67.2
PFM** D	23	0.68	2.43	-11.7	32.0	-1.4	16.6
PFM** E	23	0.52	2.49	-29.4	46.3	-2.2	22.1
Neutral	44	0.97	2.81	6.5	31.1	-4.6	12.1
Impingement	45	0.72	3.56	-15.5	65.0	-	-
Neutral-Impingement Combination	44	0.76	3.14	-10.0	62.9	-	-

Note: Estimated concentrations for one case hour were zero according to COMPLEX II (Class F,T), Neutral and the Neutral-Impingement combination models. Consequently, geometric statistics were computed over 44 case hours for these models, instead of over 45 case hours, as in the other statistics.

*The Turner objective scheme is used to determine the hourly stability class.

**PFM was run for case-hours in which $H \geq H_{crit} + 5$ m.

On the basis of the lognormal statistics, the Neutral model best estimates the highest observed concentration each hour (in the sense that it gives the smallest values of $\overline{\epsilon^2} = \overline{\epsilon}^2 + \sigma_{\epsilon}^2$). It shows a slight bias toward overestimation ($m_g = 0.97$). The Neutral-Impingement hybrid, the Impingement model, and COMPLEX I (class D) follow closely in performance with mean biases of 0.66 to 0.76. These are the only models in the test group that, on average over at least 44 test cases, estimate the highest observed concentration to within a factor of 2. A second group of models has a bias factor of about 0.4. This group includes COMPLEX I (class E, F, and appropriate stability class), and COMPLEX II (class D).

Model ranking mostly depends on the magnitude of $m_g(\overline{\epsilon})$ because s_g (or σ_{ϵ}) shows less variability among the models. The models that show the largest biases are in increasing order: the Valley model, $m_g = 0.29$; Valley centerline, $m_g = 0.28$; COMPLEX II (class E), $m_g = 0.23$; COMPLEX II (appropriate stability class), $m_g = 0.16$; and finally COMPLEX II (class F), $m_g = 0.13$.

The relative performance of COMPLEX I and COMPLEX II indicates that 1-hour average calculated maximum concentrations at CCB are overestimated by greater margins when:

- 22.5° sector averaging is not used, and
- stable plume configuration is used.

The best combination includes 22.5° sector averaging and a 0.5 plume path coefficient (COMPLEX I, class D), but it is not clear if best performance is due primarily to the difference between class E and class D dispersion coefficients or to the difference in plume trajectory assumptions (partial lift rather than impingement). For example, it is possible that the use of class E plume spread coefficients in combination with the 0.5 path coefficient might yield m_g value closer to unity, but this has not been explored.

A similar picture of relative model performance emerges if the (untransformed) concentration errors are assumed to be normally distributed. Mean residuals and standard deviations of the residuals between calculated and observed maximum concentrations are plotted in Figure 76. The models with the smallest mean residuals are Neutral, Neutral/Impingement, COMPLEX I

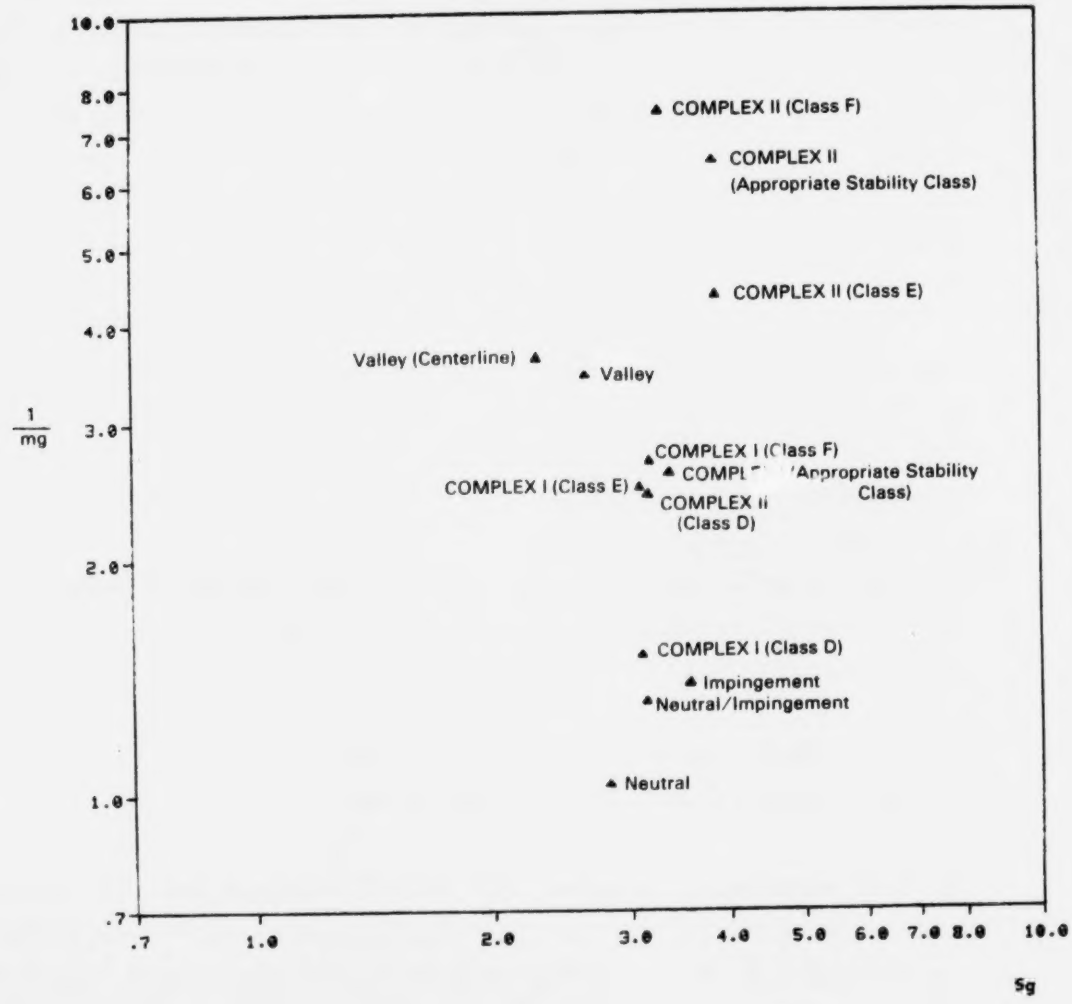

Figure 75. Relative performance of models tested with 45 case hours of data from CCB with model performance based on ratios of maximum calculated and observed hourly SF_6 concentrations.

Note: m_g and s_g are the geometric mean and geometric standard deviation of the ratio C_o/C_p.

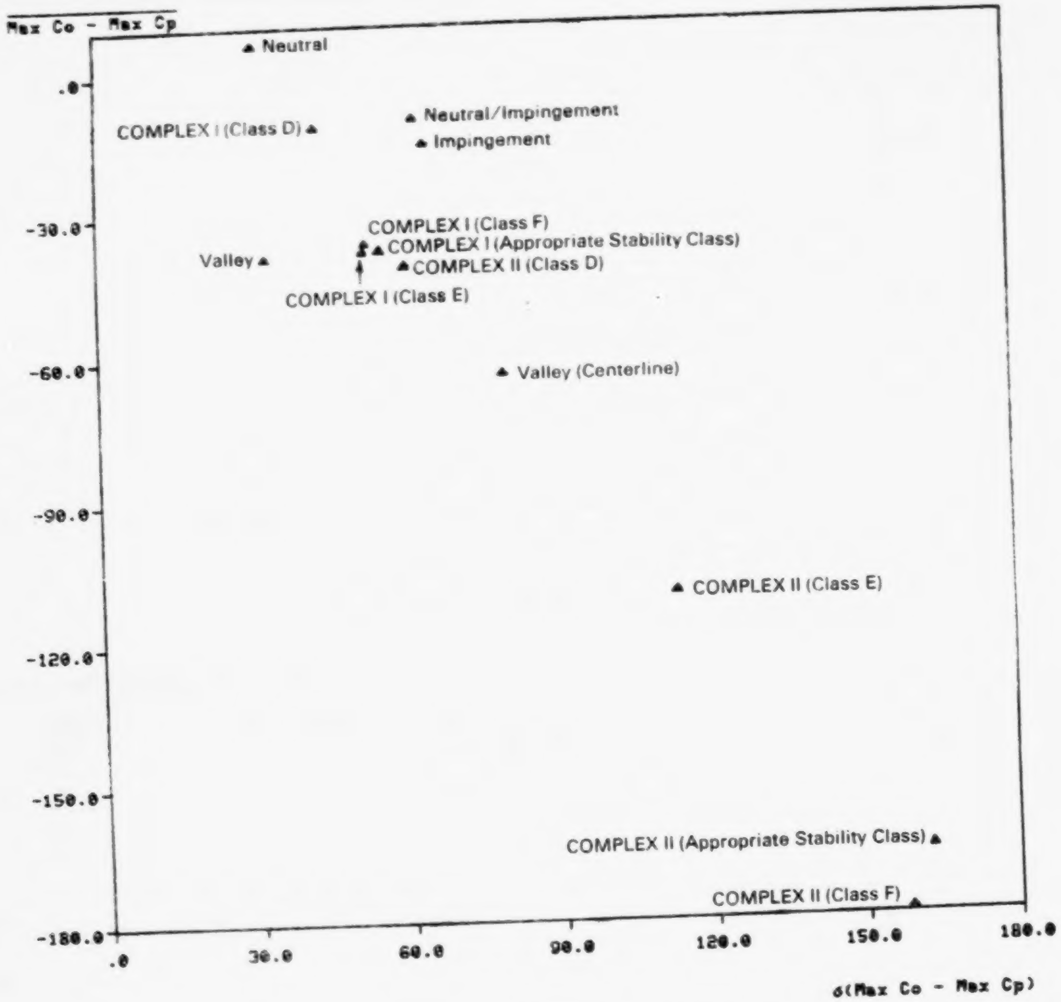

Figure 76. Relative performance of models tested with 45 case hours of data from CCB with model performance based on residuals of maximum calculated and observed hourly SF_6 concentrations.

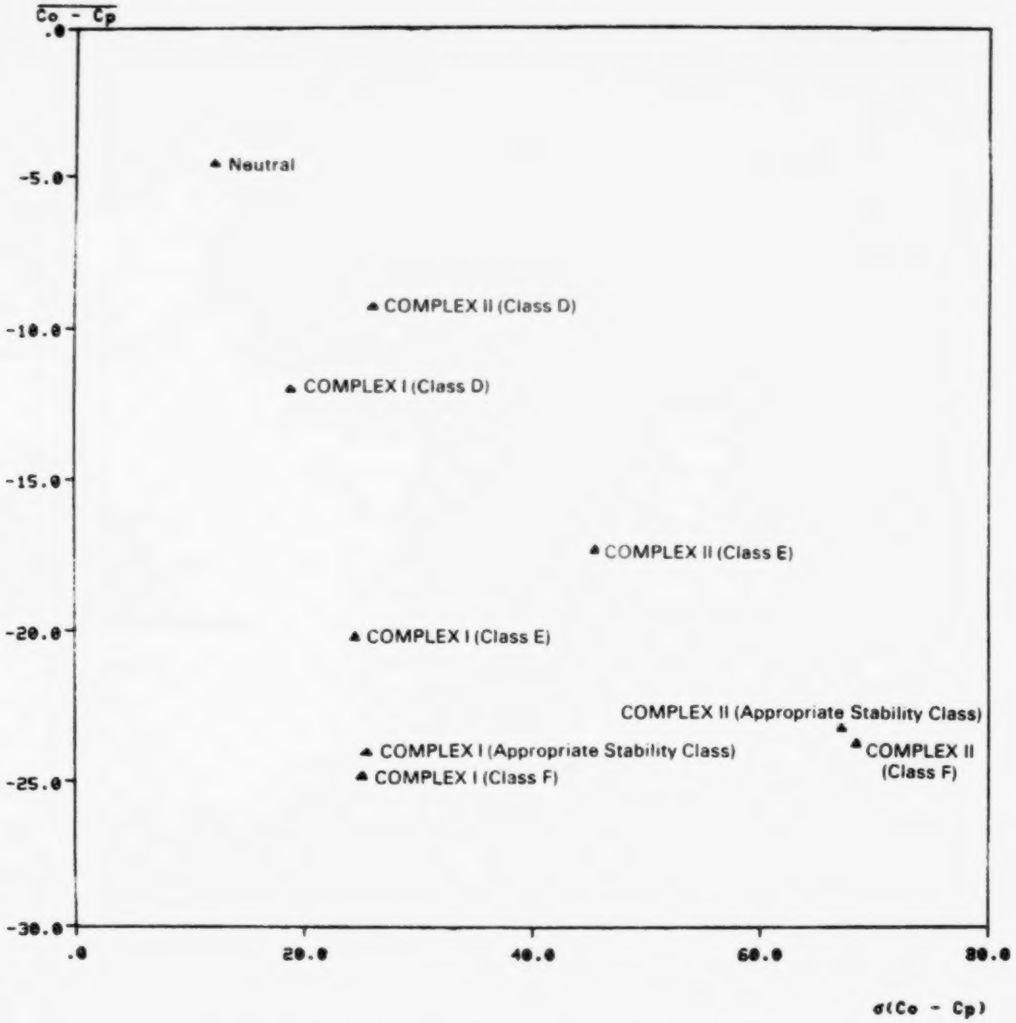

Figure 77. Relative performance of models tested with 45 case hours of data at CCB with model performance based on residuals of calculated and observed hourly SF_6 concentrations at all samplers.

(class D), and Impingement. (The Neutral model underestimates maximum concentrations on the average, but it still exhibits the best performance in terms of $\overline{\varepsilon^2}$. The next best model is COMPLEX I (class D).) Those with the largest mean residuals are Valley centerline and COMPLEX II (stable classes). Valley, COMPLEX I (stable classes), and COMPLEX II (class D) are grouped not far from the relatively better models.

A different relative ordering is found when paired residuals from all sampling points are evaluated in terms of $\overline{\varepsilon^2}$ (see Figure 77). The Neutral model is again nearest to a zero mean residual. COMPLEX II (class D) now ranks ahead of COMPLEX I (class D), COMPLEX II (class E) is virtually tied with COMPLEX I (class E), and COMPLEX II (class F) is poorer than COMPLEX I (class F). The Valley and Impingement model results are not presented because they estimate only the maximum concentration.

The relative performances of COMPLEX I and COMPLEX II become clearer when added importance is attached to the standard deviation of the residuals (σ_ε). COMPLEX I results show uniformly smaller σ_ε values than do COMPLEX II results. Therefore, the mean residuals for COMPLEX II are probably closer to zero than the corresponding COMPLEX I residuals because underestimates and overestimates tend to balance. This interpretation is consistent with the fact that COMPLEX I is a sector-averaged model, whereas COMPLEX II is a narrow plume model.

PFM performance was not included in the foregoing comparisons because it was run for only 23 of the 45 test cases. Instead, PFM is separately compared against the Neutral model and against the COMPLEX models for those 23 case hours during which the release height was equal to or greater than H_{crit} plus 5 m. Table 48 presents the residual statistics for this comparison and these results are displayed in Figures 78 to 80.

PFM ranks about the same as COMPLEX II (class D) and COMPLEX I (stable classes) in estimating the maximum concentrations, both with and without the log transformation. Its bias (m_g) is 0.68. The only models with a bias closer to unity are Neutral (m_g = 1.03) and COMPLEX I, class D (m_g = 1.10). Point-by-point residual analysis (see Figure 80) shows PFM (class D) to have the smallest mean residual, but its mean square error ($\overline{\varepsilon^2}$) is not as small as that for the Neutral model.

TABLE 48. SUMMARY OF ANALYSIS OF C/Q RESIDUALS FOR HOURS IN WHICH $H \geq H_{crit} + 5m$

Model	N	m_g	s_g	$\overline{\text{Max } C_o - \text{Max } C_p}$	$(\text{Max } C_o - \text{Max } C_p)$	$\overline{C_o - C_p}$	$\sigma(C_o - C_p)$
PFM D	23	0.68	2.43	-11.7	32.0	-1.37	16.6
PFM E	23	0.52	2.49	-29.4	46.3	-2.24	22.1
Neutral	22	1.03	2.46	6.2	22.6	-2.1	11.5
COMPLEX I D	23	1.10	2.56	-1.3	39.9	-7.5	17.6
COMPLEX I E	23	0.64	2.63	-20.1	50.6	-13.7	22.3
COMPLEX I F	23	0.60	2.55	-11.0	30.0	-15.4	18.5
COMPLEX I T*	23	0.64	2.84	-14.1	40.4	-13.7	19.3
COMPLEX II D	23	0.64	2.47	-15.7	41.9	-2.5	18.1
COMPLEX II E	23	0.32	2.60	-56.9	67.0	-6.9	28.5
COMPLEX II F	23	0.19	2.60	-103.2	80.4	-9.0	37.7
COMPLEX II T*	23	0.25	3.34	-76.6	69.3	-8.1	33.1

---

*The Turner objective scheme is used to determine the hourly stability class.

Note: Estimated concentrations for one case hour were zero according to the Neutral model. Consequently, geometric statistics were computed from 22 case hours for this model instead of 23 hours, as in the other statistics.

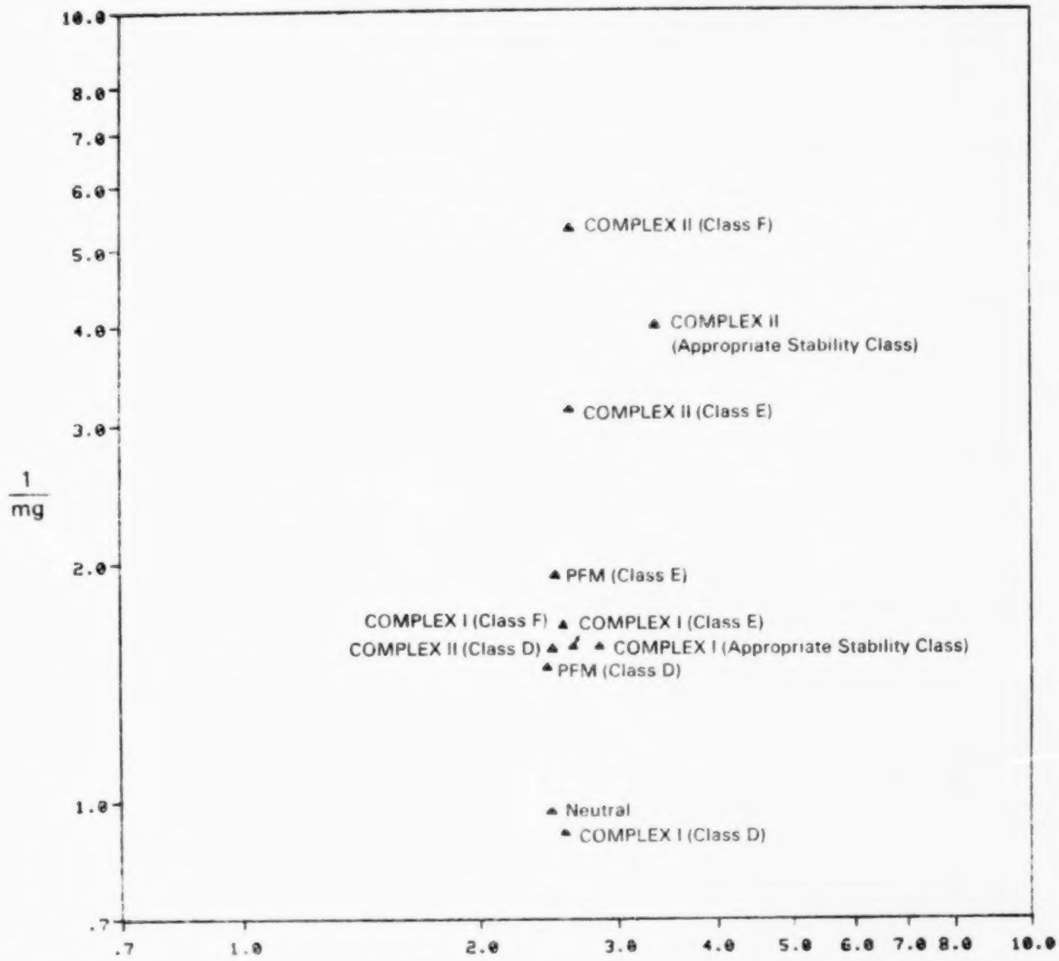

Note: m_g and s_g are the geometric standard deviation of the ratio C_o/C_p.

Figure 78. Relative performance of models tested with 23 hours case hours (release height > H_{crit}) of data at CCB with model performance based on ratios of maximum calculated and observed hourly SF_6 concentrations.

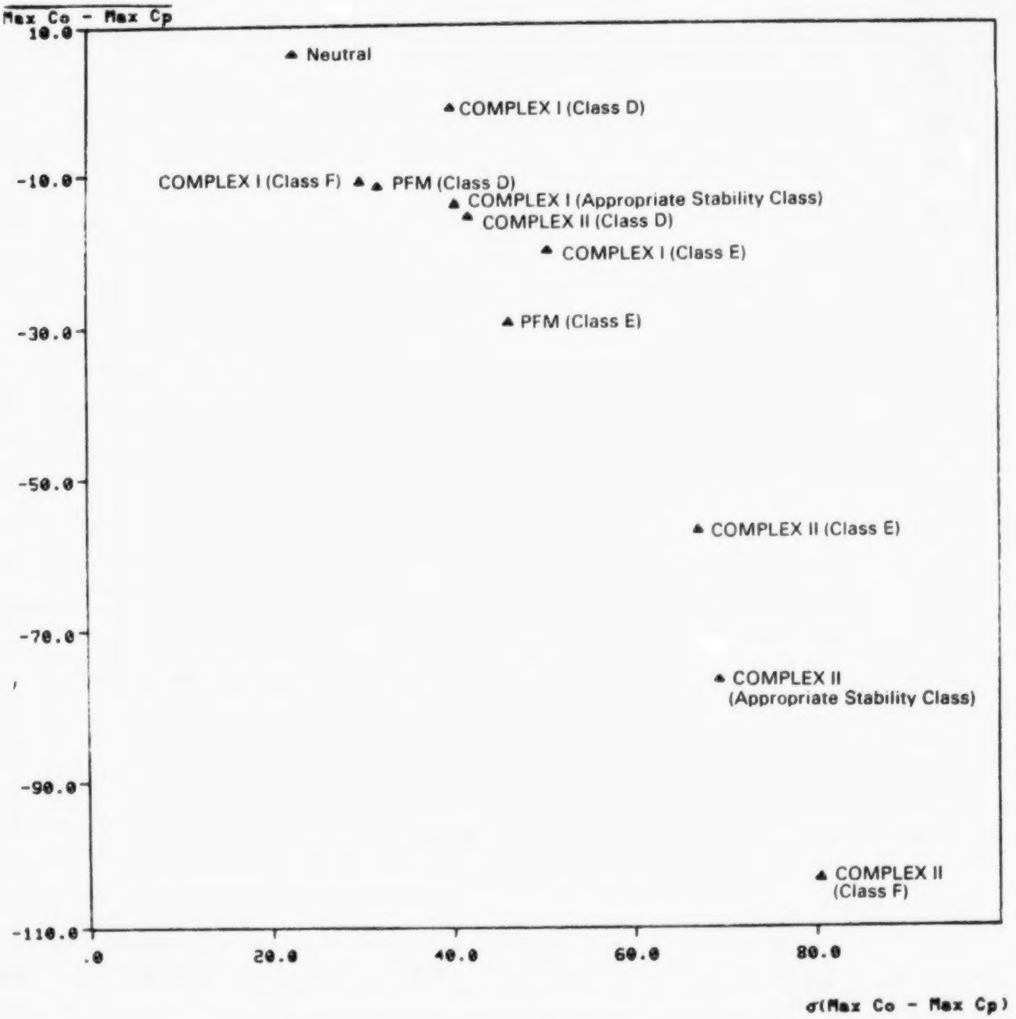

Figure 79. Relative performance of models tested with 23 case hours (release height > H_{crit}) of data at CCB with model performance based on residuals of maximum calculated and observed hourly SF_6 concentrations.

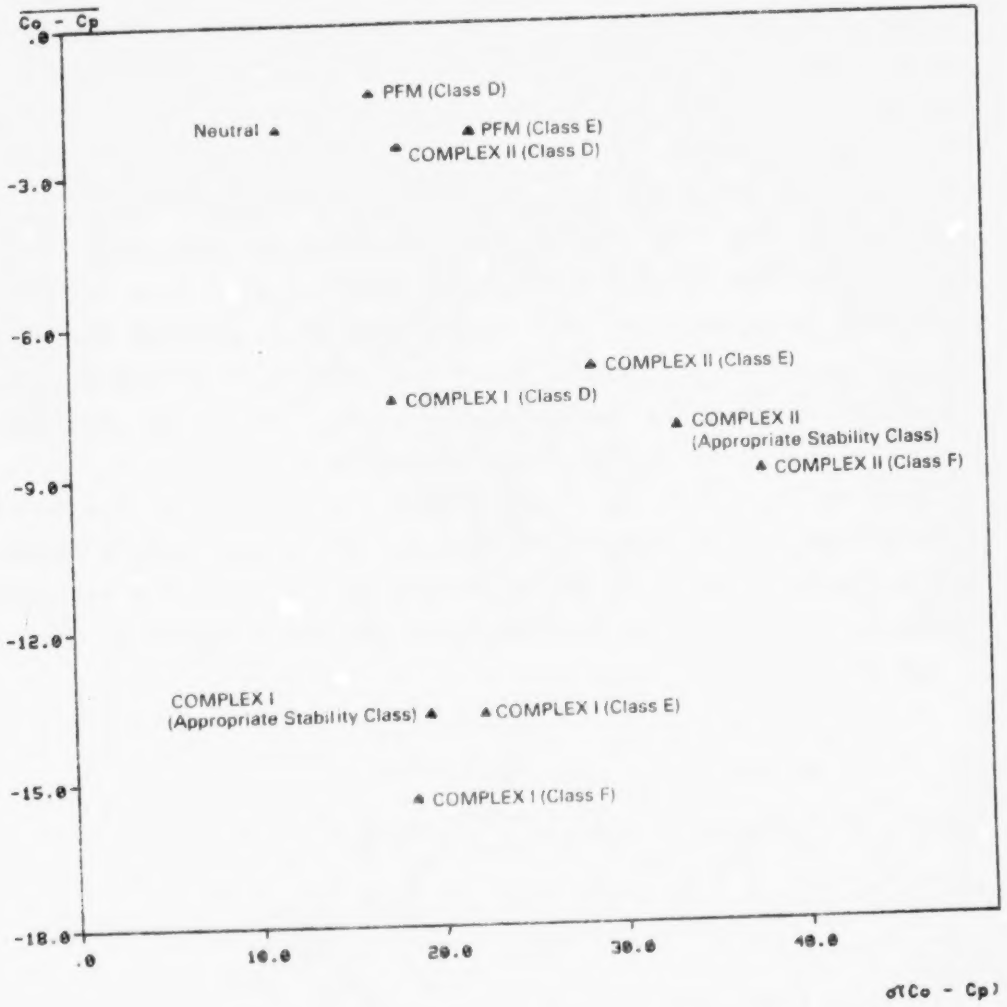

Figure 80. Relative performance of models tested with 23 case hours (release height > H_{crit}) of data at CCB with model performance based on residuals of calculated and observed hourly SF_6 concentrations at all samplers.

Figures 78 through 80 also show that the models perform better on the subset of case hours during which the release was above H_{crit} than they do on the entire 45-hour set. For example, only the COMPLEX II (stable) computations overestimate maximum observed concentrations by more than a factor of 2. Furthermore, the COMPLEX II estimates provide a marginally better description of the overall distribution of concentrations than the COMPLEX I estimates. This suggests that the flow was generally steadier when the release was above H_{crit}, and, consequently, that nonsector-averaged models tend to do as well or better than sector-averaged models in describing plume spread over 1-hour periods for this class of flow. This is best demonstrated with PG class D dispersion rates.

Model performance may also be addressed by quantifying the uncertainty in model estimates in terms of confidence intervals computed from the error statistics (mean and standard deviation). One approach to computing confidence intervals is described in Appendix C.

The evaluations of model performance presented above show that there is clearly room for improving the reliability of Gaussian models intended for use in complex terrain settings. ERT's plans for further development of models with data from the experiments at CCB are presented in the next section.

SECTION 6

CONCLUSIONS AND RECOMMENDATIONS FOR FURTHER ANALYSIS AND DEVELOPMENT

6.1 Accomplishments in Overview

The Cinder Cone Butte study, the initial field study in EPA's continuing program to develop and validate reliable dispersion models for applications in complex terrain, has achieved its stated objectives (Holzworth 1980) of providing both a set of visual observations of smoke plumes interacting with an isolated terrain feature in generally stably stratified flows and a detailed data base of meteorological and tracer measurements with which to develop appropriate models for these interactions.

The field program has verified the basic concepts of the experimental design. The flexibility provided by the release of gaseous and visible tracers from mobile cranes allowed experiments to be run cost-effectively under various meteorological conditions. The study has also demonstrated the value of a meteorological data-handling system that collects, processes, and displays information to guide the experiments in real time.

Moreover, the CCB study has confirmed the utility and effectiveness of scaled physical modeling within the overall program. The general features of the flows visualized at CCB replicated the flows produced at the Fluid Modeling Facility, thereby verifying that to a very useful extent, the essential physics of stably stratified flows over complex terrain features can be reduced to the laboratory scale in order to examine particular flow conditions and to guide experimental design.

For example, during the design of the CCB field study, information derived from experiments in the FMF's stably stratified water tank was valuable in siting the 150 m tower outside the perturbing influences of the butte. Pictures of dye streaklines in tank experiments were the primary basis for choosing the array of sampler locations on CCB and for relocating some samplers in response to meteorological forecasts. In addition, a series of quantitative laboratory experiments provided important support for the Hunt-Snyder critical streamline height, which in turn was the basis for positioning the heights of tracer releases in response to computed Froude numbers during the field experiments.

Laboratory modeling of case hours from the CCB experiments is continuing at the FMF to aid in the interpretation of the field observations. The detailed fluid modeling study of one case hour is reported in Appendix B. This study shows the influence on hourly averaged concentrations of the use of sequential 5-minute flow data instead of hourly averaged flow data. Before any general conclusions may be deduced, however, additional data from both physical and mathematical models should be obtained for other case hours, and results of sequential simulations should be compared with hourly averaged results as well as with field data. Although laboratory fluid modeling cannot simulate the real world exactly (because of differences in scales and intensity of turbulence, differences in wind and temperature profiles, and lack of meander in the laboratory flows, as well as for other reasons), it is nonetheless a valuable adjunct to field experiments; as Holzworth (1980) states, "by allowing the controlled variation of independent variables, laboratory experiments will provide deeper insight and understanding of the fundamental physics."

The CCB field program has provided a detailed, reliable data archive with which to evaluate the accuracy of the present generation of complex terrain models as well as to develop more reliable models. The data archive includes the following:

- meteorological measurements,
- observations of the patterns of tracer concentrations on the butte,
- lidar-derived plume sections, and
- photographic evidence.

The edited data archive is unique in its detailed and reliable documentation of stable flow and dispersion near an isolated hill. Moreover, In addition to its quantitative content, this data base also has important qualitative value: many of the photographs clearly demonstrate that plumes interact with elevated terrain features in a complicated variety of ways under stable flow conditions and that the simple impingement description used in some current dispersion models may not be in accord with the behavior of plumes.

Substantial progress has also been made in developing improved dispersion models for projecting ground-level concentrations on complex terrain from elevated point sources in stably stratified flows. We have developed new statistical techniques for evaluating the performance of air quality models and have applied these techniques to current complex terrain models. Preliminary new models have been constructed that incorporate some on-site turbulence data and only the simplest sort of field observations--that is, the two distinct regimes of plumes released above or below the dividing streamline height. Even these first attempts at more physically realistic models show better performance than current models. The evaluations of the performance of these preliminary models point to the need for further development of complex terrain models of known reliability and demonstrated applicability for regulatory use.

Of course, the results of these evaluations cannot be simply applied to other sites with different scales, such as power plants near mountains, or to different sorts of terrain elements, such as bluffs, ridges, or mesas where the potential for blocking of the flow is greater and where the dividing streamline height is related to the flow characteristics in a different way. The data base of the CCB field study cannot be used to address all these problems directly--nor was the experiment intended to address them. Other field experiments must be designed and performed for these purposes, as the EPA's program has recognized.

We have only begun to exploit the data gathered at CCB, however. We anticipate that because of the good quality of the meteorological and tracer measurements, these data contain valuable information on the characteristics of the flow over the butte and on the effects of both 5-minute and 1-hour turbulence on the observed patterns of tracer gases. This information will lead to an improved understanding of transport and diffusion around the butte--which will, in turn, point the way to better models of these processes. The remainder of this report summarizes comparative performance evaluations of the several models tested (Section 6.2) and presents recommendations for further analysis of CCB data and further model development with this data base (Section 6.3).

6.2 Comparative Model Performance Evaluations

Valley, COMPLEX I, COMPLEX II, and PFM computations of 1-hour average SF_6 concentrations were compared with measured SF_6 concentrations from as many as 45 experiment case hours in the CCB data archive. Two new experimental models were also evaluated with the same data. This evaluation serves to document how well each of these models performed with the CCB data, in both an absolute and a relative sense.

The Valley model is a screening algorithm intended for estimating the highest expected 24-hour average concentration of pollutants released from large point sources in complex terrain. It is based upon a univariate Gaussian plume formula incorporating 22.5° horizontal sector averaging and postulated worst-case meteorology leading to stable impingement situations. The comparison of Valley with CCB SF_6 tracer concentrations only tests how well the model simulates 1-hour average concentration estimates at CCB, not the way the Valley model is used in regulatory practice for estimating 24-hour average concentrations by persisting the assumed worst-case meteorology for six hours.

In 39 of the 45 test case hours, the concentration maximums were overestimated by Valley, and in four of the case hours, maximum concentrations were appreciably underestimated. The mean ratio (over all 45 hours) of the Valley model estimate to the observed concentration is 5.3 and the geometric mean ratio is 3.4.

The four cases in which Valley underestimated peak observed values may be "explainable" by the scale of the CCB experiment. The Valley model and its assumed worst-case meteorological conditions are supposed to apply to real sources in complex terrain, where source heights and transport distances are generally much larger than the source-terrain geometry of the CCB experiment. But during the experiments, wind speeds at release heights were frequently less than 2.5 m/sec, and as the plume approached the impingement point, σ_z was at times significantly smaller than the 10 m plume centerline stand-off distance assumed by the model. This phenomenon is associated, of course, with the small scale of the CCB experiment. For most regulatory applications of the Valley model, σ_z is large by comparison to the 10 m stand-off distance, and therefore the model concentraton estimates usually correspond closely to maximum plume centerline values.

Unlike Valley, COMPLEX I, COMPLEX II, and PFM are sequential air quality models. These models are intended to produce 1-hour concentration estimates using on-site meteorology. COMPLEX I and COMPLEX II were tested with 45 experiment case hours, and PFM was tested with 23 of these hours in which the SF_6 tracer was released at least 5 m above the critical dividing streamline height. The 1-hour average meteorology used to drive these models was estimated for the tracer release height. No "tuning" of the model inputs was done to improve the performance of these models.

COMPLEX I was found to overestimate in the mean when peak observed concentrations were compared to peak modeled concentrations (regardless of location) and when the hourly stability class was derived from the Turner scheme. The mean of the ratios of the peak modeled to peak observed concentrations is 5.3 and the geometric mean is 2.6, both nearly the same as Valley.

COMPLEX II was also found to overestimate maximum observed concentrations when the hourly stability class was derived from the Turner scheme. The mean of the ratios of peak concentrations is 14.4, and the geometric mean is 6.3. Therefore, COMPLEX I, with the constant sector averaging to simulate crosswind diffusion, appears to do a better job of estimating the magnitude of peak hourly concentrations at CCB than COMPLEX II.

Additional evaluations of the COMPLEX models were made by fixing the stability class for all test hours. Each model was run with stability classes D, E, and F in turn. Note that both COMPLEX I and COMPLEX II include the following default values for plume path coefficients as functions of stability class. For stability class D the plume path coefficient is 0.5. For stability classes E and F, the plume path coefficients is 0.0, and full surface reflection (doubling of concentrations) is assumed. The COMPLEX I and COMPLEX II model runs were made with these default values.

Both models overestimated peak concentrations on the average but the bias toward overestimation decreased as the stability class was changed from F to D. However, the scatter in the data (as characterized by the standard deviation of the residual $\sigma(C_o-C_p)$) was not significantly affected.

These models performed better, however, on the subset of hours in which the tracer was released above the dividing streamline height of the flow. The overall bias toward overestimation was reduced, and the scatter in the data was also reduced, although it remained large. Again, COMPLEX I performed better than COMPLEX II.

PFM was compared with COMPLEX I and COMPLEX II using Turner σ_y and σ_z values for PG stability classes D and E on the same subset of hours. PFM appears to offer some improvement over COMPLEX II, particularly for stability class E (when COMPLEX II adopts the Valley model stable impingement plume path). PFM does not appear to offer improvement over COMPLEX I.

Two new experimental models were also tested and compared with COMPLEX I and COMPLEX II. The Neutral model is similar to COMPLEX II (class D). Like COMPLEX II, it uses a 0.5 plume path coefficient for neutral stability, but unlike COMPLEX II, it uses on-site turbulence intensities to calculate dispersion coefficients. The Impingement model also uses on-site turbulence data. It estimates the maximum 1-hour concentration for a plume that impinges upon the terrain and then passes around the sides of the terrain feature.

The Neutral model performs better than the other models evaluated in terms of mean bias and offers an improvement in terms of the standard deviation of residuals over all the data, but no improvement in the standard deviation of the residuals of peak concentrations.

A hybrid model that combines the Neutral model (for cases in which the tracer is released above the critical dividing streamline) and the Impingement model (for cases in which the tracer is released below) was disappointing--both the bias and standard deviation of the residuals increased over those obtained when the Neutral model alone was used for all hours.

It appears that the use of on-site turbulence data does, to some extent, improve model performance at CCB and that the use of horizontal sector averaging over 22.5° (in lieu of turbulence data) to describe effective crossplume spread over an hour is more helpful than the use of the σ_y inferred from the Turner surface stability class. For this data base, however, none of the models tested to date yielded precise estimates.

6.3 Recommendations for Further Research

Although the CCB field program has provided good visual and quantitative data on the interactions of stable plumes with an isolated hill, much remains to be done to achieve the goal of practical, easily comprehensible, and reliable dispersion models applicable to stable flows in complex terrain and transferable to other sites. This section describes the research and development we plan to perform with the data already obtained from the CCB experiments. We expect that substantial progress toward the program's goal will result from these efforts.

The key to successful modeling of observed tracer concentrations at CCB lies in relating the meteorological data to the observed behavior of the visible plume. Over the course of the field program, smoke plumes exhibited a wide range of shapes, dimensions, and trajectories as they passed near the hill.

A dominant feature of plume trajectories at CCB is the sensitivity of plume path in the horizontal to small changes in wind direction or source position. As the stability of the atmosphere increased and the mean wind speed decreased, the plume rested on one side of the hill or the other but spent very little time in between. During experiment hours in which the mean wind was directed toward the center of the hill, the plume generally swept quickly across the hill, coming to rest on alternate sides of the hill in turn. This behavior is consistent with the notion of flow beneath the critical dividing streamline.

For periods of weaker thermal stratification or greater wind speed at source height, horizontal trajectories were steadier and the plumes rose over part of CCB for significant periods during some hours. At times, in passing over the crest of the hill, plumes appeared to shrink in vertical extent, and gave at least the visual impression they were not in contact with the surface. This behavior is consistent with the notion of flow above the critical dividing streamline.

Often, however, the distinction between these two conceptual descriptions was not well defined in the visual appearance of the plumes. The appearance of the plumes varied from hour to hour and quite often varied a great deal during the course of one hour. Sometimes the plume was very wide and flat; at other times, it was a well-collimated "pencil beam"; and undulations, waves, and even spiraling pulsations were occasionally observed. For initially narrow plumes, some increase in spread upwind of the hill was often noted if the plume was transported toward the center of the hill, but no such spread was seen if the plume curved around the side. This suggests that the hill influenced at least locally the upwind flow field and turbulence levels.

The model comparison and evaluation studies described in this report underscore the importance of these qualitative plume features. Models that employed unaltered PG σ_y and σ_z values did least well because horizontal meander over time scales of 10 minutes to an hour often produced plume spread much larger than that described by the stable (class E and F) σ_y curves. Horizontal sector averaging improved model performance, but a fixed sector width is not applicable to all stable-flow plume phenomena or to all source-terrain geometries. A model that uses on-site turbulence data to estimate plume size performed better than similar models that use PG sigmas with or without sector averaging. Yet although on-site turbulence data contain information about plume spread and meander, the use of such data also introduces new sources of uncertainty into the modeled concentration estimates. Systematic errors in meteorological instrumentation, for example, produce errors in modeled σ_z estimates. It is therefore essential to correct the data for documented deficiencies in order to take fuller advantage of the data's ability to characterize observed plume behavior.

The development of mathematical models incorporating the effects of these phenomena will require further analysis of the CCB data base. This analysis will involve refinements of the data base, identification and formulation of model components for describing important transport and dispersion phenomena, testing and evaluation of new model formulations, and continued improvement and refinement of these formulations.

Refinement of the Meteorological Data

Refining the meteorological data will include adjusting wind and turbulence data to account for non-cosine response characteristics of the propeller anemometers. The knowledge and use of these kinds of adjustments is especially important for evaluating model performance.

As noted earlier, the values of mean wind derived at CCB from the propeller anemometers often disagreed with corresponding values derived from the cup-and-vane anemometers. Where the source of the discrepancy is obvious--misalignment of the instrument on the tower or a seized propeller, for example--the anemometer data can be corrected (or deleted) on the basis of the information at hand. But other sources of discrepancy arise from differences in the way the two kinds of systems respond to winds at various angles of incidence, differences in the way they react to the same levels of turbulence intensity, or for kindred reasons. In a few cases, the discrepancies in mean wind speed may be so large that winds derived from propeller systems could imply $H_{crit} > H$, whereas winds from cups could imply $H_{crit} < H$. Moreover, the discrepancies in turbulence intensities cause uncertainties in some of the σ_y and σ_z estimates used in the modeling. It will therefore be worthwhile to explore differences between propeller anemometers and cup-and-vane anemometers in more detail.

As a first step, we suggest applying corrections found in the literature for similar systems (Horst 1973; Izumi and Barad 1970) to see if they bring the two sets of speed and direction data into better correspondence. A second step could include a short series of experiments at the NCAR tower under various meteorological conditions in order to compare the Climatronics F-460 (cup-and-vane) and WC-13 (propeller) systems with a sonic anemometer system and to calculate the turbulence quantities IX, IY, and IZ from both the WC-13 and sonic data.

Identification and Testing of Model Components

Aided by observational evidence, we will continue to develop and test model components such as flow-field, turbulent diffusion, boundary-layer, and wake components. These components will individually undergo sensitivity tests, refinements, and calibrations until their theoretical formulations are as consistent as possible with the observations. The tests will serve to define acceptable ranges for parameters and to permit a structured tuning of the complete model with observed tracer concentrations. (Tuned models will be evaluated with a data set separate from that used to adjust model parameters.)

Observational evidence will be assembled from a "learning" subset of the CCB data to support additional case study analyses. The analyses done to date have been performed largely without the benefit of correlative CCB data--nephelometer, sonde, lidar, sampling mast concentrations, and photographs--that could help in quantifying plume transport and diffusion phenomena. The purpose of continuing case study analyses is to delineate these phenomena as well as possible using all available information (including cae hours of near-zero tracer concentrations), so that we can understand the evolution of the measured 1-hour tracer concentration distributions within the resolution of the 5-minute average meteorological data and the 10-minute average tracer data in the CCB data base.

The 5-minute meteorological data base is essential to our understanding of the CCB experiments. Many of the theoretical descriptions of plume behavior near terrain are linked to notions about streamline patterns. These, in turn, depend critically upon the spatial and temporal variability in wind speed and wind direction. It has been shown, for example, that the mean wind field used in the models exerts a critical influence on the inferred flow regime ($H < H_{crit}$, $H > H_{crit}$) and especially on the magnitudes and locations of the maximum concentrations. It is therefore important to seek ways to infer the time-dependent structure of the flow field from supporting short-term data.

One suggested approach to this task is to construct the streamlines at CCB implied by the 10 m and 30 m potential temperature data on the butte, taking as a working assumption that streamlines are constrained to travel along surfaces of constant potential temperature, at least during fairly steady-state periods. The streamlines thus derived could be used to determine from what elevations, in the approach flow over the plain, air parcels over the butte appear to originate. (Leeward 10 m temperatures may be contaminated by heat exchange with the butte surface, but this could be checked by comparing windward and leeward temperatures.) These implied streamlines could then be compared to estimates of one or more candidate flow models.

The short-term data will prove valuable in other ways as well. We have not begun to explore the wealth of information that could be extracted from time series of the mean wind and turbulence fields or from their autocorrelations and cross-correlations in time and space. Spectral analyses of these data may lead to a better understanding of stable boundary layer processes, to new insight into the mechanics of plume meander and turbulent growth at CCB, and to more successful algorithms for relating small-scale turbulence to large-scale flow characteristics.

Supplementary data akin to those in the 5-minute and 10-minute average data base will be obtained in simulated flows set up in EPA's towing tank. These data will help to refine, extend, and test model components. For example, to explore further the use of the CCB potential temperature data as a quantitative indication of streamline patterns, it would also be worthwhile to simulate these same flow situations in the towing tank in order to ascertain how well the laboratory model describes the flow fields inferred from the observed temperature fields. We recognize that it may be difficult or impractical to set up in the towing tank the corresponding nonuniform density gradient; however, if even an approximate correspondence in the profile of N(z) can be established, the experiments could be very instructive.

Another example of such testing of model components is the analysis of how plume deformation and plume growth effects combine during stable impingement conditions. To help distinguish these effects, we suggest performing a series of towing tank experiments to simulate case hours of strongly stable plume impingement. The purpose of these runs would be to observe and record the lateral and vertical growth of the plume as it approaches the butte in a nonturbulent flow--that is, to estimate the pattern of plume growth resulting from flow distortion only. Where possible, the plume dimensions estimated from the tank experiments could be compared with the CCB photographs and lidar results. Because the tank flows would be almost entirely nonturbulent, the (scaled) laboratory plume should be smaller than the plume observed at CCB. If initial plume dimensions can be ignored or readily accounted for, any relative differences found in the plume's crosswind or vertical spread would measure the additional plume dispersion caused by local small-scale turbulence or drainage winds.

The quantitative correspondence cannot be taken at face value because of essential differences between flows in the laboratory model experiment and the prototype flow at CCB--differences in surface boundary layer characteristics, in hill roughness, in profiles of temperature (density) and winds in the approach flow, in steadiness of the flow, and so forth. At least qualitatively, however, any significant differences in plume dimensions should suggest the relative magnitude of distortion and diffusion processes at CCB under impingement conditions.

Evaluation of Models

Models formulated and adjusted by means of the learning data set must be evaluated on a test data set. Individual case hours within this data set should be studied in the same detail as is done for the learning set, so that sufficient data are available to run the models and so that enough familiarity with the data is obtained to gauge the expected imprecision in model estimates.

Model performance will be primarily gauged by comparing estimated tracer concentrations to observed concentrations. Where possible, we will test individual model components to assess the adequacy of the components that make up the model (as well as the adequacy of the model as a whole) and to identify important deficiencies. Residuals between observed and modeled variables will be analyzed in accordance with the methods presented in Section 5. Efforts will also be made to include a broader range of statistical tests consistent with recommendations of the AMS Workshop on Dispersion Model Performance (Fox 1981).

Improvement and Refinement of Model Formulations

Model formulation and testing is viewed as an iterative process. First attempts, such as those described in Section 4, are made to investigate the scope of the problem and to set a model performance mark to be exceeded by more refined approaches. It is our intent to develop and evaluate a number of models over the course of this project and to assemble a hierarchy of modeling techniques, accuracies, and data needs.

The data needs are especially critical. For practical use in various regulatory applications, complex terrain models will not always have available as much research-grade meteorological data as that gathered at CCB. The range of turbulence measurements available at CCB--for example, the 5-minute average and 1-hour average winds and turbulence intensities at 16 locations from the propeller anemometers--might represent a monitoring program for a critical siting study planned well in advance of the model application. However, the CCB data base may yield useful information for estimating turbulence statistics (such as σ_v or σ_w) or other important features that govern flow (such as N(z)) entirely from surface and low-level measurements. If such empirical formulae are found and understood within a sound theoretical framework, perhaps they can be generalized for testing in full-scale plume-terrain geometries under different meteorological conditions. It is therefore suggested that such relationships in the CCB data base be explored and their possible utility evaluated for routine operational use in improved complex terrain models.

As an example of areas in which a hierarchy of modeling approaches may be studied, consider two major elements of the transport and dispersion process, plume transport or flow and plume diffusion or spread. Several models evaluated in Section 5 use simple empirical terrain adjustments to the plume height above the ground to simulate flow distortion and use the standard PG coefficient for plume spread. One of the new models also uses a simple terrain adjustment but uses on-site turbulence data instead of the PG sigmas to estimate plume spread. The new model therefore represents a step in the hierarchy toward more refined models that require additional on-site data.

A hierarchy of approaches to the flow and diffusion components of a complex terrain air quality dispersion model is suggested below. We do not want to imply, however, that the full hierarchy would have to be pursued to develop an adequate complex terrain model.

- Flow Module Component

1) Empirical terrain adjustment: An empirical terrain correction factor is incorporated into a straight-line Gaussian air quality model. (The "half-height" correction is an example.)
2) Simple potential flow: The flow is assumed to be inviscid and stratification is ignored. Potential flow theory is used to calculate the flow around a terrain feature.
3) Stratification adjustment to potential flow: An empirical adjustment is made to potential flow to ensure that streamline deflections become more horizontal with increasing stratification. For small stratification, the adjustment factor becomes inoperative.
4) Linearized inviscid flow: The flow is assumed to be inviscid, but density stratification is included. The resulting momentum equation may be solved if it is assumed that the hill is so small that the boundary condition for vertical velocity may be applied at the surface of the plain ($z = 0$) rather than at the hill's surface ($z = z(x,y)$). In principle, this approximation allows the flow field to be computed for arbitrary hill shapes.
5) Numerical solutions: In this approach, the momentum equation is solved by numerical methods. Turbulence is modeled with any one of the several approximations available.

- Dispersion Module Component

1) Sigma curves: Here, the plume spread is estimated with stability classification schemes. It is also assumed that the hill does not affect turbulence.

2) Turbulence data: Again, turbulence is assumed to be unaffected by the hill; however, the sigmas are estimated from measurements of turbulence intensity.

3) Terrain-modified sigmas: Turbulence intensities over the hill are modified by empirical factors based on simple theories (such as rapid distortion theory) or from turbulence data from the tower on the butte.

4) Turbulence models: Here, the evolution of turbulence is estimated from models of turbulence. An example of this would be the k-ε model suggested by Launder and Spalding (1972).

REFERENCES

Bass, A. 1980. Towing Tank Studies in Support of Field Experiments at Cinder Cone Butte, Idaho. Phase II: Plume Behavior with Froude Number and Incident Wind Direction. Environmental Research and Technology, Inc., Concord, MA.

Bass, A., D.G. Strimaitis, and B.A. Egan 1981. Potential Flow Model for Gaussian Plume Interaction with Simple Terrain Features. EPA-600/54-81-008. U.S. Environmental Protection Agency, Research Triangle Park, NC.

Box, G.E.P., W.G. Hunter, and J.S. Hunter 1978. *Statistics for Experimenters: An Introduction to Design, Data Analysis, and Model Building.* New York: John Wiley & Sons.

Budney, L.J. 1977. *Guidelines for Air Quality Maintenance Planning and Analysis*. Volume 10 (revised): *Procedures for Evaluating Air Quality Impact of New Stationary Sources*. EPA-450/4-77-001 (OAQPS No. 1.2-029R). U.S. Environmental Protection Agency, Research Triangle Park, NC.

Burt, E.W. 1977. *Valley Model User's Guide*. EPA-450/2-77-018. U.S. Environmental Protection Agency, Research Triangle Park, NC.

Csanady, G.T. 1973. *Turbulent Diffusion in the Environment*. D. Reidel, Dordrecht-Holland.

Drazin, P.G. 1961.. On the Steady Flow of a Fluid of Variable Density Past an Obstacle. *Tellus* *13*: 239-251.

Egan, B.A. 1975. Turbulent Diffusion in Complex Terrain. *Lectures on Air Pollution and Environmental Impact Analyses*. American Meteorological Society, Boston, MA.

Fox, D.G. 1981. Judging Air Quality Model Performance. A Summary of the AMS Workshop on Dispersion Model Performance, Woods Hole, MA, September 1980. *AMS Bulletin* *62*: 599-609.

Holzworth, G.C. 1980. *The EPA Program for Dispersion Model Development for Sources in Complex Terrain*. Second Joint Conference on Applications of Air Pollution Meteorology, New Orleans, LA. American Meteorological Society, Boston, MA.

Horst, T.W. 1973. Corrections for Response Errors in a Three-Component Propeller Anemometer. J. Appl. Meteorol. 12: 716-725.

Hovind, E.L., M.W. Edelstein, and V.C. Sutherland 1979. Workshop on Atmospheric Dispersion Models in Complex Terrain. EPA-600/9-79-041. U.S. Environmental Protection Agency, Research Triangle Park, NC.

Hunt, J.C.R. and R.J. Mulhearn 1973. Turbulent Dispersion from Sources near Two-Dimensional Obstacles. J. Fluid Mech. 61: 245-274.

Hunt, J.C.R. and J.S. Puttock, and W.H. Snyder 1979. Turbulent Diffusion from a Point Source in Stratified and Neutral Flows around a Three-Dimensional Hill (Part I - Diffusion Equation Analysis). Atmos. Environ. 13: 1227-1239.

Hunt, J.C.R. and W.H. Snyder 1978. Flow Structure and Turbulent Diffusion around a Three-Dimensional Hill. (Part II - Surface Concentrations Due to Upstream Sources - unpublished manuscript).

Hunt, J.C.R. and W.H. Snyder 1980. Experiments on Stably and Neutrally Stratified Flow over a Model Three-Dimensional Hill. J. Fluid Mech. 96: 671-704.

Isaacs, R.G., A. Bass, and B.A. Egan 1979. Application of Potential Flow Theory to a Gaussian Point Source Diffusion Model in Complex Terrain. Fourth Symposium on Turbulence, Diffusion, and Air Pollution, Reno, NV. American Meteorological Society, Boston, MA.

Izumi, Y., Barad, M.L. 1970. Wind Speeds as Measured by Cup and Sonic Anemometers and Influenced by Tower Structure. J. Appl. Meteorol. 9:851-6.

Launder, B.E. and D.B. Spaulding 1972. Lectures in Mathematical Models of Turbulence. New York: Academic Press.

Maggs, R.J., P.L. Joynes, A.J. Davies, and J.E. Lovelock 1971. The Electron-Capture Detector - A New Mode of Operation. Anal. Chem. 43: 1966-1971.

Milne-Thompson, L.M. 1968. Theoretical Hydrodynamics. New York: The MacMillan Company.

Papoulis, A. 1965. Probability, Random Variables, and Stochastic Processes. New York: McGraw Hill Book Company

Snyder, W.H. 1980a. Towing Tank Studies in Support of Field Experiments at Cinder Cone Butte, Idaho. Phase III: Verification of Formula for Prediction of Dividing Streamline Height. U.S. Environmental Protection Agency, Research Triangle Park, NC.

Snyder, W.H. 1980b. Towing Tank Studies in Support of Field Experiments at Cinder Cone Butte, Idaho. Phase I: Influence of Hill on Wind Field at the Meteorological Tower Site. U.S. Environmental Protection Agency, Research Triangle Park, NC.

Strimaitis, D.G., J.S. Scire, and A. Bass 1981. COMPLEX/PFM. Air Quality Model User's Guide. Final Draft Report, EPA Contract No. 68-02-2759. Environmental Research & Technology, Inc., Concord, MA.

Van Ulden, A.P. 1978. Simple Estimates for Vertical Diffusion From Sources near the Ground. Atmos. Environ. 12: 2125-2129.

Yanskey, G.R., E.H. Markee, Jr., and A.P. Richter 1966. Climatography of the National Reactor Testing Station. Report IDO-12048. U.S. Atomic Energy Commission.

APPENDIX A

SUMMARY OF TRACER DATA ANALYZED FOR TESTS 201-218

TABLE A-1. CASE 201 (10/16/80 - 1700-2500)

Hour	No. 1-Hour Ave Samples SF$_6$	No. 1-Hour Ave Samples CF$_3$Br	No. 10-Min Ave Samples SF$_6$	No. 10-Min Ave Samples CF$_3$Br	Total
1	11		70		81
2	11		82		93
3	3		39		42
4	13		54		57
5	8		31		49
6	11		14		25
7	10		2		12
8	6		0		6
TOTAL	73		292		365

TABLE A-2. CASE 202 (10/17/80 - 1700-2500)

Hour	No. 1-Hour Ave Samples SF$_6$	No. 1-Hour Ave Samples CF$_3$Br	No. 10-Min Ave Samples SF$_6$	No. 10-Min Ave Samples CF$_3$Br	Total
1	14		113		127
2	19		136		155
3	24		56		80
4	23		46		69
5	23		21		44
6	22		23		45
7	24		9		33
8	20		0		20
TOTAL	169		404		573

TABLE A-3. CASE 203 (10/20/80 - 0000-0800)

Hour	No. 1-Hour Ave Samples		No. 10-Min Ave Samples		Total
	SF_6	CF_3Br	SF_6	CF_3Br	
1	1		57		58
2	21		67		88
3	20		49		69
4	2		29		31
5	9		55		64
6	7		64		71
7	3		49		52
8	16		70		86
TOTAL	79		440		519

TABLE A-4. CASE 204 (10/21/80 - 0000-0800)

Hour	No. 1-Hour Ave Samples		No. 10-Min Ave Samples		Total
	SF_6	CF_3Br	SF_6	CF_3Br	
1	32		53		85
2	33		66		99
3	12		47		59
4	26		61		87
5	29		51		80
6	28		72		100
7	32		74		106
8	30		83		113
TOTAL	222		507		729

TABLE A-5. CASE 205 (10/23/80 - 0000-0800)

Hour	No. 1-Hour Ave Samples		No. 10-Min Ave Samples		Total
	SF_6	CF_3Br	SF_6	CF_3Br	
1	20		6		26
2	12		11		23
3	29		41		70
4	31		78		109
5	33		69		102
6	35		70		105
7	33		69		102
8	32		78		110
TOTAL	225		422		647

TABLE A-6. CASE 206 (10/24/80 - 0000-0800)

Hour	No. 1-Hour Ave Samples		No. 10-Min Ave Samples		Total
	SF_6	CF_3Br	SF_6	CF_3Br	
1	1		11		12
2	33		78		111
3	34		62		96
4	34		58		92
5	30		58		88
6	29		57		86
7	31		62		93
8	36		60		96
TOTAL	228		446		674

TABLE A-7. CASE 207 (10/25/80 - 0000-0800)

Hour	No. 1-Hour Ave Samples		No. 10-Min Ave Samples		Total
	SF_6	CF_3Br	SF_6	CF_3Br	
1	2		5		7
2	31		65		96
3	30		55		85
4	25		75		100
5	2		63		65
6	3		66		69
7	30		72		102
8	27		68		95
TOTAL	150		469		619

TABLE A-8. CASE 208 (10/27/80 - 1700-2500)

Hour	No. 1-Hour Ave Samples		No. 10-Min Ave Samples		Total
	SF_6	CF_3Br	SF_6	CF_3Br	
1	15	2	63	6	86
2	15	2	72	14	103
3	28	11	69	16	124
4	33	15	73	21	142
5	4	1	38	15	58
6	35	17	60	28	140
7	3	0	19	14	36
8	40	16	67	29	152
TOTAL	173	64	461	143	841

TABLE A-9. CASE 209 (10/28/80 - 1700-2500)

Hour	No. 1-Hour Ave Samples SF_6	No. 1-Hour Ave Samples CF_3Br	No. 10-Min Ave Samples SF_6	No. 10-Min Ave Samples CF_3Br	Total
1	46		78		124
2	49		65		114
3	48		78		126
4	1		2		3
5	3		5		8
6	3		6		9
7	48		65		113
8	42		69		111
TOTAL	240		368		608

TABLE A-10. CASE 210 (10/30/80 - 0000-0800)

Hour	No. 1-Hour Ave Samples SF_6	No. 1-Hour Ave Samples CF_3Br	No. 10-Min Ave Samples SF_6	No. 10-Min Ave Samples CF_3Br	Total
1	39	9	73	11	132
2	31	15	83	17	146
3	42	22	60	15	139
4	35	15	74	13	137
5	3	1	23	0	27
6	43	22	84	15	164
7	43	19	65	16	143
8	15	6	9	2	32
TOTAL	251	109	471	89	920

TABLE A-11. CASE 211 (10/31/80 - 0000-0800)

Hour	No. 1-Hour Ave Samples		No. 10-Min Ave Samples		Total
	SF_6	CF_3Br	SF_6	CF_3Br	
1	40	20	90	26	176
2	35	18	70	13	136
3	31	17	63	4	115
4	36	19	76	11	142
5	42	21	82	5	150
6	34	16	78	4	132
7	34	20	72	8	134
8	39	18	65	10	132
TOTAL	291	149	596	81	1,117

TABLE A-12. CASE 212 (11/2/80 - 1700-2500)

Hour	No. 1-Hour Ave Samples		No. 10-Min Ave Samples		Total
	SF_6	CF_3Br	SF_6	CF_3Br	
1	11		37		48
2	10		34		44
3	17		25		42
4	1		0		1
5	8		3		11
6	18		42		60
7	20		53		73
8	1		8		9
TOTAL	86		202		288

TABLE A-13. CASE 213 (11/4/80 - 0000-0800)

Hour	No. 1-Hour Ave Samples		No. 10-Min Ave Samples		Total
	SF_6	CF_3Br	SF_6	CF_3Br	
1	3	1	4	0	8
2	3	1	2	0	6
3	4	2	0	0	6
4	29	10	41	27	107
5	43	13	84	28	168
6	47	12	75	9	143
7	42	10	82	15	149
8	45	13	64	14	136
TOTAL	216	62	352	93	723

TABLE A-14. CASE 214 (11/5/80 - 0200-1000)

Hour	No. 1-Hour Ave Samples		No. 10-Min Ave Samples		Total
	SF_6	CF_3Br	SF_6	CF_3Br	
1	0	0	0	0	0
2	26	8	81	32	147
3	38	11	80	35	164
4	36	9	65	36	146
5	42	3	75	24	144
6	7	1	0	0	8
7	41	15	89	33	178
8	43	14	88	34	179
TOTAL	233	61	478	194	966

TABLE A-15. CASE 215 (11/6/80 - 0000-0800)

	No. 1-Hour Ave Samples		No. 10-Min Ave Samples		
Hour	SF_6	CF_3Br	SF_6	CF_3Br	Total
1	45	9	83	75	212
2	47	11	94	56	208
3	43	11	96	53	203
4	50	2	103	0	155
5	46	16	97	80	239
6	46	15	94	77	232
7	1	0	0	0	1
8	0	0	0	0	0
TOTAL	278	64	567	341	1,250

TABLE A-16. CASE 216 (11/9/80 - 0000-0800)

	No. 1-Hour Ave Samples		No. 10-Min Ave Samples		
Hour	SF_6	CF_3Br	SF_6	CF_3Br	Total
1	52	15	94	16	177
2	47	14	97	14	172
3	54	14	89	30	187
4	48	11	92	28	179
5	57	15	103	34	209
6	51	13	107	26	197
7	53	14	105	19	191
8	6	2	0	0	14
TOTAL	368	98	693	167	1,326

TABLE A-17. CASE 217 (11/10/80 - 0200-1000)

Hour	No. 1-Hour Ave Samples		No. 10-Min Ave Samples		Total
	SF_6	CF_3Br	SF_6	CF_3Br	
1	50	8	96	0	154
2	50	10	95	0	155
3	52	8	89	5	154
4	1	0	5	0	6
5	48	15	97	15	175
6	45	15	97	24	181
7	49	21	102	26	198
8	44	18	83	18	163
TOTAL	339	95	664	88	1,186

TABLE A-18. CASE 218 (11/12/80 - 0200-1000)

Hour	No. 1-Hour Ave Samples		No. 10-Min Ave Samples		Total
	SF_6	CF_3Br	SF_6	CF_3Br	
1	50	6	65	10	131
2	45	12	95	21	173
3	44	7	92	30	173
4	50	8	105	31	194
5	49	13	103	32	197
6	44	7	95	26	172
7	51	9	87	9	156
8	49	12	71	10	142
TOTAL	382	74	713	169	1,338

APPENDIX B

LABORATORY SIMULATION OF STABLE PLUME DISPERSION OVER CINDER CONE BUTTE

LABORATORY SIMULATION OF STABLE PLUME DISPERSION OVER CINDER CONE BUTTE

Comparison with Field Data

by

William H. Snyder*

and

Robert E. Lawson, Jr.*

Meteorology and Assessment Division
Environmental Sciences Research Laboratory
U.S. Environmental Protection Agency
Research Triangle Park, NC 27711

May 1981

---

*On assignment from National Oceanic and Atmospheric Administration, U.S. Department of Commerce.

INTRODUCTION

The purpose of this series of experiments was to duplicate, in the laboratory, the field experiments performed by Environmental Research and Technology, Inc. (ERT) at Cinder Cone Butte, Idaho. In particular, one hour (0500-0600) of case 206 was modeled. As case 206 was representative of very stable atmospheric conditions, the Fluid Modeling Facility towing tank was selected as the proper facility for these experiments. Measurements made during the towing tank experiments included ground level concentration, vertical distributions of concentration at selected points, plume dispersion in the absence of the hill, and visual observations of plume characteristics and trajectories. In the following pages, the conduct of this study is described (not necessarily in chronological order) along with some observations in regard to the correlation of field and laboratory data.

SUMMARY OF FIELD OBSERVATIONS

Meteorological Data

The field meteorological data has been summarized in a separate data report (Cinder Cone Butte Meteorological Data, Lawson, March 1981), but there are several points of interest which require further explanation. A considerable portion of the meteorological data was missing due to failure of the instruments or data collection system. At the 40 m-level (which is the level nearest the source height), only the westerly component of wind speed was available. This was overcome to some extent by assuming a wind direction of 122°. The southerly wind component and hence the mean wind speed were then calculated. Since no information was available to indicate the distribution of wind direction at this level, the frequency distribution of wind directions at the source height was assumed to be the same as that at the 80 m-level. Where temperature data was missing, it was possible in some cases to interpolate between data for the previous time period and data for the following time period in order to obtain a reasonable estimate for the missing data point. The values of H_c reported by ERT and summarized in the above mentioned report were revised using the estimated wind speeds at the 40 m-level and some interpolated temperatures. This resulted in an increase in the average value of H_c from about 34 m to about 41 m. Figures 1 and 2 show the mean wind speed and temperature profiles for the one hour period. Table 1 provides a listing of the newly computed values of H_c for each 5-minute period within the hour. Figure 3 shows the variation of wind direction at the 80 m-level during the hour. Note the slight shift in wind direction during the hour. The mean wind direction (derived from the mean westerly and southerly wind speeds) is 122.3°. In Figure 4, an admittedly crude attempt was made to determine the frequency distribution of wind direction. As noted, this distribution is for the 80 m-level. Although the number of data points used to form this distribution was small, the bimodality of the distribution is apparent, with the main peak occurring around 121° and a secondary one near 125.5°. Similar plots were produced for H_c as shown in Figures 5 and 6. There appears to be no systematic trend in H_c and the distribution shows a single peak around 41 m.

No analysis of the remaining meteorological tower data was attempted as most of the data was reported as missing. The lower-level winds, as indicated by the instruments at the 2 and 10 m elevations, appeared to be decoupled from the upper level winds.

Concentration Data

Field concentration data for case 206 were acquired using sulfur hexafluoride (SF_6) as a tracer source, the concentrations being reported in parts per trillion. The SF_6 was released at a rate of 0.063 grams/second from a height of 35 m. The source was reportedly located at 122°/597 m from the hill center but examination of photographs of the source and maps of the road on which the source was known to be located indicated a more likely position to be 124.6°/597 m. This alteration of the source coordinates was supported by ERT.

As both the source height and meteorological tower data were referenced to local ground level, these heights were adjusted to reference all measurements to the base of the hill. Careful examination of the topographic maps showed the met tower to be located at an elevation of 941 m (3087 ft), while the source was located at an elevation of 939 m (3081 ft). The met tower was thus 3.9 m and the source 5.8 m lower than the base of the hill. This then means that the source height relative to the base of the hill was 29.2 m, and all H_c values calculated from met tower data should be reduced by 3.9 m in order to maintain comparability relative to the hill. Although the source height used in the model is shown as 31 m, the 1.8 m difference was deemed insignificant in relation to the errors in estimating elevations from the topographic maps.

Figure 7 shows the one-hour average concentration distribution over the hill. The wind direction indicated on this plot is from 122°. The distribution is seen to favor the northeast side of the hill with the axis of the distribution on a southeast-northwest line. The maximum concentration is located in the east draw near the 30 m elevation contour. There is a rather tight concentration gradient along the southwest side of the distribution with the tightest gradient being directly between the two peaks.

Although not plotted, there were several 10-minute average concentration samples available. These samples were used to form one-hour averages for comparison with the data plotted in Figure 7. The resulting one-hour averages were in good agreement with data from the one-hour average samplers.

Sampler location 60X (FMF sample port 34) showed an anomalously low value (15 ppt) and is believed to be in error.

Slides

Several 35 mm slides of the case 206 field experiments were available for analysis. While it was not possible to obtain quantitative data from these slides, several qualitative observations were made. The plume was initially observed to split with a portion traveling around the north side of the hill and the remainder traveling through the draw and over the hill. Approximately half-way through the hour the plume trajectory was directly through the draw. There was some evidence that the plume was being downwashed on the upwind side of the hill. The slides indicate that the area of peak surface concentration may have been at a somewhat greater elevation (~ 50 m contour) than indicated by the concentration data. The fact that the plume was initially observed to split around the north butte and later traveled directly through the draw is in apparent contradiction to the reported 80 m wind directions. It should be noted that the travel time from the source to the hill was on the order of 6 minutes and this must be taken into account when comparing observations with met data.

The slides were also used to visually confirm the location and release height of the source.

EXPERIMENTAL DETAILS

Model Specifications

The model was constructed of acrylic plastic by a vacuum forming technique. The nominal model scale was 1:640; after fabrication, the model scale was determined to be 1:647 horizontal and 1:694 vertical (model height = 14.4 cm). The model was mounted on a circular platform (1.7 m dia.) which was inserted into a circular, recessed cutout in a 2.5 m square baseplate to allow for rotation to various wind directions. The baseplate provided an upstream fetch of about 0.7 m and a downstream fetch of about 0.2 m; its width was 3 cm less than the width of the towing tank (2.5 m). Both baseplate and model were covered with small gravel (average diameter on the order of 2 mm) in order to simulate surface roughness. The gravel size was chosen by application of Jensen's criterion (Snyder, 1981),

$$\frac{z_{om}}{z_{op}} = \frac{L_m}{L_p} .$$

With a prototype $z_{op} \sim 5\text{-}8$ cm, then $z_{om} \sim 0.07\text{-}0.12$ mm, and since $z_0 \sim \varepsilon/30$, where ε is the grain size, $\varepsilon \sim 2\text{-}3$ mm. To be aerodynamically rough, $U_\star z_0/\nu \geq 2.5$. Assuming $U_\star/U_\infty \sim 0.045$, and a tow speed of 10 cm/sec, the value of $U_\star z_0/\nu$ is on the order of 0.5. In spite of this small value of roughness Reynolds number, the boundary layer on the baseplate approaching the hill was visually observed to be turbulent, albeit quite thin ($\sim$ 2 cm). Under the strongly stratified flows, the surface flow on the hill itself was not observed to be turbulent.

Sample ports were located on the model at the same locations as in the field study although port identification numbers were altered for more efficient data processing. The ports projected approximately 2 mm above the surface roughness, except for the mast mounted samplers, which were scaled in height in proportion to their field counterparts. The ports were fabricated from 0.24 cm O.D. brass tubing with equal lengths of vinyl tubing leading from the ports to the sampling system.

The source was simulated with a 0.32 cm I.D. brass tube with the upper portion bent over such that the tracer dye was released parallel to the approach flow.

The tracer dye was a mixture of concentrated blue food dye (Warner Jenkinson No. 393), towing-tank water drawn through the stack, and small amounts of either saturated salt water or alcohol. The diluent (salt water or alcohol and towing-tank water) was mixed in such proportions that the final mixture - 1 part concentrated dye with 10 parts diluent - was neutrally buoyant. The emission rate of tracer dye was nominally 190 cc/min, the exact rate being determined each tow.

0, 30, 60, and 90 m contour lines were added to the model to aid in visualization and photography. Index marks were placed around the periphery to aid in aligning both source and model in relation to the desired wind direction.

Stratification of Towing Tank

The water channel was stratified using layers of salt water as described by Hunt, et al (1978). Linear stratification was used to simulate the potential temperature profile derived from Figure 2. The sharp gradient near the surface was ignored as it translates to a layer of only 1.4 cm depth and cannot, for practical reasons, be maintained in the water channel. This appears justified because, as mentioned earlier, the surface winds in the field were decoupled from the higher level winds.

As successive experiments lead to erosion of the density profile near the surface, it was necessary after each two to three tows to siphon 3 to 6 centimeters of water from the surface layer and to add the same volume of saturated salt water to the bottom. This had the effect of restoring the original linear profile to the surface.

The dye tracer used as the effluent also discolored the water after two to three tows; hence, in conjunction with the siphoning process, the water was chlorinated to bleach out the residual dye. The chlorine treatment was followed by dechlorination with sodium thiosulfate to insure that tracer samples were not also bleached out.

The density profile and water quality were checked each day prior to initiating a series of tows. A typical density profile is shown as Figure 8.

Photography

Photographic records of each test were made using 35 mm cameras. One camera was used to photograph a plan view of the model while a second was used to record a side view. In addition to these still photos, 16 mm movies were made of each tow. A polaroid-back Graflex camera was used to provide black-and-white photos for immediate evaluation and comparison. A list of available photographic records is seen in Table 2.

Colorimetric Technique for Concentration Measurements

The technique used for measuring concentrations is conceptually very simple. Samples were withdrawn through the sample ports via a vacuum system which deposited each port sample in a separate test tube. The contents of each tube were then analyzed for concentration using a Brinkman PC-600 colorimeter. The PC-600 utilizes a fiber-optic probe with fixed path length which is simply dipped into the contents of each tube. The output of the instrument is a voltage which is related to the opacity of the solution being tested. This voltage is sampled by computer and converted to concentration in percent dye. The conversion from voltage to concentration utilizes a calibration curve formed by recording the output voltage vs. concentration for 12 "standards" which consist of accurately known dilutions of the same dye used for the tracer source. A "Beer's Law" type of curve is then best-fit to the standards for use in converting the voltage from the unknown sample into a dye concentration. Although the instrument required some care in use, frequent checks of the calibration showed excellent repeatability. A typical calibration curve is shown in Figure 9.

Procedure Followed

The sequence of events leading to a daily series of tows was as follows:

1. Measure density profile.
2. If density profile is not linear, then siphon from surface to restore the profile and add an equal volume of brine at the bottom of the channel to restore the original depth.
3. Withdraw a sufficient quantity of water through the stack to mix the dye tracer. Mix the dye, diluent water, and alcohol such that the effluent specific gravity is the same as that at the source height.
4. Use program IMPINGE to determine, from the density profile, the tow speed appropriate to the desired H_c.
5. Place one drop of sodium thiosulfate solution in each sample test tube to insure that any residual chlorine does not affect the sample concentration.
6. Check and/or adjust the source flow rate and the sample flow rate. Check vacuum seals on sampling device.
7. Check that all cameras and lights are ready - also check alignment of stack vs. wind direction.
8. Set desired tow speed on carriage controller and check timer used to monitor actual tow speed.
9. Initiate tow, monitoring source flow rate and sample time during the tow - sampling is initiated only after the starting transient has decayed and conditions are stabilized.
10. After the tow, record all pertinent data immediately, then remove the sample test tubes and proceed with analysis of samples.
11. At the end of each day's experiments, or more frequently if necessary, chlorinate the water to remove the residual dye - this must be followed by dechlorination and a check of the density profile.

A total of 41 tows was made. A summary list showing all tests conducted is provided in Table 3 along with remarks on visual observations made after each tow.

Observations of Erratic Behavior of the Plume

The only erratic behavior observed during the entire series of tests was a tendency for the plume to be deflected slightly toward the north side of the hill during the last 1/3 of the tow. This was not observed during the tests with the flat baseplate, rather some slight horizontal meandering of the plume was observed. No tests were conducted to investigate this phenomenon as it did not appear to be significantly affecting the concentration measurements.

Flat Baseplate Measurements

The last nine tows were conducted with the model hill removed and a flat disk inserted in its place. The disk was coated with gravel of the same size as that on the model and was equipped with a cross-rake of sampling ports. The rake was mounted at three locations during the experiments, corresponding to model distances of 48.5, 91.4, and 134.2 cm and full-scale distances of 314, 591, and 868 m downwind from the source. Samples were drawn from the cross-rake using the vacuum sampling system and similarly analyzed for dye concentration. The resulting measurements provided an indication of concentration in the absence of the hill and estimates of the vertical and horizontal spread of the plume.

Conversion of Model Concentrations to Field Concentrations

Model concentrations were recorded in percent of dye by volume, these values then being converted to nondimensional form by the following equation:

$$\chi = \frac{CUH^2}{Q} ,$$

where χ is the nondimensional concentration, U is the tow speed, H is the hill height, and Q is the effluent flow rate. These nondimensional concentration values were then used to convert the model concentrations to their field equivalents as follows:

$$\chi_{model} = \chi_{field} ,$$

so $$\chi_m = \chi_f = \frac{C_f U_f H_f^2}{Q_f},$$

and $$C_f = \frac{\chi_m Q_f}{U_f H_f^2}.$$

Field concentrations were reported in parts-per-trillion (ppt) of SF_6 which has a density of 6.5 grams/liter at 20°C and 760 mm Hg. The height of the hill, H_f, was 100 m, and the wind speed at the source height was 1.3 m/s. Making the substitutions,

$$C(\text{ppt}) = \frac{(.063\ \text{gm/s})(1\ \text{m}^3/10^3\ell)(10^{12}\ \text{ppt})\chi}{(6.5\ \text{gm}/\ell)(1.3\ \text{m/s})(100\ \text{m})^2}$$

$$= 746\ \chi.$$

Thus, conversion of nondimensional model concentrations to equivalent field concentrations in ppt is simply a matter of multiplying by 746. Note that the conversion factor is inversely proportional to wind speed and, since the wind speed data near the source height was missing, this value was estimated from the wind profile as was previously discussed.

PRESENTATION AND DISCUSSION OF RESULTS

Dispersion in the Absence of the Hill

Nine tows were made to characterize plume dispersion in the absence of the hill. During each tow, lateral and vertical concentration profiles were measured in one cross-section (one downwind distance). Tests were conducted at three towing speeds, corresponding to H_c values of 24, 44 and 60 m, and lateral and vertical concentration profiles were measured at downwind distances corresponding to 314, 591, and 868 m. Typical profiles are shown in Figures 10 and 11. These results (as well as the remainder of data to be presented) are displayed in terms of full scale equivalents. "Best-fit" Gaussian profiles are also displayed; it may be observed that the concentration distributions are very close to Gaussian in shape.

Standard deviations of horizontal and vertical plume widths are shown in Figure 12. As the average effluent flow speed was 40 cm/s, the effluent was emitted as a turbulent jet; the jet was visually observed to expand rapidly initially both in the vertical and horizontal directions. Horizontal growth continued at a slower rate, but vertical growth approached zero, with a hint of plume collapse (negative growth) further downwind. These qualitative observations are substantiated by the growth curves displayed in Figure 12. Neither horizontal nor vertical plume widths appear to be strongly affected by the towing speed.

Figure 13 shows the variation of plume centerline concentration versus downwind distance. Table 4 summarizes the plume statistics in the absence of the hill.

Let us address the correspondence between these laboratory measurements in the absence of the hill and the field plume behavior. The field plume was generated by a thermal fogger suspended from a crane. Because of the rapid mixing of the jet in the wake of the fogger, and because the fogger was free to rotate about a vertical axis, ERT (Strimaitis, 1981) has estimated virtual plume widths of $\sigma_{zo} \sim 2$ m and $\sigma_{yo} = 3$ m. When the field plume was observed "missing" the hill under strongly stable conditions, it was frequently described as looking like a "piece of yarn", i.e., a long, reasonably straight plume with slightly ruffled edges and near-zero growth. Hence, for short time periods ($\sim$ 5 min), the plume dimensions may be very roughly estimated as $\sigma_z = 5$ m and $\sigma_y = 15$ m. The laboratory values shown in Table 4 and Figure 12 are comparable to these estimated, short-term field values.

On the other hand, plume meander, as was immediately apparent in the field, was obviously lacking in the laboratory simulations. Also lacking were the low frequency fluctuations in wind speed (or H_c). Since adequate field measurements of plume dimensions and concentrations as functions of averaging time were unavailable at this time, it was not possible to draw firmer conclusions concerning the relationship between laboratory and field measurements of plume behavior in the absence of the hill. However, some elementary attempts at simulating the fluctuating wind speed and direction in the presence of the hill were made (see next section).

Concentration Patterns on the Butte

A total of 32 tows with the model of Cinder Cone Butte in place was made, representing different source locations (by mistake), wind directions and wind speeds. A summary of all tows is given in Table 3. A map of port numbers is provided in Figure 14 for later reference and a cross-reference list to ERT sampler locations is given in Table 5. In Figure 14, the precise port location is the lower left corner of the dot matrix from which the number is configured.

The first 9 tows were preliminary in nature; only the highlights will be described here.

Figure 15 shows top and side views of the plume diffusing over the hill during Tow 8. The source height H_s was 31 m, the dividing streamline height H_c was 38 m, and the wind direction was 122°. Under these conditions, the flow was observed to be limited in vertical travel such that the plume passed around and between the two peaks, but did not surmount them.

Tows 1 and 2 were done approximately 2 hours apart under ostensibly identical conditions for the purpose of testing repeatability. The two concentration distributions may be compared by examination of Figure 16. The one-digit numbers on these maps are relative concentrations (same scaling factor on both maps). The decimal points associated with the numbers are located at the sampler locations. Care should be exercised in reading the maps, i.e., if the number is to the left of the decimal point, the relative concentration is a whole number; if to the right, a fractional number. (These numbers are truncated, not rounded.) Also, 100 samples were collected during each tow. If no number appears at a port location, it is because a visual inspection of the contents of the sample collection test tube revealed no dye, and the sample was not analyzed. If the sample was analyzed and the relative concentration was found to be less than 0.1, then a 0 appears on the map (sampler location is at the bottom center of the zero).

Figure 17 compares the concentrations from the two tows on a scatter diagram. Except for one obvious outlier (which is unexplained at this point), concentrations generally match to within 10 to 20% of each other without any obvious bias over the range from 0.02 C_{mx} to C_{mx}, and is considered excellent repeatability. The obvious departures at the very low concentrations is most likely due to slight secondary flows in the towing tank.

Tows 7 and 8 were also done for the purpose of testing repeatability, but in this case, two high speed tows and a twenty-four hour delay occurred between the two; the density profile was not restored by skimming as was usual, so that the two profiles differed somewhat, as shown in Figure 18. Note that the towing speeds differed between the two tows (see Table 3) such that H_c was the same, according to Hunt's formula (Snyder, 1980):

$$\tfrac{1}{2}\,\rho U^2 = g \int_{H_c}^{h} (h-z)\left(-\frac{d\rho}{dz}\right) dz \ .$$

The scatter diagram for tows 7 and 8 is shown in Figure 19, where it may be observed that the scatter is very much larger than in the previous comparison. Variations between the two tows do not appear to have significant bias, but are typically factors of 3 to 5 apart. The conclusion that may be drawn from this test, then, is that the precise shape of the density profile is quite important in determining the concentration distribution, i.e., a gross characterization of the stability (such as by specifying H_c alone) is clearly not sufficient.

Figure 20 shows a 3 x 6 matrix of concentration distributions, covering all combinations of three wind directions (117°, 122°, and 127°) and six values of H_c (24, 31, 38, 44, 49 and 60 m). Concentration isopleths have been drawn by eye so that the distributions can be more readily comprehended. Several points are to be noted from this figure. First, at the wind direction of 122°, as H_c increased from 24 to 60 m, the location of the maximum shifted from the downwind side of the hill to the top and finally to the upwind side. The crosswind width of the distributions increased as H_c increased, but the value of the maximum concentration changed relatively little (less than a factor of 2). At H_c = 60 m, the maximum surface concentration was located at nearly the same elevation as the source. Second, changes of only ±5° in wind direction had dramatic effects on the distributions, moving the locations of the maximum concentrations from the north skirt of the hill at a wind direction of 127°, to the centerline at 122°, then to the south skirt at 117°. Again, the values of the maximum concentrations changed relatively little with changes in H_c and/or wind direction, although the values of the maximums were noticeably less at 127°. Third, for centerline winds (122°), the shapes of the distributions change substantially with changes in H_c, whereas for off-axis winds (117° or 127°), the distributions are, for practical purposes, independent of H_c. Unfortunately, very few field samplers were located within the areas of maximum concentration for the off-axis winds. During this hour, only two samplers were working within the 1600 ppt SF_6 contour on the south side of the hill. Finally, it is noteworthy that the maximum surface concentration was 1/2 to 2/3 of the plume centerline concentration in the absence of the hill (cf., Figure 13).

A scatter diagram comparing concentration distributions measured in three of these tows (11,12, and 13) with field distributions is presented in Figure 21. There is one obviously suspicious field measurement point (port 34; ERT sampler location 60X; see Figure 14 for sampler location and Figure 7 for field concentration distribution). Ignoring that, it is generally apparent that maximum model concentrations were much higher than maximum field concentrations (by factors of 3 to 10) and low model concentrations were much lower than low field values; there were many ports on the model where zero-concentrations were observed, whereas in the field, all the samplers showed at least a trace concentration. It is impossible, of course, to show these points properly on the logarithmic scatter diagram of Figure 21; they are indicated, however, by the hand-drawn points on the bottom of the figure.

As mentioned earlier, low-frequency fluctuations in wind speed and direction as observed in the field were obviously lacking in the towing tank. This is almost certainly the explanation for the discrepancies between the model and field data of Figure 21. The previous series of 18 tows was done in an attempt to determine whether a superposition of concentration patterns from tows done at a series of discrete wind speeds (various H_c's) and wind directions could be used to simulate field conditions with continuous distributions of wind speed and direction. As mentioned earlier, however, the 40 m-level winds were lacking, so that proper choices for particular wind speeds and directions to simulate and superpose were difficult to make. The particular choices for the previous series of tows (122° ±5° and $24 \text{ m} \leq H_c \leq 60 \text{ m}$) were made on an ad hoc basis after studying the field photographs of plume behavior and available meteorological data at other levels on the tower.

The first attempt at superposition is shown in Figure 22. It was constructed as the simple arithmetic average of the distributions from each of the 18 tows. Figure 23, a scatter plot of resulting model concentrations versus field concentrations, showed a marked improvement over the previous single-tow comparisons. The highest model concentrations here are within a factor of 2 of the highest field values. Whereas the low model concentrations are still lower than the low field values, there were no zero-model-concentration values. The indication for improving the correspondence is, therefore, an even larger series of tows, although particular choices to be made for other wind speeds and/or directions are not immediately obvious.

Three points on the scatter plot of Figure 23 deserve discussion. The two points marked 49 and 61 (port numbers) were the only two operating field samplers on the south side of the hill, and both of them indicated quite small values of concentration. Evidently the choice of the 117° wind direction was a poor one; it created the lobe of the concentration distribution around the south side of the butte. In an attempt to improve the correspondence, the 6 tows at the 117° wind direction were eliminated from the superposition; this process reduced model concentrations at these two points to only a factor of 2 higher than the observed field values. However, it increased nearly all remaining concentrations by approximately 50%; such a simple solution is therefore not sufficient.

The point marked 31 on the scatter plot was located at the 25 m elevation, i.e., 5 m lower than the source; it happens to be the location of the highest concentration measured during this hour in the field. This may at first appear anomalous. However, Hunt and Venkatram (private communication) have reported similar observations during other very stable periods. Hunt has further postulated as a possible mechanism a vortex roll-up on the windward side of the hill and has done some preliminary calculations showing that such vortex roll-up is plausibly due to shear in the approach flow. Vortex roll-up was not observed on the windward side of the CCB model, as shear in the approach flow was absent. Such vortex roll-up has been observed in the towing tank, however, on model hills of much steeper slope (Hunt and Snyder, 1980).

Other combinations and superpositions from this set of 18 tows were attempted, but the superposition of the entire set (Figures 22 and 23) appeared to yield the best results.

Five additional tows were made, 3 at 120° and 2 at 125.5°, so that superpositions could be made on the basis of the probability distribution of H_c and the bimodal distribution of wind direction at the 80 m-level (Figures 6 and 4, respectively). Various combinations of distributions including those from these 5 tows were made, using uniform as well as weighted averaging. None of these superpositions were as successful as those shown in Figures 22 and 23.

Figures 24 and 25 show the variation of maximum surface concentration with H_c and wind direction, respectively. No systematic variation of C_{mx} with H_c is observed, but there is a definite tendency for the maximum concentration to peak around a wind direction of 120°. It is also to be noted that the maximum surface concentration at this wind direction is approximately equal to the plume centerline concentration in the absence of the hill.

CONCLUSIONS

1. Repeatability of the concentration distributions in the towing tank was good. Under ostensibly identical conditions, concentrations can be matched to within 10 to 20% upon successive tows.

2. Gross stability classifications are not sufficient for characterizing concentration distributions. It appears that the detailed shape of the density profile is quite important in determining concentrations on a point-by-point basis. However, such a gross classification would appear to be reasonable for predicting the values of maximums as well as ranges of values of concentration (but not locations).

3. Surface concentration distributions around the hill are extremely sensitive to changes in wind direction under stable conditions. In these experiments, $24 \text{ m} \leq H_c \leq 60 \text{ m}$, the location of the maximum concentration shifted through an angle of approximately 60° (looking from the source) with a shift of only 10° in wind direction.

4. The value of the maximum surface concentration changed relatively little with changes in wind direction or wind speed; over the entire range of $24 \text{ m} \leq H_c \leq 60 \text{ m}$ and $117° \leq \theta \leq 127°$, the maximum changed by only a factor of 3.5.

5. For "on-axis" wind directions (i.e., plume aimed directly toward hill center), the location of the maximum surface concentration moved from the lee side to the windward side as H_c increased from 24 to 60 m. The value of the maximum surface concentration changed by only a factor of 1.5 over this same range of H_c.

6. For "off-axis" wind directions (on the order of ±5°), the locations and values of the maximum surface concentrations are, for practical purposes, independent of H_c.

7. Because of the absence of low frequency fluctuations in wind speed and direction in the tank, the concentration distributions observed in the tank were exceedingly narrow; maximum concentrations were 5 to 10 times larger than those observed in the field.

8. An ad hoc attempt was made to simulate the low frequency wind fluctuations by superposing concentration patterns from tows done at a series of discrete wind speeds and wind directions. This attempt was moderately successful in that 80% of the model concentrations were within a factor of 2.5 of the field concentrations. The highest model concentrations were a factor of 2.5 larger than field values. The points where the model showed concentrations lower than field values were located on the extreme edges of the distributions, indicating that tows at very slightly different wind directions could have brought these points in-line.

9. The ad hoc attempt was made because of malfunctions in the measurement system at the 40-m level (closest to plume elevation), so that a detailed analysis of 80-m level winds was made. Additional tows were made on the basis of the frequency distribution of wind directions at the 80-m level. Several superpositions on this basis yielded results less satisfactory than did the ad hoc attempt. Frequency distributions of wind speed and direction at plume elevation are evidently essential in order to improve performance of the model.

10. For "on-axis" winds in the model, maximum surface concentrations approached those at the centerline of the plume in the absence of the hill, i.e., $C_{mx} = aC_o$, where $0.5 \leq a \leq 1$. However, because of the extreme sensitivity of the location of maximum concentration to wind direction, the plume is "smeared" broadly across the hill surface as the wind direction changes by only a few degrees. Hence, short term (~5 min) in the field may be expected to approach C_o; larger term averages (~1 hr) may be expected to be reduced by factors of 5 to 10 (or more depending, of course, on the magnitudes of σ_u and σ_θ).

REFERENCES

Hunt, J.C.R. and Snyder, W.H., 1980: Experiments on Stably and Neutrally Stratified Flow over a Model Three-Dimensional Hill, J. Fluid Mech., v. 96, pt. 4, p. 671-704.

Hunt, J.C.R., Snyder, W.H., and Lawson, R.E. Jr., 1978: Flow Structure and Turbulent Diffusion around a Three-Dimensional Hill: Fluid Modeling Study on Effects of Stratification: Part I: Flow Structure, Envir. Prot. Agcy. Rpt. No. EPA 600/4-78-041, Res. Tri. Pk., NC.

Snyder, W.H., 1980: Towing Tank Studies in Support of Field Experiments at Cinder Cone Butte, Idaho; Phase III: Verification of Formula for Prediction of Dividing Streamline Height, Rpt. to Envir. Res. & Tech., Aug. 29, 12p.

Snyder, W.H., 1981: Guideline for Fluid Modeling of Atmospheric Diffusion, Envir. Prot. Agcy. Rpt. No. EPA-450/4-81-004, Res. Tri. Pk., NC, 200p.

Strimaitis, D.G., 1981: private communication.

TABLE 1: VALUE OF H_c DURING EACH 5-MINUTE PERIOD OF THE HOUR 0500-0600

TIME (END)	FIVE-MINUTE PERIOD NUMBER	H_c (m)
0505	1	40.9
0510	2	38.9
0515	3	42.9
0520	4	42.2
0525	5	40.9
0530	6	38.5
0535	7	38.8
0540	8	40.2
0545	9	44.5
0550	10	40.3
0555	11	40.3
0600	12	40.7

Average H_c = 40.8 m σ_{H_c} = 1.7 m

Note: H_c was calculated assuming a hill height of 100 m. These values are referenced to local ground level.

TABLE 2. PHOTOGRAPHIC RECORDS AVAILABLE

TYPE OF RECORD	LOCATION AND EXPERIMENTS RECORDED
16 mm motion picture film	all tows - plan view only
35 mm color prints	all tows - plan view
35 mm color prints	all tows - side view
Polaroid b & w prints	tows 10-41 - plan view only

TABLE 3. SCHEDULE OF TOWS

TOW # DATE	FILE #	θ	H_s	H_c	TOW SPEED	EFFLUENT RATE	SAMPLE TIME	REMARKS	DENSITY PROFILE #
- 1981	CCBRD.	degrees	m (cm)	m (cm)	cm/sec	cc/min	sec	----	CCBRS.
1 4/3	1	122	35 (5.0)	32 (4.6)	12.59	194.7	102.0	source at 597 m/122° very little dye reaching south peak need to check field source height	36
2 4/3	2	122	35 (5.0)	32 (4.6)	12.59	187.5	105.0	repeat of tow #1 to check repeatability	37
3 4/6	3	122	31 (4.5)	31 (4.5)	13.73	192.5	93.0	adjusted source height to correct for differences in local ground level	38
4 4/6	4	122	31 (4.5)	24 (3.5)	15.21	188.4	96.0		38
5 4/6	5	122	31 (4.5)	38 (5.51)	12.36	190.0	113.0	slight roll-up on windward side of model - may be effect of boundary layer	38
6 4/7	6	122	31 (4.5)	60 (8.64)	7.91	188.8	126.4	source location changed to 597 m/126.5°	39
7 4/7	7	122	31 (4.5)	38 (5.51)	12.33	189.3	105.3	ran two high speed tows for JCRH following this tow	39
8 4/8	8	122	31 (4.5)	38 (5.51)	9.42	186.9	112.5	repeatability check	40
9 4/8	9	122	31 (4.5)	38 (5.51)	9.41	43.4	115.2	effluent released isokinetically	41
10 4/9	10	122	31 (4.5)	38 (5.51)	11.69	192.1	97.4	source location moved to 597 m/124.6°, plume splits around north butte	42
11 4/9	11	122	31 (4.5)	31 (4.5)	12.55	192.4	102.1	a little more dye getting through the draw	42
12 4/9	12	122	31 (4.5)	24 (3.5)	13.55	195.5	100.8	plume goes primarily through (over?) the draw	42
13 4/13	13	122	31 (4.5)	60 (8.64)	7.38	189.6	126.2	very little dye through the saddle - most splits around the sides	45
14 4/13	14	122	31 (4.5)	49 (7.06)	8.97	190.3	132.0		45
15 4/16	15	122	31 (4.5)	44 (6.4)	11.48	194.8	101.9		49
16 4/17	16	127	31 (4.5)	60 (8.64)	7.41	192.5	137.8	changed wind direction to 127° all of plume goes around the north butte - max ~ 30 m contour	50
17 4/17	17	127	31 (4.5)	38 (5.51)	10.84	193.4	103.5	not very different from previous tow	50
18 4/17	18	127	31 (4.5)	24 (3.5)	13.72	195.0	102.2	plume doesn't go over hill - plume very thin at top of hill, not reaching top of masts	50
19 4/20	19	127	31 (4.5)	31 (4.5)	11.93	194.4	108.9	no plume over the north peak large wake with uniformly low concentration	51
20 4/20	20	127	31 (4.5)	44 (6.4)	9.98	195.4	126.7		51
21 4/21	21	127	31 (4.5)	49 (7.06)	8.77	195.0	127.8		52
22 4/21	22	117	31 (4.5)	31 (4.5)	11.34	193.8	104.9	changed wind direction to 117°	52

TABLE 3. SCHEDULE OF TOWS (continued)

TOW # DATE	FILE #	θ	H_s	H_c	TOW SPEED	EFFLUENT RATE	SAMPLE TIME	REMARKS	DENSITY PROFILE #
- 1981	CCBRD.	degrees	m (cm)	m (cm)	cm/sec	cc/min	sec	----	CCBRS.
23 4/22	23	117	31 (4.5)	60 (8.64)	8.49	191.9	142.4	plume goes around south side of hill - large uniform wake	53
24 4/22	24	117	31 (4.5)	24 (3.5)	14.13	194.7	100.2	small portion of plume went over top of hill	53
25 4/22	25	117	31 (4.5)	38 (5.51)	11.85	193.4	114.4	very similar to tow #24 - slight wisp over draw about 2/3 of way down the channel	53
26 4/23	26	117	31 (4.5)	44 (6.4)	11.33	193.7	106.1	mostly around south side - but, about 2/3 of way down the channel got some around north side and draw	55
27 4/23	27	117	31 (4.5)	49 (7.06)	10.31	194.6	119.2	very similar to previous tow some shift about 2/3 of way down the channel	55
28 4/29	28	120	31 (4.5)	38 (5.51)	12.87	194.5	110.9	changed wind direction to 120° plume splitting around both peaks similar to higher H_c	56
29 4/30	29	120	31 (4.5)	31 (4.5)	13.87	195.1	96.2		58
30 5/1	30	120	31 (4.5)	31 (4.5)	13.61	200.0	99.1		59
31 5/1	31	125.5	31 (4.5)	38 (5.51)	11.86	195.2	106.3	changed wind direction to 125.5°	59
32 5/4	32	125.5	31 (4.5)	31 (4.5)	12.98	192.6	104.6	plume spreads mostly around north butte - occasionally goes over north butte - get shift 2/3 of way down channel	60
33 5/11	33 (z) 34 (y)	0	31 (4.5)	24 (3.5)	14.47	194.5	105.2	model removed and flat baseplate installed with cross rake 48.5 cm from source	61
34 5/12	35 (z) 36 (y)	0	31 (4.5)	60 (8.64)	7.89	198.1	156.3	observe no shift of plume centerline during the tow	63
35 5/12	37 (z) 38 (y)	0	31 (4.5)	44 (6.4)	10.85	198.2	124.5		63
36	39 (z) 40 (y)	0	31 (4.5)	24 (3.5)	15.25	196.8	95.8	moved cross rake downstream to 91.4 cm from source	64
37 5/13	41 (z) 42 (y)	0	31 (4.5)	60 (8.64)	7.87	196.4	154.8	toward end of tow, plume centerline wavers a bit	64
38 5/13	43 (z) 44 (y)	0	31 (4.5)	44 (6.4)	11.28	195.9	118.3		64
39 5/15	45 (z) 46 (y)	0	31 (4.5)	24 (3.5)	14.84	192.8	97.3	moved cross rake downstream to 134.2 cm from source	65
40 5/15	47 (z) 48 (y)	0	31 (4.5)	60 (8.64)	7.49	194.7	153.0	toward end of tow, plume centerline wavers a bit	65
41 5/15	49 (z) 50 (y)	0	31 (4.5)	44 (6.4)	10.85	192.5	117.9	last tow for case 206	65

TABLE 4. SUMMARY OF FLAT BASEPLATE MEASUREMENTS

X (m)	H_c (m)	σ_z (m)	σ_y (m)	C^z_{max} (ppt)	C^y_{max} (ppt)
313.8	24	4.8	7.3	25,350	24,978
313.8	44	5.0	8.7	21,026	20,504
313.8	60	4.5	9.4	15,658	15,881
591.4	24	4.7	11.7	19,758	16,925
591.4	44	4.0	13.4	17,894	14,166
591.4	60	3.8	13.7	14,912	13,719
868.3	24	4.6	11.2	21,996	21,250
868.3	44	3.8	13.7	17,074	14,912
868.3	60	3.7	14.5	14,688	13,644

TABLE 5. LOCATION OF SAMPLERS ON CINDER CONE BUTTE

FMF PORT	ERT PORT	ANGLE DEG.	R m	x m	y m
1	37.01000	8.00000	510.00000	70.97845	505.03071
2	37.02000	8.00000	449.00000	62.48866	444.63034
3	37.03000	8.00000	391.00000	54.41681	387.19475
4	37.04000	8.00000	308.00000	42.86541	305.00256
5	37.05000	8.00000	275.00000	38.27269	272.32[illegible]
6	37.06000	8.00000	250.00000	34.79335	247.5[illegible]
7	37.07000	8.00000	227.00000	31.59237	224.79[illegible]
8	37.09000	8.00000	177.00000	24.63370	175.2[illegible]
9	37.10000	8.00000	154.00000	21.43271	152.50129
10	37.11000	8.00000	122.00000	16.97916	120.81271
11	37.12000	8.00000	81.00000	11.27305	80.21172
12	37.20000	8.00000	193.00000	26.86047	191.12177
13	37.26000	8.00000	19.00000	2.64429	18.81509
14	34.10000	30.00000	146.00000	73.00016	126.43967
15	31.90000	52.00000	146.00000	115.04976	89.88632
16	31.96000	53.00000	154.00000	122.99007	92.67924
17	31.07000	53.00000	200.00000	159.72736	120.36265
18	31.09000	53.00000	154.00000	122.99007	92.67924
19	31.26000	53.00000	107.00000	85.45414	64.39402
20	31.05000	53.00000	246.00000	196.46465	148.04687
21	29.04000	68.00000	187.00000	173.38358	70.05093
22	28.26000	71.00000	420.00000	397.11826	136.73749
23	29.11000	75.00000	75.00000	72.44456	19.41119
24	27.03000	83.00000	260.00000	258.06213	31.68519
25	26.03000	90.00000	360.00000	360.00000	-0.00135
26	26.05000	90.00000	208.00000	208.00000	-0.00078
27	26.06000	90.00000	142.00000	142.00000	-0.00053
28	63.03000	98.00000	315.00000	311.93430	-43.84081
29	62.03000	105.00000	190.00000	183.52571	-49.17640
30	60.03000	120.00000	362.00000	313.50034	-181.00150
31	60.04000	120.00000	297.00000	257.20886	-148.50122
32	60.22000	120.00000	235.00000	203.51543	-117.50097
33	60.23000	120.00000	164.00000	142.02779	-82.00067
34	60.24000	120.00000	124.00000	107.38686	-62.00051
35	60.25000	120.00000	94.00000	81.40617	-47.00039
36	60.26000	120.00000	43.00000	37.23899	-21.50018
37	60.01000	120.00000	510.00000	441.67175	-255.00209
38	60.02000	120.00000	410.00000	355.06946	-205.00169
39	58.08000	135.00000	195.00000	137.88507	-137.88660
40	58.07000	137.00000	240.00000	163.67863	-175.52593
41	57.25000	143.00000	327.00000	196.79202	-261.15500
42	57.26000	143.00000	140.00000	84.25346	-111.80948
43	57.96000	143.00000	165.00000	99.29873	-131.77545
44	57.13000	143.00000	165.00000	99.29873	-131.77545
45	57.90000	147.00000	162.00000	88.23071	-135.86517
46	56.03000	150.00000	255.00000	127.49866	-220.83729
47	56.04000	150.00000	198.00000	98.99895	-171.47365
48	56.05000	150.00000	86.00000	42.99955	-74.47845
49	55.03000	158.00000	250.00000	93.65015	-231.79659
50	55.13000	158.00000	204.00000	76.41852	-189.14601
51	55.96000	158.00000	204.00000	76.41852	-189.14601
52	55.26000	159.00000	165.00000	59.12974	-154.04114
53	55.90000	159.00000	196.00000	70.23896	-182.98221
54	54.04000	165.00000	301.00000	77.90256	-290.74420
55	53.03000	171.00000	139.00000	21.74345	-137.28883
56	53.04000	173.00000	260.00000	31.68423	-258.06223
57	39.21000	187.00000	37.00000	-4.50945	-36.72417
58	39.01000	187.00000	510.00000	-62.15722	-506.19812
59	39.02000	187.00000	411.00000	-50.09141	-407.93613
60	39.03000	187.00000	348.00000	-42.41317	-345.40576
61	39.05000	187.00000	291.00000	-35.46618	-288.83069
62	39.07000	187.00000	251.00000	-30.59110	-249.12888
63	39.12000	187.00000	115.00000	-14.01584	-114.14271
64	39.17000	187.00000	180.00000	-21.93784	-178.65816
65	39.18000	187.00000	150.00000	-18.28154	-148.88179
66	39.20000	187.00000	77.00000	-9.38452	-76.42599
67	45.24000	232.00000	107.00000	-84.31778	-65.87498
68	45.07000	232.00000	224.00000	-176.51572	-137.90651
69	45.10000	232.00000	158.00000	-124.50562	-97.27334
70	48.12000	255.00000	63.00000	-60.85350	-16.30495
71	48.02000	255.00000	411.00000	-396.99664	-106.37038
72	48.03000	255.00000	327.00000	-315.85864	-84.63043
73	48.05000	255.00000	258.00000	-249.20956	-66.77264
74	48.07000	255.00000	211.00000	-203.81093	-54.60863
75	48.10000	255.00000	150.00000	-144.88928	-38.82130
76	50.07000	270.00000	238.00000	-238.00000	0.00267
77	64.05000	277.00000	282.00000	-279.89764	34.37034
78	64.10000	277.00000	159.00000	-157.81464	19.37902
79	65.03000	285.00000	252.00000	-243.41238	65.22526
80	67.01000	300.00000	510.00000	-441.66986	255.00542
81	67.02000	300.00000	416.00000	-360.26404	208.00441
82	67.04000	300.00000	343.00000	-297.04462	171.50363
83	67.05000	300.00000	311.00000	-269.33200	155.50330
84	67.06000	300.00000	284.00000	-245.94948	142.00301
85	67.13000	300.00000	230.00000	-199.10445	115.00244
86	67.23000	300.00000	247.00000	-213.90677	123.50262
87	67.24000	300.00000	178.00000	-154.15144	89.00189
88	67.25000	300.00000	130.00000	-112.58251	65.00138
89	67.26000	300.00000	54.00000	-46.76504	27.00057
90	69.07000	315.00000	200.00000	-141.41957	141.42316
91	69.26000	315.00000	325.00000	-229.80679	229.81262
92	70.08000	322.00000	151.00000	-92.96336	118.99082
93	70.26000	322.00000	108.00000	-66.49035	85.10602
94	[illegible]	333.00000	275.00000	-124.84406	245.0[illegible]
95	72.27000	338.00000	285.00000	-106.75929	264.24[illegible]
96	72.24000	338.00000	211.00000	-79.03934	195.6[illegible]
97	73.10000	345.00000	127.00000	-32.86974	122.67304
98	73.11000	345.00000	105.00000	-27.17461	101.42259
99	74.03000	353.00000	310.00000	-37.77516	307.68985
**	74.04000	353.00000	197.00000	-24.00850	195.53184

Reproduced from best available copy.

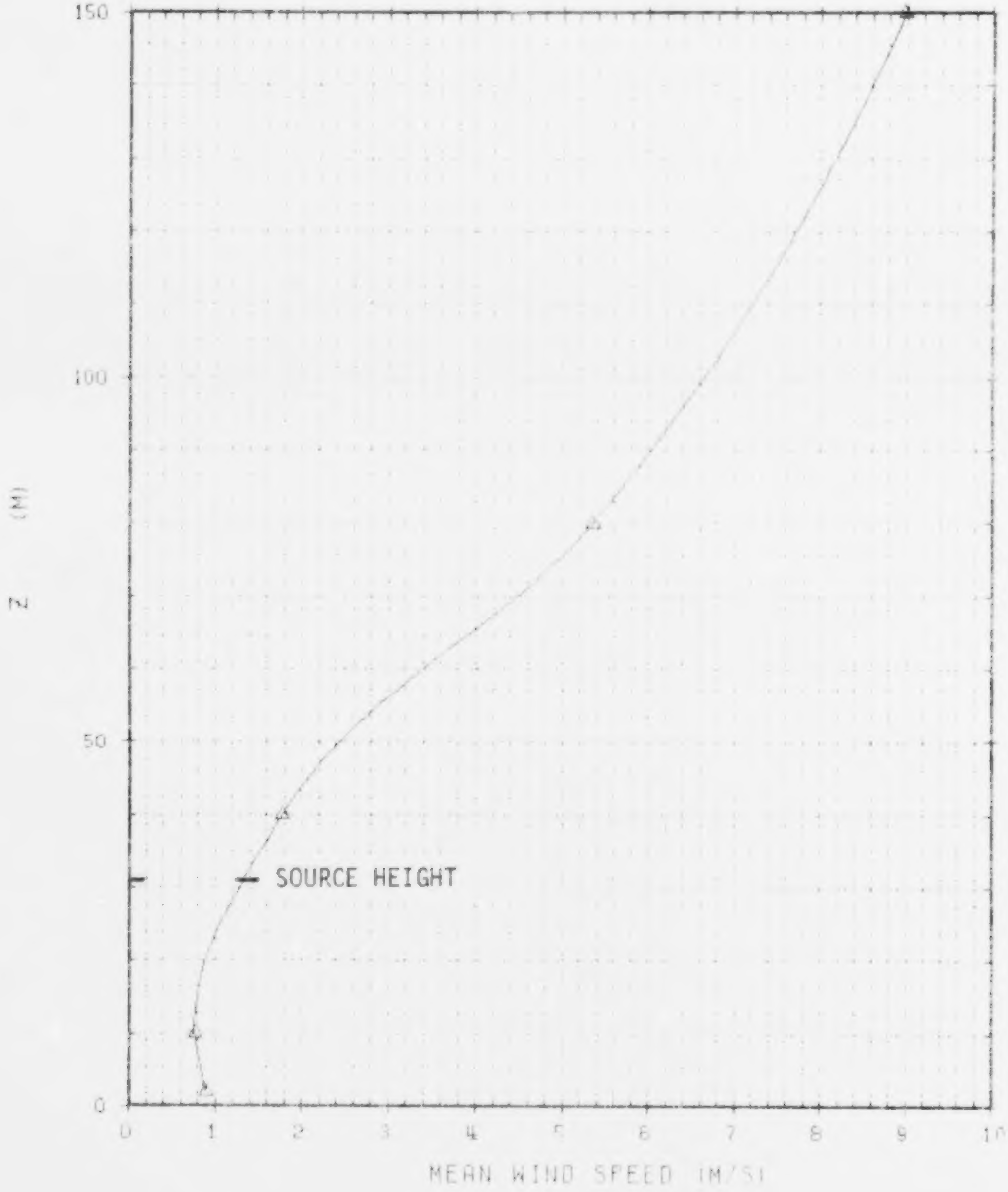

Figure 1. Average Wind Speed Profile, 0500-0600.

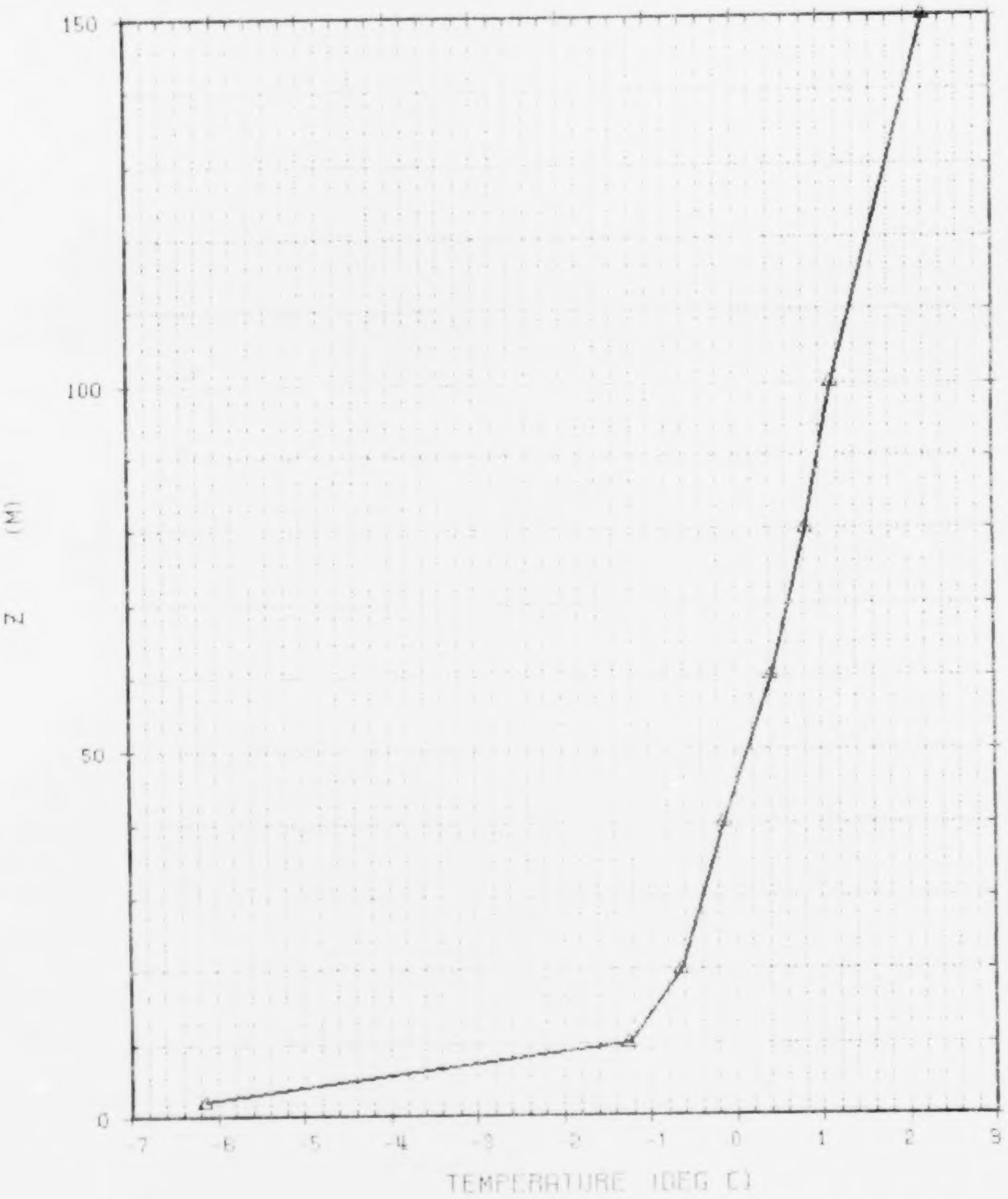

Figure 2. Average Temperature Profile, 0500-0600

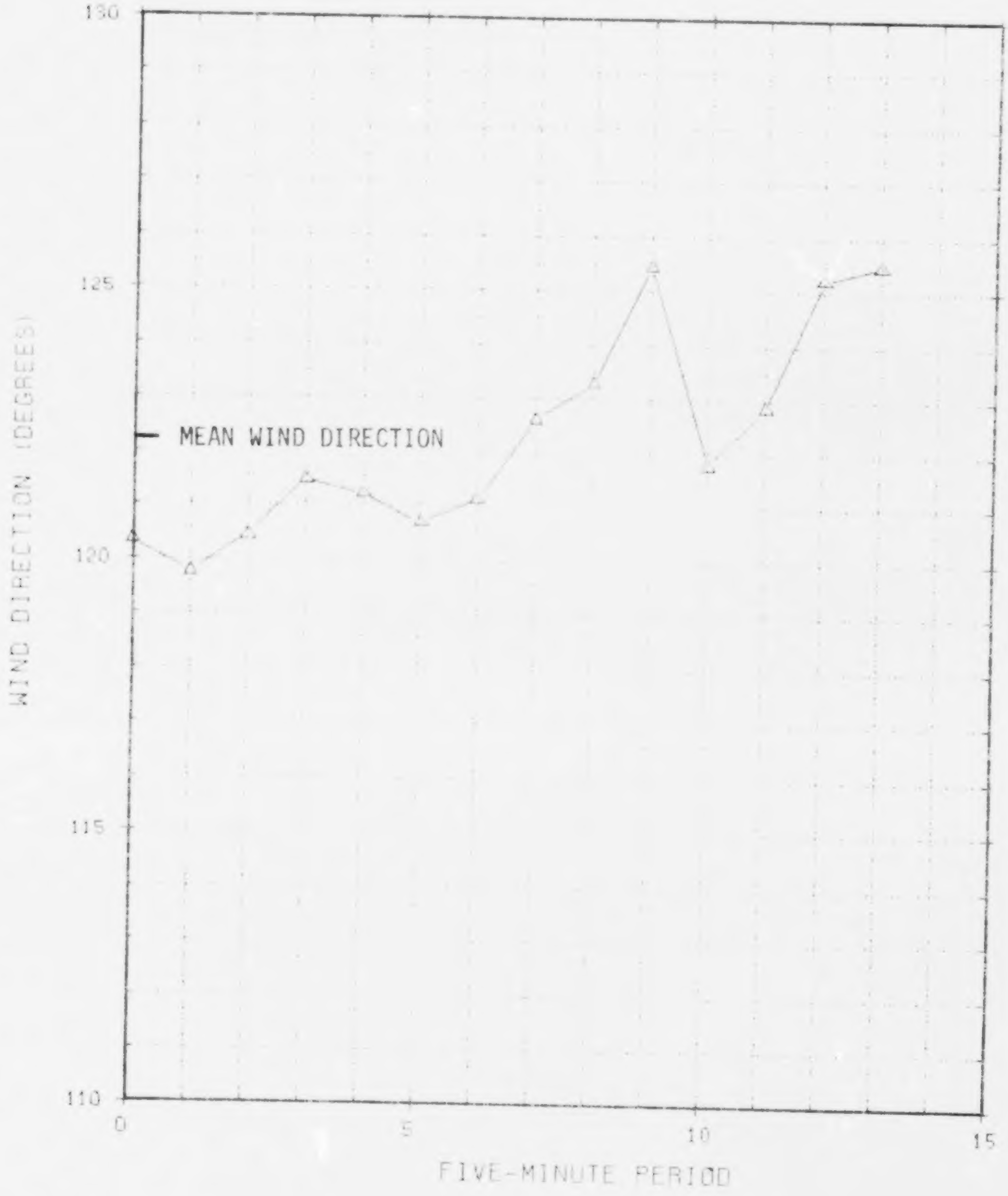

Figure 3. Variation of 80 m Wind Direction During the Hour.

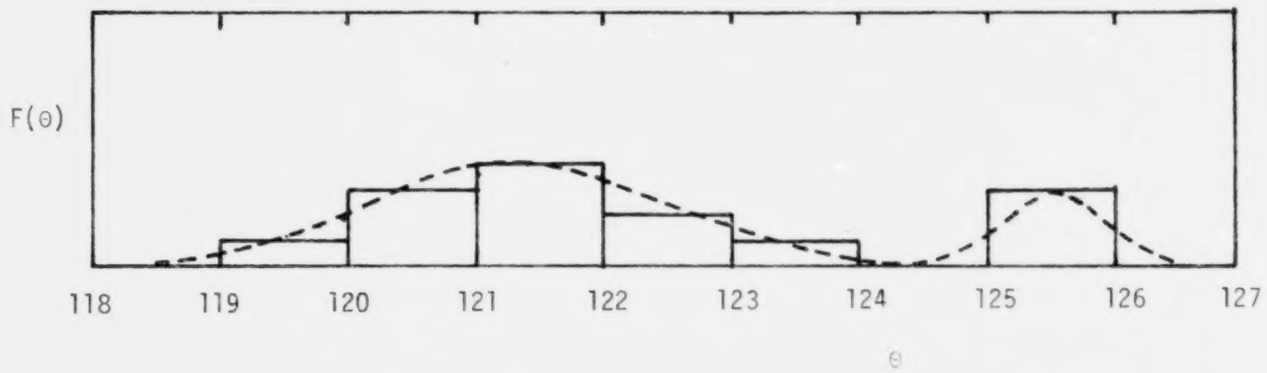

Figure 4. Frequency Distribution of Wind Directions.

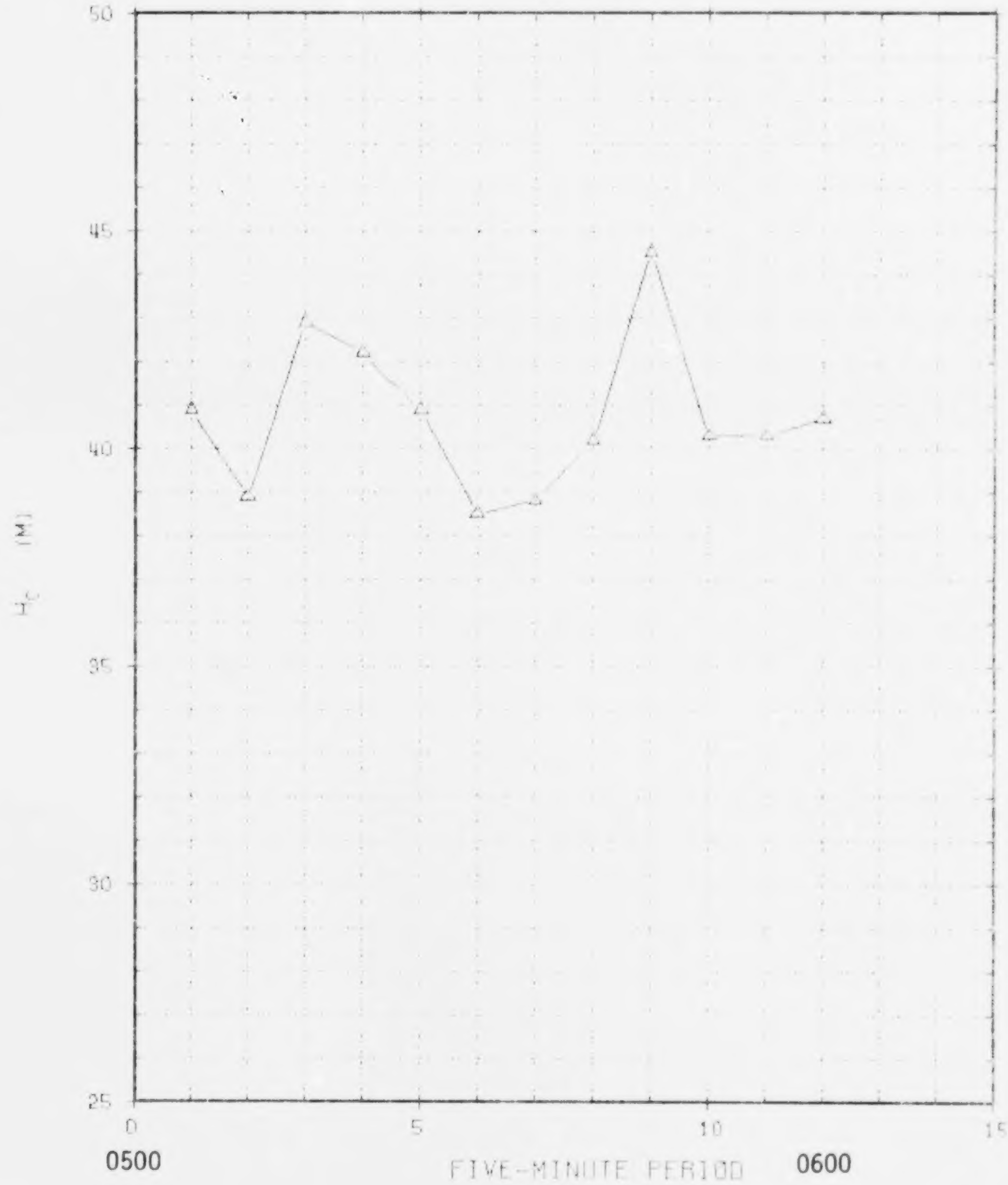

Figure 5. Variation of H_c During the Hour.

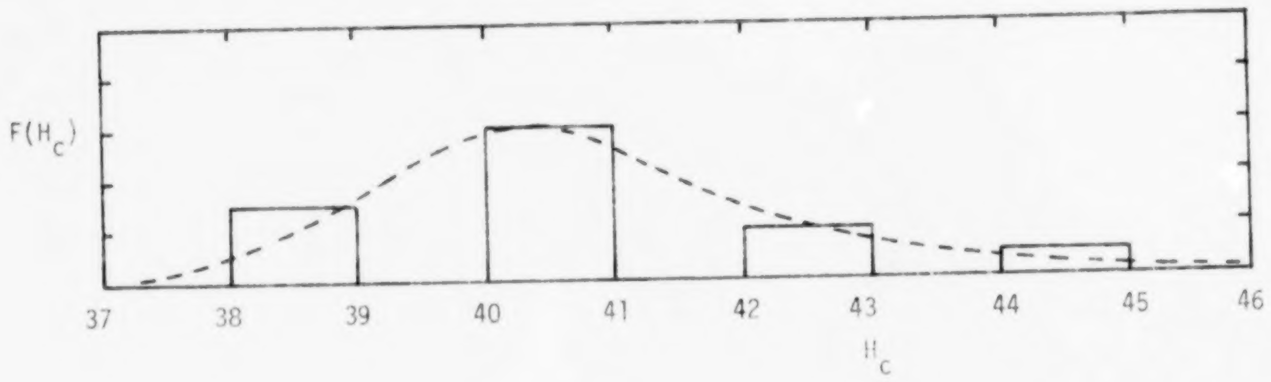

Figure 6. Frequency Distribution of H_c.

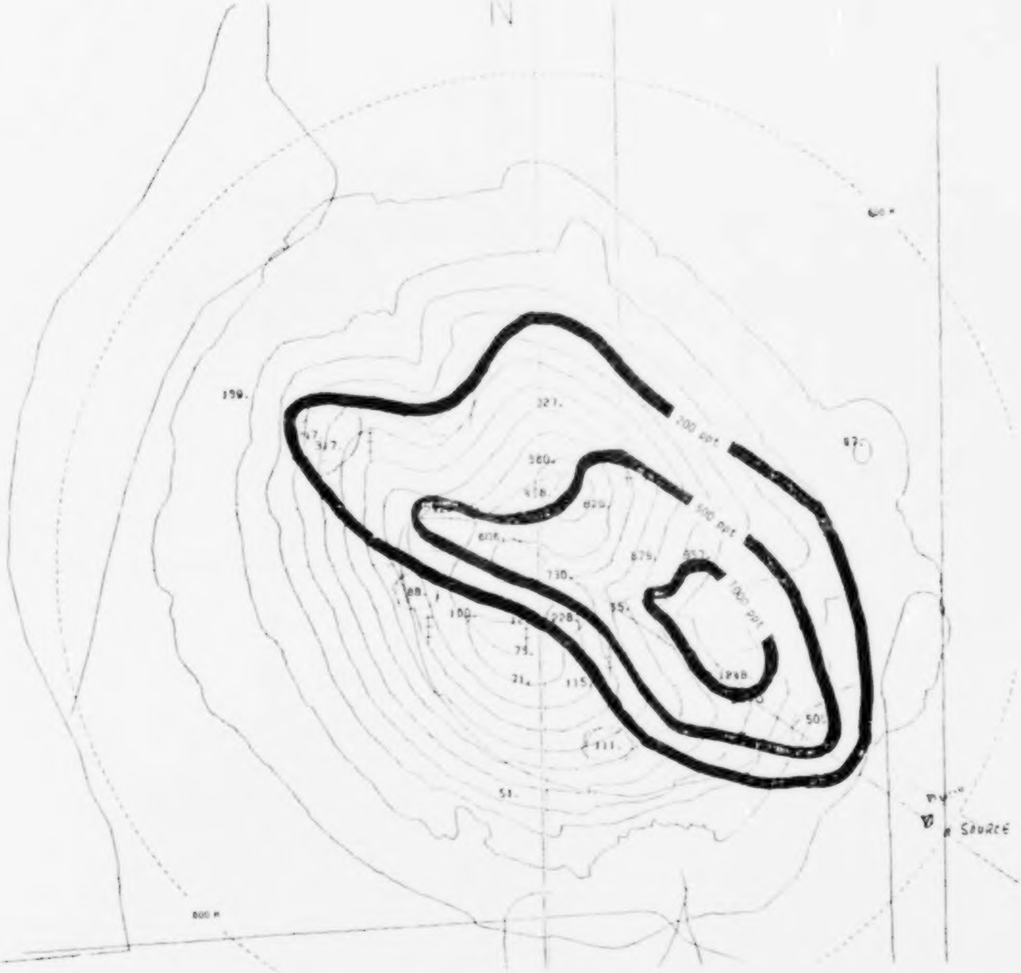
N
199.
227.
347.
380.
418.
620.
608.
200 ppt
500 ppt
1000 ppt
875.
852.
730.
88.
100.
228.
55.
75.
21.
115.
1248
50.
111.
51.
97.
800 m
SOURCE

Figure 7. One-Hour-Average SF_6 Concentrations from Field Data.

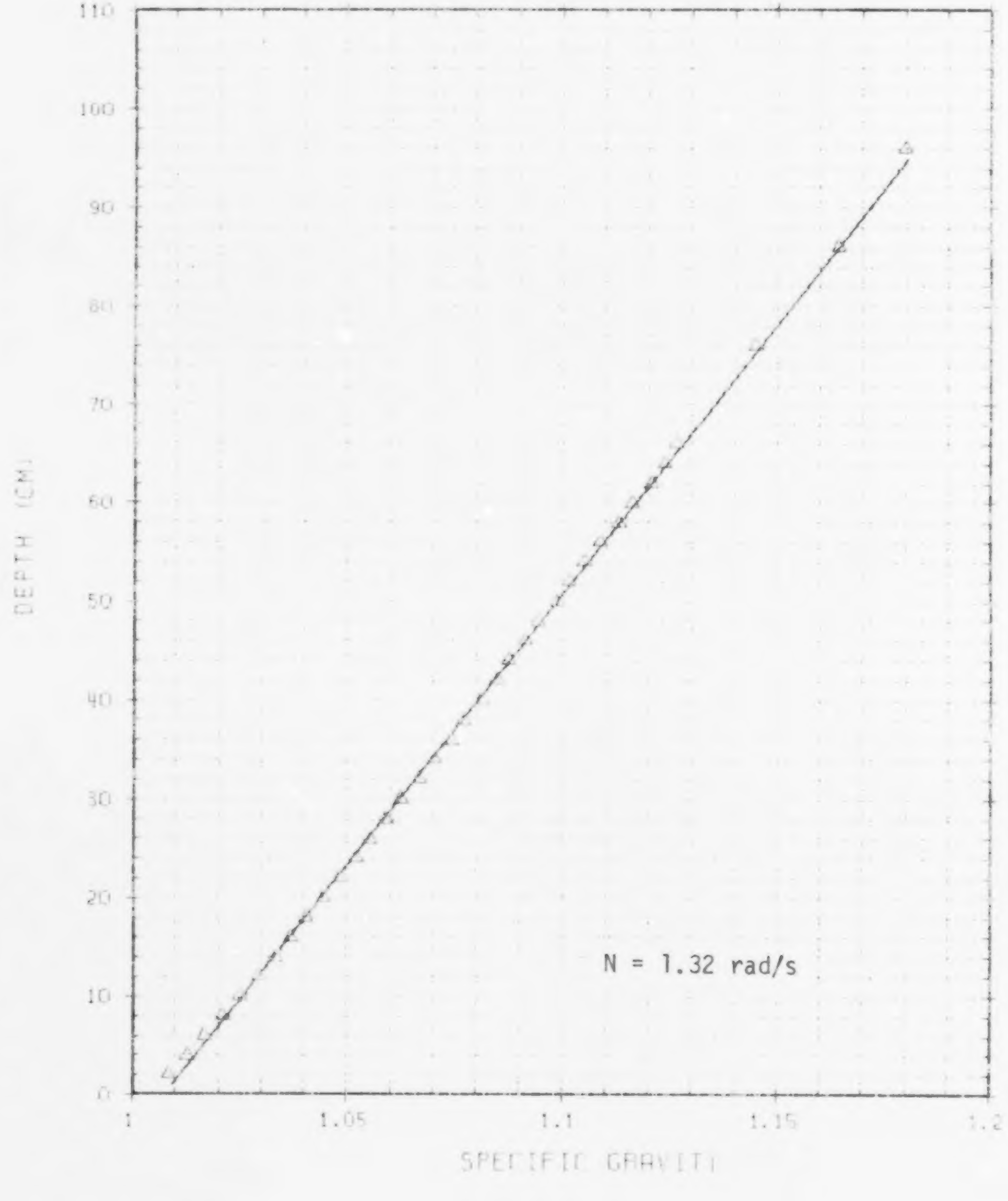

Figure 8. Typical Density Profile in Towing Tank.

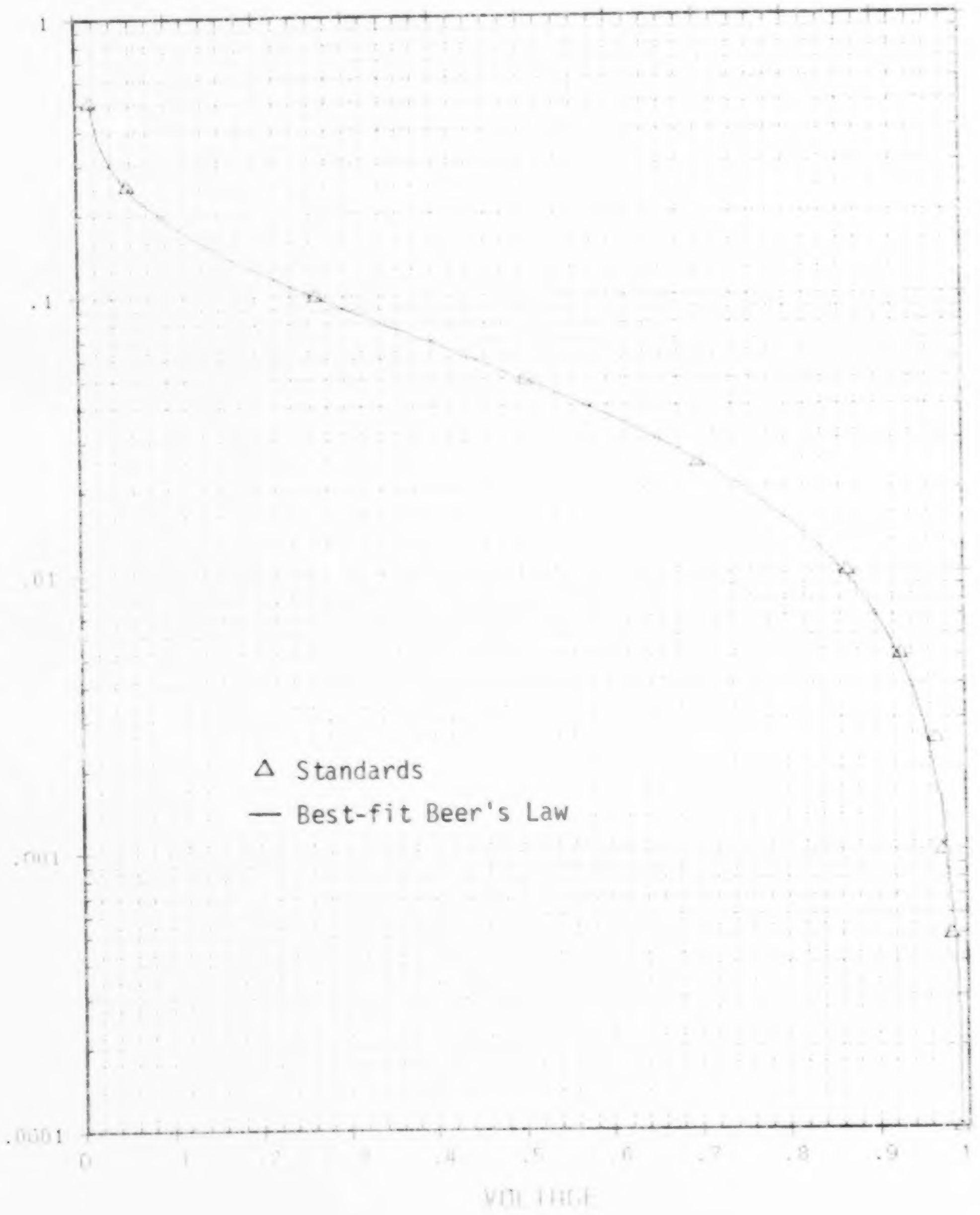

Figure 9. Colorimeter Calibration Curve

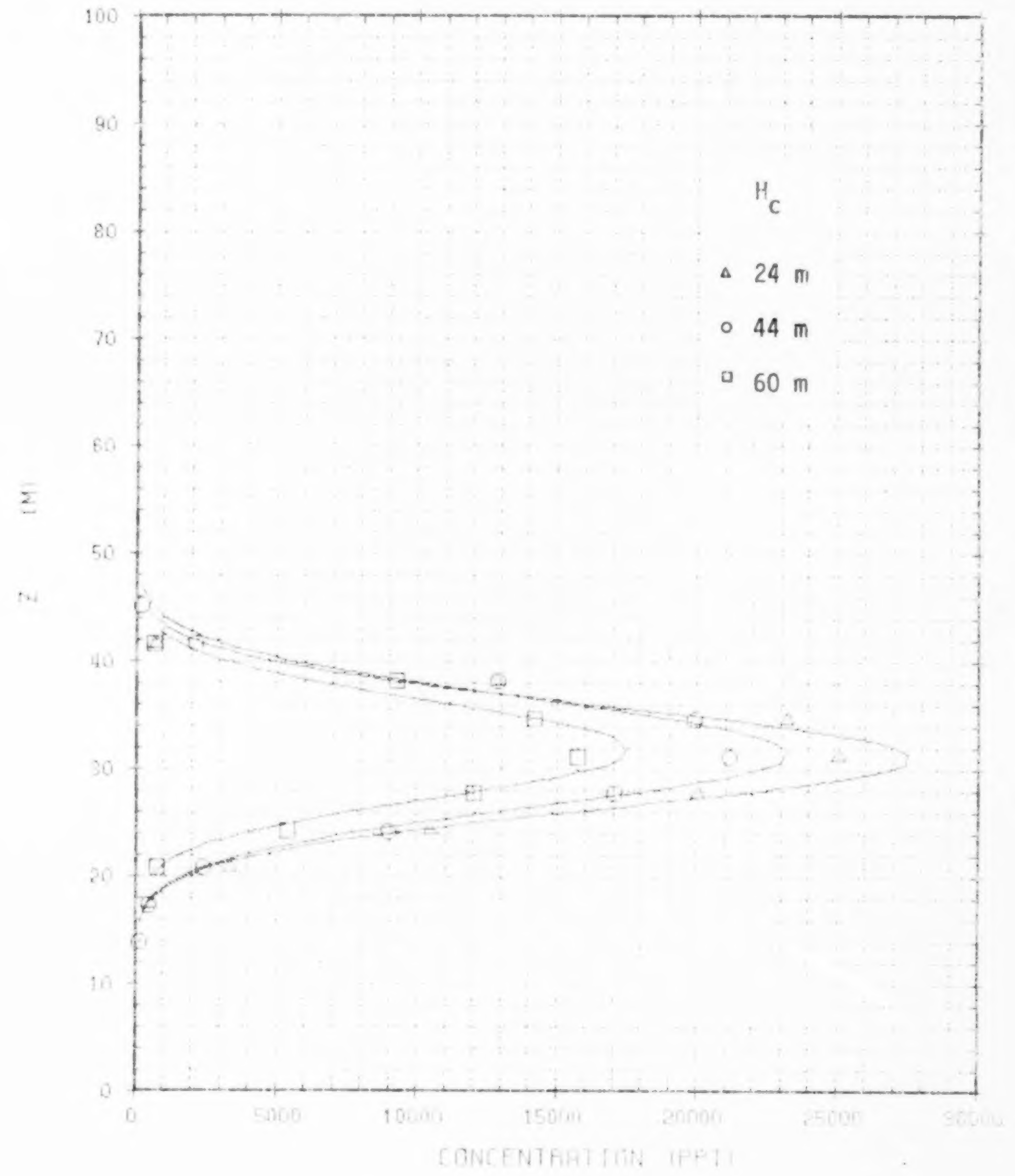

Figure 10. Vertical distributions of plumes over flat baseplate 48.5 cm (314 m) downwind of source.

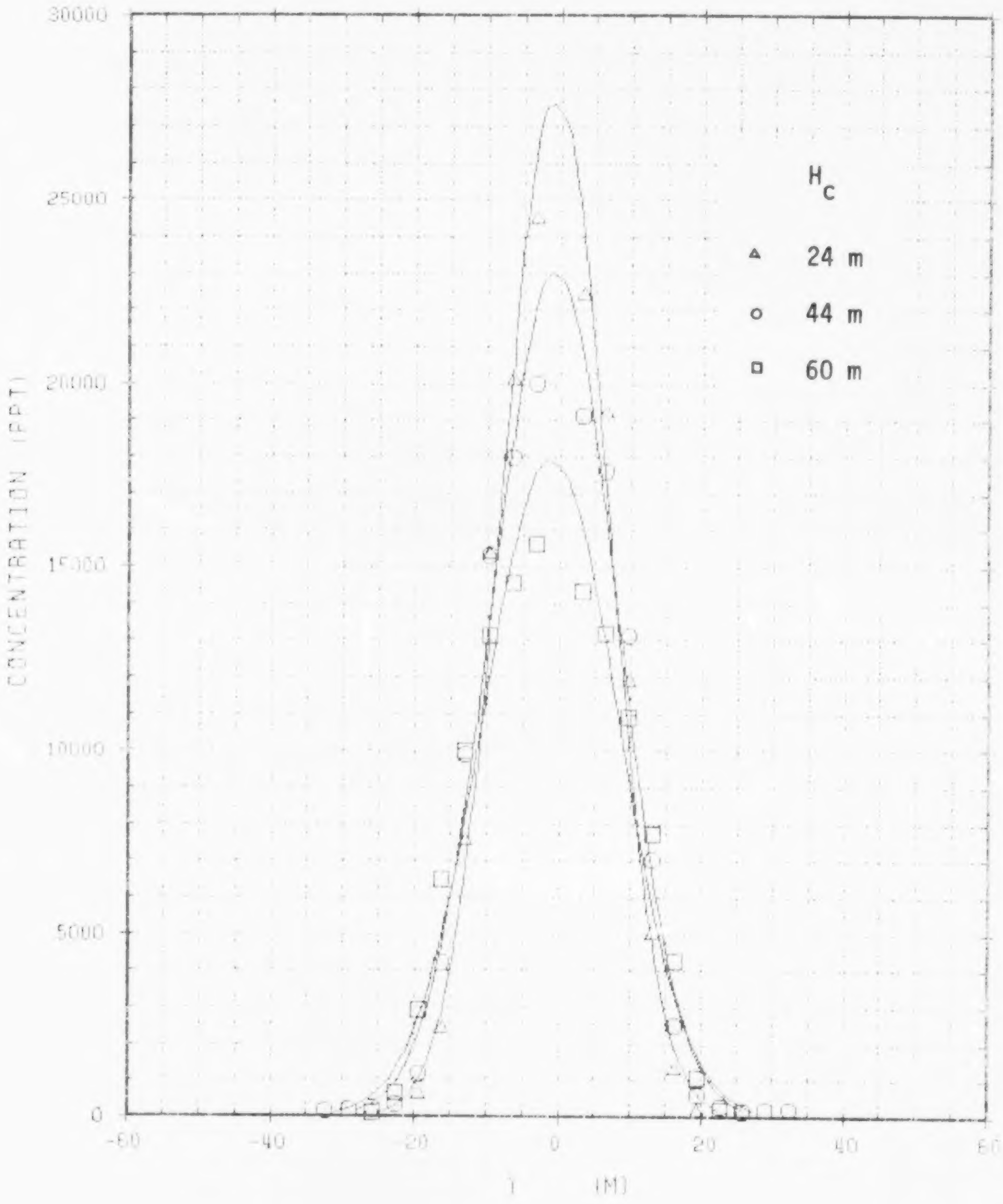

Figure 11. Horizontal distributions of plumes over flat baseplate 48.5 cm (314 m) downwind of source.

Reproduced from best available copy.

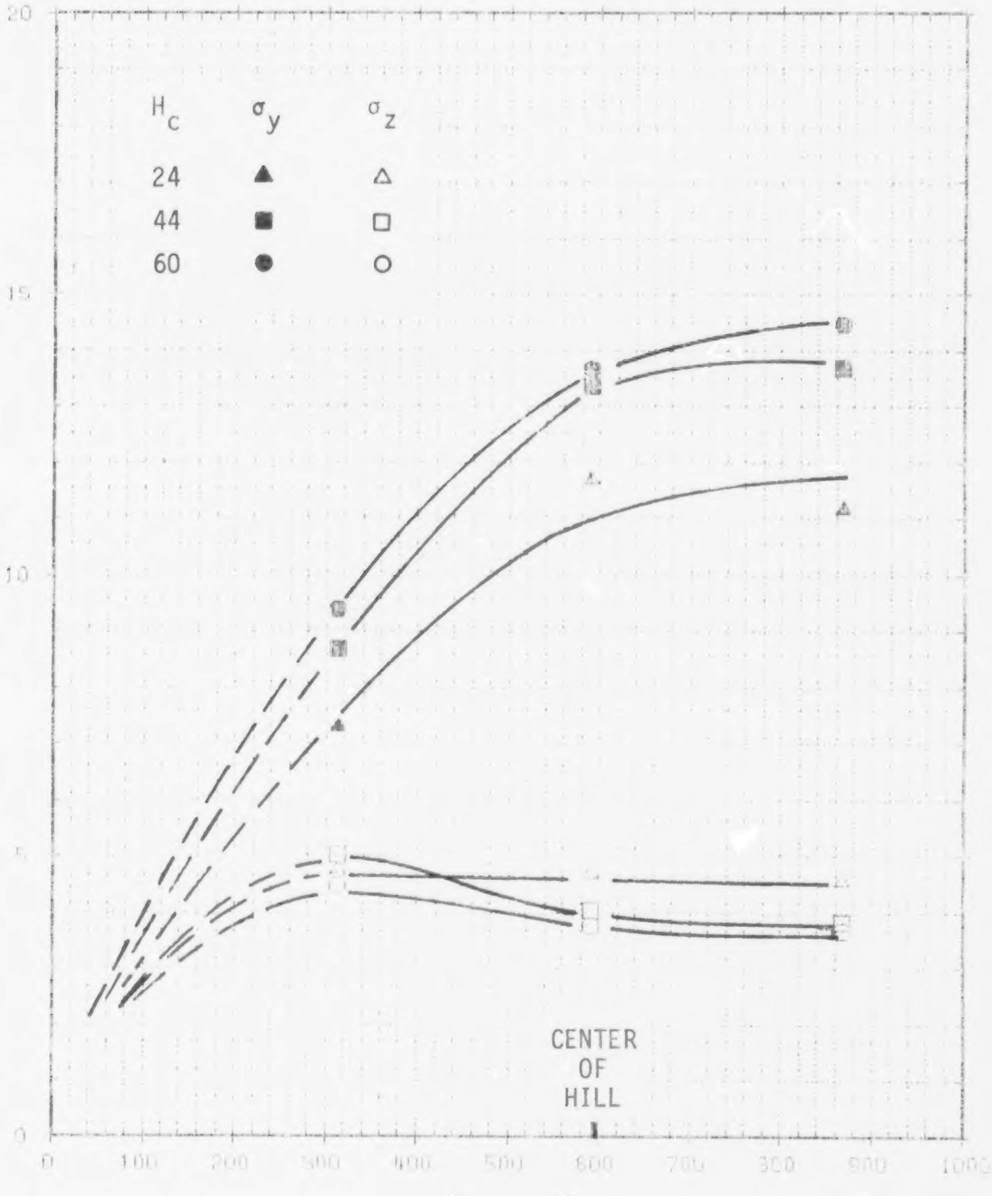

Figure 12. Plume Widths in the Absence of the Hill.

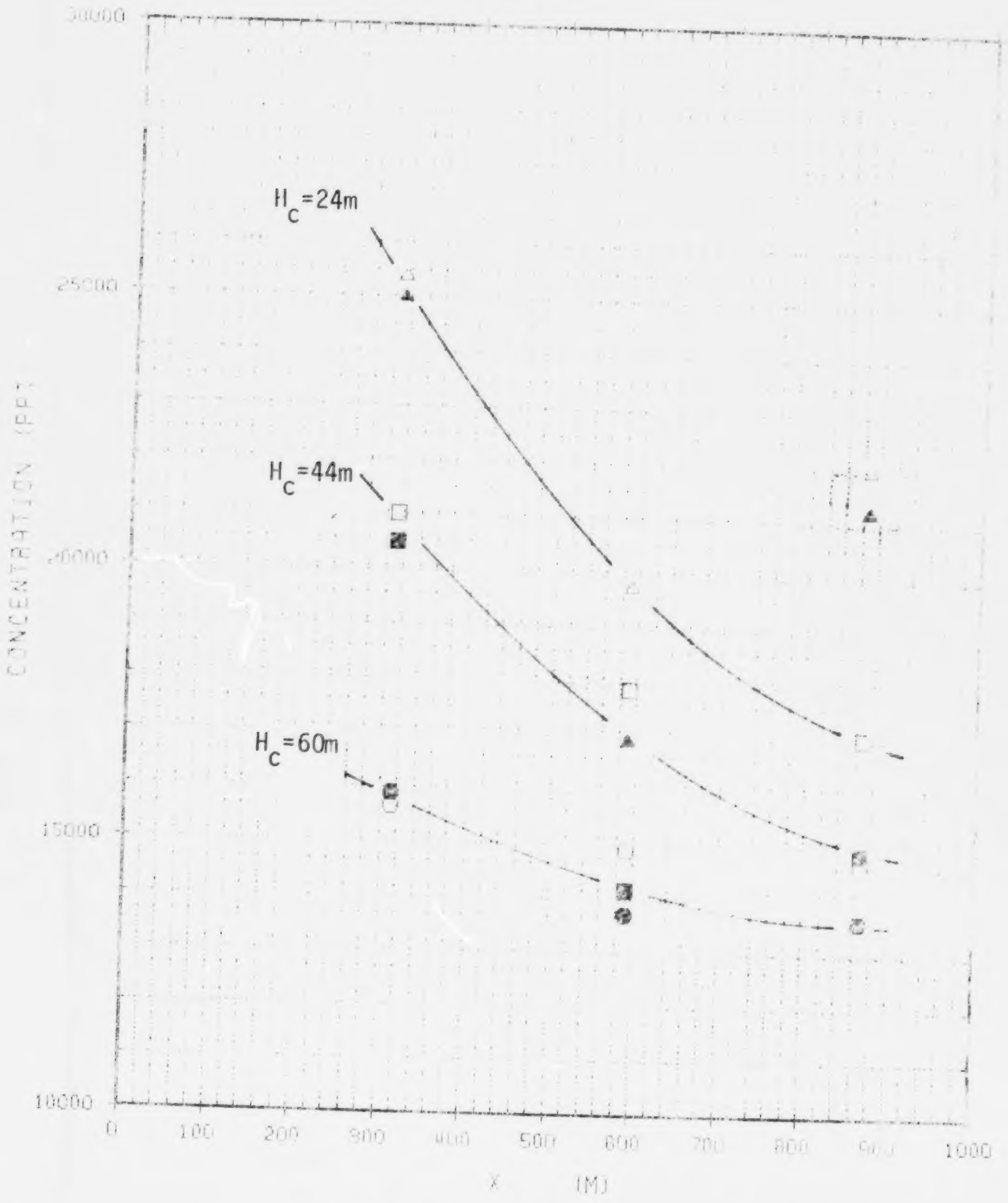

Figure 13. Concentration vs. downwind distance in the absence of the hill. Open points from vertical distributions; closed points from horizontal distributions.

Reproduced from
best available copy.

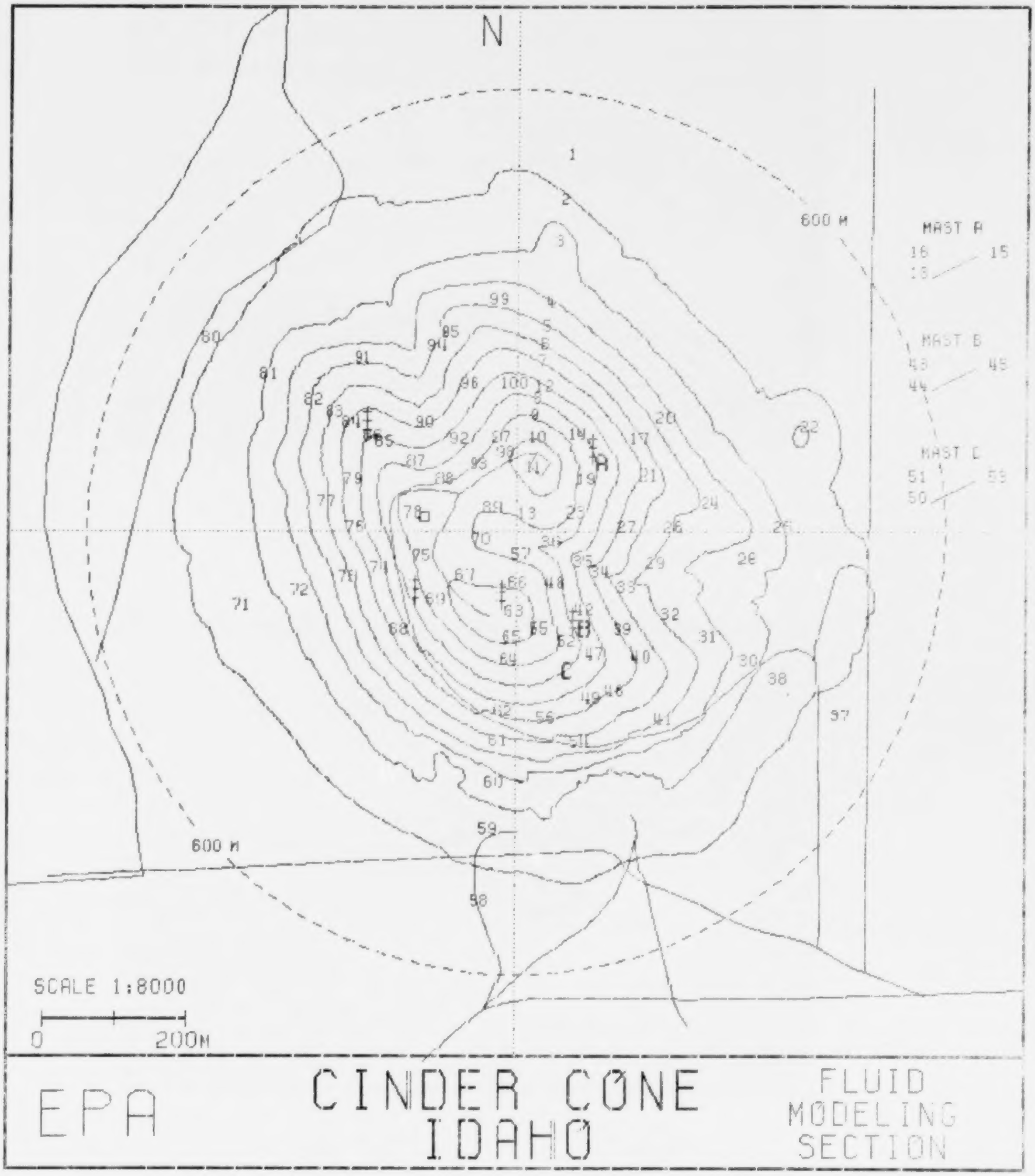
N
600 M
MAST A
16
15
13
MAST B
43
45
44
MAST C
51
53
50
A
B
C
1
2
3
4
5
6
7
8
9
10
11
12
13
14
17
19
20
21
23
24
25
26
27
28
29
30
31
32
33
34
35
36
37
38
39
40
41
46
47
48
49
52
54
56
57
58
59
60
61
62
63
64
65
66
67
68
69
70
71
72
73
74
75
76
77
78
79
80
81
82
83
84
85
86
87
88
89
90
91
92
93
94
95
96
97
98
99
100
SCALE 1:8000
0
200M
EPA
CINDER CONE
IDAHO
FLUID
MODELING
SECTION

Figure 14. Sampling Port Location Map.

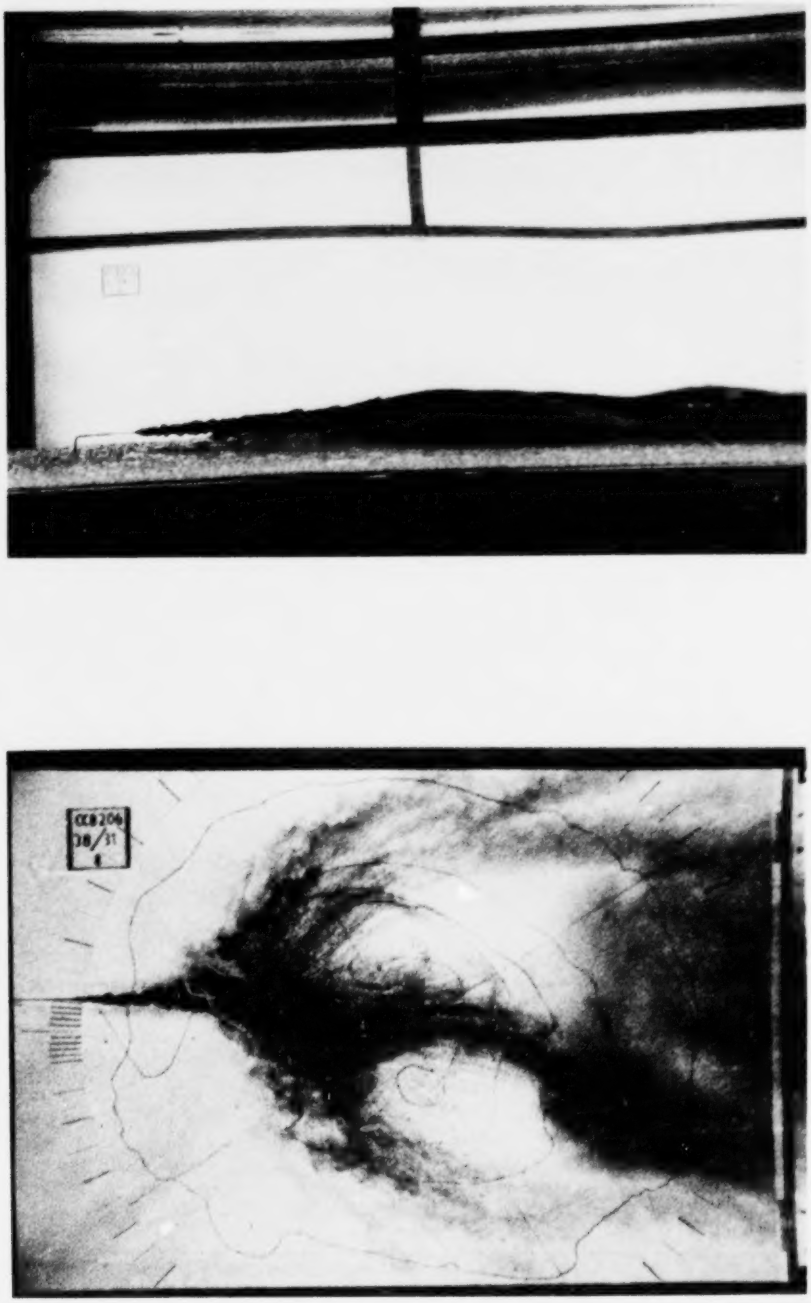
CC8206
38/31
8

Figure 15. Side and Top Views of Model during Tow 8.

Reproduced from
best available copy.

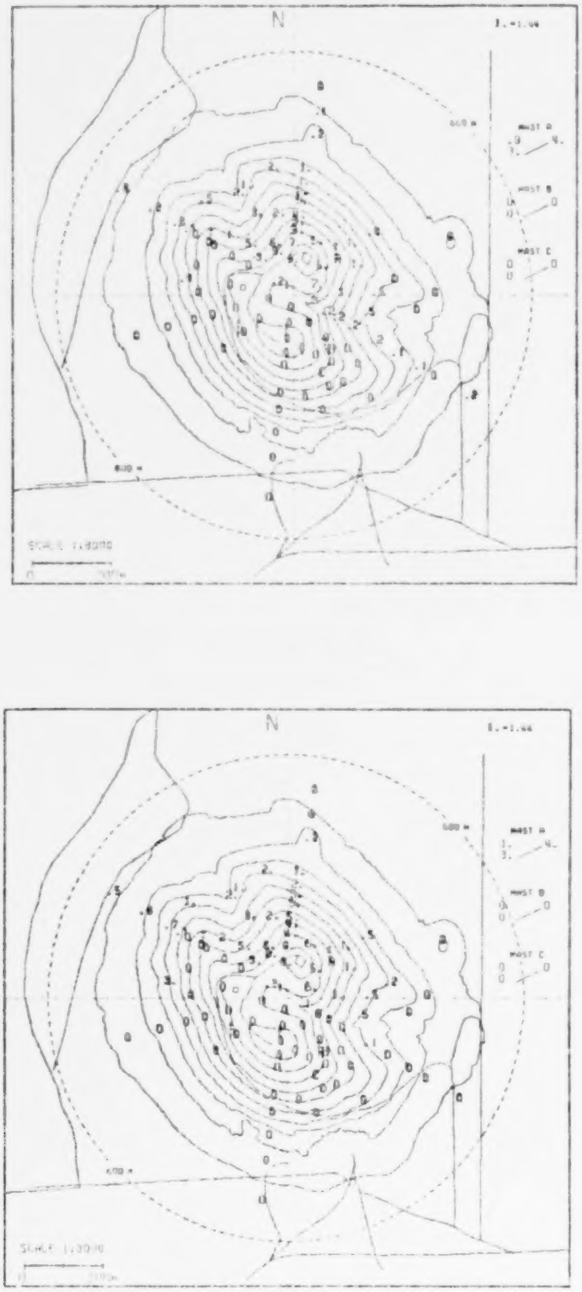
N
MAST A
MAST B
MAST C
N
MAST A
MAST B
MAST C

Figure 16. Concentration Distributions from Tows 1 (top) and 2 (bottom).

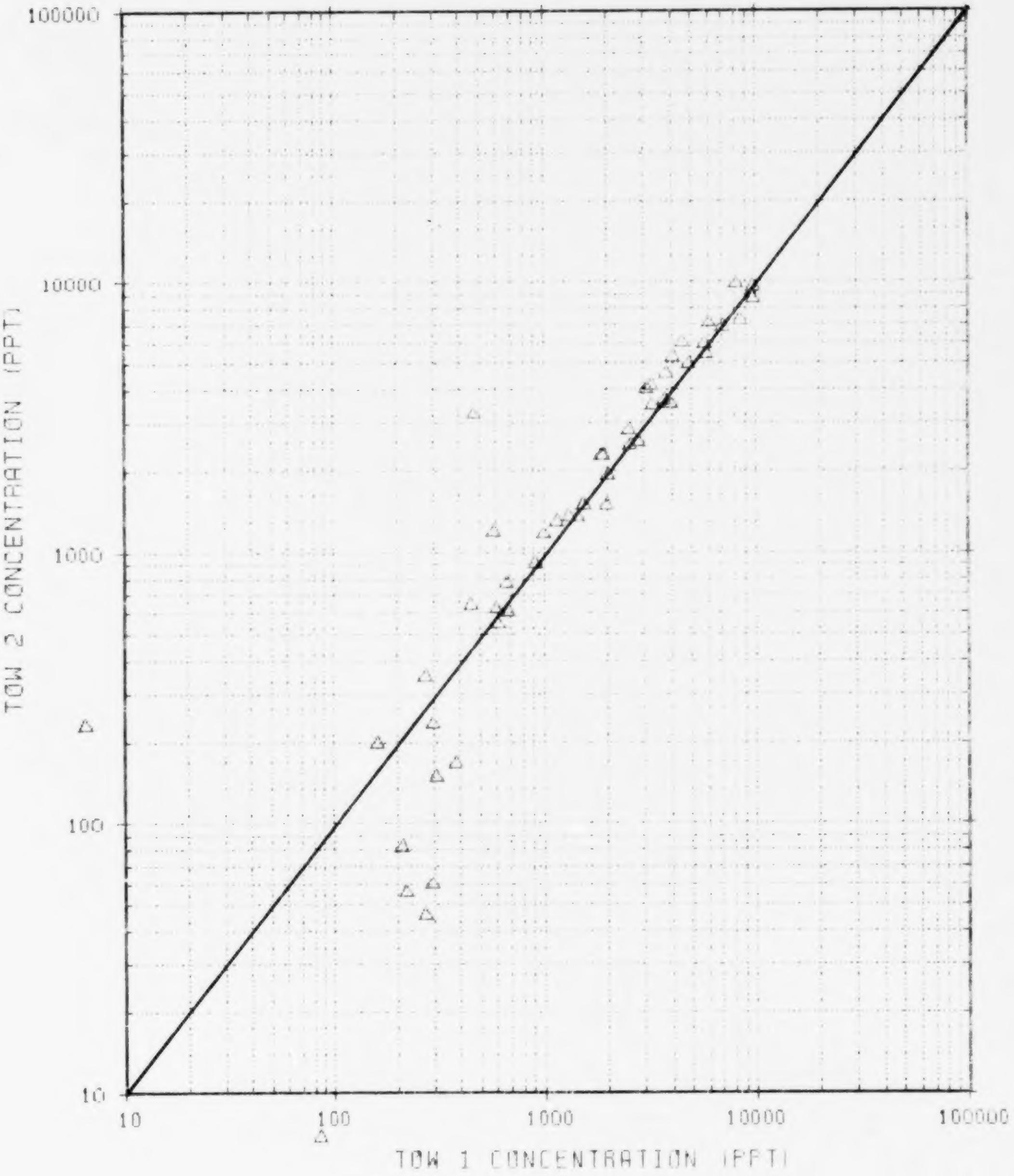

Figure 17. Scatter Diagram Showing Repeatability Between Successive Tows.

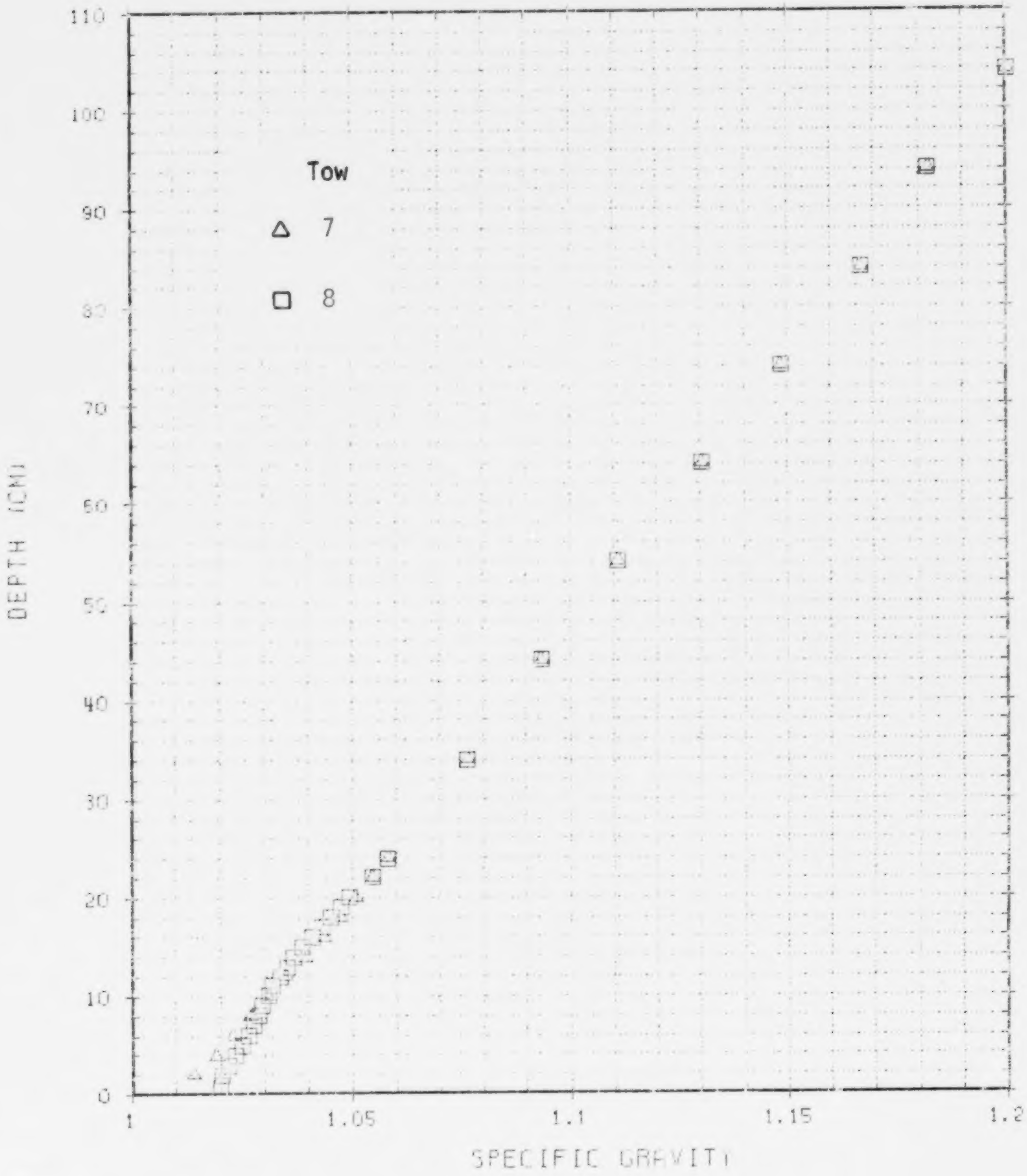

Figure 18. Density Profiles for Tows 7 and 8.

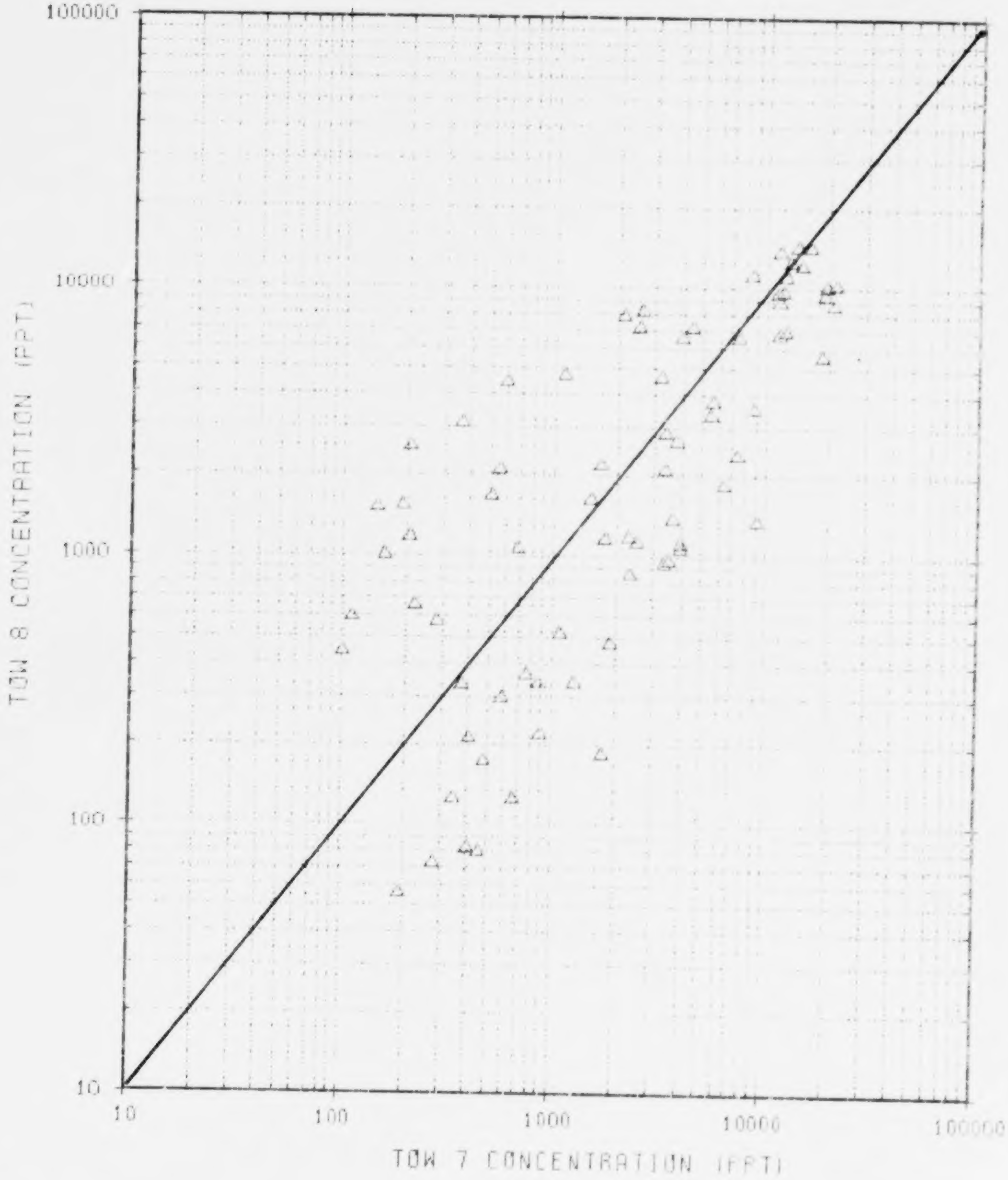

Figure 19. Scatter Diagram Showing Effects of Change in Shape of Density Profile.

Reproduced from
best available copy.

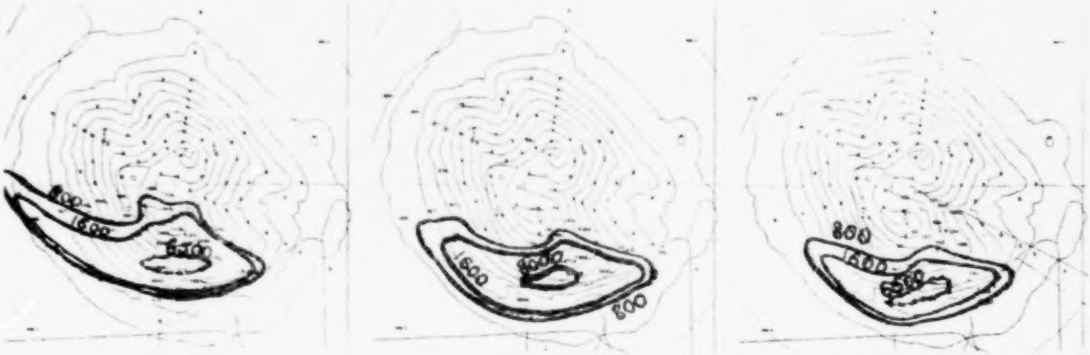

TOW 24
H_c = 24 m; θ = 117°

TOW 22
H_c = 31 m; θ = 117°

TOW 25
H_c = 38 m; θ = 117°

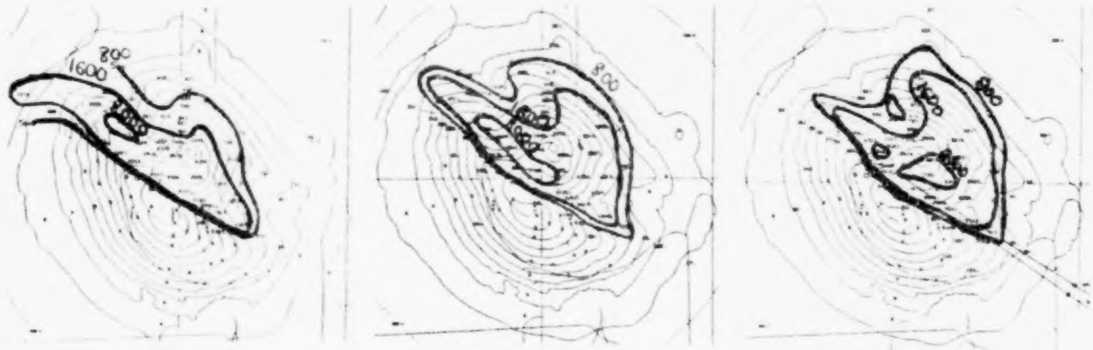

TOW 12
H_c = 24 m; θ = 122°

TOW 11
H_c = 31 m; θ = 122°

TOW 10
H_c = 38 m; θ = 122°

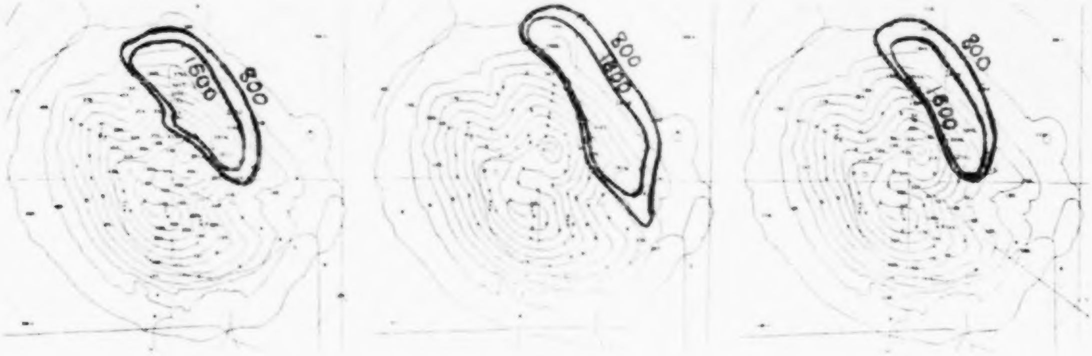

TOW 18
H_c = 24 m; θ = 127°

TOW 19
H_c = 31 m; θ = 127°

TOW 17
H_c = 38 m; θ = 127°

Figure 20: Concentration Distributions Resulting from TOWS at 3 Wind Directions and 6 Values of H_c; H_s = 31 m.

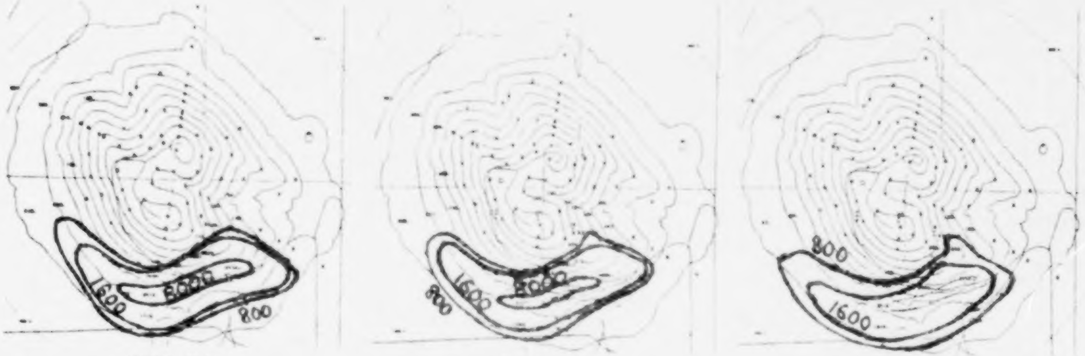

TOW 26
H_c = 44 m; θ = 117°

TOW 27
H_c = 49 m; θ = 117°

TOW 23
H_c = 60 m; θ = 117°

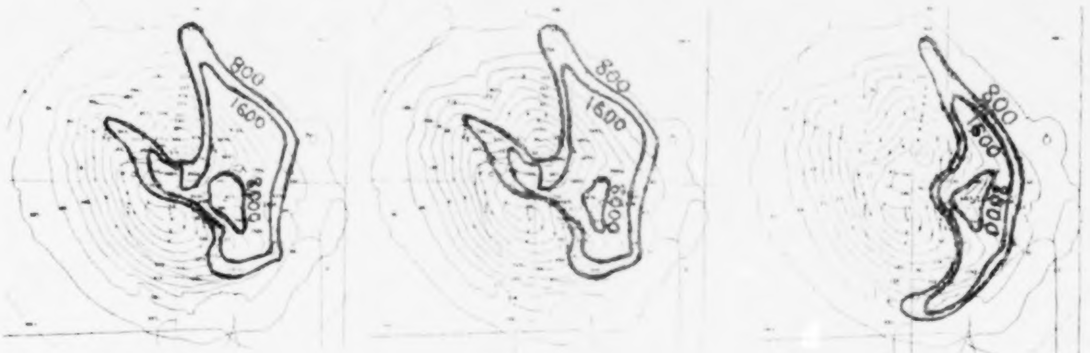

TOW 15
H_c = 44 m; θ = 122°

TOW 14
H_c = 49 m; θ = 122°

TOW 13
H_c = 61 m; θ = 122°

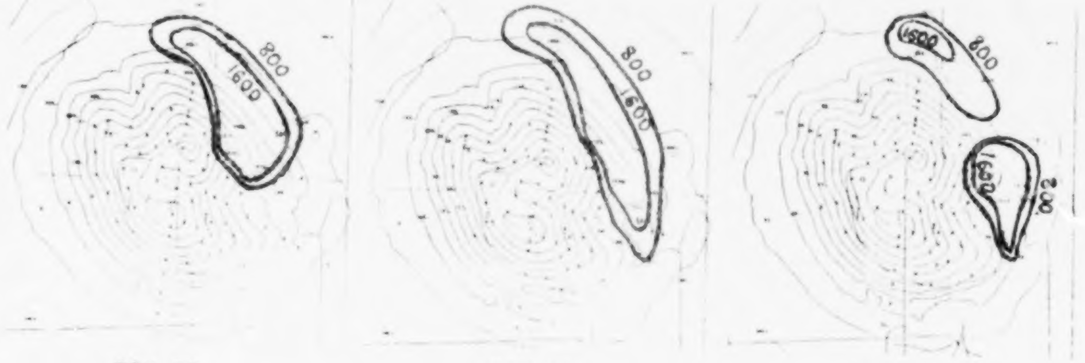

TOW 20
H_c = 44 m; θ = 127°

TOW 21
H_c = 49 m; θ = 127°

TOW 16
H_c = 60 m; θ = 127°

Figure 20: (continued)

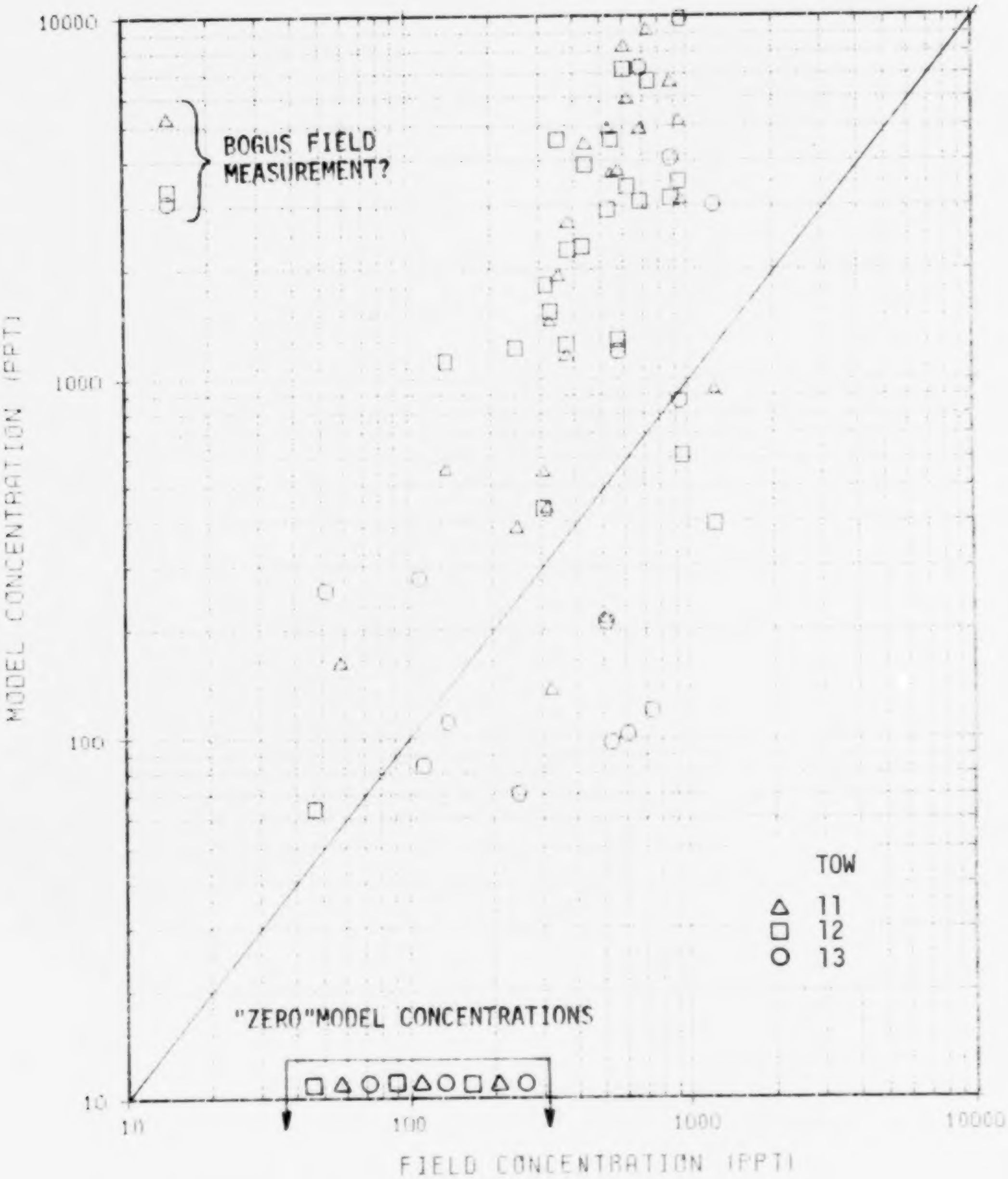

Figure 21. Scatter Diagram Comparing Concentration Distributions from 3 Individual Tows with Field Distributions.

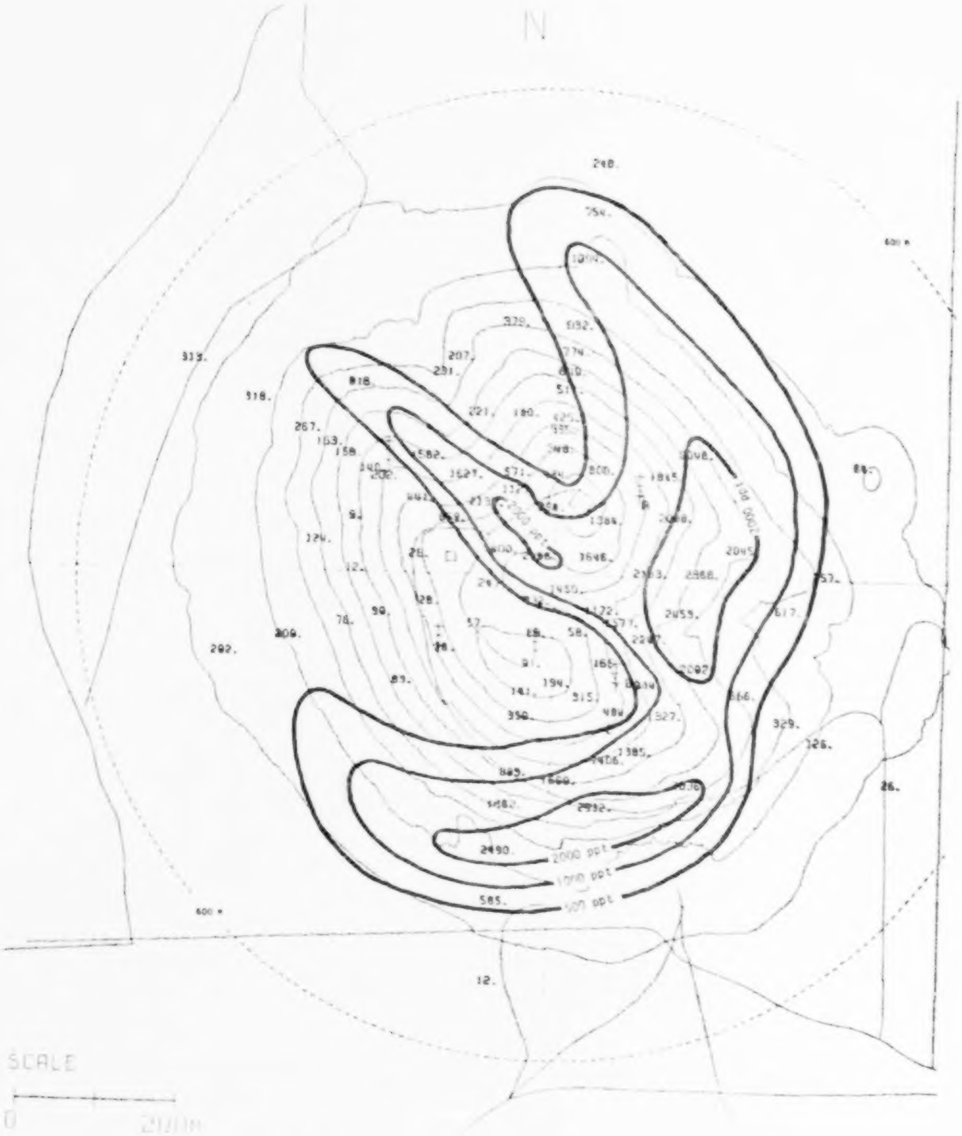
N
2000 ppt
1000 ppt
500 ppt
600 m
SCALE
0
200m

Figure 22. Concentration Distribution from Superposition of 18 Tows.

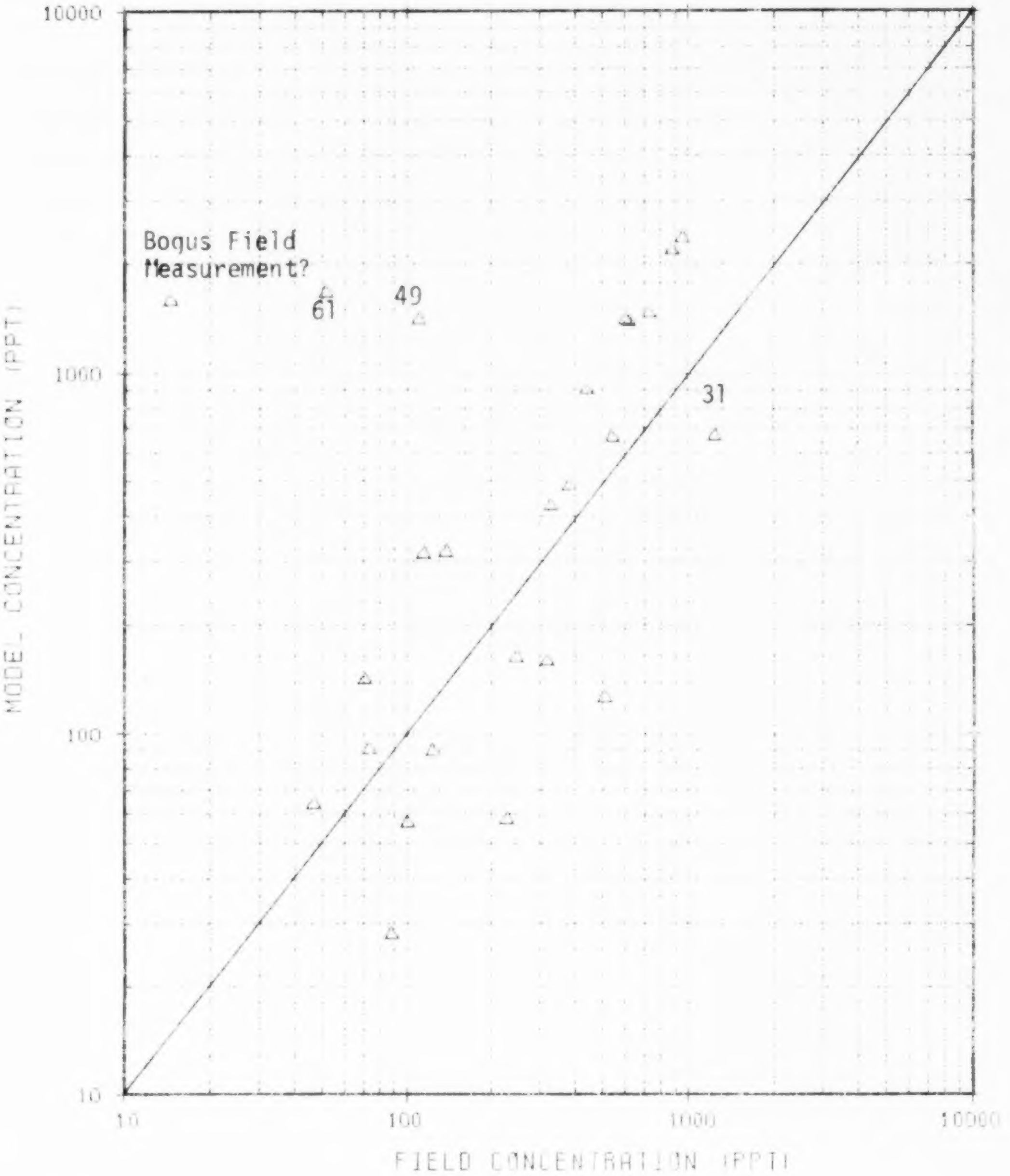

Figure 23. Scatter Diagram Comparing Superposition of Concentration Distributions from 18 Tows with Field Distributions.

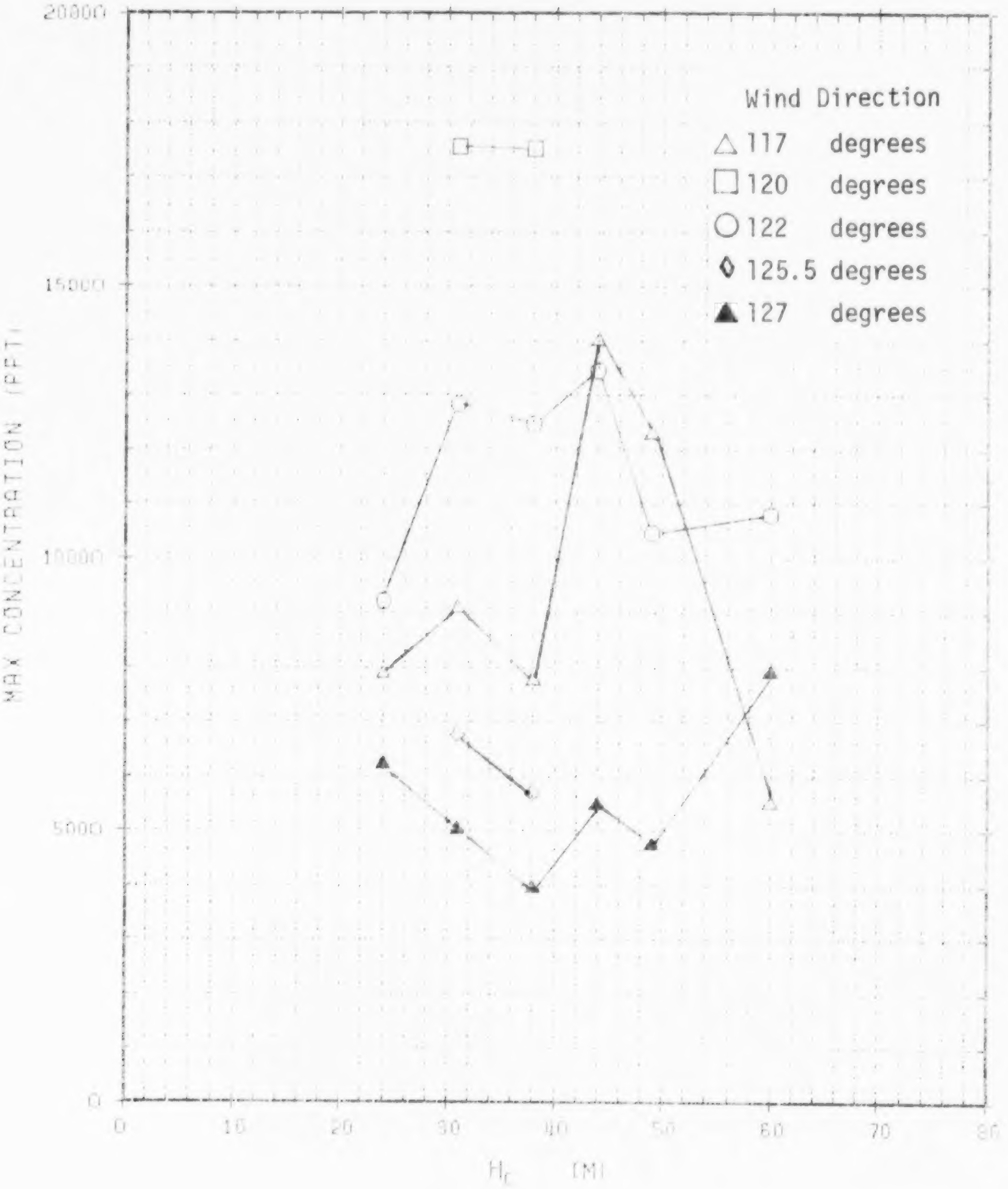

Figure 24. Variation of Maximum Concentration with H_c.

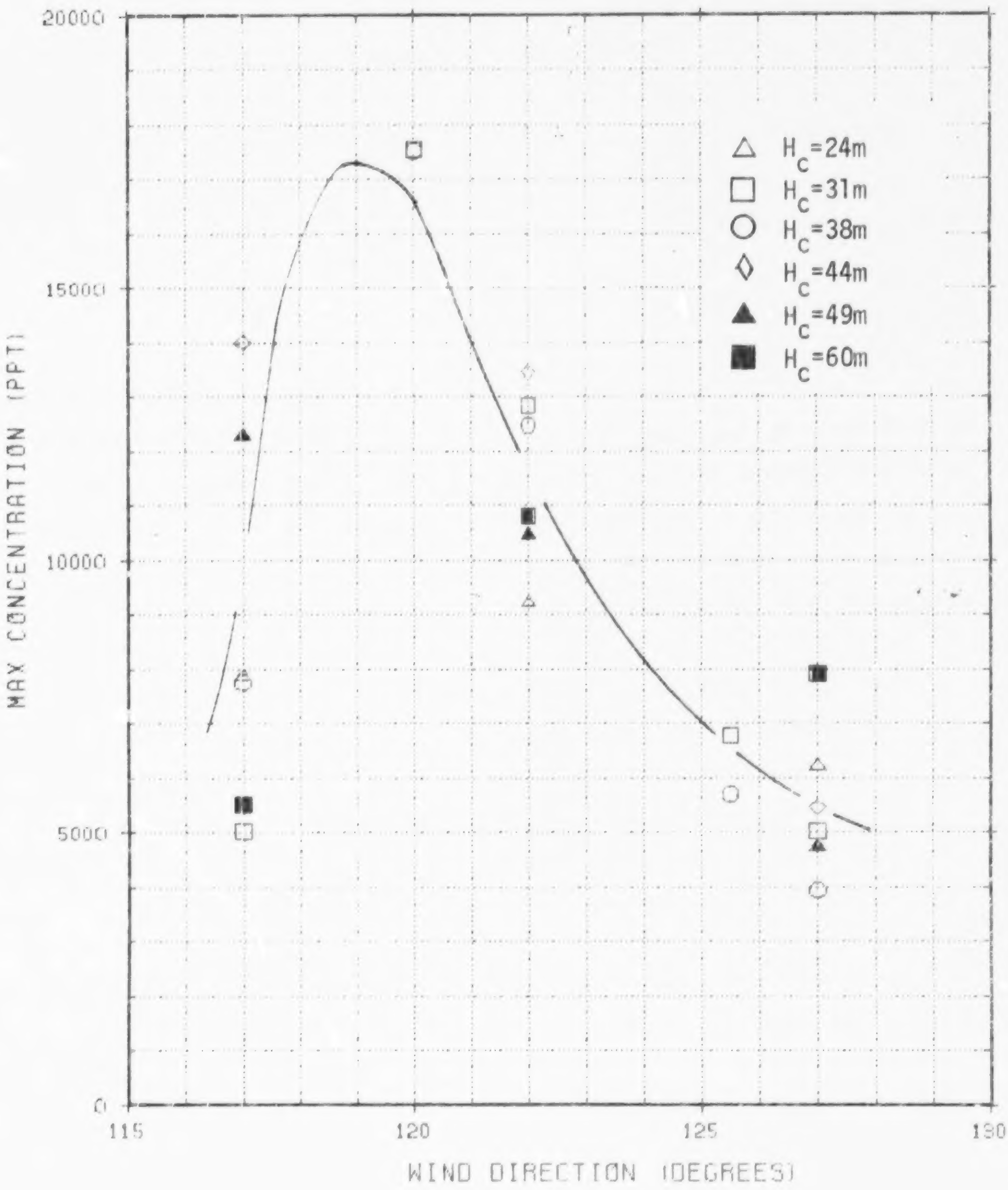

Figure 25. Variation of Maximum Concentration with Wind Direction.

APPENDIX C

USE OF MODEL PERFORMANCE STATISTICS

The model tests discussed in Section 5 are based on the following hypothesized relationship between an observation C_o and the corresponding model estimate C_p:

$$C_o(x_1, x_2) = C_p(x_1) + \varepsilon\,(x_2) \tag{1}$$

where x_1 are known model inputs, and x_2 are unknown variables. Recall that because x_2 is unknown, the estimate C_p can be associated with an infinite ensemble of possible observations. This ensemble is in effect described by the distribution of the residuals ε.

To understand how the statistics of ε can be used to link model estimates with observations, the following questions might be asked:

1) Given a model estimate C_p, what is the probability that the corresponding observation C_o will exceed a specified concentration C_s?
2) Given an estimate C_p, what fraction of corresponding observations are expected to lie within a factor of 2 of the modeled concentration?

To answer these questions assume that ε is normally distributed with zero mean. Then the sample variance of ε is given by

$$S^2 = \frac{1}{N}\sum_{i=1}^{N} (C_{oi} - C_{pi})^2 \tag{2}$$

where N is the number of observations. It can be readily shown that $(C_{oi} - C_{pi})/S$ follows a Student-t distribution with N degrees of freedom.*

To answer Question 1, we construct the following t-statistic, t_r

$$t_r = (C_s - C_p)/S \tag{3}$$

The probability $Pr(t > t_r)$ can be readily obtained from statistical tables. For example, consider the standard deviation of the residuals associated with log-transformed concentrations

$$S \equiv \ln s_g = \left[\frac{1}{N} \sum (\ln C_{oi} - \ln C_{pi})^2\right]^{1/2} \tag{4a}$$

The log-transformation of concentrations allows us to restate Question 1 as: What is the probability that the observed concentration C_o will exceed x times the predicted concentration C_p? Let us take x = 2 and $s_g = 2.5$ for N = 45 so that t_r becomes

$$t_r = \frac{\ln(xC_p) - \ln C_p}{\ln s_g} = \frac{\ln 2}{\ln 2.5} = 0.76 \tag{4b}$$

From tables, we find $Pr\ (t>t_r) \simeq 26\%$.

This calculation immediately allows us to answer Question 2. Because the t-distribution is symmetric, we expect 26% of the observations to be less than one-half the estimated concentration and 26% to be greater than twice the estimated concentration. Therefore, 48% of the observations are expected to lie within a factor of 2 of the estimate.

---

*See Box, G.E.P., W.G. Hunter, and J.S. Hunter 1978. Statistics for Experiments: An Introduction to Design, Data Analysis, and Model Building. New York: John Wiley & Sons.

We can also estimate confidence intervals for the model calculations. Specifically, we can express the $(1 - \gamma)$ confidence interval for the ratio C_o/C_p as follows:

$$S^{-j} < C_o/C_p < S^{j} \qquad (5)$$

where $j = t_{\gamma/2}$ (n degrees of freedom). As an example, the 95% confidence interval corresponding to $s_g = 2.5$ (45 degrees of freedom) can be estimated by noting that $t_{\gamma/2} = 2$. Then,

$$0.16 < C_o/C_p < 6.25 \qquad (6)$$